UNIVERSIDADE
BEIRA INTERIOR

Produção de novos materiais de elevado desempenho a partir de celulose vegetal nano/microfibrilada

Vera Lúcia Dias da Costa

Tese para obtenção do Grau de Doutor em
Química
(3º ciclo de estudos)

Orientador: Prof. Doutor Rogério Manuel dos Santos Simões

julho de 2022

Júri das provas de Doutoramento em Química

As provas de doutoramento realizaram-se no dia 04 de julho de 2022, pelas 14h30, sendo o júri constituído pelos seguintes elementos:

Presidente:

Doutor Joaquim Mateus Paulo Serra, Vice-Reitor da Universidade da Beira Interior

Vogais:

Doutor Paulo Jorge da Silva Almeida, professor catedrático da Universidade da Beira Interior;

Doutor Rogério Manuel dos Santos Simões, professor associado da Universidade da Beira Interior;

Doutor Dmitry Victorovitch Evtyugin, professor associado da Universidade de Aveiro (Arguente);

Doutor Paulo Jorge Tavares Ferreira, professor associado da Faculdade de Ciências e Tecnologia da Universidade de Coimbra (Arguente);

Doutora Ana Paula Nunes de Almeida Alves da Costa, professora auxiliar da Universidade da Beira Interior;

Engenheiro Vitor Reinaldo dos Santos Lucas, Especialista na produção de pasta para papel, Diretor industrial da Biotek, Grupo Altri.

Para ti, querido Pai, como mais uma busca incansável pelo teu orgulho e amor, na certeza de que o meu coração, bem como os corações de todos os que te amam, são a tua verdadeira e derradeira morada.

Para o meu Filho, que vem a caminho, na esperança de que também ele, um dia, ele se orgulhe da Mãe.

Para a minha família: a minha pedra angular.

Acknowledgements

Este doutoramento foi financiado por uma bolsa de investigação no âmbito do protocolo celebrado entre a Universidade da Beira Interior e a Celtejo - Empresa de Celulose do Tejo, S.A.. O meu agradecimento à Celtejo por esta possibilidade.

Agradeço à minha família o apoio incondicional, o respeito e o carinho que me dedicaram ao longo dos anos em que construí esta tese. Um agradecimento especial ao meu marido, o meu pilar, colo e porto de abrigo; à minha mãe, fonte inesgotável de resistência e otimismo; à minha irmã, pela constante sensatez e compreensão; às minhas afilhadas, cuja inocência e amor me deram alento e perspetiva em dias menos bons; à minha avó, pelo carinho e alegria contagiante a cada nova etapa concluída; ao meu saudoso pai, cuja alma de cientista e espírito de sacrifício carrego como exemplo todos os dias.

Um agradecimento sincero por todo o apoio, ensinamentos e orientação ao meu orientador, Professor Doutor Rogério Simões e, de uma forma geral, a todas as pessoas que cruzaram o meu caminho na UBI, incluindo os docentes e funcionários do departamento de Química e colegas, cuja amizade permaneceu para lá da vida académica.

A todos, a minha sentida gratidão!

“Look again at that dot. That's here. That's home. That's us. On it everyone you love, everyone you know, everyone you ever heard of, every human being who ever was, lived out their lives. The aggregate of our joy and suffering, thousands of confident religions, ideologies, and economic doctrines, every hunter and forager, every hero and coward, every creator and destroyer of civilization, every king and peasant, every young couple in love, every mother and father, hopeful child, inventor and explorer, every teacher of morals, every corrupt politician, every "superstar," every "supreme leader," every saint and sinner in the history of our species lived there - on a mote of dust suspended in a sunbeam.”

Carl Sagan in Pale Blue Dot, 1994

Abstract

Cellulose is the most abundant, renewable and sustainable biopolymer on the planet, having many desirable characteristics that make it a suitable material for many applications. Cellulose fibrils from renewable resources have been gaining increasing interest due to their sustainable and biodegradable nature, combined with other mechanical, optical, thermal, and fluidic properties. Cellulose fibrils are therefore attractive for the production of a variety of materials, from composites to porous membranes and gels, filaments and films. The investigation developed throughout this work aimed to explore both the rheological behavior of nanofibrillated cellulose (NFC) suspensions using different liquid media, and mechanical, optical and barrier properties of structures produced from this material.

Regarding the investigation of NFC suspensions' rheological behavior, the undertaken study focused on the morphological effects of the fibrils present in aqueous suspensions, on the addition of ethanol or acetone to the medium and on the increase of the medium's ionic strength through the addition of high NaCl concentrations. For this purpose, two different NFC suspensions were used: a carboxymethylated NFC aqueous suspension obtained from Innventia (Stockholm, Sweden) (NFC-carb); and a NFC aqueous suspension produced in the laboratory using a commercial eucalyptus bleached sulfite pulp, subjected to a 2,2,6,6-tetramethylpiperidine-1-oxyl (TEMPO) mediated oxidation pretreatment in a TEMPO/NaBr/NaClO system, which was subsequently subjected to high pressure homogenization at the RAIZ (Institute for Research on Forest and Paper) facilities (NFC-TEMPO). The morphological analysis of the suspensions through SEM (Scanning Electron Microscopy) and TEM (Transmission Electron Microscopy) allowed to infer a higher percentage of nanoelements in the NFC-TEMPO suspension compared to the NFC-carb. The physicochemical analysis of the fibrils on both suspensions was performed: the intrinsic viscosity was 397 ml/g for NFC-carb and 85 ml/g for NFC-TEMPO, corresponding to cellulose polymerization degrees of 696 and 149, respectively; the quantification of carboxylic groups was 698 μmol/g for NFC-carb and 1900 μmol/g for NFC-TEMPO. These results confirmed that the used suspensions were morphologically and physicochemically very different.

In order to study the effect of the liquid medium's characteristics in which the nanofibrils are suspended, on the rheology of the suspension, the addition of ethanol or acetone to the medium was explored, and concentrations between 2.5 and 40% of

ethanol or acetone were investigated, using the NFC-carb. On the other hand, to study the effect of increasing ionic strength on the suspensions' rheological behavior, NaCl was added in order to obtain concentrations between 50 mM and 1000 mM, for both studied nanofibrils (NFC-carb and NFC-TEMPO). The solids content of both studied suspensions was adjusted to 1.3%. The suspensions were subjected to rheological measurements in flow and oscillatory modes, using a tension-controlled rheometer, equipped with a cone and plate geometry, with either smooth or rough surfaces. In the later case, sandpaper with known roughness was attached to the surface of both tools.

The study of the geometry roughness effect on the NFC-carb suspensions' rheological behavior showed higher shear stresses and viscosity for the rough geometry at lower shear rates (0.05 to 5 s^{-1}), but at higher rates (up to 100 s^{-1}) the measurements were less influenced by either flow instabilities or the geometry's roughness, closely representing the bulk properties of the suspension. The subsequent rheological measurements were carried out with sandpaper with a roughness of 58.5 μm.

Regarding the study of ethanol or acetone addition effect on the NFC-carb suspension, results showed that an addition of 2.5 wt.% of either solvent decreased the viscosity and dynamic modulus, while a 40 wt.% addition increased the shear stress for values higher than those of the corresponding aqueous suspensions, particularly at low or moderate shear rates, indicating higher interfibrillar interaction. The suspension containing 40wt.% ethanol enabled to further double the storage modulus and allowed the extension of the gel-like behavior to higher shear stress values.

Concerning the effect of ionic strength, increasing the NaCl concentration from 50 mM to 100 mM drastically increased the viscosity of both NFC-carb and NFC-TEMPO suspensions, while the network's energy storage modulus the in the elastic region linearly increased with the increase of NaCl concentration from 100 mM to 1000 mM, suggesting improved interfibrillar interaction with increasing salt concentration. This result is in agreement with the expected decrease in electrostatic repulsion between fibrils due to salt addition. In practical terms, the suspensions elastic domain was extended from 10 Pa to 50 Pa with the addition of 40 wt.% of acetone, and to above 500 Pa with NaCl addition at a concentration of 1000 mM.

Despite the much lower cellulose degree of polymerization of the NFC-TEMPO sample, compared to that of the NFC-carb (149 vs 696), the NFC-TEMPO aqueous suspension without added salt exhibited a markedly higher shear stress over the entire studied shear rate range. This result evidences the importance of particle size, as well as specific

surface area, on the suspension's rheological behavior, as the NFC-TEMPO sample has a higher nanoelements (nanofibrils) content than the NFC-carb (based on SEM and TEM analysis).

In addition to film production, NFC gel can be used to produce filaments for potential applications in the textile industry. In the present work, the effect of suspension's solids content and spinning rate on the mechanical properties of filaments produced via wet spinning were studied. For this purpose, two commercial eucalyptus bleached pulps, one obtained by a kraft process and the other one obtained by a sulfite process, were used as sources of cellulose fibers to produce NFC suspensions. Firstly, both pulps were submitted to a refining process in a PFI mill. Then, the refined sulfite pulp was subjected to TEMPO-mediated oxidation in a TEMPO/NaBr/NaClO system, while the refined kraft pulp was subjected to TEMPO-mediated oxidation in a TEMPO/NaClO/$NaClO_2$ system. Both oxidized pulps were subsequently subjected to high pressure homogenization in the RAIZ facilities. The initial characteristics of the pulps and the different applied oxidative treatments led to products with very different degrees of cellulose polymerization. For the sulfite pulp, the cellulose degree of polymerization in the NFC-s was 202, while the NFC resulting from kraft pulp (NFC-k) had a cellulose degree of polymerization of 848. The highest cellulose degree of polymerization of the NFC-k is a consequence of the higher initial value of the pulp and also the less aggressive oxidation treatment with the TEMPO/NaClO/$NaClO_2$ system. The suspensions' solids content was adjusted to a range from 2.5 to 3.22 % and were used to produce cellulosic filaments *via* wet spinning, with spinning rates of 0.45 to 1.7 m min^{-1} into a 1M NaCl coagulation bath, followed by an ethanol fixation bath. Some of the produced filaments were also subjected to an additional water bath, in order to wash out the salt still present in the filaments. The filaments ends were pinned, maintaining the filaments' length and were air dried under standard conditions of temperature and relative humidity. Subsequently, filaments' mechanical performance was tested.

The filaments were void-free and had an approximately circular cross section, which was not substantially altered by the spinning rate variation in the studied range, nor by the reimmersion in the washing bath and second drying.

The results showed that an increase in wet spinning rate improved the mechanical performance of the filaments, indicating some level of fibril alignment. On the other hand, the increase in the suspensions' solids content did not translate into an improvement in the filaments' strength, due to the higher viscosity and reduced

alignment capacity of the fibrils. The filaments produced from the NFC-s suspension exhibited superior mechanical performance, despite the much lower cellulose degree of polymerization. On the other hand, the microscopic analysis of the suspension shows a higher fibrillation extent and a higher nanoelements content, which again highlights the role of fibril morphology in the structure/performance of the filaments.

After additional washing of the filaments, and as a consequence of removing some amount of salt, the linear mass and cross-sectional diameter of the filaments significantly decreased, thus a drastic increase in tensile strength, tenacity and strength-to-failure was observed due to interfibrillar interaction reestablishment. A broader and deeper exploration of filaments production from NFC gels requires a more advanced experimental setup, namely one that allows to increase the spinning rate, which was not available.

With regard to cellulose films, in addition to mechanical properties, barrier properties are very important in several applications. Thus, at a given stage of the undertaken work, the effect of hot calendering on the physical and water vapor barrier properties of bacterial and vegetable cellulosic films was studied. The production of bacterial cellulose was carried out using *Gluconacetobacter xylinus* at the University of Minho facilities and the films were produced and tested at the University of Beira Interior. To produce the films, bacterial cellulose was fragmented in a blender and the solid content of the resulting suspension was adjusted to 0.354 %. Part of this suspension was subjected to ozonization in order to improve the optical properties of the resulting films.

Films were produced by vacuum filtration from non-ozonized (BC) and ozonized (BCO) bacterial cellulose suspensions. After draining the water, the filter cakes were adhered to metal discs and pressed between blotting papers using a procedure analogous to paper production. Then, the films were dried overnight, between perforated metal rings under pressure applied to the ends of the sheets to prevent the films from shrinking, under standard conditions of temperature and relative humidity. For properties comparison, vegetable cellulose films were also produced from highly refined bleached kraft eucalyptus pulp with approximately the same grammage as the bacterial cellulose films. To study the calendering effect, some films were subjected to a hot calendering process.

Results showed that BC and BCO suspensions formed much denser films than those from vegetable cellulose, forming much more compact and closed structures, in

agreement with the smaller dimension of the constituent elements. As a consequence of the high density, the Young's modulus and tensile index of BC and BCO films were much higher than those obtained for vegetable cellulose.

Calendering substantially increased the transparency of the films and ozonation was effective in increasing the brightness and transparency of the BCO films regarding the BC films. However, both processes slightly decreased the mechanical performance of the films. The water vapor transfer rate was lower for bacterial cellulose films than for vegetable cellulose films and decreased by 70% with calendering. Concluding, hot calendering can be used to obtain bacterial cellulose (or nanofibrillated vegetable cellulose) films suitable for various applications, where the water vapor barrier represents an important functionality. Ozonation can be used as a way to improve the optical properties of the films, although it is necessary to establish a compromise between the benefits of ozonization and calendering, and the decrease in the mechanical performance of the films induced by these processes.

Subsequently, research was carried out in order to provide hydrophobicity to films made from a NFC suspension, through coating with stearic acid (SA) and particles of modified precipitated calcium carbonate (PCC). The NFC used in this work, oxidized with a TEMPO/NaBr/NaClO system, contained a cellulose with a degree of polymerization of 367 and a carboxylic group content of 997 μmol/g.

An SA aqueous suspension was prepared following a procedure that involved raising the temperature of a SA/water mixture and sonicating it, followed by cooling in an ice bath. The modification of the PCC was carried out by adding PCC to the priorly made SA suspension and subjecting it to ultrasounds. After drying in an oven, the modified PCC was collected and manually ground, resulting in a fine white powder. Both the SA aqueous suspension and the modified PCC were used as a coatings in the production of hydrophobic NFC films. The films were produced by vacuum filtration and later surface-modified, resulting in three different sets: a first set of neat, uncoated NFC films; a second set coated with a layer of stearic acid (NFC-SA) and a third set coated with a layer of stearic acid and an additional layer of modified PCC (NFC-LBL). The films were dried overnight, between perforated metal rings under pressure applied to the ends of the sheets, under standard conditions of temperature and relative humidity. Subsequently, some of the coated films were subjected to heat treatment in an oven at 68ºC or 105ºC. Next, the films were analyzed in terms of their mechanical performance, water vapor and oxygen barrier properties, as well as static/dynamic contact angle measurements.

The results showed that the coatings and heat treatments did not affect the mechanical performance of the films. Heat treatments decreased the water vapor transmission rate and oxygen permeability of both NFC-SA and NFC-LBL films. Coating with SA rendered hydrophobic films as the measured static contact angle reached 122°. Non-heat-treated NFC-LBL films achieved a contact angle of up to 150° and a contact angle hysteresis of 3.1°. The NFC-LBL films treated at 68°C exhibited near superhydrophobicity, with a contact angle of up to 140° and a contact angle hysteresis of 5°. The coating of NFC-LBL films without heat treatment was easily removed by friction, but the heat treatment turned the films' coating the hydrophobicity persistent, resisting to friction and handling.

Taking into account that the production of nanofibrillated cellulose films through filtration is a slow process, based on previous rheology studies it was decided to study the effect of ethanol addition to the suspension on the drainage time during the production of NFC films by vacuum filtration and the mechanical, optical and barrier properties of the resulting films. For this, aqueous / alcoholic suspensions of NFC with an ethanol content up to 75 wt.% were used in the production of films, monitoring the drainage progression by measuring the collected filtrate. The films were air-dried under standard conditions of temperature and humidity or in an oven at 70°C for 4 hours. Mechanical and optical performance as well as water vapor barrier properties were tested.

The results showed that the filtration time drastically decreased with increasing ethanol content, from about 2 hours to 2 minutes for ethanol suspensions with 0 (zero) and 75 wt.%, respectively. The increase in ethanol content did not significantly affect the mechanical performance of air-dried films, despite the increase in the global porosity of the structures. On the other hand, oven drying provided the films with tensile properties superior to those exhibited by air-dried films, both produced from purely aqueous suspensions, despite the increase in elongation at break and the higher value of specific light scattering coefficient. The water vapor transmission rate increased for films produced from 75 wt.% ethanol suspensions and was even higher for oven dried films. The combination of drying the films in an oven and producing the film from an alcoholic/aqueous suspension provided the opportunity to manipulate the transparency of the film and the water vapor transmission rate, preserving the mechanical performance of the films. Briefly, with this study, it was possible to develop a relatively fast and simple method to produce NFC films with mechanical and barrier properties with potential for several applications, such as membranes, where mechanical strength, toughness, low density, controlled permeability and porosity and

high specific area are important, fuel cells, liquid purification and filtration, tissue engineering, protein immobilization and separation, and protective clothing.

In short, the investigation carried out throughout this work allowed to prove the great potential of cellulosic fibrils in numerous applications, mainly in the manufacture of films. Regarding calendering, the present work demonstrated that this unitary operation is highly effective in improving the water vapor barrier properties of cellulosic fibril films. With regard to the production of films by vacuum filtration from highly fibrillated cellulose suspensions, the most reported difficulty by several authors referenced in the literature is the fact that this is an extremely slow process, making the production of NFC films impractical at the industrial level. The present work presents important developments regarding this aspect, suggesting a simple modification from the purely aqueous medium of suspensions to a medium with a mixture of water/ethanol. This technique, in addition to drastically reducing film formation time and using a solvent that is easily and quickly recovered by evaporation, preserves the mechanical properties of the produced films. Another aspect that complicates the application of NFC in several areas and, consequently, of films made from NFC, is its hydrophilic nature. The present work developed methods for the production of NFC films with strong hydrophobic properties, resistant to handling and friction, applying surface coatings of stearic acid and precipitated calcium carbonate, combined with a heat treatment, in an environmentally friendly technique and possibly industrially scalable.

Keywords

Nanofibrillated cellulose (NFC); bacterial cellulose; aqueous/ ethanol NFC suspensions; drainage time; morphology; rheology; filaments; films; mechanical performance, optical properties; barrier properties.

Resumo

A celulose é o biopolímero mais abundante, renovável e sustentável do planeta, possuindo muitas características desejáveis que a tornam um material adequado para diversas aplicações. As fibrilas de celulose obtidas a partir de recursos renováveis têm vindo a ganhar um crescente interesse devido à sua natureza sustentável e biodegradável, combinada com outras propriedades mecânicas, óticas, térmicas e fluídicas. As fibrilas de celulose são, portanto, atraentes para o fabrico de diversos materiais, desde compósitos a membranas porosas e géis, filamentos e filmes. A investigação desenvolvida ao longo deste trabalho visou explorar quer o comportamento reológico de suspensões de celulose nanofibrilada (NFC) usando diferentes meios líquidos, quer as propriedades mecânicas, óticas e de barreira das estruturas produzidas a partir deste material.

Relativamente à investigação do comportamento reológico de suspensões de NFC, o estudo realizado focou-se nos efeitos da morfologia das fibrilas presentes em suspensões aquosas, na adição de etanol ou acetona ao meio e no aumento da força iónica do meio através da adição de elevadas concentrações de NaCl. Para tal, foram utilizadas duas suspensões diferentes de NFC: uma suspensão aquosa de NFC carboximetilada obtida através da Innventia (Estocolmo, Suécia) (NFC-carb); e uma suspensão aquosa de NFC produzida no laboratório usando uma pasta comercial de eucalipto ao sulfito branqueada, submetida a um pré-tratamento de oxidação mediada por 2,2,6,6-tetrametilpiperidina-1-oxil (TEMPO) num sistema TEMPO/NaBr/NaClO, que posteriormente foi submetida a homogeneização de alta pressão nas instalações do RAIZ (Instituto de Investigação da Floresta e do Papel) (NFC-TEMPO). A análise morfológica das suspensões através de SEM (Scanning Electron Microscopy) e TEM (Transmission Electron Microscopy) permitiu inferir uma maior percentagem de nanoelementos na suspensão NFC-TEMPO relativamente à NFC-carb. Foi efetuada a análise físico-química das fibrilas presentes em ambas as suspensões: a viscosidade intrínseca foi de 397 ml/g para a NFC-carb e 85 ml/g para a NFC-TEMPO, correspondendo a graus de polimerização da celulose de 696 e 149, respetivamente; a quantificação de grupos carboxílicos foi de 698 μmol/g para a NFC-carb e 1900 μmol/g para a NFC-TEMPO. Estes resultados confirmaram que as suspensões usadas tinham propriedades morfológicas e físico-químicas substancialmente diferentes.

Para estudar o efeito das características do meio líquido em que as nanofibrilas estão suspensas sobre a reologia da suspensão, explorou-se a adição de etanol ou acetona ao meio, tendo-se investigado concentrações entre 2,5 e 40% de etanol ou acetona, utilizando a NFC-carb. Por outro lado, para o estudo do efeito do aumento da força iónica no comportamento reológico das suspensões, foi adicionado NaCl com vista a obter concentrações entre 50 mM e 1000 mM, tendo-se estudado ambas as nanofibrilas (NFC-carb e NFC-TEMPO). O teor de sólidos das duas suspensões estudadas foi ajustado para 1,3 %. As suspensões foram submetidas a medições reológicas nos modos de fluxo contínuo e oscilatório, usando um reómetro controlado por tensão, equipado com uma geometria de cone e prato, com superfície lisa ou rugosa, sendo que, no caso da geometria rugosa, papel de lixa com rugosidade conhecida foi colado na superfície de ambas as peças.

O estudo do efeito da rugosidade da geometria no comportamento reológico das suspensões NFC-carb evidenciou tensões de cisalhamento e viscosidade mais elevados para a geometria rugosa a taxas de cisalhamento mais baixas (0.05 a 5 s^{-1}), mas a taxas mais elevadas (até 100 s^{-1}) as medições foram menos influenciadas quer por instabilidades de fluxo, quer pela rugosidade da geometria, aproximando-se das propriedades do *bulk* da suspensão. As medições reológicas que se seguiram foram realizadas com papel de lixa de rugosidade 58.5 μm.

Relativamente ao estudo do efeito da adição de etanol ou acetona à suspensão NFC-carb, os resultados mostraram que uma adição de 2,5% em peso de qualquer destes solventes diminuiu a viscosidade e os módulos dinâmicos, enquanto uma adição de 40% aumentou as tensões de cisalhamento para valores superiores às das correspondentes suspensões aquosas, principalmente a taxas de cisalhamento baixas ou moderadas, indicando maior interação interfibrilar. A suspensão contendo 40% de etanol provocou ainda a duplicação do módulo de armazenamento e permitiu a extensão do comportamento do tipo gel para valores de tensão de cisalhamento mais elevados.

Relativamente ao efeito da força iónica, o incremento na concentração de NaCl de 50 mM para 100 mM aumentou drasticamente a viscosidade de ambas as suspensões NFC-carb e NFC-TEMPO, enquanto que o módulo de armazenamento de energia pela rede na região elástica aumentou linearmente com o aumento da concentração de NaCl de 100 mM para 1000 mM, sugerindo o aumento da interação interfibrilar com o aumento da concentração do sal. Este resultado está em concordância com a expectável diminuição da repulsão eletrostática entre as fibrilas por efeito da adição do sal. Em

termos práticos, o domínio elástico das suspensões foi alargado de 10 Pa para 50 Pa com a adição de 40 % de acetona, e para mais de 500 Pa com a adição de NaCl à concentração de 1000 mM.

Apesar do muito menor grau de polimerização da celulose da amostra de NFC-TEMPO, face à NFC-carb (149 *vs* 696), a suspensão aquosa de NFC-TEMPO sem adição de sal exibiu uma tensão de cisalhamento marcadamente superior para toda a gama de taxa de cisalhamento estudada. Este resultado revela a importância da dimensão das partículas, bem como da área específica, sobre o comportamento reológico da suspensão, já que a amostra NFC-TEMPO tem um teor mais elevado de nanoelementos (nanofibrilas) do que a NFC-carb (com base na análise de SEM e TEM).

Para além da produção de filmes, o gel de celulose nanofibrilada pode ser usado para produzir filamentos para eventuais aplicações na área têxtil. No presente trabalho, estudou-se o efeito do teor de sólidos da suspensão e a velocidade de fiação sobre as propriedades mecânicas dos filamentos produzidos via *wet spinning*. Para este efeito, duas pastas comerciais de eucalipto branqueadas, uma obtida pelo processo kraft e outra pelo processo ao sulfito, foram usadas como fontes de fibras de celulose para produzir as suspensões de NFC. Primeiramente, ambas as pastas foram submetidas a um processo de refinação em moinho PFI. Seguidamente, a pasta ao sulfito refinada foi submetida a oxidação mediada por TEMPO num sistema TEMPO/NaBr/NaClO, enquanto a pasta kraft refinada foi submetida a oxidação mediada por TEMPO num sistema TEMPO/NaClO/$NaClO_2$. Ambas as pastas oxidadas foram posteriormente submetidas a homogeneização a alta pressão nas instalações do RAIZ. As caraterísticas iniciais das pastas e os diferentes tratamentos oxidativos aplicados conduziram a produtos com graus de polimerização da celulose muito diferentes. Para a pasta ao sulfito o grau de polimerização da celulose na NFC-s foi de 202, enquanto que a NFC resultante da pasta kraft (NFC-k) apresentou um grau de polimerização da celulose de 848. O maior grau de polimerização da celulose na NFC-k é uma consequência do maior valor inicial da pasta e do tratamento menos agressivo da oxidação com o sistema TEMPO/NaClO/$NaClO_2$. O teor de sólidos das suspensões foi ajustado para uma gama de 2,5 a 3,22 %, e estas foram usadas para produzir filamentos celulósicos via *wet spinning*, com velocidades de fiação de 0,45 a 1,7 m min^{-1} para banho de coagulação de NaCl 1M, seguido por um banho de fixação de etanol. Alguns dos filamentos produzidos foram ainda submetidos a um banho adicional de água, com o intuito de fazer uma lavagem do sal ainda presente nos filamentos. Os filamentos foram presos pelas pontas com comprimento fixo e foram secos ao ar em condições padrão de

temperatura e humidade relativa. Posteriormente, o desempenho mecânico dos filamentos foi testado.

Os filamentos são maciços e de secção transversal aproximadamente circular, que não foi substancialmente alterada pela variação da velocidade de fiação na gama estudada, nem pela reimersão no banho de lavagem e segunda secagem.

Os resultados mostraram que um aumento na velocidade de *wet spinning* melhorou o desempenho mecânico dos filamentos, indicando algum nível de alinhamento das fibrilas. Por outro lado, o aumento do teor de sólidos não se traduziu na melhoria da resistência dos filamentos, devido à maior viscosidade e menor capacidade de alinhamento das fibrilas. Os filamentos produzidos a partir da suspensão de NFC-s exibiram um desempenho mecânico superior, apesar do muito menor grau de polimerização da celulose. Em contrapartida, a análise microscópica da suspensão evidencia maior extensão da fibrilação e maior teor de nanoelementos, o que realça de novo o papel da morfologia das fibrilas na estrutura/desempenho dos filamentos.

Após a lavagem adicional dos filamentos e como consequência da remoção de alguma quantidade de sal, a massa linear e o diâmetro da seção transversal dos filamentos diminuíram significativamente, pelo que foi observado um aumento drástico na resistência à tração, tenacidade e tensão de rotura devido ao restabelecimento da interação interfibrilar. Uma exploração mais ampla e profunda da produção de filamentos a partir de gel de NFC requer um *setup* experimental mais avançado, nomeadamente que permita aumentar a velocidade de fiação, o que não se encontra disponível.

No que respeita aos filmes de celulose, para além das propriedades mecânicas, as propriedades barreira são importantíssimas em muitas aplicações. Assim, numa dada etapa do trabalho, foi estudado o efeito da calandragem a quente nas propriedades físicas e de barreira ao vapor de água em filmes de celulose bacteriana e vegetal. A produção de celulose bacteriana foi levada a cabo usando *Gluconacetobacter xylinus* nas instalações da Universidade do Minho e os filmes foram produzidos e testados na Universidade da Beira Interior. Para produzir os filmes, a celulose bacteriana foi fragmentada num liquidificador e o teor de sólidos da suspensão resultante foi ajustado para 0.354 %. Parte desta suspensão foi submetida a ozonização com o intuito de melhorar as propriedades óticas dos filmes resultantes.

Foram produzidos filmes por filtração a vácuo a partir das suspensões de celulose bacteriana não ozonizada (BC) e ozonizada (BCO). Após o escoamento da água, os bolos de filtração foram aderidos a discos metálicos e prensados entre papel mata-borrão usando um procedimento análogo à produção de papel. Seguidamente, os filmes foram secos durante a noite, entre anéis metálicos perfurados sob pressão aplicada na extremidade das folhas para evitar que os filmes encolhessem, em condições standard de temperatura e humidade relativa. Para comparação de propriedades, foram também produzidos filmes de celulose vegetal a partir de pasta de eucalipto kraft branqueada fortemente refinada com aproximadamente a mesma gramagem dos filmes de celulose bacteriana. Para estudar o efeito da calandragem, alguns filmes foram submetidos a um processo de calandragem a quente.

Os resultados mostraram que as suspensões de BC e BCO formaram filmes muito mais densos que a celulose vegetal, formando estruturas muito mais compactas e fechadas, em concordância com a menor dimensão dos elementos que as constituíam. Como consequência da alta densidade, o módulo de Young e o índice de tração dos filmes de BC e BCO foram muito maiores do que os obtidos para a celulose vegetal.

A calandragem aumentou substancialmente a transparência dos filmes e a ozonização foi eficaz em aumentar a brancura e a transparência dos filmes de BCO face aos filmes de BC. No entanto, ambos estes processos diminuíram ligeiramente o desempenho mecânico dos filmes. A taxa de transferência de vapor de água foi menor para os filmes de celulose bacteriana do que para os filmes de celulose vegetal e diminuiu 70% com a calandragem. Concluiu-se que a calandragem a quente pode ser usada para obter filmes de celulose bacteriana (ou de celulose vegetal nanofibrilada) adequados para várias aplicações, onde a barreira ao vapor de água represente uma funcionalidade importante. A ozonização pode ser usada com uma forma de melhorar as propriedades óticas destes filmes, mas é necessário estabelecer um compromisso entre os benefícios da ozonização e calandragem, e a diminuição do desempenho mecânico dos filmes induzido por esses processos.

Posteriormente, foi realizado trabalho de investigação no sentido de conferir hidrofobicidade a filmes feitos a partir de uma suspensão de NFC, através do revestimento com ácido esteárico (SA) e partículas de carbonato de cálcio precipitado (PCC) modificado. A NFC usada neste trabalho, produzida com base no sistema TEMPO/NaBr/NaClO, continha uma celulose com um grau de polimerização de 367 e um conteúdo de grupos carboxílicos de 997 μmol/g.

Uma suspensão aquosa de SA foi preparada seguindo um procedimento que envolveu elevar a temperatura da mistura SA /água e submetê-la a ultrassons, e posterior arrefecimento em banho de gelo. A modificação do PCC foi efetuada adicionando PCC à suspensão de SA preparada anteriormente e submetendo-a a ultrassons. Após a secagem em estufa, o PCC modificado foi recolhido e moído manualmente, resultando num pó branco e fino. Tanto a suspensão aquosa de SA como o PCC modificado foram usados como revestimento na produção de filmes de NFC hidrofóbicos. Os filmes foram produzidos por filtração a vácuo e posteriormente modificados superficialmente, resultando em três conjuntos diferentes: um primeiro conjunto de filmes de NFC simples, sem revestimento; um segundo conjunto revestido com uma camada de ácido esteárico (NFC-SA) e um terceiro conjunto revestido com uma camada de ácido esteárico e uma camada adicional de PCC modificado (NFC-LBL). Os filmes foram secos durante a noite, entre anéis metálicos perfurados sob pressão aplicada na extremidade das folhas, em condições standard de temperatura e humidade relativa. Posteriormente, alguns dos filmes revestidos foram submetidos a um tratamento térmico em estufa a 68ºC ou 105ºC. Seguidamente, os filmes foram analisados em termos da sua performance mecânica, das propriedades de barreira ao vapor de água e oxigénio, bem como medidas de ângulo de contato estático / dinâmico.

Os resultados mostraram que os revestimentos e tratamentos térmicos não afetaram o desempenho mecânico dos filmes. Os tratamentos térmicos diminuíram a taxa de transmissão de vapor de água e a permeabilidade ao oxigénio de ambos os filmes NFC-SA e NFC-LBL. O revestimento com SA tornou os filmes hidrofóbicos, uma vez que o ângulo de contato estático medido atingiu os 122º. Os filmes NFC-LBL sem tratamento térmico atingiram um ângulo de contato de até 150º e uma histerese do ângulo de contato de 3,1º. Os filmes NFC-LBL tratados a 68ºC exibiram q*uasi* superhidrofobicidade, com um ângulo de contato de até 140º e uma histerese do ângulo de contato de 5º. O revestimento dos filmes NFC-LBL sem tratamento térmico era facilmente eliminado por fricção, mas o tratamento térmico permitiu a permanência do revestimento e persistência da hidrofobicidade, resistindo à fricção e manuseamento dos filmes.

Tendo em conta que a produção de filmes de NFC por filtração é um processo lento, com base nos estudos anteriores da reologia decidiu-se estudar o efeito da adição de etanol à suspensão sobre o tempo de drenagem durante a produção de filmes de NFC por filtração a vácuo e nas propriedades mecânicas, óticas e de barreira dos filmes resultantes. Para isso, suspensões aquosas / alcoólicas de NFC com teor de etanol até 75% em peso foram utilizadas na produção dos filmes, monitorizando a progressão da

drenagem por meio da medição do filtrado coletado. Os filmes foram secos ao ar em condições padrão de temperatura e humidade ou em estufa a 70ºC por 4 horas. O desempenho mecânico e ótico, e as propriedades de barreira ao vapor de água foram testados.

Os resultados mostraram que o tempo de filtração diminuiu drasticamente com o aumento do teor de etanol, de cerca de 2 horas para 2 minutos para suspensões de etanol com 0 (zero) e 75% em peso, respetivamente. O aumento do teor de etanol não afetou significativamente o desempenho mecânico dos filmes secos ao ar, apesar do aumento da porosidade global das estruturas. Por outro lado, a secagem em estufa proporcionou aos filmes propriedades de tração superiores às exibidas pelos filmes secos ao ar ambos produzidos a partir de suspensões puramente aquosas, apesar do aumento do alongamento à rotura e do maior valor do coeficiente específico de dispersão de luz. A taxa de transmissão de vapor de água aumentou para filmes produzidos a partir de suspensões com 75% de etanol e foi ainda maior para filmes secos em estufa. A combinação da secagem dos filmes em estufa e da produção do filme a partir de uma suspensão alcoólica/aquosa proporcionou a oportunidade de manipular a transparência do filme e a taxa de transmissão do vapor de água, preservando o desempenho mecânico dos filmes. Em resumo, com este estudo, foi possível desenvolver um método relativamente rápido e simples para produzir filmes de NFC com propriedades mecânicas e de barreira com potencial para diversas aplicações, tais como membranas, onde a resistência mecânica, tenacidade, baixa densidade, permeabilidade e porosidade controladas e elevada área específica são importantes, células de combustível, purificação e filtragem de líquidos, engenharia de tecidos, imobilização e separação de proteínas e roupas de proteção.

Em suma, a investigação levada a cabo ao longo deste trabalho permitiu comprovar o grande potencial das fibrilas celulósicas em numerosas aplicações, principalmente no fabrico de filmes. Relativamente à calandragem, o presente trabalho demonstrou que esta é uma operação unitária altamente eficaz na melhoria das propriedades barreira ao vapor de água de filmes de fibrilas celulósicas. No que diz respeito à produção de filmes por filtração a vácuo a partir de suspensões de celulose altamente fibrilada, a dificuldade mais reportada por variados autores referenciados na literatura é o facto de este ser um processo extremamente lento, tornando a produção de filmes de NFC impraticável ao nível industrial. O presente trabalho apresenta desenvolvimentos importantes relativamente a este aspeto, sugerindo uma simples modificação do meio puramente aquoso das suspensões, para um meio com mistura água/etanol. Esta técnica, além de reduzir drasticamente o tempo de formação do filme e usar um

solvente fácil e rapidamente removido por evaporação, preserva as propriedades mecânicas dos filmes produzidos. Outro aspeto que complica a aplicação da NFC em várias áreas e, consequentemente, dos filmes feitos a partir de NFC, é a sua natureza hidrofílica. O presente trabalho desenvolveu métodos de produção de filmes de NFC com propriedades fortemente hidrofóbicas, resistentes ao manuseamento e fricção, aplicando revestimentos superficiais de ácido esteárico e carbonato de cálcio precipitado, combinados com tratamento térmico, numa técnica não prejudicial ao meio ambiente e possivelmente aplicável à escala industrial.

Palavras-chave

Celulose nanofibrilada; celulose bacteriana; suspensões aquosas/ alcoólicas; tempo de drenagem; morfologia; reologia; filamentos; filmes; performance mecânica; propriedades óticas; propriedades de barreira.

Index

Figure list

Table list

Acronym list

AGU	Anhydroglucose units
ARCA	Advancing and receding contact angles
BC	Bacterial cellulose
CA	Contact angle
CED	Cupriethylenediamine
CNC	Cellulose nanocrystals
CNF	Cellulose nanofibrils
CrI	Crystallinity index
DMA	N, N-dimethylacetamide
DP	Degree of polymerization
FE-SEM	Field emission scanning electron microscopy
FTIR	Fourier transform infrared spectroscopy
HC	Hard calender
LBL	Layer-by-layer
MFC	Microfibrillated cellulose
NCC	Nanocrystalline cellulose
NFC	Nanofibrillated cellulose
NMMO	N-methyl morpholine-N-oxide
NREL	National Renewable Energy Laboratory
PCC	Precipitated calcium carbonate
PDADMAC	Poly(diallyldimethylammonium chloride)
PLA	Polylactic acid
PVA	Poly(vinyl alcohol)
OP	Oxygen permeability
OTR	Oxygen transmission rate
SA	Stearic acid
SEM	Scanning electron microscopy
TEM	Transmission electron microscopy
TEMPO	2,2,6,6-tetramethylpiperidine-1-oxyl
VC	Vegetal cellulose
XRD	X-ray diffraction
WVTR	Water vapor transfer rate
WVP	Water vapor permeability

Chapter 1 - Introduction

In recent decades, natural fibrous materials, namely cellulose nanofibrils, have received increasing attention due to their potential to produce filaments and films with high mechanical performance, respecting environmental and social requirements. These structures represent the building blocks for biomaterials with low environmental impact, low production cost, high mechanical performance and susceptible to nanoscale functionalization. On the other hand, drawbacks that impair their application in several fields, such as the difficult control over fibril alignment, the extremely long time necessary to films formation from cellulosic nanofibril suspensions and the intrinsic hydrophilic nature of cellulose nanofibrils represent a challenge.

In this context, the aim of the present work focuses on the manufacture of filaments and films from native cellulosic fibrils (not resorting to the solubilization of cellulose macromolecules) searching for alternative and effective techniques of increasing the orientation of the nanofibrils in filaments, speed up the production of films and hydrophobicity improvement, while retaining the mechanical properties of the structures, using simple, scalable, and environmentally friendly processes.

The main specific objectives of the present work are summarized below.

Concerning the rheological behavior of nanofibrillated cellulose (NFC) suspensions, the objective of the present work was to study the effects of organic solvents addition (namely ethanol or acetone) to the NFC suspensions aqueous medium and also the effect of high ionic strength on the rheological response of two chemically and morphologically different NFC suspensions.

Delving into structures produced from native cellulose fibrils, and regarding the production of filaments, the objective was to investigate the influence of solid content and operating conditions on the mechanical performance of filaments produced from aqueous NFC suspensions, through a wet spinning technique. Regarding the production of films, this work aimed to explore the influence of ozonation on bacterial cellulose and the effect of a hot-calendering operation on the mechanical, optical–structural, and water vapor barrier properties of films produced from bacterial cellulose, using a process similar to papermaking and vegetal cellulose fibers as reference.

It was also an objective of this work to produce NFC films through vacuum filtration of NFC aqueous suspensions and study their hydrophobicity improvement through surface coating with either stearic acid alone or a layer-by-layer assembly of stearic acid and modified precipitated calcium carbonate coatings, combined with heat treatments.

Finally, the present work had the objective of investigating the effect of NFC aqueous/ethanol suspensions composition on the drainage time during NFC films formation through vacuum filtration and its impact on mechanical performance, as well as on the water vapor barrier properties of the resulting films.

Hereupon, this work is organized in five chapters according to the following structure: *Chapter 1 – Introduction*, establishes the framework and justification for this work, clarifying the global and specific objectives; *Chapter 2 – State of the art*, provides a contextualization for this work's theme and gives an overview on the most important contributions found in the literature; *Chapter 3 - Publications and other developed investigation*, contains the papers published in the course of the developed work as well as other research contributions regarding the objectives of the work; *Chapter 4 - General conclusions and future perspectives*, summarizes the main conclusions of the undertaken investigation and the challenges that have yet to be faced and issues that need improvement; finally, *Chapter 5 – References*, lists the accessed literature referenced throughout the text.

Chapter 2 – State of the art

2.1. Cellulose

Since the beginning of mankind, there has been a continuous search for renewable natural resources that could be somehow useful. For many decades now, we have been exploring nature to find them. The best example of such a resource is cellulose. Cellulose is the most abundant, renewable, and sustainable biopolymer on earth (Prabhu and Li, 2015; Rojas *et al.* 2015). The annual biomass production of cellulose is around $1.5x10^{12}$ tons, as it is considered an almost inexhaustible source of raw materials that can fulfill the increasing demand, due to its large-scale bioavailability (Poletto and Pistor 2013; Prabhu and Li 2015).

Apart from its availability, cellulose has many desirable characteristics that make it a suitable material for several applications and in a vast array of fields. It is a colorless, odorless, and nontoxic solid polymer with a good biodegradability and biocompatibility. It is also highly rigid, with great mechanical strength, crystalline, insoluble in common organic solvents, hydrophilic, with an alterable optical appearance and it is relatively inexpensive (Prabhu and Li, 2015; Tayeb *et al.* 2018).

2.2. Structure of cellulose

The empirical formula of the cellulose polymer is $(C_6H_{10}O_5)_n$, where n is the degree of polymerization, which can vary between 10 000 and 15 000, depending on the cellulose's source material. Although cellulose may be originated through several ways, this molecule is common to all types of cellulose, regardless of their origin. Cellulose is a long chain polymer, and its repetition unit is called cellobiose which consists of two anhydroglucose units (AGU) joined by the β-1,4 glycosidic bond, shown in Figure 1.1 (Eichhorn *et. al.*, 2010; Chinga-Carrasco 2011; Poletto and Pistor 2013).

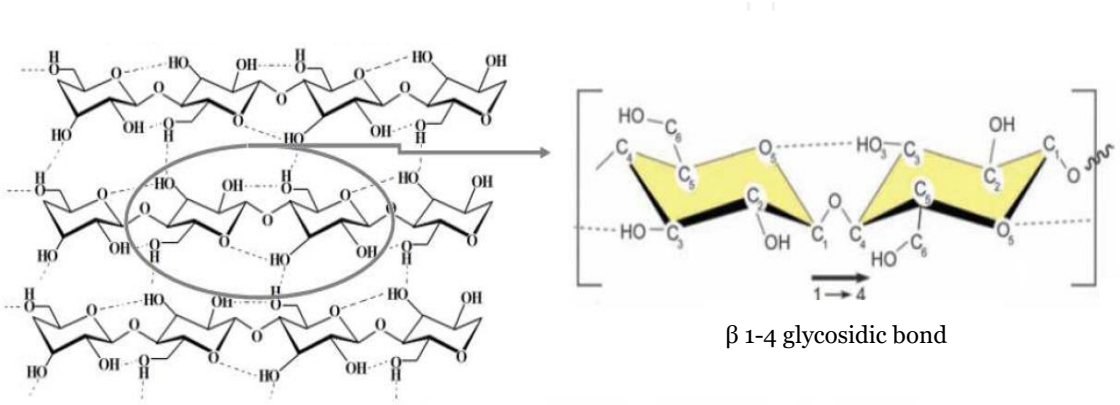

Figure 1. Molecular structure of a cellulose unit, showing the intrachain hydrogen bonding (dotted lines) and the β 1-4 glycosidic bond (Adapted from Poletto and Pistor 2013)

Each AGU bears three hydroxyl groups that have the ability to form strong hydrogen bonds. The intrachain hydrogen bonding (figure 1) between hydroxyl groups and oxygens of the adjoining ring molecules stabilizes the linkage and results in the linear configuration of the cellulose chain (Moon *et al.* 2011).

The cellulose chains are organized in a supramolecular structure, generating the elementary fibrils, where the cellulose chains are arranged in highly ordered structures, which are dubbed crystalline regions, and disordered regions, also known as amorphous regions. The ratio between amorphous and crystalline structures in cellulose differs according to its source of production (O'sullivan 1997; Eichhorn *et. al.* 2010; Chinga-Carrasco 2011).

There are four types of cellulose polymorphs which can be the result of wide variation of molecular orientation and hydrogen bonding network in the crystalline region. They are cellulose I, II, III, and IV. Cellulose I, native cellulose, is the form found in nature, and it occurs in two allomorphs, Iα and Iβ. Cellulose II, which is the most stable crystalline form, is the regenerated cellulose that emerges after re-crystallization or mercerization with aqueous sodium hydroxide. These two forms of cellulose differ essentially in the layout of their atoms (parallel and antiparallel packing for cellulose I and II, respectively). Finally, celluloses III and IV are obtained though the modification of the previously mentioned ones (Siqueira *et al.* 2010; Mahmud *et al.* 2019; Zugenmaier 2021).

2.3. Sources of cellulose

Cellulose can either be produced by tunicates, synthesized by bacteria under specific culture conditions, or it can be obtained from plants (Eichhorn *et. al.*, 2010).

2.3.1. Cellulose from Tunicates

Although cellulose can also be produced from the cell walls of certain algae and bacteria (Habibi *et al.* 2010), tunicates, members of the subphylum Urochordata, are a group of about 1250 species of marine animals and are the only known animals that can be a source of cellulose (Hirose 2009; Raven *et al.* 2011). An example of a tunicate is depicted in figure 1.2.

The name of these ocean animals is derived from their unique integumentary tissue called the ‘tunic’, which covers the entire epidermis of the animal (figure 2). The tunic has several biological functions, such as phagocytosis, impulse conduction, tunic contractility, bioluminescence, photosynthetic symbiosis and allorecognition (Hirose 2009). Cellulose is synthesized through cellulose-synthesizing enzyme complexes found in the plasma membrane of tunicates’ epidermal cells (Kimura and Itoh 2007).

In order to produce and use the cellulose from tunicates, further treatments must be performed so as to isolate and purify the cellulose obtained from the tunic, such as mechanical fragmentation, hydrolysis, kraft cooking and bleaching, since it has been reported to contain

approximately 60 wt.% cellulose and 27 wt.% nitrogen-containing components, among other minor compounds (Zhao and Li 2014; Dunlop *et al.* 2018).

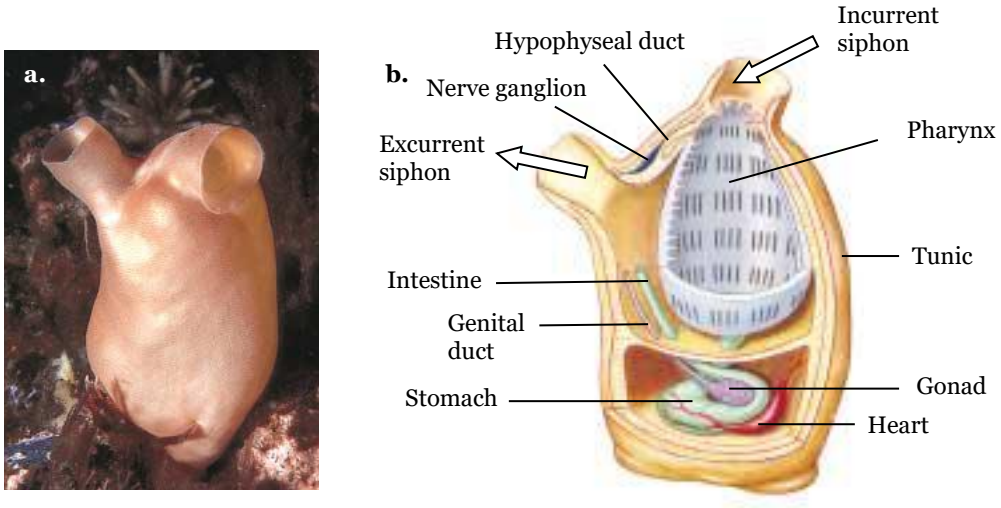

Figure 2. Halocynthia auranthium, a tunicate also known as the sea peach (a); Diagram of the structure of an adult tunicate (b) (Adapted from Raven *et al.* 2011)

2.3.2. Bacterial cellulose

Bacterial cellulose is often called nanocellulose, because unlike the cellulosic material prepared from vegetal sources, this material has a width strictly in the nanoscale. These cellulose nanofibers are secreted extracellularly into an aqueous culture medium by specific Gram-negative bacterial cultures, mainly by *Gluconacetobacter* genus (figure 3) (Klemm *et al.* 2011).

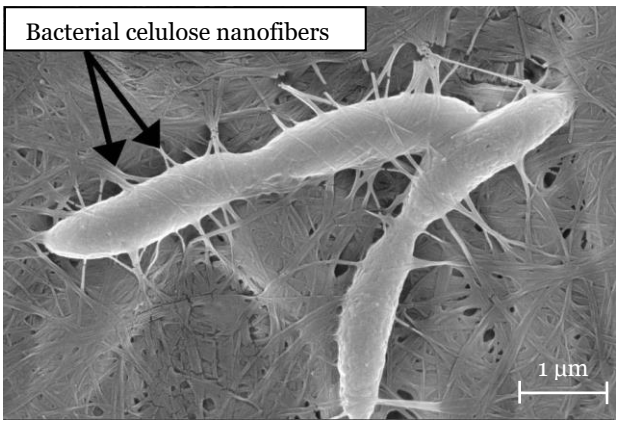

Figure 3. Gluconacetobacter bacteria forming cellulose nanofibers. Secreted nanofibers are marked with arrows (Adapted from Virginia Tech, 2008)

Bacterial cellulose consists of purely randomly assembled, <100 nm wide ribbon-shaped cellulose fibrils, composed of 7 to 8 nm-wide elementary nanofibrils aggregated in bundles. It exhibits a combination of exclusive properties, such as flexibility, high hydrophilicity and water holding capacity, high crystallinity and mouldability of the tridimensional network into different shapes (Gorgieva and Trček, 2019).

Although this gel-like material has a typical solid content of around one percent, it is composed of pure cellulose containing no lignin or other extraneous substances, making its isolation and purification a relatively simple process, not requiring energy or chemical intensive treatments. Furthermore, its unique fibrillar nanostructure provides it with excellent physical and mechanical properties such as high tensile strength and high elastic modulus (Iguchi *et al.* 2000; Svensson *et al.* 2005; Siró & Plackett, 2010; Keshk 2014). Furthermore, the biocompatibility of bacterial cellulose makes it suitable for many biomedical applications (Wasim, 2020).

2.3.3. Vegetal cellulose

Vegetal cellulose is present in plants and algae. The biggest source of vegetal cellulose is the cell wall of wood fibers along with other constituents such as hemicelluloses and lignin. Figure 4 presents an overview of the general hierarchical structure of a tree.

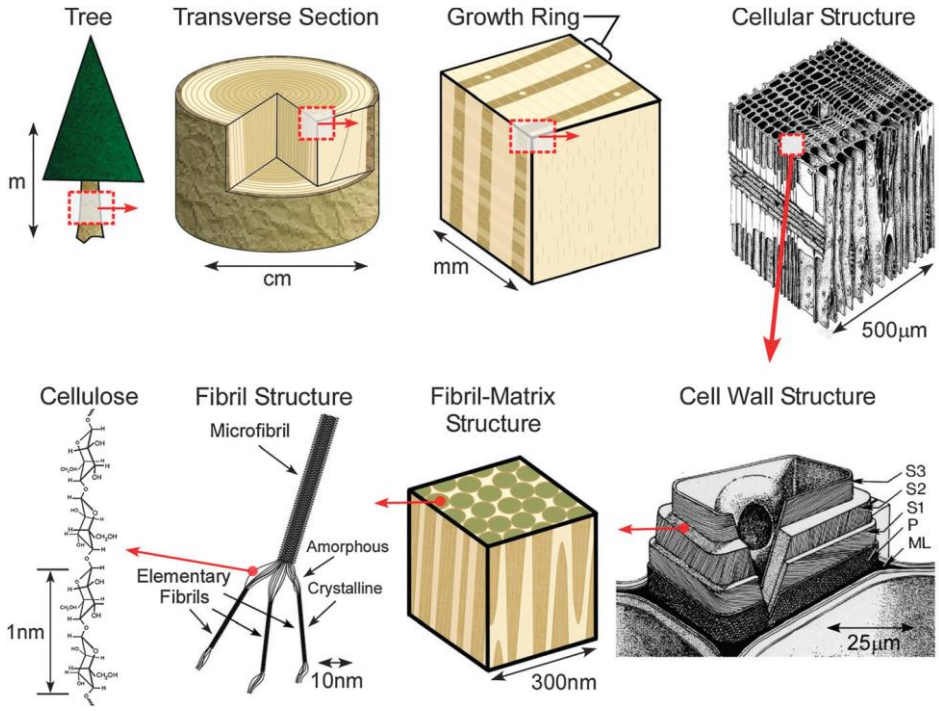

Figure 4. Hierarchical structure of a tree (Adapted from Postek *et al.* 2011)

The fibers are composed by a primary wall (P in figure 4) and a secondary wall which is built by three layers (S1, S2 and S3 in figure 4) (Fengel and Wegener, 1984). Of these, the secondary layer S2 of the wall stands out because it is thicker and because its macrofibrillar structures are better oriented and with an alignment closer to the fiber axis (Chinga-Carrasco 2011).

The space between fibers is called the middle lamella (ML in figure 4) and is filled with a lignin matrix. The walls are composed of cellulose macrofibrils with diameters between 8 and 60 nanometers and these, in turn, are made up of microfibrils, which are composed of elementary fibrils: during cellulose biosynthesis, van der Waals bonds and intermolecular hydrogen bonds

between hydroxyl groups and oxygens of adjacent molecules (figure 1) promote a parallel assembling of multiple cellulose chains forming elementary fibrils, measuring 2–20 nm in diameter and about a few micrometers in length, which are the basic structural units. According to Habibi *et al.* (2010), around 36 individual cellulose molecules are assembled together into elementary fibrils, which in turn are packed into larger units called macrofibrils (Moon *et al.* 2011; González *et. al.*, 2012; Rojas *et al.* 2015).

The organization and orientation of the fibrils in the different layers of the fiber provides them with different mechanical strengths, which are important in several applications (Chinga-Carrasco 2011).

Depending on the origin of the cellulose, the fibers might have different characteristics: this has to do with their dimensions and the composition and structure of the cell wall, as well as its percentage of cellulose, hemicellulose and lignin. The percentages of these last three constituents differ depending on whether the raw material comes from leaved trees (hardwood), from coniferous trees (softwood), shrubs or other plant sources (Isogai *et al.* 2011; Bacakova *et al.* 2019).

In the case of woody plants such as pine (softwood) and eucalyptus (hardwood), with kraft cooking and pulp bleaching, more than half of the hemicelluloses and almost all of the lignin can be removed by dissolution. Although cellulose might be partially degraded by these processes, it does not dissolve. The content of hemicelluloses in the resulting pulp is an important feature: if, on the one hand, hemicelluloses enable the absorption of water or reagents because they are very hydrophilic, on the other hand, they hinder the access of these same compounds since they produce more compact pulps. In short, they are chemically favorable and physically unfavorable to water absorption. As for lignin, if it is not removed it will also hinder the access of the reagents to the fiber. All these aspects influence the fibrillation capacity of the fibers, as well as the different methods of extraction of the fibrils (Duchesne *et. al.* 2001).

Other sources of cellulose such as agricultural crops and their by-products such as sugar beet, potato tuber, soybean, wheat straw, rice straw, rapeseed and corn fibers have been gaining increasing interest since, unlike woody species, they have shorter growing cycles and lower lignin contents, leading to easier delignification processes and thus making the mechanical fibrillation a less energy demanding process (Dufresne *et al.*, 1997; Dufresne *et al.*, 2000; Wang and Sain, 2007; Alemdar and Sain, 2008; Chaker *et al.*, 2014).

2.4. Cellulose dissolution

In order to shape and tailor cellulose-based materials according to design requirements and functionality, dissolution of cellulose might be a prerequisite. The relatively high length of the cellulose molecular chains and their dense and strong conformation through numerous

hydrogen bonds make cellulose dissolution a tough process to achieve. Therefore, the development of solvents for cellulose is essential for the successful use of cellulose as a component of polymeric materials (Wang *et al.*, 2016b).

Derivatization and direct dissolution of cellulose have been commonly performed, giving rise to regenerated cellulose (Olsson and Westman, 2012; Sayyed *et al.*, 2019). Dissolving pulp, a refined bleached pulp with a high cellulose content is commonly used to manufacture regenerated celluloses (Paunonen, 2013). Figure 5 shows the systematic classification of different cellulose regeneration processes.

Besides the production of regenerated cellulose by derivatization, other methods are available for direct processing of physically dissolved cellulose. The fundamental difference between the derivatizing processes and direct dissolution processes is that, in the later, cellulose directly dissolves in an organic solvent without the formation of an intermediate compound (Sayyed *et al.* 2019). Having unique structural and chemical features, native and regenerated cellulose can be assembled into several nanoscale configurations to meet the required design needs. Currently, cellulose-based structures such as fibers and thin films are developed according to the intended application (Wang *et al.*, 2017).

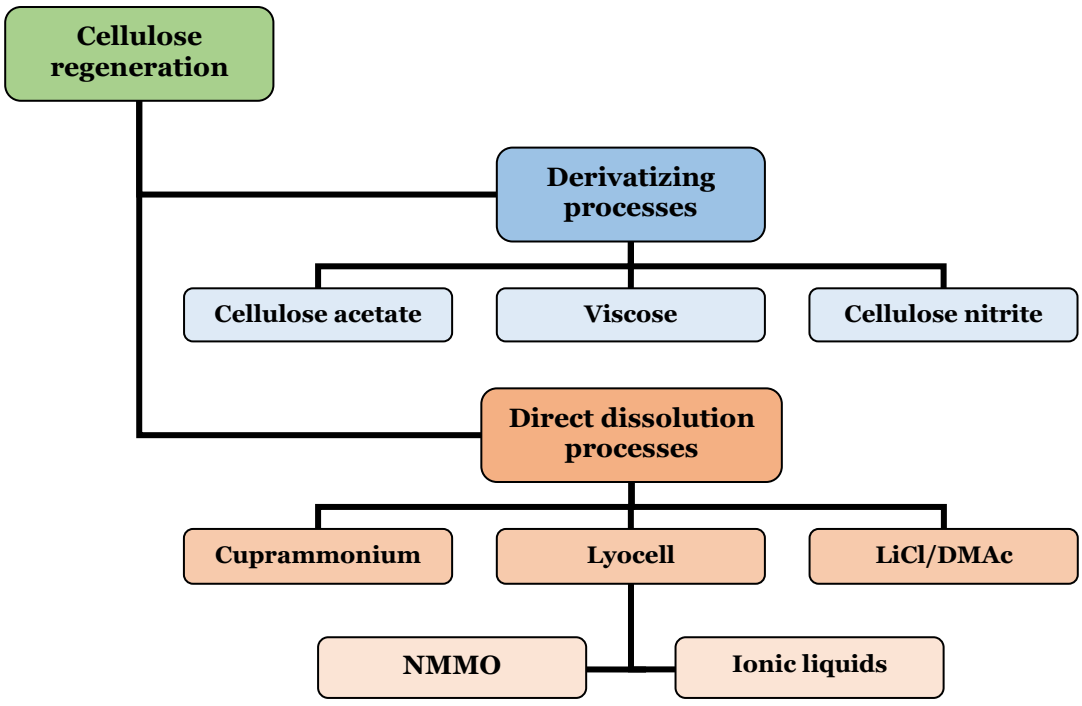

Figure 5. Systematic classification of cellulose regeneration processes (Adapted from Sayyed *et al.* 2019)

2.4.1. Cellulose-based fibers and films

One of the most common load-bearing architectures found in nature are fibers. This kind of building block can be found everywhere from plant cell walls to fibrous tissues of animals. Trying to mimic nature, mankind has attempted to manufacture continuous fibers from several materials and for a variety of applications, such as composites, filters or textiles, allowing a wide flexibility in the design and manufacture, controlling the orientation and the architecture of the fibers (Clemons, 2016).

Man-made fibers can be divided into the two categories: regenerated fibers and synthetic fibers. Synthetic fibers such as polyamides (commonly known as nylons), acrylics, polyesters, and polypropylene are produced from synthetic high molecular weight polymers obtained through the polymerization of the respective monomers (Singh and Bhalla 2017)

Polymeric fibers are essentially produced through spinning processes, which consist of forcibly passing a polymer solution or a polymer melt through a device containing small orifices known as the spinneret at a controlled rate. The holes from which the solution or melt is forced through are referred to as nozzles. Depending on the solidification or setting method, the process can be termed melt spinning (commonly referred to simply as extrusion or melt extrusion), dry spinning if a highly volatile solvent is used and the spun filaments are air dried in order to set, or wet spinning if the solvent has low volatility and the filaments need to go through solvent exchange in contact a liquid phase so as to coagulate (Chen *et al.* 2014; Imura *et al.,* 2014; Mount, 2017). The different spinning processes are depicted in Figure 6.

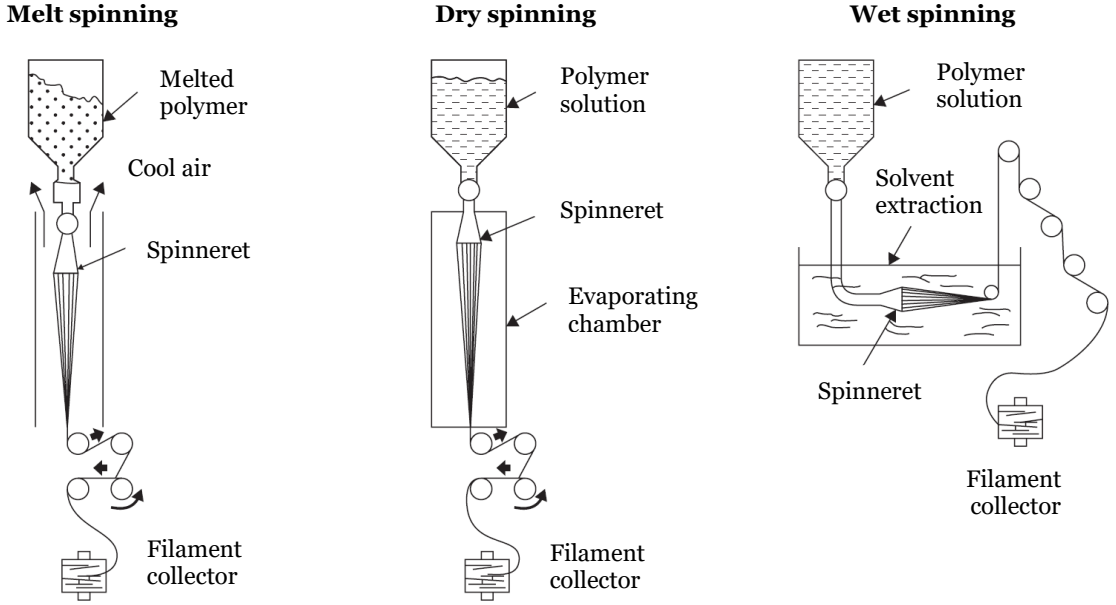

Figure 6. Schematic representation of melt, dry, and wet spinning processes (Adapted from Imura *et al.*, 2014)

Several authors have performed a subcategory spinning method dubbed dry jet-wet spinning (or simply dry wet spinning), in which the filament leaving the spinneret is stretched in an air gap before entering the regeneration bath. This process leads to high molecular orientation and improved mechanical performance of the spun fibers (Kim *et al.,* 2005a; Hauru *et al.* 2014).

Although synthetic fibers have a low production cost and high production rate and are more durable and versatile than natural fibers, they are mostly non-biodegradable and the production process is hazardous for both human health and environment (Singh and Bhalla 2017).

Cellulose-based fibers appear as an alternative to overcome the limitations of synthetic fibers (Rose and Palkovits, 2011). However, as cellulose will decompose before melting, a melt extrusion process, commonly applied to synthetic polymers, would not be effective for shaping the original material in the form of filament. Thus, derivatization aided dissolution and direct dissolution of cellulose have been performed as an alternative to melting cellulose and regenerate it into filaments (Olsson and Westman, 2012; Sayyed *et al.*, 2019).

Due to the complex hydrogen bonding network and dense packing, cellulose exhibits a low solubility in most common solvents. The derivatizing processes for producing fibers from cellulose come up as a solubilization strategy by chemically altering the cellulose into cellulose derivative precursors for subsequent dissolution (Rose and Palkovits, 2011; Olsson and Westman, 2012).

While the fibers result from spinning a solution into a coagulation bath through a spinneret, a film can be produced from the same material, extruding the solution through a narrow slit into a coagulation bath or air-dried in controlled conditions (Paunonen, 2013). Several fields such as food packaging, medicine and electronics demand flexible, robust, transparent and thermally stable films with good barrier properties, especially gas barrier properties in order to prevent deterioration of products. Like synthetic fibers, films made from petroleum-derived polymers meet these requirements besides having low manufacturing costs and being easily processed, hence they are extensively used. In recent years, however, increased environmental consciousness has promoted the exploration of biopolymers such as cellulose to produce cellulose based or cellulose composite films (Österberg *et al.*, 2013). Derived celluloses are more resistant to microbial attacks and enzymatic cleavage than the native ones. Cellulose is readily biodegraded by cellulase-using organisms but cellulose acetate, for instance, requires the presence of esterases for the first step of biodegradation, making it more resistant to those organisms. Modified forms of cellulose have been gaining much attention, mainly in food packaging, where mechanical and barrier properties are crucial to provide structural support to the product and increase its shelf life. The applications range of modified celluloses go from freestanding wrapping films to edible water-soluble films in direct contact with the food product (primary packaging), since modified cellulose can be tuned to have higher mechanical performance as well as oxygen, water, carbon dioxide, light, microbes, and grease barrier

properties, providing the food item with a superior shelf life. Traditional packaging that are not in direct contact with the food product, on the other hand, do not require the use of cellulose derivatives. For such purposes, ordinary native or regenerated cellulose-based materials will do (Puls *et al.*, 2011; Paunonen, 2013).

2.4.1.1. Cellulose acetate

Cellulose acetate is produced trough esterification by reacting cellulose pulp with acetic anhydride and acetic acid in the presence of sulfuric acid (Ertas and Uyar 2017). It is then subjected to a partial hydrolysis, removing the sulfate and introducing an appropriate number of acetate groups, according to the cellulose acetate's desired properties (Watabe *et al.*, 2018). The introduction of acetate substituents inhibits hydrogen bonding to a large extent. During the production of cellulose acetate fibers, the cellulose acetate solution is extruded through a spinneret and the solvent is subsequently evaporated in controlled conditions. The cellulose acetate dry-spun filaments usually have a round cross section but, depending on the evaporation rate and on the nozzle's shape, they can take on irregular cross section shapes (Chen *et al.* 2014; Yang *et al.*, 2019). In combination with appropriate plasticizers, cellulose acetate (as well as other cellulose esters such as cellulose butyrate or cellulose acetate-butyrate) can be processed like a common thermoplastic (Ganster and Fink, 2013). This material is widely used in food packaging industry as a rigid wrapping film (along with cellulose diacetate and triacetate, according to the degree of substitution) and it has also been used in other fields such as membranes. Commercial freestanding cellulose acetate films are optically clear, printable and adequate for mixing with appropriate additives, rendering industrially desired features, such as antioxidant or antimicrobial properties (Paunonen, 2013).

2.4.1.2. Viscose and Cellophane

Viscose fibers are frequently dubbed viscose rayon as a generic term. The basic fiber forming process starts with wood pulp and removal of noncellulosic components (dissolving pulps are often used as a raw material) and involves the cellulose regeneration from a cellulose xanthate which is a derivative of cellulose and carbon disulfide (Paunonen, 2013; Vecchiato *et al.,* 2017).

The viscose process is characterized by its high versatility because the modification of process parameters in either one or more steps of the process can give rise to wide variety of viscose fibers with varying characteristics. Many modifications can be introduced from varying the initial's pulp degree of polymerization, to adding salts to the cellulose solution or controlling the operating conditions on the coagulation bath, to stretching during the fibers processing. Thus, the operating conditions must be carefully controlled and closely monitored in order to produce fibers with the desired end quality and properties such as fiber length, cross-sectional shape and coarseness (Bredereck and Hermanutz, 2008; Vecchiato *et al.,* 2017). An outline of the viscose dissolution process is shown in figure 7.

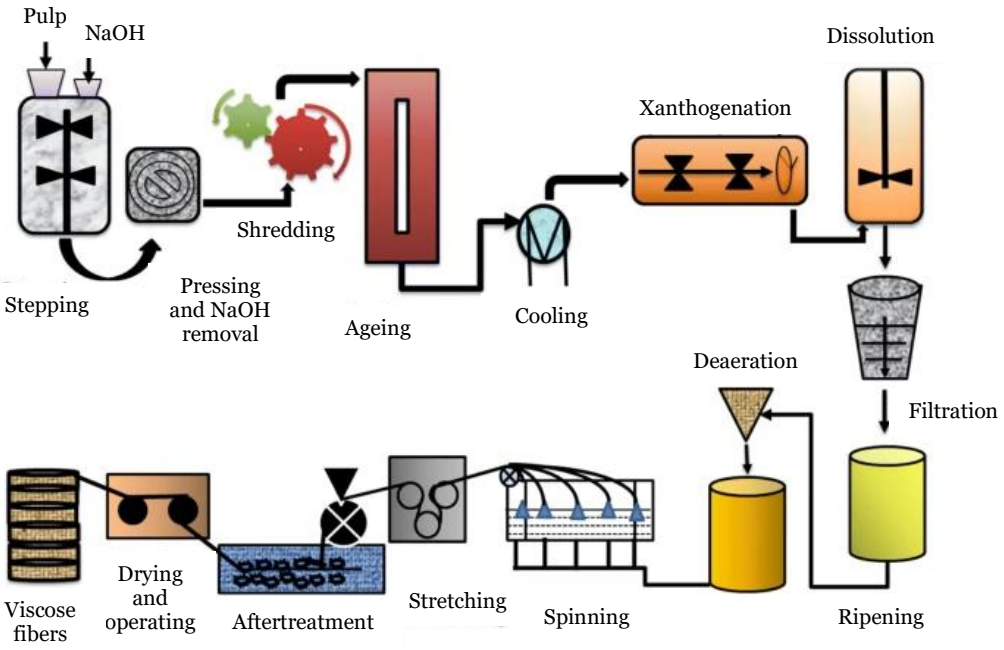

Figure 7. General scneme oı a viscose process (Adapted from Sayyed *et al.* 2019)

In a first stage, cellulosic pulp is treated with NaOH (steeping stage on figure 7) thus swelling and changing the crystalline structure of the native cellulose (a phenomenon known as mercerization) increasing its reactivity and enabling the penetration of carbon disulfide for the derivatization process. After steeping, the pulp is pressed and excess NaOH is as much removed as it is possible in order to avoid any side reactions with carbon disulfide (which would lead to by-products formation). The excess NaOH is usually recovered and returned to the process for reuse. The alkali pressed cake is then shredded to crumbles to ensure uniform distribution of the NaOH and ease the penetration of the derivatization reagents. At this point the shredded material is aged under heat to promote oxidative depolymerization and reduction of molecular weight, followed by the derivatization of the cellulose (xantogenation in figure 7), where a reaction with carbon disulfide takes place, giving rise to cellulose xanthate. The xantogenation step is very prone to by-products formation that cause a yellowing of the viscose, especially at higher temperatures: a compromise between reaction temperature and time must be achieved at this point. The cellulose xanthate is dissolved in dilute NaOH under high shearing. Before spinning, the solution is filtered and aged (ripening in figure 7) to guarantee a more even distribution of the substituent groups from the C2 and C3 positions of the anhydroglucose units to the position C6. Deaeration is usually performed at this point to remove any dispersed gases that might cause bubbles to form as the viscose filaments are extruded. Sulfuric acid is commonly used to regenerate the cellulose from the coagulated viscose. The stretching of the fibers is maximized by controlling the rates of coagulation and regeneration rates, thus orienting, and aligning the cellulose molecules along the fiber axis to get the best mechanical properties. (Wilkes, 2001; Bredereck and Hermanutz, 2008; Sayyed *et al.*, 2019).

Viscose can yet be chemically modified by adding chemical compounds to the solutions or to the coagulation bath and the cross-sectional shape of the fibers can be differently shaped by varying the spinneret design (Bredereck and Hermanutz, 2008).

While the fibers resulting from spinning a viscose solution are referred to as viscose fibers, cellophane is the result of extruding the same viscose solution through a narrow slit into an acid bath, thus it is the film form of a viscose process. Commercial cellophane films are versatile, clear and transparent and are susceptible of chemical surface modification (Paunonen, 2013).

2.4.1.3. Cuprammonium rayon

Another commercial regenerated fiber is cuprammonium rayon, which is made from cellulose dissolved in a cuprammonium solution. Amongst the commercial regenerated cellulose-based fibers, cuprammonium rayon is perhaps the one that most resembles silk fibers, being very thin, smooth, and glassy in appearance, for which reason it replaces natural silk, and it is frequently referred to as artificial silk (Kamide and Nishiyama, 2001; Rana *et al.,* 2014; Sayyed *et al.*, 2019).

In this process, cellulose is dissolved in an aqueous cuprammonium hydroxide solution and is wet spun through a capillary into a dilute acid, ethanol, or concentrated cresol bath. At this point, cellulose precipitates immediately, giving rise to solid filaments, as copper and ammonium are removed into the spinning bath. The produced filaments are subsequently stretched in dilute hydrochloric acid. The remaining copper and ammonium present in the filaments are chemically reacted to form copper and ammonium chloride, which are easily dissolved and removed from the filaments (Kamide and Nishiyama, 2001).

Although cuprammonium rayon is widely used, the process is expensive and environmentally harmful due the release of copper in the waste stream and the use of wasteful auxiliary hazardous chemicals, reason why its manufacture is illegal in the United States (Kamide and Nishiyama, 2001).

2.4.1.4. Lyocell

Although many solvents can be used to directly dissolve cellulose, so far, the most successful cellulose direct solvents are the N-methyl morpholine-N-oxide (NMMO) and ionic liquids, representing a significant and growing industry for producing textile fibers under the generic name Lyocell (Chavan and Patra, 2004; Jiang *et al.,* 2020).

Direct dissolution of cellulose in NMMO was developed as replacement of other polluting processes such as the viscose process, since this aqueous solvent is non-toxic and can easily be recovered and recycled into the process, which is commonly performed since this reagent is also very expensive. This process has been widely used industrially as several companies differently branded fibers produced from this technology: Tencel (Lenzing); Alceru (TITK Rudolstadt);

Newell (Akzo Nobel); Acelon (Greencell) and Excel (Grasim) (Bredereck and Hermanutz, 2008; Sayyed *et al.* 2019; Jiang *et al.,* 2020). A general scheme of the Lyocell process is shown in figure 8.

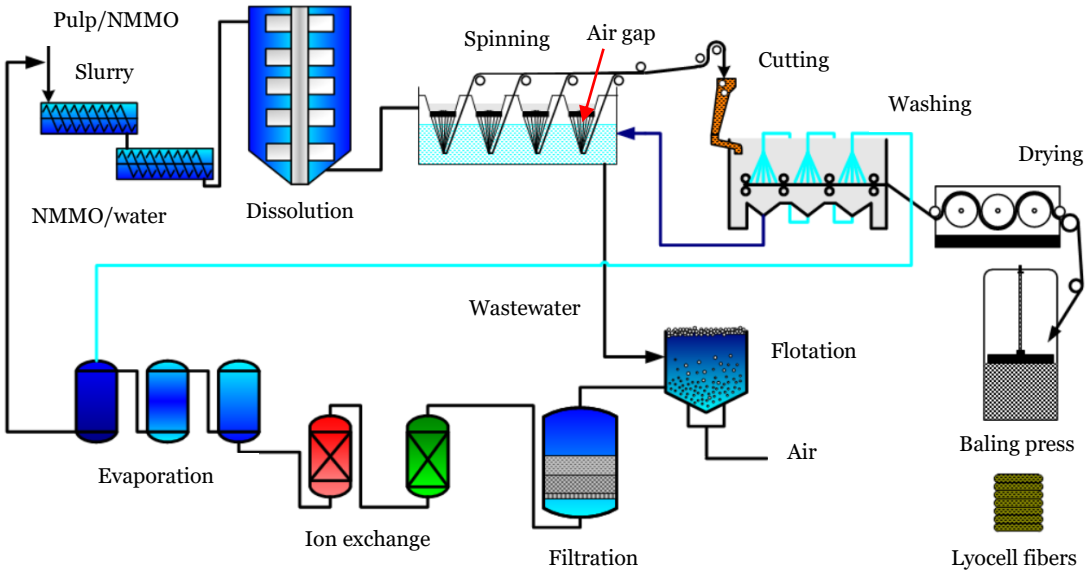

Figure 8. General scheme of a Lyocell NMMO process (Adapted from Sixta, 2016)

The process of dissolving cellulose in NMMO involves cellulose swelling, during which the solvent molecules (NMMO and water) penetrate the inter- and intra-crystalline regions of the cellulose structure and bulge the pulp fibers to a certain extent. Due to the high polarity of the N—O bond, NMMO has an extremely high dissolving capacity in water and is prone to hydrogen bonding with the cellulose, leading to the cleavage of intermolecular hydrogen bonds of cellulose chains. The entire crystalline structure of cellulose is destroyed, giving rise to a homogeneous solution (Chaudemanche and Navard, 2011; Medronho and Lindman, 2014; Sayyed *et al.*, 2019).

As simple as it may appear, the cellulose dissolution in NMMO is actually a rather troublesome process: while cellulose very rapidly dissolves in high-concentration NMMO aqueous solution, the resultant solution can be heterogeneous, therefore a low-concentration NMMO aqueous solution must be used. Furthermore, high water concentration favors swelling of cellulose molecules before dissolution, resulting in a homogeneous spinning dope. The difficulties in cellulose dissolution can be attributed to the cellulose narrow solubility region, the accurate control of water content solution and the occurrence of thermal decomposition of NMMO during preparation of the spinning solutions at 90-110°C and exothermic decomposition at 130°C (Perepelkin 2007; Jiang *et al.,* 2020).

The cellulose solution goes through a dry jet-wet spinning process, where the spun filaments leaving the spinneret are pulled in the air gap (enduring extensional stress) and regenerated in aqueous NMMO coagulation bath (figure 8). The air gap length, along with the spinning rate, are critical factors for the molecular orientation of the lyocell fibers. This oriented assembly is fixed once the spun filaments enter the coagulation bath (Sixta, 2016; Jiang *et al.,* 2020).

Lyocell fibers and viscose fibers differ in structure and morphology. Lyocell fibers are less flexible than those obtained from the previously described viscose process due to the high orientation achieved during stretching in the air gap. Lyocell fibers have a unique property profile though, including high strength, good dyeability and tendency to wet fibrillation: a phenomenon characterized by splitting along the fiber axis under the action of swelling, mechanics and friction, always in the wet state, which can have many industrially desirable purposes (Bredereck and Hermanutz, 2008; Zhang *et al.*, 2018; Jiang *et al.,* 2020).

Concerning ionic liquids, they have been used either to dissolve the cellulose or to create an appropriate media for its functionalization. While ionic liquids are usually composed of imidazolium, pyridinium, or organic ammonium cations and anions, the first one displays the best performance (Swatloski *et al.* 2002).

Unlike dissolution in NMMO, ionic liquid-based lyocell process has not yet been commercialized due several processing difficulties: the presence of water in the ionic liquid has to be controlled since its presence decreases the solubility of cellulose, probably through competitive hydrogen-bonding (Swatloski *et al.* 2002); although cellulose solutions in imidazolium-based ionic liquids containing a chloride anion lead to spun fibers with high tenacity (Kosan *et al.*, 2008), the presence of the chloride anion limits their practical application in processing; some ionic liquids require high temperatures for cellulose dissolution, which on one hand possibly results in thermal decomposition and on the other hand ionic liquids show high temperature corrosion properties, potentially limiting industrial applications (Perissi *et al.*, 2006; Cao *et al.*, 2009); adding to this, ionic liquids are typically petroleum-derived, going against the desirable greener and environmentally friendly processes (Zhu *et al.*, 2009).

2.4.1.5. Electrospinning

Electrospinning has been recognized as an efficient technique for the production of polymer nanofibers (Huang *et al.*, 2003). This method uses an electrical driving force rather than a mechanical one (Frey, 2008). Figure 9 depicts the general scheme of an electrospinning process.

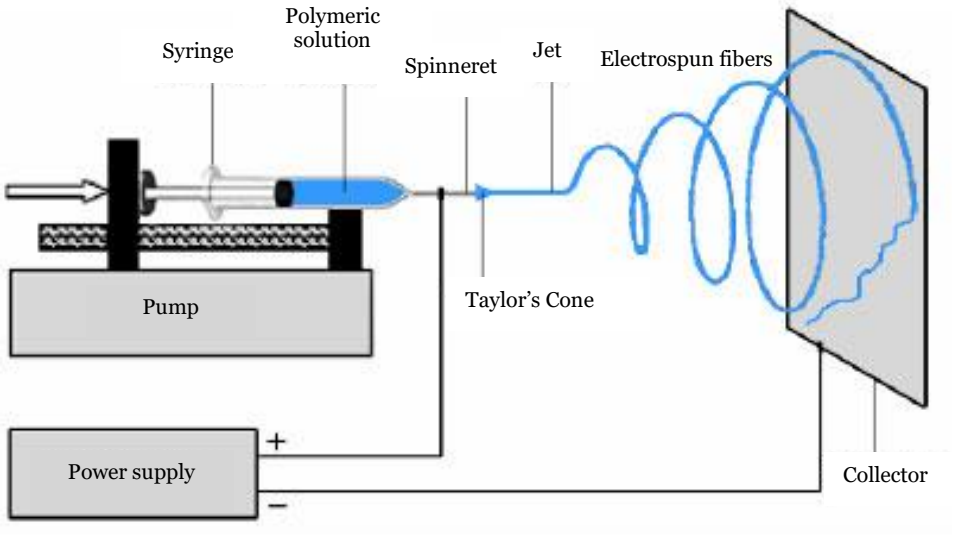

Figure 9. General scheme of an electrospinning process (Adapted from Ziabari *et al.,* 2009)

In electrospinning, a high voltage is applied to a droplet of polymer solution, creating a large electric field between the spinneret and a grounded electrode (collector). When the charge at the droplet's surface overcomes its surface tension, uniaxial elongation of the droplet takes place, forming the often-called Taylor's cone and a fine electrically charged jet is projected from it, traveling in a straight line for a few centimeters as it is drawn, substantially decreasing its diameter, before going through a directional instability (convective flow), in which the diameter continues to decrease along its trajectory. Finally, the jet is collected, solidifying in the form of nanofibers deposited on the collector's surface (figure 9) (Dersch *et al.*, 2003; Frey, 2008).

In order to manufacture fibers from polymer solutions through electrospinning, a volatile solvent is generally preferred, since solvent evaporation along the jet path is a requirement for gathering solid individualized fibers in the collector, although the fiber's fine diameters contribute to a rapid evaporation of the solvent. For this reason, electrospinning can be considered a particular case of dry spinning (Clemons, 2016).

The electrospinning operating conditions, such as the solution composition, degree of polymerization, applied voltage, collector type and distance to the spinneret, temperature, solvent evaporation rate, as well as post-spinning treatments, are known to affect the morphology of the spun fibers (Liu and Hsieh, 2002; Kim *et al.*, 2006). Furthermore, a good molecule alignment on the spun fibers is usually achieved though electrospinning, since the shear forces compelling the droplet to elongate into a jet, combined with rapid solvent evaporation and the extreme confinement in a very small diameter help induce molecular alignment (Dong *et al.*, 2012).

Several solvents suitable for either wet or dry spinning of cellulose and cellulose derivatives have likewise been considered as solvents for cellulose electrospinning. However, due to the low volatility of these solvents, an additional step is required to completely remove the solvent from the spun fibers. Cellulose acetate in acetone-containing solvents has been spun under a wide variety of operating conditions and subsequently deacetylated to form cellulose nanofibers (Liu and Hsieh, 2002; Tungprapa *et al.*, 2007; Han *et al.*, 2008; Konwarh *et al.*, 2013). Kim *et al.* (2005b, 2006) have performed electrospinning of cellulose directly dissolved in LiCl/DMA and NMMO into collectors at different temperatures, followed by coagulation baths in order to efficiently remove the solvents. The previously described approaches use organic solvents for electrospinning, which are toxic, expensive, or hard to remove from the nanofibers, limiting the application in growing field of research such as biomedicine. Recently, Zhang *et al.* (2020) have managed to produce water resistant electrospun nanosized cellulose fibers using a periodate oxidation—adipic acid dihydrazide crosslinking strategy, where the periodate oxidation of cellulose generated water-soluble aldehyde cellulose, thus avoiding unfavorable organic solvents in the electrospinning process.

2.5. Cellulose nanocrystals and nanofibrils

Nanocellulosic materials have generated great interest from the research community, governmental bodies, and the industry over several decades due to several important and exciting properties and the possibility of producing the materials from a multitude of sustainable resources (Naderi 2017). Depending on the applied pretreatments, two kinds of nanocellulosic materials can be extracted from vegetal sources, namely cellulose nanocrystals (CNC), also frequently called cellulose nanowhiskers or nanocrystalline cellulose, and cellulose nanofibrils (CNF) which, according to the nomenclature found in the literature, can also called nanofibrillated cellulose (NFC) or microfibrillated cellulose (MFC) (NFC and MFC terms can arguably be used either interchangeably or according the dimension range of the obtained fibrils (Sehaqui *et al.* 2011)). Figure 10 depicts CNC and NFC imaged through Transmission Electron Microscopy (TEM).

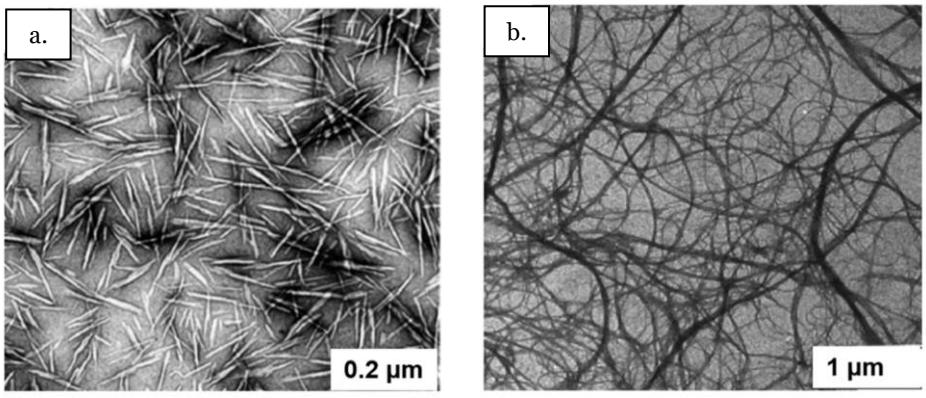

Figure 10. TEM images of a dried dispersion of cellulose nanocrystals (a) (Source Habibi *et al.*, 2008) and a dispersion of cellulose nanofibrils (Source Dufresne *et al.*, 1997)

CNC exhibits elongated crystalline rod-like shapes, as can be seen in figure 10 with a very limited flexibility compared to NFC (Brinchi *et al.*, 2013). While CNCs are usually obtained though chemical hydrolysis of the amorphous regions of cellulose, CNFs are obtained by subjecting cellulose to a series of mechanical, chemical or enzymatic processes, or a combination of these (Rol *et al.* 2019).

Concerning the particle size, CNCs are typically 100 to 250 nm long and their diameters range from 5 to 70 nm, while individualized NFCs have comparable diameters (5 to 60 nm) but their length can reach up to several micrometers (figure 10) (Klemm *et al.* 2011).

Figure 11 Shows examples of what NFC and CNC look like at the end of the obtention processes.

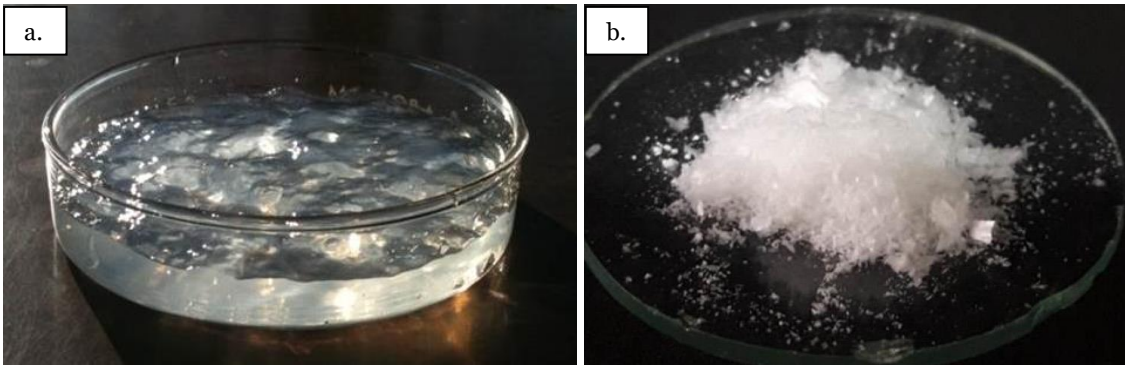

Figure 11. Appearance of an NFC aqueous suspension (a) (Source: Wise, 2014) and CNC powder (Source: Di Giorgio *et al.*, 2020)

While NFC is usually obtained as a translucent gel (figure 11 a.) with a solid content around 1 wt.%, whose transparency degree differs according to the carboxyl content and morphological features (Besbes *et al.*, 2011), CNC is obtained as a white dry powder through spray dry or lyophilization (figure 11 b.) or as a liquid suspension (Brinchi *et al.*, 2013; Di Giorgio *et al.*, 2020).

2.6. Nanofibrillated cellulose obtention

Cellulose fibers are currently being manufactured from several different cellulosic sources, being the lignocellulosic materials the most important industrial source of cellulosic fibers, and the main raw material used to produce NFC. Bleached kraft pulp is most often used as a starting material for NFC production, followed by bleached sulfite pulp (Klemm *et al.* 2011).

The interest in the use of NFC is mainly focused on taking advantage of the crystalline areas of this material, since they promote high hardness and resistance. It is for this reason that one seeks to break down the fibers through the amorphous zones until obtaining nanofibers with high crystallinity (Alila *et al.* 2013).

2.6.1. Mechanical treatments

Numerous mechanical treatments have been used to manufacture NFC, depending on the type of NFC that is desired or target dimension range of the fibrils.

2.6.1.1. Microfluidization

In the microfluidization process, the aqueous suspension is led through thin (in the range 200–400 μm) z-shaped chambers under high pressure (above 2000 bar). When the pressurized product enters the interaction chamber at high speed, the suspension is subjected to very high shear rates (up to 10^7 s^{-1}) due to collisions with the equipment walls and upon itself. Finally, the suspension leaves the chamber through a zone of low pressure, in the form of cellulose nanofibers and a heater exchanger returns it to ambient temperature (Aulin *et al.*, 2009; Siqueira *et al.,* 2010).

2.6.1.2. High-pressure homogenization

High-pressure homogenization consists of passing an aqueous cellulose fibers suspension with a solid content of 1 to 2 wt.%, in a high-pressure homogenizer. This equipment makes the fibers go through two stages where they are subjected to high pressures and collide against a valve that opens and closes in rapid succession, so the fibers are subjected to a large pressure drop under high shearing forces. This combination of forces promotes a high degree of fibrillation of the cellulose fibers (Nakagaito and Yano, 2004; Alcalá *et. al*., 2013; Kalia *et al*. 2013; Khalil *et al.,* 2014a).

In order to obtain a good degree of fibrillation, the fiber suspension must go through this process several times. The number of required passes easily runs to 10 (Taipale *et al*., 2010) and can even reach as high as 30 (Iwamoto *et al.,* 2005).

The final product is a homogeneous gel-like material where the nanocelluloses form a three-dimensional structure (González *et. al*., 2012; Nakagaito and Yano, 2004). Although this is an efficient method of defibrillation, due to the intense mechanical treatment that the fibers undergo in this process, they present a high degree of physical degradation. In fact, Benhamou *et al*. (2014) reported that the number of passes through the homogenizer has a visible effect on the crystallinity index of the NFC. The production of NFC through high-pressure homogenization requires a considerably high energy consumption because the degree of fibrillation that is achieved is directly proportional to the energy consumption (Chauhan and Chakrabarti, 2012). Furthermore, there is a high risk of clogging of the valve of the homogenizer, hence the pulp should undergo a pretreatment in order to ease the defibrillation process (Li *et al*. 2012).

2.6.1.3. Cryocrushing

The cryocrushing technique consists of freezing the cellulose fibers with liquid nitrogen, and then subject them to high shear forces applied through a pestle in order to break the cell walls of the fibers to release the microfibrils (Chakrabort *et al.* 2005). This process becomes more efficient if there is a previous refining of the fibers to promote their swelling and delamination (Hubbe *et al.*, 2008).

2.6.1.4. Grinding

The principle of this process consists of breaking down the cell wall structure due to the shearing forces generated between grinding stones: The pulp passes between static and rotating grindstones revolving at about 1500 rpm. The nanofibers that compose the cell wall become thus individualized. This manufacturing process does not differ much from that using a single- or double-disc refiner, except that the gap-clearance is narrower in this case, and that the rotor and stator are usually ceramic (Iwamoto *et al.*, 2007).

Unlike the high-pressure homogenization process, grinding apparently requires fewer passes to obtain NFC without requiring any fiber-shortening pretreatment. The grinding method is also clog-free and can grind aqueous fiber suspensions at higher solid contents (2-5 wt.%). However, this process can degrade the pulp fibers and significantly decrease their length, which might affect the reinforcement and physical properties of the final material (Iwamoto *et al.*, 2007; Osong *et al.* 2016).

2.6.2. Chemical treatments

Despite the mechanical treatments being useful and efficient processes because no additives are required, if a very intensive method is not used, mostly bundles of microfibrils are obtained, rather than individual microfibrils. On the other hand, chemical treatments can aid the disintegration of cellulose into individual microfibrils via modification of the surface properties (Iwamoto et al. 2009).

2.6.2.1. TEMPO mediated oxidation

Several chemical functionalities can be achieved by manipulating the reactive surface of the hydroxyl (–OH) groups of cellulosic fibers in order to attain different surface properties (Moon *et al.* 2011). Currently, introducing charged carboxylate groups through TEMPO-mediated oxidation (TEMPO = 2,2,6,6-tetramethylpiperidine-1-oxyl) is the more commonly used and most promising technique for achieving the surface modification of native cellulose fibers (Lavoine *et al.* 2012).

TEMPO mediated oxidation is expected to result in NFC systems with smaller and narrower particle size distributions when compared to an enzymatic pretreatment process, for instance

due to the high number of charges that originate electrostatic repulsion between the fibers, leading to an effective delamination in a later mechanical process (Tanaka *et al.*, 2012a).

TEMPO-mediated oxidation is usually carried out with a pH in the range of 9 to 11, at ambient temperature and atmospheric pressure, in the presence of NaBr as an additional catalyst and using NaClO as oxidant (TEMPO/NaBr/NaClO system) (Perez *et al.,* 2003; Isogai *et al.*, 2011). During the catalytic oxidation, either NaOH is added, or the reaction can be carried out in a buffer solution in order to maintain a constant pH (Xu *et al.* 2012). As the reaction occurs, the mixture turns into a yellowish color due to the release of free chlorine (Besbes *et al.,* 2011).

Figure 12 shows a scheme of TEMPO/NaBr/NaClO system oxidation in water under alkaline medium.

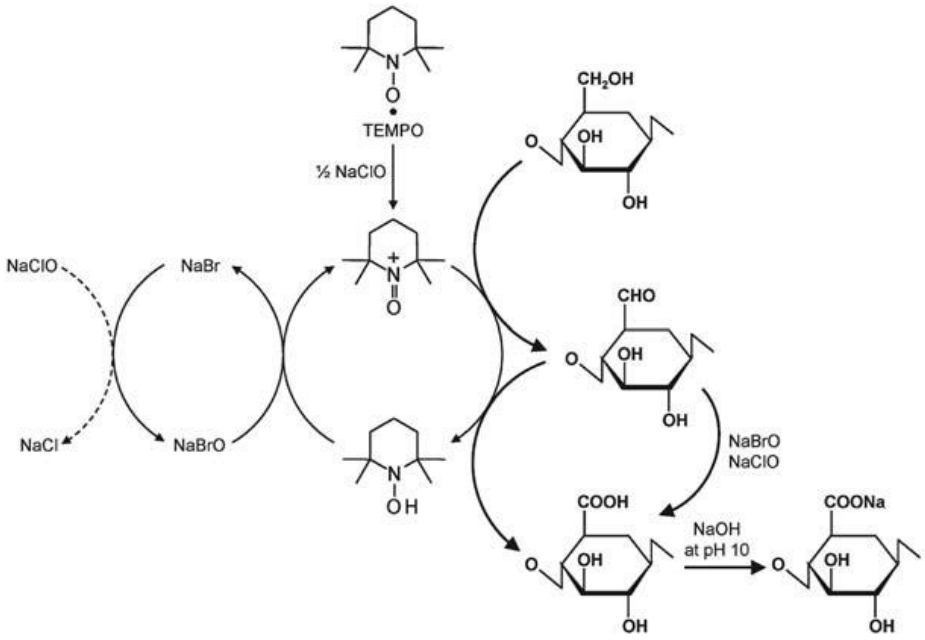

Figure 12. Selective oxidation of C6 primary hydroxyls of cellulose to C6 carboxylate groups by TEMPO/NaBr/NaClO system oxidation with alkaline conditions. (Adapted from Isogai *et al.* 2011)

This method promotes the selective oxidation of primary hydroxy groups at C6 of the cellulose molecules, introducing charged carboxylic and aldehyde functional groups under mild aqueous conditions (figure 12). Thus, strong electrostatic repulsions are created between the fibrils, facilitating their separation (Isogai *et al.* 2011).

Despite de oxidation effectiveness of the TEMPO/NaBr/NaClO system, under alkaline conditions, side reactions are inevitable, including a noteworthy depolymerization of cellulose (Saito and Isogai, 2004; Shibata and Isogai, 2003). As the cellulose degree of polymerization (DP) greatly impacts the strength, length, and flexibility of individual cellulose fibrils, it can also affect their properties and applications. Benhamou *et al.* (2014) also reported that while increasing the oxidation time facilitates the extraction procedure, it significantly degrades the cellulose, lowering the aspect ratio of the NFC. Furthermore, aldehyde groups are formed to

some extent as intermediates, impairing the proper dispersion of individualized fibrils in water (due to partial formation of hemiacetal linkages between the fibrils) and remaining in the oxidized fibrils, causing discoloration when they are heated or dried at more than 80°C (Saito and Isogai, 2004; Saito and Isogai, 2006).

To overcome this downside, TEMPO-mediated oxidation under neutral or slightly acidic conditions using $NaClO_2$ as oxidant instead of NaClO (TEMPO/NaBr/$NaClO_2$ system) has also been performed by many authors, successfully preventing significant decrease in cellulose DP and favoring the selective oxidation process to carboxyl without leaving residual aldehyde groups (Shibata and Isogai, 2003; Saito and Isogai, 2004; Saito *et al.*, 2009).
Figure 13 Shows a scheme of TEMPO/NaBr/$NaClO_2$ system oxidation in water under neutral medium.

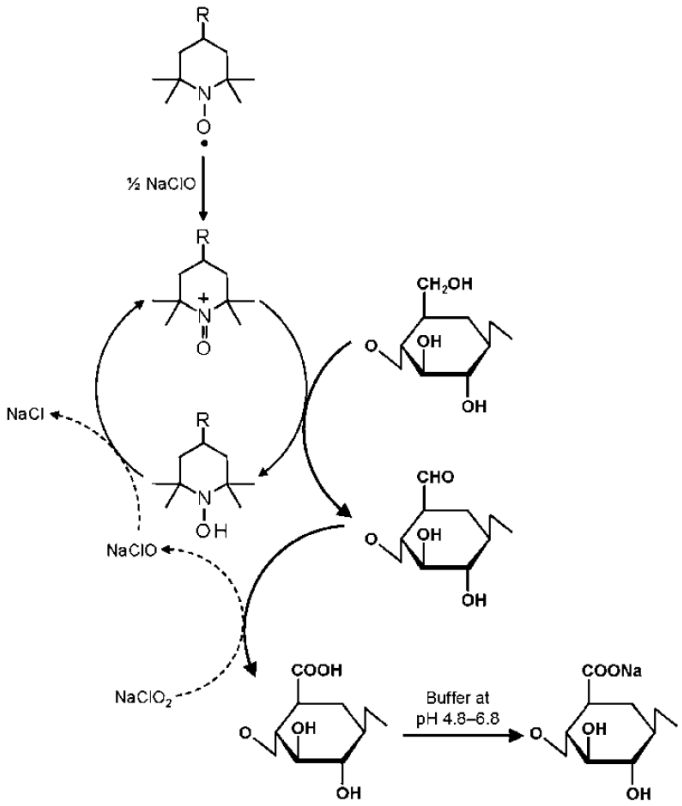

Figure 13. Selective oxidation of C6 primary hydroxyls of cellulose to carboxylate groups by TEMPO/NaBr/$NaClO_2$ oxidation in water with neutral conditions (Adapted from Isogai *et al.* 2011)

A TEMPO-mediated oxidation pre-treatment is usually followed by a mechanical treatment, and the separation by centrifugation can be used on a laboratory scale to eliminate the incompletely fibrillated material (Lavoine *et al.* 2012).

2.6.2.2. Carboxymethylation

Another pretreatment processes that have attained considerable interest in the scientific community is carboxymethylation. In this treatment, a solvent exchange to ethanol is firstly performed on a pulp suspension. Then the pulp is impregnated with monochloroacetic acid in

isopropanol. This acid reacts with the primary O-6 and secondary O-2 and O-3 hydroxyl groups of the AGU. Then, the fibers are added to a NaOH alcoholic solution, which acts as a catalyst, under high temperature and constant agitation. Finally, the carboxymethylated cellulose fibers are washed with water and acetic acid and are subjected to high-pressure homogenization followed by ultrasonication and centrifugation to remove the residual non-fibrillated fibers. (Wågberg *et al.*, 2008; Rol *et al.*, 2019).

Figure 14 depicts the general mechanism of cellulose carboxymethylation using monochloroacetic acid.

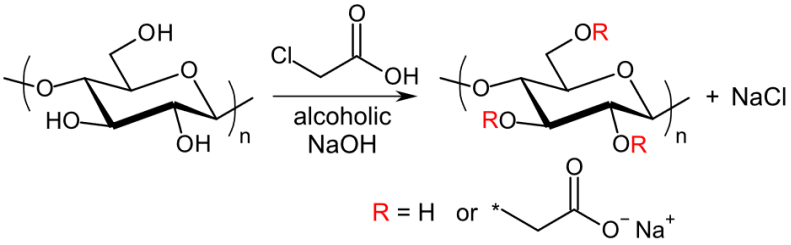

Figure 14. Carboxymethylation of cellulose using monochloroacetic acid (adapted from Nechyporchuk *et al.*, 2016)

This pretreatment increases the anionic charges through the formation of carboxyl groups on the surface of the fibrils, facilitating their disentanglement (Wågberg *et al.*, 2008; Lavoine *et al.*, 2012). Moreover, Taipale *et al.*, (2010), measured the net specific energy consumption of an MFC carboxymethylation and reported a decrease of 60% on the required energy of fluidization of a carboxymethylated MFC, against an MFC without such pretreatment. In their turn, Naderi *et al.* (2015) reported 30–50% reduction in energy consumption on repeated homogenization at lower pressures, without affecting the fibrils properties.

The main downsides of carboxymethylation reside in the use of toxic chemicals such as monochloroacetic acid and being a rather complex multi steps process (Rol *et al.*, 2019).

2.6.3. Enzymatic treatments

Enzymatic treatment (which can also be referred to as biobeating) is often used as a pretreatment in alternative to the use of chemical pretreatment approaches such as TEMPO-mediated oxidation. This kind of pretreatment improves the accessibility and reactivity of the fiber wall (Henriksson *et al.*, 2007; Pääkkö *et al.*, 2007; González *et al.*, 2013).

Enzymatic treatments are performed with the addition of cellulases in optimum conditions of temperature and pH. Cellulases can be divided into two sub-groups: cellohydrolases and endoglucanases, which respectively attack the crystalline and amorphous regions of cellulose. The most conventional cellulase used as pretreatment for the modification of pulp fibers before the main mechanical treatment is endo-1,4-β-D-glucanase (Osong *et al.* 2016). Besides,

cellulose cannot be degraded by single enzymes, hence a set of cellulases is usually involved in the process of fiber disruption (Henriksson *et al.*, 2007).

Depending on the treatment time and enzyme dosage, enzymes can assist the fibrillation of wood fibers by enhancing accessibility, reduce fiber clogging, and decrease energy during processing (Henriksson *et al.*, 2007; Pääkkö *et al.*, 2007).

2.6.4. Combined treatments

The techniques for producing NFC generally combine two or more of the previously described methods. Whether due to the low yield of nanofibrillation, inhomogeneous fibril sizes or due to the high energy cost, the currently used processes apply a chemical or enzymatic pretreatment to the fibers. It is usually only after this pretreatment that the final nanofibrillation takes place (Chinga-Carrasco *et. al.*, 2011).

According to the literature, the more commonly used technique for NFC production is mechanical homogenization. It is also possible to perform a homogenization with ultrasounds combined with the acid hydrolysis process (Isogai *et al.*, 2011). In the case of mechanical homogenization, it is essential to pretreat the fibers in order to have a relatively homogeneously sized material and diminish the number of required passages through the homogenizer. Furthermore, the pretreatment is crucial to decrease the fibers size and prevent equipment clogging (Chauhan and Chakrabarti, 2012; Zhou *et. al.*, 2012). Homogenization is usually preceded by TEMPO-mediated oxidation, since increasing the charge density eases the delamination of the fibers (Besbes *et al.*, 2011; Klemm *et. al.*, 2011; Benhamou *et al.* 2014; Lindström *et al.* 2014).

Enzymatic treatment is often used in combination with mechanical disintegration since it enables NFC manufacture with significant reduced energy consumption (Missoum *et al.*, 2013). Several authors have reported enzymatic pretreatment as an approach to producing NFC; Ankerfors *et al.* (2013) registered a patent for a method to treat pulp for the manufacture of NFC which includes refining the pulp with wood degrading enzymes at a relatively low enzyme dosage; Janardhnan and Sain (2011) explored the effectiveness of enzymatic treatment on the intermolecular and intramolecular hydrogen bonding in bleached kraft softwood pulp fibers (cellulose fibrils were afterwards isolated by high-shear refining); Pääkkö *et al.* (2007) performed enzymatic hydrolysis combined with mechanical shearing and high-pressure homogenization on bleached sulfite softwood cellulose pulp, leading to a controlled fibrillation down to nanoscale and a network of long and highly entangled cellulose I elements.

2.7. Properties and potential applications of cellulose fibrils

The several available sources of cellulose and the different production techniques result in a wide spectrum of NFCs that can be produced with different dimensions and properties and that, in turn, might have different applications (Sharma *et al.*, 2019).

NFC has potential application in several different areas, such as:

- Food additives (Lee *et al.* 2017; Agarwal *et al.* 2018);
- Reinforcing agents in nanocomposites and in paper (Zimmermann *et al.* 2010; González *et al.* 2012; Lee *et al.* 2012; Sehaqui *et al.* 2013; González *et al.* 2014; Lourenço *et al.* 2017);
- Films and barriers for food packaging and materials where selective oxygen barrier property is important (Fukuzumi *et. al.*, 2009; Lee *et al.* 2017; Storaenso, 2020);
- Medical devices, such as wound dressings and new types of bioartificial and bioactive implants, including cardiovascular grafts (Wang *et al.* 2016a; Tappa and Jammalamadaka, 2018; Bacakova *et al.* 2019);
- Foams and aerogels with superior specific area (Svagan *et al.* 2008);
- Paper coatings and additives (Luu *et al.* 2011; Torvinen *et. al.*, 2012; Brodin *et al.*, 2014; Salas *et al.*, 2019);
- Optically transparent materials and electronics (Besbes *et al.* 2011; Huang *et al.* 2013; Nogi *et al.* 2013; Fang *et al.* 2014)

The production of nano-scale cellulose fibers and their application in composite materials has gained increasing attention due to their high strength and stiffness combined with low weight, biodegradability and renewability (Klemm *et al.* 2011). NFC nanocomposite applications has been extensively reviewed (Osong *et al.* 2016; Siqueira *et al.*, 2010; Siró and Plackett, 2010; Moon *et al.* 2011; Klemm *et al.*, 2011).

Quite a few studies have been carried out to determine the Young's modulus of cellulose crystals and, although there is no absolute value, it is estimated to be around 138 GPa, varying according to the technique and / or applied model (Eichhorn *et. al.*, 2010). Table 1 compares the specific modulus (Young's modulus / density) of different engineering materials, including crystalline cellulose.

Table 1. Comparison of resistance properties of different engineering materials

Material	Young's Modulus (GPa)	Density ($t\ m^{-3}$)	Specific modulus (GPa $t^{-1}\ m^3$)
Aluminum	69	2.7	26
Steel	200	7.8	26
Glass	69	2.5	28
Crystalline cellulose	138	1.5	92

Source: Eichhorn *et. al.*, 2010

From the values in table 1, it is noticeable that the specific modulus of crystalline cellulose is much higher (and thus its mechanical strength is also superior) than that of the other compared materials. However, it is very difficult to obtain fully crystalline fibrillar structures. Although the practical values might be inferior, they are high enough for an increasing interest in NFC as a reinforcement material in different areas (Eichhorn *et. al.*, 2010).

In addition to the high crystallinity, strength and Young's modulus, NFC has a high specific surface (around 30 $m^2 g^{-1}$) and a high aspect ratio (length / diameter) (Spence *et al.* 2011). Theoretically, the performance of reinforced materials relies on the efficiency with which mechanical stress is transferred from an external energy source to the reinforcing phase through the matrix. The efficiency of transfer is a function of the amount and quality of the interfacial area between the reinforcing agent and the matrix. Overall, high-aspect ratio fibers have a better ability to sustain mechanical stress uniformly over the matrix than short fibers (Klemm *et al.,* 2011). Some studies demonstrated that the incorporation of cellulose nanomaterials in polymeric matrices leads to an increase in the rigidity and mechanical resistance of these materials (Samir *et al.,* 2005; Siqueira *et al.*, 2009; Eichhorn *et. al.*, 2010).

2.8. Water interactions of cellulose

Due to its intrinsic hydrophilicity, cellulose is sensitive to water interactions while being simultaneously water insoluble, which is mostly related to the previously mentioned strong intra- and intermolecular hydrogen bonding and crystallinity. Thus, the surface of cellulose fibers consequently builds an interface in contact with water (Samyn, 2013).

Figure 15 portrays the transition between cellulose and surrounding layers of water building over a cellulose fiber.

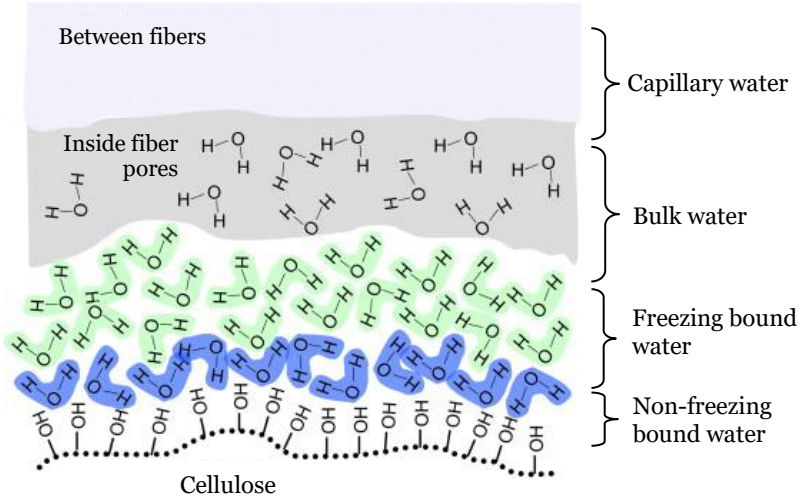

Figure 15. Layered adsorbed water forms on top of cellulose fibers (adapted from Bechtold *et al.*, 2013)

For any chemical modification of cellulose to take place the surface coverage mechanism with water must be considered, since the access of reagents will require replacement of strongly adsorbed water molecules, allowing the reagents to approach the reactive hydroxyl groups (Bechtold *et al.*, 2013). In this context, strongly adsorbed or bound water (freezing and non-freezing bound water in figure 15) is defined as the water molecules which break the intermolecular hydrogen bonding and then become closely attached to each hydroxyl group of the cellulose (Nakamura *et al.*, 1983). While bulk water does not significantly differ in its melting/crystallization temperature and enthalpy from capillary of free water (figure 15), freezing bound water is less closely associated with the polymer chains than non-freezing water, but it exhibits a crystallization phase transition and a melting point lower than 0°C, distinguishing it from the bulk water. Non-freezable bound water, on the other hand, does not show first-order phase transitions calorimetrically: it does not crystallize even when cooled down to – 100 °C (hence the designation). This implicates that when the dimensions of the pores and/or cavities of the cellulosic matrix do not exceed several Ångströms, the crystallization of water is very difficult or even impossible. Concomitantly, it is also difficult to attain a completely dry state of the cellulosic matrix (Talik and Hubicka, 2018).

Concerning the reactivity of the different hydroxyl groups at the surface of cellulose fibers towards solvents, it does not just correlate with adsorbed water but also with the degree of organization and conformation of the macromolecular cellulose chains as well as that of crystalline and amorphous sites (Mazeau and Heux, 2003; Samyn, 2013). For instance, in case of a perfect assembling or in a in highly crystalline cellulose (as bacterial cellulose, for example) some of the hydroxyl groups in the molecular side chains would be hydrogen bonded to the oxygen atom of the adjacent glucose ring, rendering these hydroxyl groups inaccessible for water penetration or solvent interaction. This is not the case, however, in cotton for instance, which has a much less organized molecular structure (Samyn, 2013).

2.8.1. Wettability of cellulose surfaces

As previously stated, cellulose is intrinsically hydrophilic. Hydrophilicity is intimately related with a concept dubbed wettability which can be generally described as the tendency of a liquid to make contact with a solid surface. Accordingly, unmodified cellulosic surfaces are intrinsically water wettable. The more spread out the water becomes on the surface, the more water wettable it is (Samyn, 2013; Hubbe *et al.*, 2015).

The most common way to assess wettability is to evaluate the contact angle (θ) of the system which is defined as the angle between the tangent to the liquid interface and the tangent to the solid interface at the contact line between the three phases in a thermodynamic equilibrium between the interfacial tension forces: solid/liquid (γ^{SL}), solid/vapor (γ^{SV}), and liquid/vapor (γ^{LV}) (Marmur, 2006; Hubbe *et al.*, 2015). The described θ determination approach is known as the sessile drop method. Although it is the most frequently used due to its convenience, other θ measurement methods can used as well (Marmur, 2006), such as the captive bubble, which

involves a fluid bubble floating in a liquid underneath the solid surface (Zhang and Hallström, 1990), or the Wilhelmy plate, involving a thin solid plate partially immersed vertically in liquid (Ramé, 1997).

A schematic illustration of the sessile drop method is depicted in figure 16.

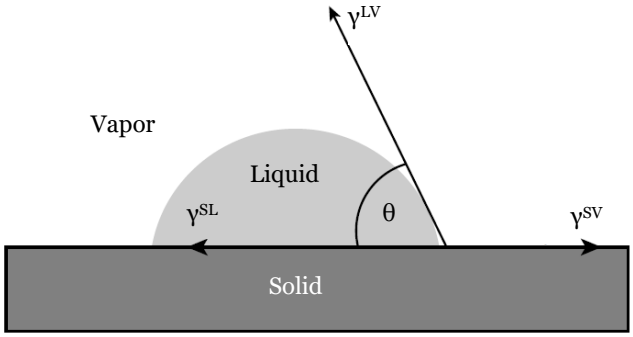

Figure 16. Schematic illustration of a liquid drop on a solid substrate: γSL, γSV and γLV are the solid/liquid, solid/vapor and liquid/vapor interfacial tension forces, respectively; θ is the contact angle (adapted from Soleimani-Gorgani, 2016)

It is noteworthy that there are many other possible configurations of systems for which the θ is measurable, such as a liquid inside a porous medium, or a solid particle floating on a liquid-fluid interface (Marmur, 2006; Hubbe *et al.*, 2015).

From a thermodynamic equilibrium point of view, it is possible to distinguish two distinct wetting regimes: complete wetting and partial wetting. In the complete wetting regime, the θ is zero and the liquid forms a thin film on the surface of the solid. On the other hand, partial wetting occurs when the θ reaches a greater than zero finite value. In such regime, if the contact angle exceeds 90°, a non-wetting situation is considered and the solid is said to be hydrophobic should the liquid be water. Otherwise, the lower the θ, the more affinity to water it has and solid is said to be hydrophilic (de Coninck *et al.*, 2001; Law, 2014).

The three-phase wetting system illustrated in figure 16 was first described by Young through the following equation:

$$\gamma^{SV} = \gamma^{SL} + \gamma^{LV} \cos(\theta)$$

Although the most acknowledged definitions in surface science are hydrophobicity and hydrophilicity, the scientific community has come to accept the definition that a surface is hydrophobic when its water θ is >90° and is hydrophilic when θ is <90°. The driving force for switching from hydrophilicity to hydrophobicity is the high surface tension of the water. The surface is said to be superhydrophobic if the θ reaches or exceeds 150°, although this later definition appears only by popular convention, having no technical rationalization to support it (Law, 2014).

As it will be further discussed, a chemical modification of cellulose with nonpolar moieties can render a given cellulose-based surface hydrophobic, but in order to attain a highly hydrophobic, or superhydrophobic surface, in addition to this chemical contribution, a complementary morphological component must be impacted on the surface: the development of micro- or/and nano-sized roughness (Gandini and Belgacem, 2015).

According to the early models there are two wetting regimes of a rough surface, first described by Wenzel (1936) and Cassie and Baxter (1944). Figure 17 shows a schematic representation of the Wenzel model opposed to the Cassie-Baxter model.

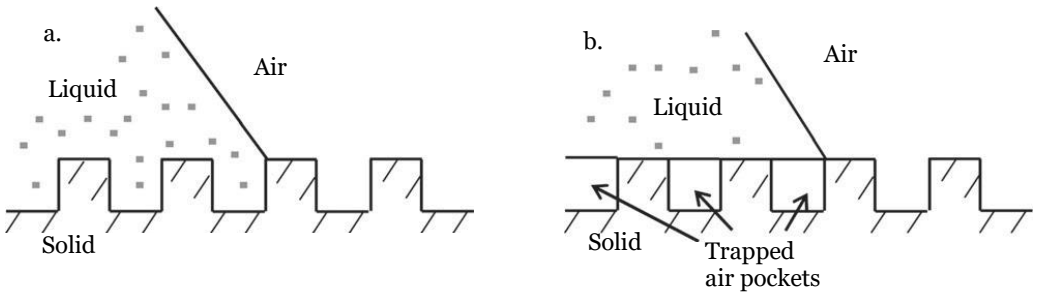

Figure 17. Different wetting models of rough surfaces: Wenzel model (a.) and Cassie-Baxter model (b.) (Adapted from Bhushan and Nosonovsky, 2010)

Both models predict that the surface roughness affects the water θ but, while the Wenzel model describes a homogeneous regime with a two-phase solid-water interface (figure 17 a.), Cassie-Baxter model describes a non-homogeneous or composite regime with a three-phase solid-water-air interface (figure 17 b.), since air pockets are trapped between the solid surface and water (Bhushan and Nosonovsky, 2010).

As a matter of fact, several biological surfaces, such as those of the lotus leaves, have a hierarchically structured surface roughness (i.e., the entire microtextured area is covered with nanoscale roughness), a characteristic that is optimized for superhydrophobicity through natural selection (Yang *et al.*, 2006; Cha *et al.*, 2010).

Figure 18 depicts the micro- and nano-scaled hierarchically structured surface roughness of a lotus leaf.

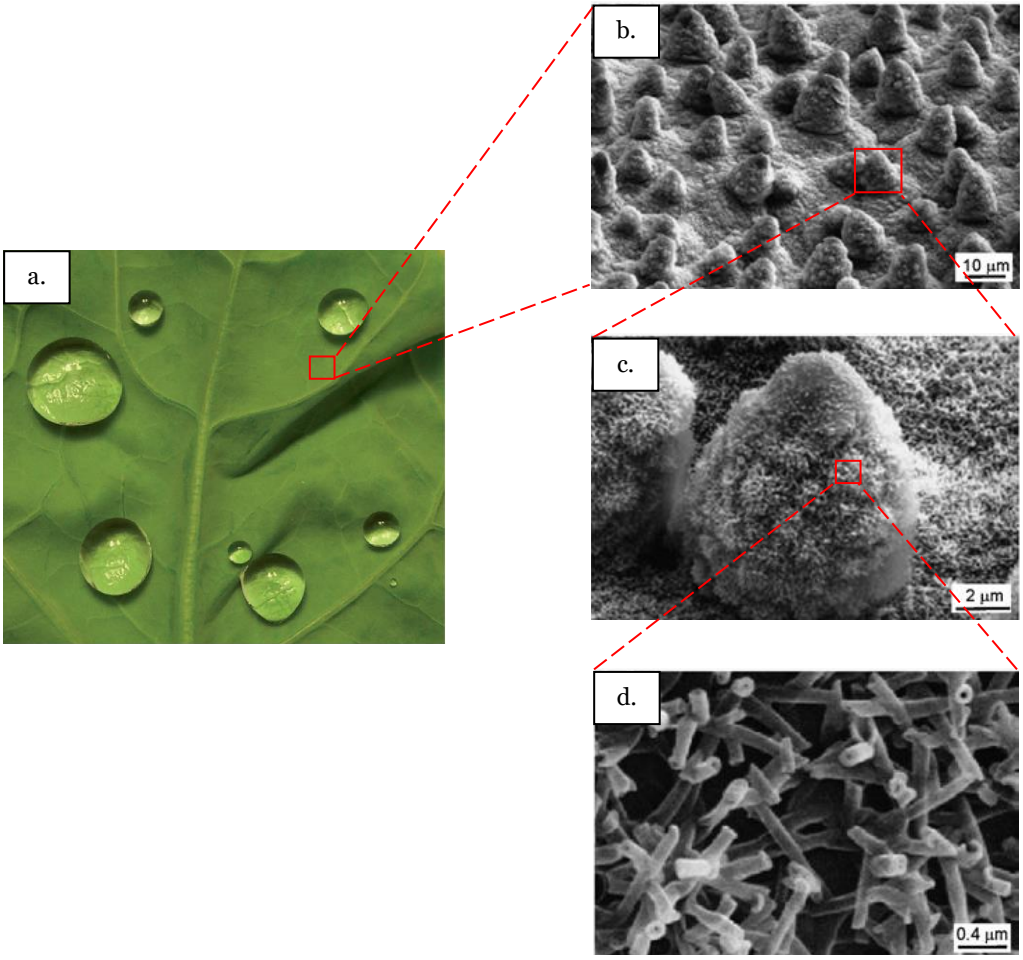

Figure 18. Photo of water droplets on a lotus leaf (a.) and SEM micrographs at three magnifications of the lotus (*Nelumbo nucifera*) leaf surface, consisting of a microstructure formed by papillose epidermal cells covered (b., c.) with a nanostructure of epicuticular wax tubules (d.) (Adapted from Koch *et al.*, 2008; Liu *et al.*, 2009)

Liu *et al.* (2009) found out that despite the surface roughness usually contributing for improving surface hydrophobicity at ambient temperature, it might actually also improve the wettability of a solid surface to hot water (50 to 80ºC) due to a decrease in the water surface tension with increasing temperature, leading to lower surface tension and thus making it a better wetting agent. In this case, the authors acknowledge that there is a transition of the wetting state from the aforementioned Cassie-Baxter state to the Wenzel state, in which the water gets into the pores and fissures of rough surfaces rather than bridging them with surface tension (figure 17 b.), which emphasizes the crucial role of surface free energy on water repellency.

Apart from static θ measurements (as it is the case for sessile drop method) which are employed to assess the wetting mechanism of a given surface, dynamic θ measurements, i.e., advancing angle (θ_A) and receding angle (θ_R) of a droplet on a tilted surface are commonly used to study wetting/dewetting and adhesion (the pull-off force when the probe droplet and the surface separate after making contact) characteristics of these surfaces, respectively. The difference

between these angles constitutes the θ hysteresis. (Law, 2014). Figure 19 depicts the dynamic contact angles of a liquid droplet on a tilted surface.

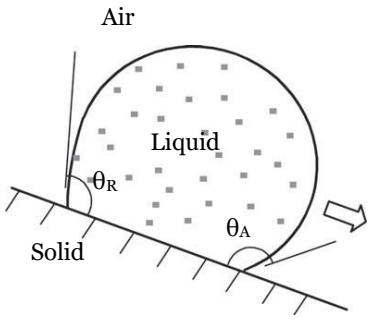

Figure 19. Schematic of a droplet on a tilted substrate showing the dynamic θs (Adapted from Bhushan and Nosonovsky, 2010)

Instead of measuring the dynamic θ on a tilted surface, one can perform these measurements by placing a probe drop on a resting horizontal surface and increase de volume of the drop by having some more liquid steadily injected by a syringe, using a needle-in-drop method, until the contact line advances: the θ_A can be measured when the contact line is just set in motion. In a similar manner, the steady partial withdrawal of liquid from the probe drop will make the contact line recced, in which case the θ_R can be measured. While tilting the sample will make the probe drop with different dynamic θ on each side (figure 19), the needle-in-drop method performed on a homogeneous surface will provide us with the same θ_A or θ_R on both sides (McHale *et al.*, 2004: Huhtamäki *et al.*, 2018).

The roll-off angle (α), i.e., the minimum inclination angle necessary for a surface droplet to roll off the surface, is also an important indicator of superhydrophobicity, mainly in the on growing field of self-cleaning surfaces which exhibit a so-called lotus leaf effect (θ greater than 160º and very low α) (Zhang *et al.*, 2016).

Despite that fact that the Young's equation is widely used to calculate θs, there is a catch: this equation was developed for ideal solid surfaces, which are defined as smooth, rigid, chemically homogeneous, insoluble, and non-reactive. According to the Young's equation, the θ would depend only on the physical-chemical nature of the three phases, and would be independent of gravity, for instance, which affects the shape of the liquid-vapor interface (but not the θ, as it is well known) (Marmur, 2006; Marmur, 2008). Solid surfaces such as wood, paper or cellulose-based films are examples of non-ideal surfaces since the wetting mechanism is affected by surface roughness due to uneven particles and porosity, capillary action, in addition to chemical heterogeneities. In such surfaces, rather than a single well defined θ, there exists a range of apparent θs (Wolansky and Marmur, 1999; Missoum, 2013). Alternative techniques which supply an average, more reliable θ have been developed: Rodríguez-Valverde *et al.* (2002) came up with a combined technique for determining the average θ of two non-ideal surfaces (wood and stone), where the axisymmetric top view diameter of a sessile drop and the axisymmetric side view shape of a captive bubble are analyzed. However, the authors asserted that the

equilibrium θ cannot be measured due to the existence of metastable states and a strong dependence of θ on the drop size.

Nevertheless, the apparent θ on a nano-roughened surface equals the equilibrium θ if the line tension (that accounts for the three-phase molecular interactions at the contact line) is negligible, since the line tension is usually only significant when the scale of roughness is over a few micrometers (Modaressi and Garnier, 2002).

2.9. Nanofibrillated cellulose surface modification

Given the high strength, dimensional anisotropy, and natural sourcing the use of NFC as a functional and renewable building block for hydrogels, as well as a reinforcing agent for polymer composites has attracted significant research interest (de France *et al.*, 2017).

As stable dispersity of NFC in non-polar media is a prerequisite for achieving reproducible results in composite manufacturing, the NFC's surface charge density is an important factor influencing the dispersity of the fibrils. The surface charge density of an NFC depends on the preparation and modification methods used. It can be harvested to both promote high dispersibility in a polar matrix and interact with other components via electrostatic or hydrogen bonding, lowering the effective threshold for NFC gelation, or to tune the physical properties of hydrogels. Nevertheless, the charged nature of cellulose fibrils interface, in addition to their tendency to aggregate in non-polar media, has made challenging the efficient incorporation and dispersion of cellulose fibrils in most conventional polymeric materials, reason why it is still difficult to develop commercial cellulose nanomaterials (de France *et al.*, 2017; Tang *et al.*, 2017; Foster *et al.*, 2018).

It is possible to obtain relatively homogeneous NFC dispersions and to prepare hydrophobic polymer/NFC nanocomposites using solvent exchange with a suitable solvent/dispersant to obtain a wet NFC precursor containing a thermoplastic or polymerizable resin. However, it is more efficient to introduce surface charge or long chain molecules to increase either the electrostatic repulsion or steric hindrance between fibrils. Proper surface modification based on the properties of specific media, aiming to change the surface hydrophilicity and improve compatibility, is an effective way to improve the dispersity of NFC (Khalil *et al.,* 2014b; Plummer *et al.*, 2015; Thomas *et al.*, 2018; Chu *et al.*, 2020). In this context, low interfacial adhesion between the nanofibrils and the polymeric matrix of the composite leads to a decrease in the mechanical performance and other properties of the final product (Hubbe *et al.*, 2008).

In short, surface modification allows to introduce new functionality and therefore make way towards new applications, while improving cellulose fibrils compatibility with hydrophobic matrices in composites manufacture (Missoum *et al.*, 2013).

Nonetheless, while surface modification can decrease the hydrophilicity of the NFC while maintaining the crystalline structure of the cellulose fibrils intact, the drying process builds up another challenge, which should be considered for incorporation of NFC in polymers because it can change the size of these materials after drying and may compromise their final properties due to the formation of irreversible hydrogen bonds between adjacent fibrils upon drying, a phenomenon known as hornification (Diniz *et al.,* 2004; Khalil *et al.,* 2014a; Islam and Rahman 2019).

The characterization of a chemically modified cellulosic material is usually done by Fourier transform infrared spectroscopy (FTIR). FTIR is a qualitative/comparative nondestructive technique based on the irradiation of infrared light on a given sample. The involved device measures the amount of light that absorbed, transmitted and / or reflected after interaction with the sample and reports the absorbance or transmittance as a function of the wave number, providing information on molecular vibrations, which can be used to identify the presence or absence of specific functional groups on the sample, reason why it is frequently used to validate the efficiency of the chemical modification, aiming functionality (Mohamed *et al.*, 2017; Hospodarova *et al.*, 2018).

2.9.1. Molecular grafting

The surface of cellulose nanofibrils can be modified and tuned by using a chemical approach to achieve covalent bonds between cellulosic substrates and a grafting agent. In this context, two general routes can be considered: molecular grafting and polymer grafting (Missoum *et al.*, 2013). Figure 20 gives an overview of some reagents used in NFC molecular grafting strategies.

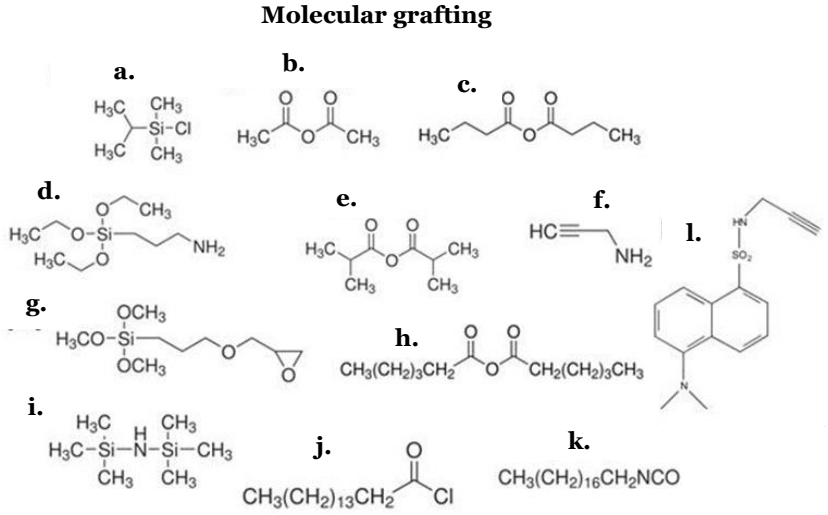

a. Chlorodimetylisopropylsilane; **b.** Acetic anhydride; **c.** Butyric anhydride; **d.** 3-aminopropyltriethoxysilane; **e.** Iso-butyric anhydride; **f.** propargyl amine; **g.** 3-glycidoxypropyltrimethoxysilane; **h.** hexanoic anhydride; **i.** Hexamethyl disilazane; **j.** Palmitoyl acid; **k.** n-octadecylisocyanate; **l.** 5-(dimethylamino)-N-(2-propyl)-1-naphthalenesulfonamide.

Figure 20. Molecules used in cellulose surface modification through molecular grafting (adapted from Missoum *et al.*, 2013)

One of the most frequent approaches to cellulose surface modification by molecular grafting is silylation. Silylation consists of introducing silane-based coupling agents onto the surface of cellulose fibrils (figure 20 a., d., and g.). The silylation process turns the hydrophilic surface of NFC into hydrophobic by attaching silyl groups to the –OH groups in the cellulose. While in the absence of water, even at high temperatures, no reaction happens between the silyl groups and the OH groups of cellulose (although they do react with lignin's phenolic OH), the presence of moisture allows this reaction to happen at high temperatures (Hubbe *et al.*, 2008).

By manipulating the degree of substitution, some authors have reported improved dispersion of cellulose fibrils in organic solvents in a non-aggregating manner (Goussé *et al.*, 2004). Other authors have successfully obtained hydrophobic structures from silylated cellulose fibrils (Andresen *et al.*, 2006; Zhang *et al.* 2014; Zhao *et al.,* 2015; Samarasekara *et al.*, 2018). Apart from silylation of cellulose fibrils, this technique can be performed to alter the characteristics of previously manufactured NFC-based structures: Chinga-Carrasco *et al.* (2012) have performed silylation on the surface of carboxymethylated NFC films to improve their hydrophobicity, achieving contact angles of 90º. Ifuku and Yano (2015) also used a silylation method to improve the mechanical properties of NFC-reinforced polymer composites, increasing their Young's modulus to 1.5 GPa, against 0.8 GPa determined for the neat NFC-based composites, due to better dispersion and compatibility.

Another molecular grafting method commonly performed on cellulose is acetylation (figure 20 b.). The principle of acetylation is the organic esterification reaction with acetic acid, introducing acetyl functional groups CH_3-C(=O)- onto the surface of cellulose which cause plasticization of the cellulosic fibrils (Bledzki *et al.*, 2008).

Esterification of cellulose fibrils is commonly performed to decrease their hydrophilicity and enhance their dispersibility and affinity to a nonpolar solvent by reducing the interfibrillar hydrogen bonding (Lavoine *et al.*, 2012). Yetiş *et al.* (2020) performed surface acetylation on high hemicellulose and lignin content MFC to significantly decrease its polarity and provide good dispersibility in (polylactic acid) PLA for biocomposites fabrication via a solvent casting method. Tingaut *et al.* (2010) have also acetylated MFC to improve its compatibility with a PLA matrix. They introduced acetyl groups onto the inner crystalline regions of the MFC and reported that an acetyl content above 4.5% promotes significant changes in the MFC's crystalline structure. Furthermore, they also reported that the acetylation prevented hornification of the material upon drying which can be a desirable feature in industrial-scale production and storage. Several researchers have suggested acetylation of cellulose fibrils rendering hydrophobic characteristics (Jonoobi *et al.*, 2010), improving dispersion and compatibilization with nonpolar solvents (Ashori *et al.*, 2014) and enhancing mechanical and/or barrier properties (Kim *et al.,* 2002; Bulota *et al.*, 2012; Cunha *et al.,* 2014, Mashkour *et al.,* 2015) as well as optical properties (Nogi *et al.*, 2006; Yang *et al.*, 2018) of cellulose fibrils-based structures.

It is noteworthy that, although the electrostatic repulsion arising from the introduction of functional groups on cellulose fibrils' surface aids the NFC dispersion, it can easily be affected by the ambient conditions, such as pH, temperature, salt concentration, among others (Qi *et al.*, 2015).

Modification of cellulose has also been performed in another approach that takes advantage of a self-reinforced effect to manufacture mono-component cellulose-based composites. This strategy has been carried out in several different ways: by partially dissolving the outer layers of cellulose, using ionic liquids, followed by cellulose regeneration (Li *et al.*, 2018) or pre-dissolving cellulosic fibers and introducing untreated fibers into the resultant solution (Nishino *et al.*, 2004); by performing oxypropylation (Gandini *et al.*, 2005: de Menezes *et al.*, 2009) or esterification (Matsumura *et al.*, 2000; Freire *et al.*, 2006) limited to the outer layers of cellulose fibers. Rather than being converted entirely with the corresponding functional groups, the cellulosic substrate is treated in order to be only partially converted. Thus, the mechanical properties of the material can be tuned depending on the degree of substitution. Hot-pressing can then be used to merge the two phases into one material, in which the modified cellulose constitutes the matrix, and the unmodified cellulose fibers make up the reinforcing elements of a novel composite made up entirely from cellulose (Missoum *et al.*, 2013; Gandini and Belgacem, 2015).

The critical facet of this process, however, is the cautious control of reagents penetration and modification extent, to avoid the total transformation of cellulose, keeping the nanofibrillar structure so as to modify only the surface of the cellulosic chains, reason why a non-swelling media is typically used in this mechanism in order to maintain the structure and properties of the cellulosic fibers. Ideally the system results in an inner core of fibrous cellulose with its mechanical properties untouched, and an outer sleeve of modified material (Missoum *et al.*, 2013; Gandini and Belgacem, 2015). This kind of composites are featured by their good interfacial compatibility due to the same cellulosic composition of the matrix and reinforcing phase, biocompatibility and biodegradability, as well as superior mechanical, optical and barrier properties (Li *et al.*, 2018). The Young's modulus and tensile strength of these kind of composites can, in some instances, surpass 10 GPa and about 100–500 MPa, respectively, which is well above those of the cellulose-reinforced thermoplastics (Gandini and Belgacem, 2015).

2.9.2. Polymer Grafting

As previously mentioned, polymer grafting is another commonly performed cellulose surface modification approach. It consists of the immobilization of long neural polymer chains onto the surface of cellulose aiming to modify its surface and hence achieving stable NFC dispersions. These grafted polymer chains tend to expand away to gain configurational entropy, generating steric or entropic repulsion between the fibrils which then have their possible steric conformations reduced. This steric repulsion is much more prone to resist environmental

interference than electrostatic repulsion, therefore leading to more stable NFC dispersions (Stenstad *et al.*, 2008; Azzam *et al.*, 2010; Harrisson *et al.*, 2011).

Figure 21 summarizes polymers used in NFC polymer grafting approaches.

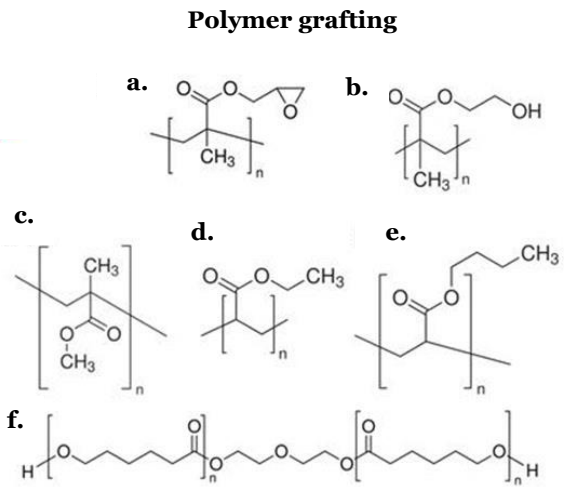

a. Poly (glycidyl methacrylate); **b.** Poly (2-hydroxyethyl methacrylate); **c.** Poly (methyl methacrylate); **d.** Poly (ethyl acrylate); **e.** Poly (butyl acrylate); **f.** Poly (ε-caprolactone).

Figure 21. Polymers used in cellulose surface modification through polymer grafting (adapted from Missoum *et al.*, 2013)

Polymer grafting comprises two main routes: "grafting onto" and "grafting from": the "grafting onto" approach, while extensively performed on cellulose fibers or CNC, it has not been used for NFC tough. This method consists of mixing the cellulose substrates with the grafting polymer and a coupling agent or else activating either the cellulose substrates or the polymer and grafting either one onto the other. The main advantage when following this strategy is the control of the resulting material's properties since one can characterize the polymer in terms of molecular weight beforehand. However, high grafting densities are usually not expectable due to steric hindrance brought up by the polymeric chains (Missoum *et al.*, 2013; Gandini and Belgacem, 2015; Rol *et al.*, 2019). On the other hand, this polymeric hindrance can be harvested to limit cellulose nanoparticles aggregations and improve their dispersion or control their assembly (Azzam *et al.*, 2016; Lin *et al.*, 2019).

The "grafting from" approach consists of mixing activated cellulose substrates with both a monomer and an initiator agent to induce a polymerization process directly from the substrate's surface to the outward direction. Contrary to the "grafting onto" strategy, this method is an effective route for generating high grafting densities, due to the lower medium viscosity and limited steric hindrance arising from a lower degree of polymerization. Hereupon, the precise determination of the grafted polymer's molecular weight, as well as the quantification of the non-grafted polymer as difficult tasks to achieve (Hansson *et al.*, 2012; Missoum *et al.*, 2013; Gandini and Belgacem, 2015; Rol *et al.*, 2019).

Another often referred to strategy in the literature is polymer grafting on a previously molecular grafted or polymer grafted cellulosic substrate, allowing further functionalization. For instance, Stenstad *et al.* (2008), apart from being the first to polymer graft NFC by means of a "grafting from" strategy performing radical polymerization of glycidyl methacrylate (figure 1.21, a.), reported modification of NFC with isocyanate followed by grafting anhydrides. Anhydrides introduce alkenyl groups that can support even further grafting. Yeo and Hwang (2014) grafted aminopropyl triethoxysilane-modified NFC to polypropylene-graft-maleic anhydride NFC aiming to not only improve the NFC dispersion, but also to increase the interfacial adhesion between the NFC and a polypropylene matrix as a way to upgrade the resulting composites' mechanical performance. Li *et al.* (2011) modified NFC surface using 2-bromoisobutyryl prior to grafting poly(butyl acrylate) (figure 21 e.) with a technique that controls the length of the grafted chains, rendering highly hydrophobic NFC with a by-layered structure with a hard core and a soft outer layer, increasing the affinity of the NFC towards poly(propylene) and providing the resulting composites with enhanced mechanical properties.

2.9.3. Physical adsorption

Surface modification of cellulose fibrils by adsorption is less complex and more environmentally friendly than grafting in the sense that it does not usually require organic solvents and can be performed in a non-hazardous aqueous media. Moreover, this strategy is easily scalable: the adsorption of commercial polymers for instance, is a well-known methodology that has been employed in pulp and paper industry for centuries (Hatton *et al.* 2015).

While grafting involves the establishment of covalent bonds between the fibril's surface and grafted fragments, surface modification by adsorption on the other hand involves noncovalent interactions such as van der Waals interactions, hydrogen bonds, ionic interactions or other affinities to cellulose (Gandini and Belgacem, 2015; Rot *et al.*, 2019).

Figure 22 presents some compounds commonly used in NFC's surface adsorption strategies.

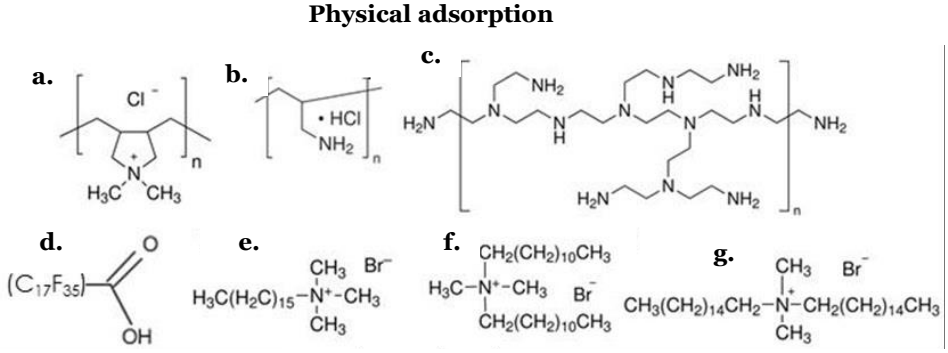

a. Poly(diallyldimethylammonium chloride); **b.** Polyethylenimine; **c.** Barnched polyethylenimine; **d.** Perfluoro-octadecanoic acid; **e.** Cetyltrimethylammonium bromide; **f.** Triethylmethylammonium bromide; **g.** Dihexadecyl ammonium bromide

Figure 22. Compounds used in cellulose surface modification through physical adsorption (adapted from Missoum *et al.*, 2013)

Physical adsorption on NFC surface has received growing attention amongst the scientific community not only as fibril dispersion aiding strategy in nonpolar media, but also as a way to develop viable bioengineering interactions (Siró and Plackett, 2010; Klemm *et al.*, 2011).

Modification of cellulosic substrates surface through physical adsorption has been reported for polyelectrolytes i.e., polymers that multiple charges along their chain, and non-polyelectrolytes, that despite being uncharged, have binding ability though van der Waals interactions or hydrogen bonding. Some biopolymers have also been reported to have a specific binding affinity for cellulose, such as hemicelluloses and some chemically modified celluloses, as carboxymethyl cellulose (Hatton *et al.* 2015).

The deposition of polyelectrolytes has been extensively applied to NFC (Larsson *et al.*, 2013) and CNC (Podsiadlo *et al.*, 2005; Cranston *et al.*, 2006). However, cationic polyelectrolytes are commonly applied to chemically modified cellulose such as carboxymethylated cellulose, due to the highly negatively charged surface, binding through electrostatic interactions (Wågberg *et al.*, 2008; Chi and Catchmark, 2018). Aarne *et al.* (2012) chose Poly(diallyldimethylammonium chloride) (PDADMAC) (figure 22 a.) and another cationic polyelectrolyte dubbed polybrene, for successfully reduce the swelling properties of the carboxymethyl cellulose treated fibers, due to their known ability to neutralize the anionic charge either exclusively on the surface or in the whole fiber, respectively.

When adsorbing polyelectrolytes on a substrate, the type of polyelectrolyte, its charge density and charge distribution along the polymer chain, are features that have to be taken into account, since investigations in the field have shown that the charge density and distribution as well as presence of salts largely affect the binding ability of the polyelectrolyte to the substrate. Thus, the ionic strength of the media can be used as a way of tuning adsorptivity of the polyelectrolyte onto the substrate (Wågberg, 2000; Galván *et al.*, 2015). Adsorption of polyelectrolytes have also been applied to NFC as a way of facilitating flocculation and water drainage, besides developing novel nanocellulose-based composite applications (Raj *et al.*, 2015; Raj *et al.*, 2016).

Layer-by-layer (LBL) assemblies have become a popular strategy of exploiting electrostatic interactions between oppositely charged molecules or polyelectrolytes. Cellulose has been employed in LBL assemblies with polyelectrolyte multilayers being constructed from a cellulose surface (Lingström *et al.*, 2007). In other approaches, CNC and NFC has been incorporated in LBL assemblies as an anionic polyelectrolyte themselves, in combination with cationic polyelectrolyte multilayers (Cranston and Gray *et al.*, 2006; Wågberg *et al.*, 2008) and were also investigated for the formation of NFC-based thermoresponsive nanocomposites with important applications on controlled release drug delivery systems, sensors, or membrane permeability control (Utsel *et al.*, 2010; Larsson *et al.*, 2013).

Surfactants have been likewise extensively used to modify the surface of cellulosic substrates in order to control suspension stability, hydrophilicity and interfacial interaction. Surfactants are usually amphiphilic organic compounds, i.e., simultaneously containing both hydrophobic groups (tails) and hydrophilic groups (heads) (Missoum *et al*., 2013).

Xhanari *et al.* (2010) used cationic surfactants with different chain lengths (cetyltrimethyl-, didodecyl- and dihexadecyl ammonium bromide, figure 22, e., f., g., respectively) to modify the surface of NFC. The results suggest the possibility of using cationic surfactants to systematically control the degree of water wettability of NFC. Kaboorani and Riedl (2015) used hexadecyltrimethylammonium bromide, a cationic surfactant, to modify CNC surface. Results showed that the adsorption of the surfactant on the CNC could be used to control the stability and dispersibility of CNC suspensions, while maintaining the crystalline structure intact. In more recent approaches, surface modification of CNC with cationic surfactants adsorption improved their barrier properties against moisture, aiming to manufacture corrosion protective nanocomposite surface coatings (Ly and Mekonnen, 2020; Mekonnen *et al.* 2021).

.

Chapter 3 - Publications and other developed investigation

3.1. Paper 1 - Nanofibrillated cellulose Rheology: Effects of morphology, ethanol/acetone addition and high NaCl concentration

Vera L.D. Costa, Ana P. Costa and Rogério M. S. Simões.
BioResources, Vol. 14 No. 4, 7636-7654, 2019
DOI 10.15376/biores.14.4.7636-7654

Nanofibrillated Cellulose Rheology: Effects of Morphology, Ethanol/Acetone Addition, and High NaCl Concentration

Vera L. D. Costa, Ana P. Costa, and Rogério M. S. Simões *

The effects of ethanol or acetone addition (2.5% to 40% w/w) and high ionic strength (50 mM to 1000 mM NaCl) on the rheology of carboxymethylated (NFC-carb) and 2,2,6,6-tetramethylpiperidine-1-oxyl (TEMPO) oxidized (NFC-TEMPO) nanofibrillated cellulose (NFC) suspensions were studied. Morphological characterization and centrifugation showed that NFC-TEMPO had a much finer overall morphology than NFC-carb. Rheological measurements were taken at 1.3 wt% using a stress-controlled rheometer equipped with cone and plate measurement tools with rough surfaces. The dynamic moduli were investigated through oscillatory stress sweeps. The results showed that as little as 2.5% (w/w) of either ethanol or acetone decreased the viscosity and the dynamic moduli, while 40% (w/w) increased the viscosity to values higher than those of the aqueous suspensions, doubled the storage modulus, and extended the gel-like behavior. Increasing the NaCl concentration from 50 mM to 100 mM drastically increased viscosity; moreover, the storage modulus in the elastic region linearly increased with increasing NaCl concentrations in the range of 100 mM to 1000 mM, suggesting the increased content of interparticle bonds with NaCl addition. The elastic domain was also extended from 10 Pa to 50 Pa and above 500 Pa with acetone addition (40%) and NaCl addition, respectively.

Keywords: Nanofibrillated cellulose; Rheology; Morphology; High ionic strength; Ethanol/acetone addition

Contact information: Department of Chemistry, Unit of Fiber Materials and Environmental Technologies (FibEnTech-UBI), University of Beira Interior, 6200-001 Covilhã, Portugal;
** Corresponding author: rmss@ubi.pt*

INTRODUCTION

Many biological materials exhibit impressive and controllable properties determined by their micro- and nanostructures (Bhushan and Jung 2011).

Nanofibrillated cellulose (NFC) is a cellulosic material with lateral dimensions usually under 100 nm, which is typically obtained *via* mechanical defibrillation of wood pulp, commonly preceded by enzymatic treatments (Janardhnan and Sain 2006; Henriksson *et al.* 2007; Pääkkö *et al.* 2007) and/or chemical treatments such as 2,2,6,6-tetramethylpiperidine-1-oxyl (TEMPO)-mediated oxidation (Saito *et al.* 2007), aqueous morpholine addition (Onyianta *et al.* 2018), carboxymethylation (Wagberg *et al.* 2008; Naderi and Lindstrom 2014), or sulfoethyltion (Naderi *et al.* 2017). These treatments result in a gel-like cellulosic aqueous suspension.

NFC recently has been the subject of much attention due to its unique characteristics, such as high aspect ratio and mechanical resistance, as well as its aptitude to set up strong entangled networks with high transparency (Nechyporchuk *et al.* 2016). In addition, NFC is a renewable and biodegradable material, among other attributes, which makes it suitable for many industrial applications, namely as a reinforcing phase in composites and in fields such as packaging, adhesives, biomedicine, *etc.* (Nechyporchuk

et al. 2016). The potential of NFC, cellulose nanocrystals and bacterial cellulose in packaging applications was also recently reviewed (Hubbe *et al.* 2017a).

The manipulation and application of NFC suspensions requires the study of their rheological behavior. Thus, research has been lately focused on the determination of the dynamic moduli (storage modulus: G' and loss modulus: G'') from the linear viscoelastic regions during oscillation measurements, as well as viscosity (η) and/or shear stress (τ) during flow measurements (Naderi *et al.* 2014a,b; Nechyporchuk *et al.* 2014).

It has been reported that the NFC suspensions' rheological properties are highly concentration dependent (Pääkkö *et al.* 2007; Karppinen *et al.* 2012; Chen *et al.* 2013; Nechyporchuk *et al.* 2015); even at solid concentrations as low as 0.125 wt%, the suspensions exhibit a shear-thinning thixotropic behavior and gel-like properties, *i.e.*, the rheological response of the suspension is elastic dominated ($G' >> G''$) (Pääkkö *et al.* 2007; Nechyporchuk *et al.* 2015). However, more recently, Fneich *et al.* (2019) stated 0.25% as the optimal solid content at which the gel-like behavior appears for a salt-free suspension although the gel-like behavior can be attained at 0.1% in the presence of 50 mM NaCl.

Apart from the solid concentration, other features that have been reported to affect the rheological properties of NFC suspensions include morphological characteristics such as the length of the nanofibrils, their aspect ratio (Ishii *et al.* 2011; Iwamoto *et al.* 2013; Benhamou *et al.* 2014; Tanaka *et al.* 2014, 2015), pH, temperature, and the ionic strength of the medium (Karppinen *et al.* 2012; Saarikoski *et al.* 2012; Naderi and Lindstrom 2014; Tanaka *et al.* 2016, Hubbe *et al.* 2017b).

Regarding the effect of ionic strength on viscosity and viscoelastic properties, apparent contradictory conclusions have been suggested by Mendoza *et al.* (2018). Naderi and Lindstrom (2014), working with carboxymethyl cellulose with a charge of 590 μeq/g of carboxyl groups at 1% solid content and a NaCl concentration in the range of 0 to 10 mM, reported a decrease in both the viscosity and the elastic moduli. Fukuzumi *et al.* (2014) explored a broader range of NaCl concentration (0 to 400 mM) and worked with TEMPO-oxidized cellulose at a 0.1% solid content and reported no significant decrease in the viscosity until 10 mM of NaCl, but also reported a drastic increase in viscosity between 10 mM and 100 mM NaCl followed by a moderate decrease thereafter. Saarikoski *et al.* (2012) also reported a very moderate increase in the storage modulus with NaCl concentration in the range 0 to 1 M for a very low surface-charge on microfibrillated cellulose (MFC). Tanaka *et al.* (2014) also reported an increase in the storage modulus with salt addition. The same research group, working with NFC having a substantially different carboxyl group content (200 μmol/g and 900 μmol/g), but simultaneously with different hemicellulose content, suggested that the carboxyl groups content has a role on the sensitivity of the salt concentration and its effect on the storage modulus (Tanaka *et al.* 2016). More recently, Xu *et al.* (2018) identified two types of solid-phases for cellulose nanocrystals suspensions: a repulsive phase at low salinity and an attractive solid phase at high salinities.

It has also been reported that inherent flow instabilities occur during rheological studies of NFC suspensions. These instabilities introduce errors in the rheological measurements: shear banding and wall-slip phenomena, also designated by wall depletion, which creates a lubrication effect and results in a lower energy state during laminar shearing (Ovarlez *et al.* 2009; Saarinen *et al.* 2009; Nechyporchuk *et al.* 2014). Shear banding arrives from a dynamic situation of competition between flock formation *vs.* consolidation over time and flock destruction due to flow, favoring fragments segregation and leading to coexisting fast and slow flowing regions. Wall depletion consists of interfacial slippage on the edge of geometry tools and the suspension due to a displacement of a disperse phase from solid boundaries. To prevent or decrease these flow instabilities,

many methods have been used, such as increasing the gap (Saarinen *et al.* 2009), using other geometry configurations like a vane-in-cup system (Mohtaschemi *et al.* 2014), or using roughened tool surfaces that take advantage of the material's cohesive forces (Naderi and Lindstrom 2015; Nechyporchuk *et al.* 2015).

Although NFC are mostly produced and processed in aqueous media, organic solvents, such as ethanol or acetone, can play a role in solvent exchange for processing, as the reaction medium for derivatization, and even as the coagulation medium in wet-spinning. In fact, several authors (Iwamoto *et al.* 2011; Håkansson *et al.* 2014) have reported the use of acetone as a coagulation or exchange medium. As far as the authors know, the rheological response to the addition of organic solvents, like ethanol, to NFC suspensions has not been yet investigated. In contrast, the effect of ionic strength of NFC suspensions on viscosity and viscoelastic behavior has been extensively reported, but some contradictory results remain, probably due to the different nanocellulose characteristics, including surface charge, the ranges of ionic strength, and studied solid contents.

Therefore, the objectives of this investigation are to study the effects of organic solvent addition (ethanol or acetone) to the NFC aqueous medium and the effect of NaCl concentration in the range of 100 mM to 1000 mM on flow and dynamic rheological behavior of two strongly different NFC suspensions, including morphological and carboxylate content levels.

EXPERIMENTAL

Materials

For this study, a carboxymethylated NFC aqueous suspension containing a 2.2 wt% solid content, obtained from Innventia (Stockholm, Sweden), was used. This suspension will be designated as NFC-carb in the study.

An NFC suspension was also produced in the authors' lab from a commercial bleached sulphite eucalyptus pulp. The pulp was subjected to a TEMPO-mediated oxidation pretreatment under previously reported reaction conditions (Saito *et al.* 2007) and then subjected to two successive homogenization steps (500 bar and 1000 bar), using a GEA Niro Soavi (model Panther NS3006L; GEA, Parma, Italy). The solid content of the suspension was initially kept at 1%; afterwards, the solids content was increased to approximately 2.2% *via* evaporation at room temperature with occasional stirring; when required, additional water was removed from the gel by absorption using blotting paper. The obtained NFC from this process will henceforth be called NFC-TEMPO.

Methods

Microscopic observations

The NFC-carb and NFC-TEMPO suspensions were diluted with distilled water to attain a solid content of 0.1 wt% and were subsequently sonicated for 5 min to improve the dispersion of the fibrils. A drop of each diluted suspension was allowed to air dry overnight at room temperature on a microscopic slide, and it was later attached on a microscope sample holder with double-sided tape. Microscopic observations were performed using scanning electron microscopy (SEM) (Hitachi S-2700; Hitachi, Tokyo, Japan) operated at 20 kV. All of the samples were previously gold-sputtered by cathodic spraying (Quorum Q150R ES; Quorum Technologies, Ltd., East Sussex, UK).

For the transmission electron microscope (TEM) imaging, drops of 0.001 wt% NFC-carb and NFC-TEMPO suspensions were deposited on carbon-coated electron microscopic grids and negatively stained with 2 wt% uranyl acetate. The grids were air-

dried and analyzed with a Hitachi HT-7700 TEM (Hitachi, Tokyo, Japan) with an acceleration voltage of 80 kV.

NFC carbohydrate composition

The neutral sugar compositions of NFC-carb and NFC-TEMPO suspensions were determined by quantitative saccharification upon acid hydrolysis according to the National Renewable Energy Laboratory's (NREL) proceeding guidelines for the determination of structural carbohydrates and lignin in biomass (Sluiter *et al.* 2012). Thin layers of NFC-carb and NFC-TEMPO were oven-dried at 50 °C for 4 h and were finely fragmented with scissors prior to the acid hydrolysis. The structural carbohydrates were quantified using an HPLC system that integrates a pump (Perkin Elmer Binary LC Pump 250; Perkin Elmer, Waltham, MA, USA), equipped with an UV/Vis detector (LC290; Perkin Elmer, Waltham, MA, USA), a refraction index detector (HP 1047A RI Detector; Hewlett Packard, Palo Alto, CA, USA) and a liquid chromatography column (Aminex HPX-87H; Bio-Rad Laboratories, Inc., Hercules, CA, USA).

Degree of polymerization in NFC polysaccharides

The determination of the NFC limiting viscosity [η], was achieved with a cupriethylenediamine (CED) solution as a solvent, using a capillary viscometer according to the ISO 5351 (2012) standard. The degree of polymerization (DP) was calculated using the Mark–Houwink–Sakurada equation $[\eta] = 0.57 \times DP$ (Smith *et al.* 1963).

Total acidic groups content in NFC

The content of total acidic groups in NFC was determined *via* a conductivity titration method, according to the standard SCAN-CM 65:02 (2002). First, the NFC was suspended in an HCl solution to protonate the NFC. Due to filtration issues, the vacuum filtration washing after the protonation step was substituted by sequential 15 min centrifugations at 3000 g. The supernatant was discarded and the process of adding distilled water and mixing after each centrifugation was continued until the supernatant attained a conductivity of 5 µS/cm. The suspensions were afterwards titrated with a NaOH solution to pH = 11. The amount of weak acid groups was determined from break points in the conductivity *vs*. added volume of NaOH from the curves obtained from the conductivity titrations.

Preparation of the NFC suspensions for rheological measurements

Suspensions of NFC with 1.30 wt% solid content were produced from the original NFC-carb and NFC-TEMPO through the addition of the appropriate amount of distilled water, organic solvent, or NaCl aqueous solutions. The homogenization of the suspension was obtained through vigorous agitation in a vortex mixer with four successive steps lasting 1.0 min each with handshaking in-between.

Ethanol or acetone were added to the original NFC aqueous suspensions to attain the suspension medium with ethanol/(ethanol + water) percentages of 2.5%, 5.0%, 10.0%, 20.0%, and 40.0% (w/w). The NaCl solutions were added to attain the final concentrations of 5 mM, 100 mM, 300 mM, 500 mM, and 1000 mM.

Prior to the rheological measurements, all suspensions were sonicated for 5 min to ensure proper homogenization and air bubble removal. After this step, the NFC suspensions were loaded in the rheometer and rested for 1.0 min before the rheological assays. The samples were not subjected to preshearing in the rheometer with the purpose of avoiding the distortion of the initial NFC structure before the measurements (Nechyporchuk *et al.* 2015).

Zeta potential measurements

The previously prepared 1.3 wt% NFC-carb and NFC-TEMPO suspensions with NaCl concentrations of 0 mM, 50 mM, 100 mM, and 1000 mM, as well as NFC-carb suspensions with 2.5% and 40% (w/w) ethanol were diluted to a solids content of 0.1 wt% with distilled water, the pH was adjusted to 7, and the resulting suspensions were sonicated for 5 min. A rough estimative of the surface particles charge was obtained by a streaming current detector (Mütek PCD-02; BTG Product Digest, Herrsching, Germany).

Rheological measurements

The rheological measurements were recorded using a stress-controlled rheometer (RheoStress® RS 150; Haake Technik GmbH, Vreden, Germany). A cone and plate geometry with a 2° angle cone sensor (C35-2°) with a diameter of 35 mm and a gap of 0.105 mm were used to study the NFC suspensions in both flow and oscillation modes. To study the effect of the tool's roughness on the rheological measurements, a sandpaper with a roughness of either 58.5 µm or 18.3 µm, depending on the assay, was attached to both the plate and cone using double-sided tape. When roughened surfaces were used, the thickness of the sand paper was taken into account, maintaining the same gap as in the assays with smooth surfaces. To minimize water or ethanol evaporation, all of the rheological measurements were performed under a homemade transparent cover.

In flow mode, controlled rate flow tests were conducted with a shear rate (γ) in the range of 0.05 s^{-1} to 1000 s^{-1} for 180 s. Shear stress (τ) and viscosity (η) were analyzed.

The viscoelastic behavior was studied through oscillatory stress sweeps performed with a τ in the range of 0.07 Pa to either 100 Pa or 10000 Pa, depending on the suspension's rheological performance, with a frequency of 1.0 Hz. The dynamic moduli (G^*), *i.e.*, the storage modulus (G') and the loss modulus (G'') were analyzed. The suspensions were tested at room temperature (22 ± 1 °C). All of the described assays were performed in duplicate and the results represent the arithmetic average in each point.

RESULTS AND DISCUSSION

Morphological Characterization of the Fibrils

The morphology of the fibrils was investigated through SEM and TEM analyses using various magnifications to capture the micro- and nano-scale particles. Figure 1 gives an overview of the morphological characteristics of the NFC-carb and NFC-TEMPO fibrils.

As shown in Figs. 1a and 1c, the fibrillation of the material appears not to have been homogeneous and particularly incomplete, especially for NFC-carb. Although the fine fibrillar structures with diameters in the nanometer range can be spotted in both materials (Figs. 1b and 1d), the relative proportion of the fibers with micrometer dimensions was clearly higher in NFC-carb. The pretreatments performed on NFC-TEMPO led to a substantial deconstruction of the fibrillar cell wall of the sulphite eucalyptus pulp, thus resulting in shorter fibrillar structures and a finer overall morphology when compared to the NFC-carb fibrils produced from softwood kraft pulp.

To roughly quantify the relative proportions of nano- and microelements, extremely dilute suspensions (0.05 wt%) of both materials were adjusted to a pH of 4 (to protonate most parts of the carboxylate groups; pKa = 4.8) and were submitted to centrifugation at 9000 g for 20 min. The obtained sedimented material was quantified. The experimental results showed nearly 84% and 57% of the initial material has sedimented for NFC-carb and NFC-TEMPO, respectively, confirming the higher percentage of nanoelements in NFC-TEMPO. Therefore, the two materials had substantially different morphological

properties. While most of the NFC-carb's elements were predominantly at microscale range, the NFC-TEMPO's were made up of many more elements in the nanoscale range.

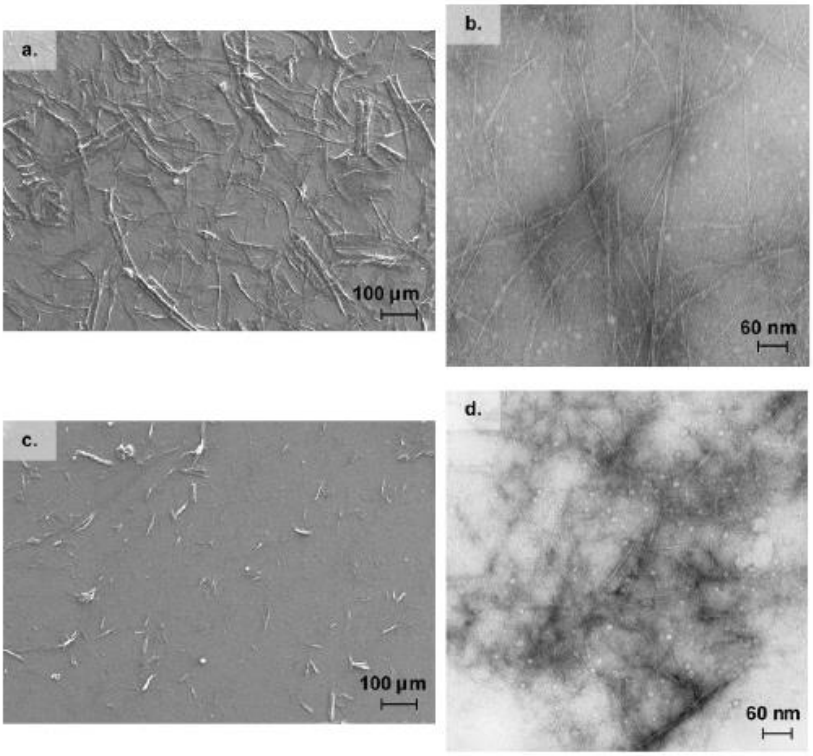

Fig. 1. NFC-carb (a and b) and NFC-TEMPO (c and d) fibrils imaged through SEM (a and c) at a solid content of 0.1 wt% and TEM (b and d) at a solid content of 0.01 wt%

Physico-chemical Characterization of the Fibrils

The structural carbohydrates in NFC-carb were quantified through acid saccharification. The material was made up of 88.4% cellulose and approximately 11.6% hemicelluloses. The NFC-carb's limiting viscosity was 397 mL/g, which corresponded to an average DP of 696, suggesting a good preservation of the DP of the initial raw materials. Assuming that the weak acidic groups were predominantly carboxylic acid groups introduced during the carboxymethylation pretreatment stage in the course of the NFC production, its carboxyl group content was determined as 698 µmol/g. This value was in good agreement with those reported by NFC produced *via* a similar process (Naderi *et al.* 2014a).

Concerning the NFC-TEMPO material, the resulting limiting viscosity was 85 mL/g, corresponding to an average DP of 149, and the resulting carboxyl group content was 1900 µmol/g. Both the carboxylic group content and the polysaccharides' DP were in good agreement with the values reported in the literature for similar pretreatments (Shinoda *et al.* 2012). From Fig. 1 and the physicochemical data, it was clearly demonstrated that the two materials used in the present work were representatives of two morphologically and physio-chemically different materials.

Effect of Geometry Surface Roughness

Many authors have reported that a distortion of the rheological measurements of NFC suspensions (mostly during flow mode measurements) occurs due to wall-slip

phenomena and hence at least one roughened or serrated tool surface was introduced to overcome this issue (Iotti *et al.* 2011; Naderi *et al.* 2014b; Nechyporchuk *et al.* 2014; Nechyporchuk *et al.* 2015). For example, Nechyporchuk *et al.* (2014) have suggested attaching sandpaper (roughness of approximately 120 µm) on the surfaces of cone and plate measurement tools to prevent wall-slippage of a 1.0 wt% TEMPO-oxidized NFC suspension during rheological flow measurements. In the present study, preliminary rheological studies were performed to determine the influence of different surface roughness on the measurements. Sandpapers with various roughness values (58.5 µm and 18.3 µm) were attached to the surface of both the plate and sensor. Controlled rate flow assays were performed with both mentioned sandpapers and also without the sandpaper (smooth surface) using a 1.3 wt% NFC-carb aqueous suspension.

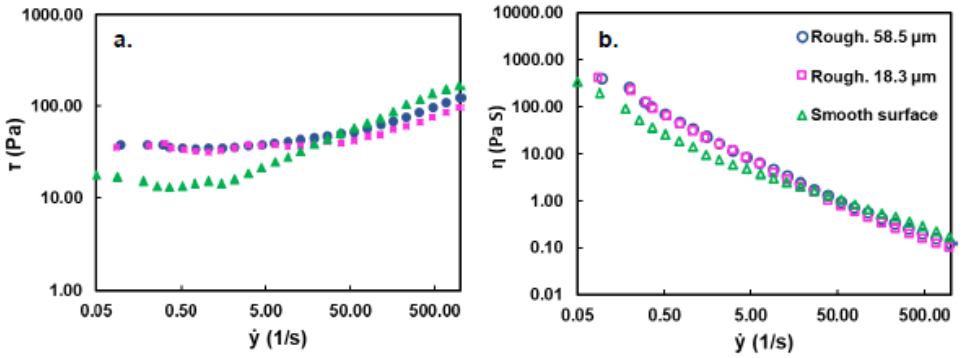

Fig. 2. Shear stress (a) and viscosity (b) curves of a 1.3 wt% NFC-carb aqueous suspension performed with smooth, 58.5 µm, and 18.3 µm roughened surfaces

Figure 2 shows the stress rate flow curves of a 1.3 wt% NFC-carb aqueous suspension, performed with various surface roughness, where it was evident that both the measured shear stress and viscosity were higher when the assay was performed with roughened surfaces, particularly at shear rates between 0.05 s^{-1} and 5 s^{-1}. The results were in good agreement with those obtained by Nechyporchuk *et al.* (2014, 2015); however, these authors reported that wall-slip can still occur with roughened surfaces (≈ 120 µm) for the enzymatically pretreated NFC and attributed this effect to the water release from the suspension, which probably does not occur in the present case due to the higher carboxyl group content.

In accordance with what was reported by other authors, at higher shear rates (from 10 s^{-1} to 100 s^{-1}) the measurements were less influenced by the flow instabilities as well as the used geometries and their roughness, closely representing the bulk properties of the NFC suspensions (Haavisto *et al.* 2014; Nechyporchuk *et al.* 2015).

Because no substantial variation was detected between the results for the two different roughness levels (Fig. 2), the authors believe that the size of the sandpaper grain did not play an important role in keeping the cohesive forces between the bulk of the suspension and the borders for the used roughness. In fact, other authors have reported that to avoid wall-slip, the texture of the roughened surfaces only needs to be on the same scale of the studied particle size, even though exceeding this value, on the side of caution, might be prudent (Buscall 2010; Naderi and Lindström 2015). In the following assays, only measurements made with the 58.5 µm roughness sandpaper was described if nothing was otherwise mentioned.

Regarding the flow curves (Fig. 2), it was possible to clearly identify a plateau in the shear stress for a shear rate in the range of 0.05 s^{-1} to 10 s^{-1}, which translated to a decrease in apparent viscosity.

Effect of Ethanol and Acetone Concentrations in the Suspension Medium

Organic solvents, such as ethanol and acetone, have been widely used in coagulation and fixation baths for the production of NFC filaments from aqueous suspensions *via* wet spinning (Iwamoto *et al.* 2011; Walther *et al.* 2011; Håkansson *et al.* 2014) and dry jet-wet spinning (Hauru *et al.* 2014); to the authors' knowledge, no rheological study has been conducted on NFC suspensions containing these solvents. Although the NFC fibrils are assumed to make the major contribution to the rheological effects, the rheological behavior of the suspending medium, and mainly its interaction with fibrils, surely play a key role.

To evaluate the effect of ethanol and acetone additions on the rheological behavior of NFC suspensions, controlled rate flow assays and oscillatory stress sweeps were performed on the NFC-carb suspensions with various contents of either ethanol or acetone.

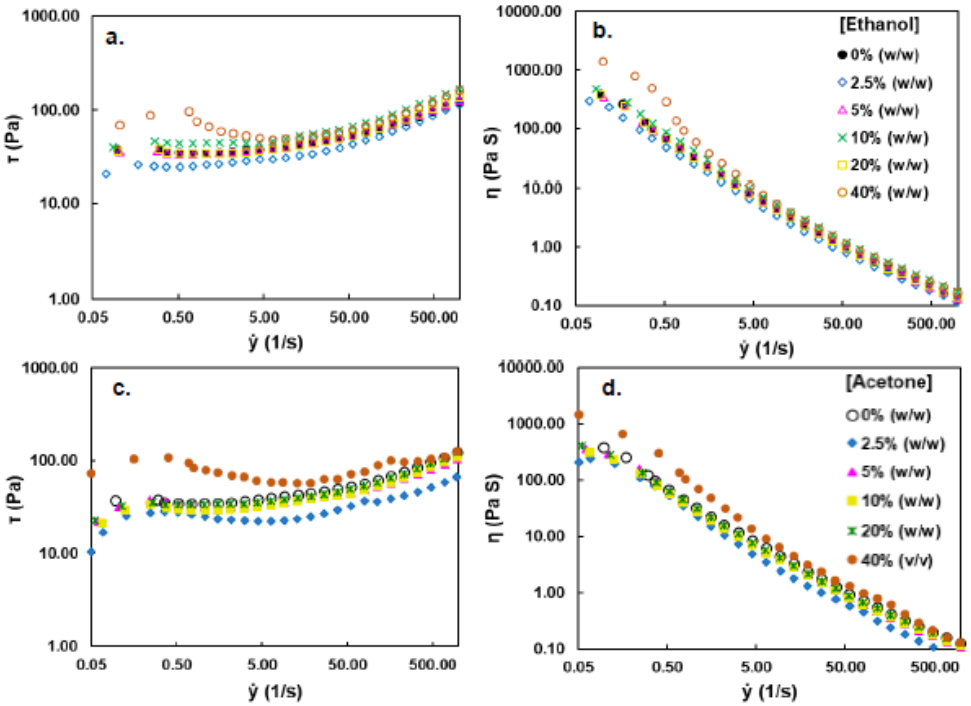

Fig. 3. Shear stress (a and c) and viscosity (b and d) flow curves of 1.3 wt% NFC-carb suspensions with 0%, 2.5%, 5%, 10%, 20%, and 40% (w/w) of ethanol (a and b) and acetone (c and d)

Figure 3 shows the stress rate flow curves of 1.3 wt% NFC-carb suspensions with 0%, 2.5%, 5%, 10%, 20%, and 40% (w/w) of either ethanol or acetone, performed with roughened surfaces. It was observed that a small concentration of either ethanol or acetone (2.5% (w/w)) somewhat decreased the shear stress and viscosity of the suspensions, probably due to an impairing of the hydrogen bonds between fibrils. However, an organic solvent concentration as high as 40% (w/w) increased the shear stress values considerably higher than those of the pure aqueous suspensions, predominantly at low and moderate

shear rates, showing higher interfibrillar interaction and viscosity. The decreasing value of the dielectric constant of the bulk solvent as the concentration of ethanol or acetone increased could explain the cohesion of the suspension. This topic will be further discussed in the paper.

Oscillatory assays were performed on the same suspensions (Fig. 4).

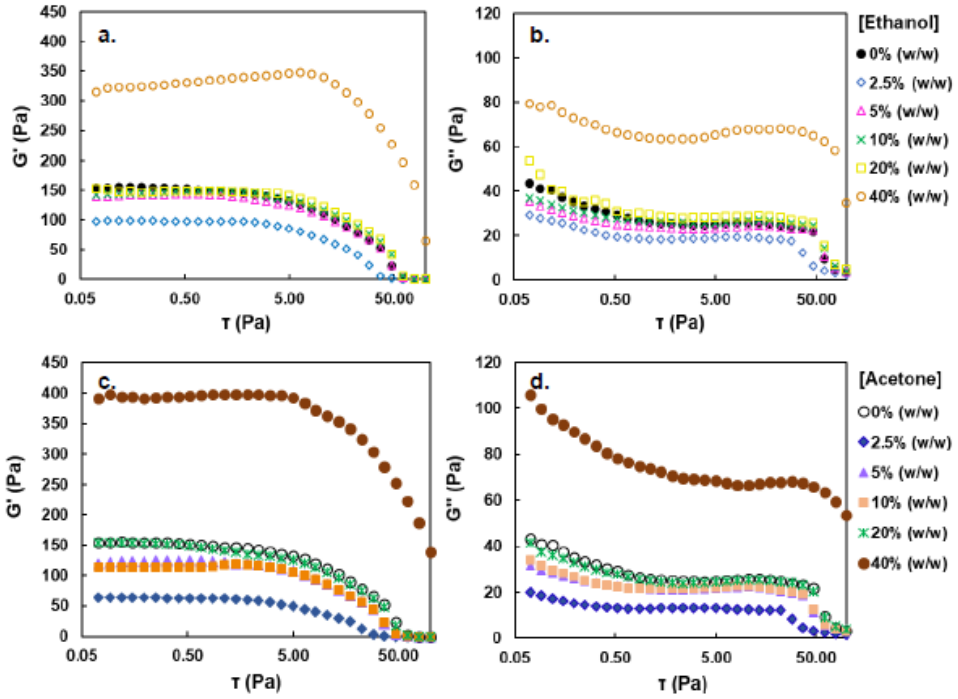

Fig. 4. Storage modulus (a and c) and loss modulus (b and d) of oscillatory stress sweep curves of 1.3 wt% NFC-carb suspensions with 0%, 2.5%, 5%, 10%, 20%, and 40% (w/w) of ethanol (a and b) and acetone (c and d)

The dynamic rheology was measured using a stress-controlled rheometer instead of the more usual strain-controlled rheometer. In the latter case, for a fixed strain, the oscillation frequency is changed while the dynamic moduli are monitored. In this study, at a fixed frequency (1.0 Hz), the shear stress was changed and the corresponding moduli were recorded. In this solicitation mode, the material was simultaneously submitted to both higher shear stress (and corresponding shear rate) and strain at the fixed frequency.

The results from this study allowed the estimation of the shear stress endured by the gel before the structure completely breaks down. The loss tangent (tan δ) values in Fig. 5, which were calculated through the ratio (G''/G') of the loss modulus (G'') to the elastic modulus (G'), identified three profiles: (i) the suspension with a small amount of acetone or ethanol, which started to lose elasticity for lower shear stress values; (ii) the 40% ethanol or acetone NFC suspensions, which clearly retained their elastic behavior until higher shear stress values; and (iii) all the remaining suspensions with intermediate elastic behavior. In short, it was clear that the addition of 40% of ethanol or acetone enabled further extension of the solid-like behavior to higher shear stress values.

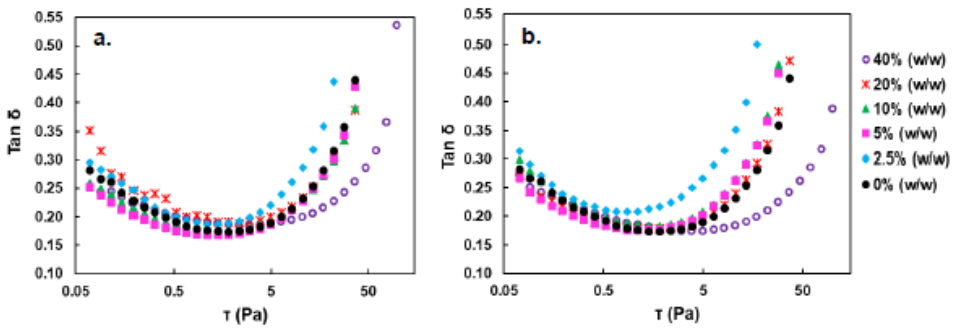

Fig. 5. Loss tangent values of 1.3 wt% NFC-carb suspensions with 0%, 2.5%, 5%, 10%, 20%, and 40% (w/w) of ethanol (a) and acetone (b)

According to Fig. 4, in the elastic domain, a small amount of ethanol or acetone (2.5 % w/w) caused a decrease in the storage modulus (and viscosity as well) of the suspensions (from 150 Pa to 100 Pa for ethanol and to 50 Pa for acetone), which suggested a destabilization of the hydrogen bonds, weakening the fiber network. In contrast, concentrations of ethanol and acetone as high as 40% (w/w) drastically increased the storage modulus from approximately 150 Pa to 350 Pa for ethanol and 400 Pa for acetone, respectively. Figure 6 represents the evolution of the output of the streaming potential detector corresponding to the particles with ethanol content of the medium, where an increased absolute value of ζ-potential for 2.5% w/w ethanol was observed (from 1175 to 1420). This condition corresponded to a decrease in the storage modulus and viscosity, probably due to the increased repulsion between the particles. The streaming current detector output recovered for 5% of ethanol and remained relatively stable until 20% of ethanol; the same trend occurred for the storage modulus (Fig. 4). However, this property increased substantially for 40% of ethanol while the streaming current detector output (absolute value) substantially decreased to 565, diminishing the corresponding particles' electrostatic repulsion, whereas the van der Waals forces, including hydrogen bonds, were also revealed. The authors concluded that the effective particles' surface charge (as represented by the streaming current detector output) explained most of the storage modulus and the apparent viscosity variations well.

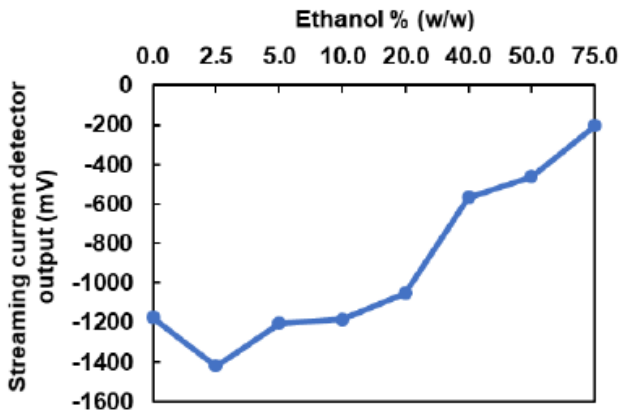

Fig. 6. Streaming current detector output of 0.1 wt% NFC-carb suspensions with 0%, 2.5%, 5%, 10%, 20%, and 40% (w/w) of ethanol

The ethanol concentration was further extended to 75% (w/w), and the results for shear stress and storage modulus are presented in Fig. 7. The experimental results showed that an ethanol concentration of 75 wt% led to an extensive decrease in shear stress for the region with the high shear rate, which was observed as strong flocculation; instability was also observed in the storage modulus for a shear stress over 10 Pa and segregation of mainly water was evident under visual observation.

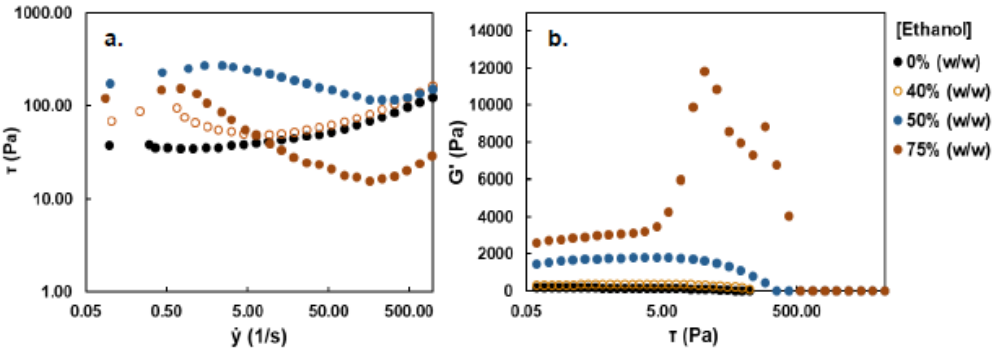

Fig. 7. Shear stress (a) and storage modulus (b) curves of 1.3 wt% NFC-carb suspensions with 0%, 40%, 50%, and 75% (w/w) of ethanol

Effect of Ionic Strength

The effect of the ionic strength on the rheological behavior of NFC-carb aqueous suspensions was determined in both flow and oscillatory rheological experiments (Figs. 8 and 10), for a wide range of NaCl concentrations (0 to 1000 mM). Contrasting behaviors were observed when low (up to 50 mM) and high (100 mM and above) NaCl concentrations were explored. When the salt concentration increased from 0 to 50 mM, a decrease in viscosity was observed. Naderi and Lindstrom (2014) worked with carboxymethylcellulose having 590 µeq/g of carboxyl groups (an NFC similar to the authors' own NFC-carb) and reported a small decrease in both viscosity and storage modulus (measured at a solid content of 1%) when the NaCl concentration was increased in the range 0 to 10 mM. Jowkarderis and Van de Ven (2014) also reported a similar decrease of intrinsic viscosity with ionic strength in the diluted regime. The behavior of samples in this study drastically changed when the salt concentration was increased to 100 mM, as can be seen in Fig. 8. Jowkarderis and Van de Ven (2014) also reported an inversion of intrinsic viscosity at 20 mM NaCl concentration, for a TEMPO-oxidized cellulose with a carboxyl content of 0.65 mmol/g.

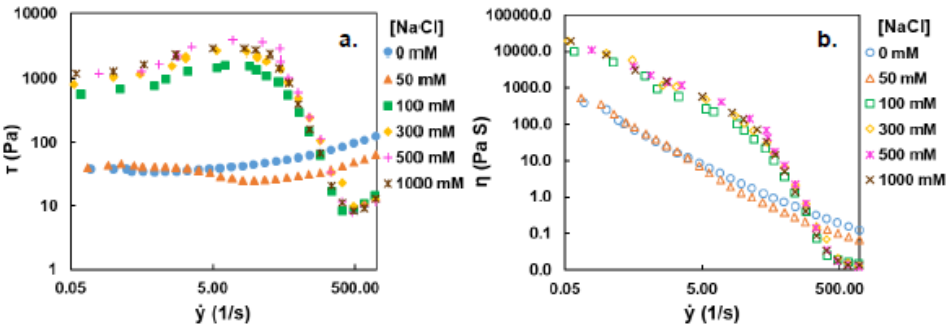

Fig. 8. Controlled rate flow curves of NFC- carb suspensions with various concentrations of NaCl: effect of ionic strength on the shear stress (a) and on the viscosity (b)

Figure 8 shows that both the shear stress and viscosity drastically increased (close to two orders of magnitude) when the NaCl concentration was changed from 50 mM to 100 mM; further increase in the NaCl concentration (until 1 M) had only a marginal effect. Moreover, observation of the suspension showed that up to a concentration of 50 mM of NaCl, the suspensions maintained their homogenous gel structure, but at higher NaCl concentrations a slight flocculation of the suspension was observed, which was in accordance with the decrease in the ζ-potential (Fig. 9).

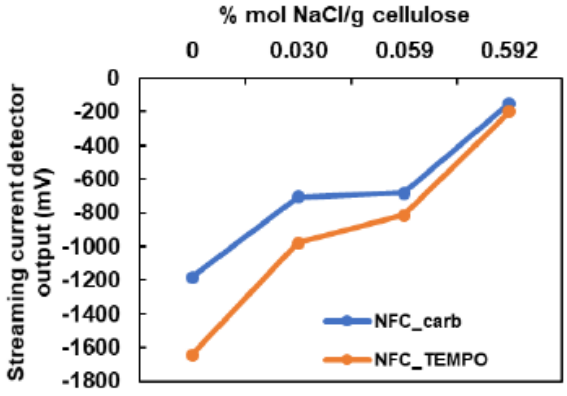

Fig. 9. Streaming current detector output for 0.1 wt% NFC-carb and NFC-TEMPO suspensions with increasing NaCl charges

The flocculation behavior, enhanced by the addition of NaCl, was in accordance with that reported by Saarikoski *et al.* (2012). As expected, higher ionic strength increased the screening of the electrical charges in the fibrils surface, decreasing the electrostatic repulsion and thus allowing the fibrils to come closer together and strengthening the connection between the contact points. Another approach suggests that the salt neutralizes the carboxylate groups, leading to the same results (Fall *et al.* 2011). The results in Fig. 9 seem to support this view.

The comparative behavior of the two NFC suspensions (NFC-carb and NFC-TEMPO) is presented in Fig. 10.

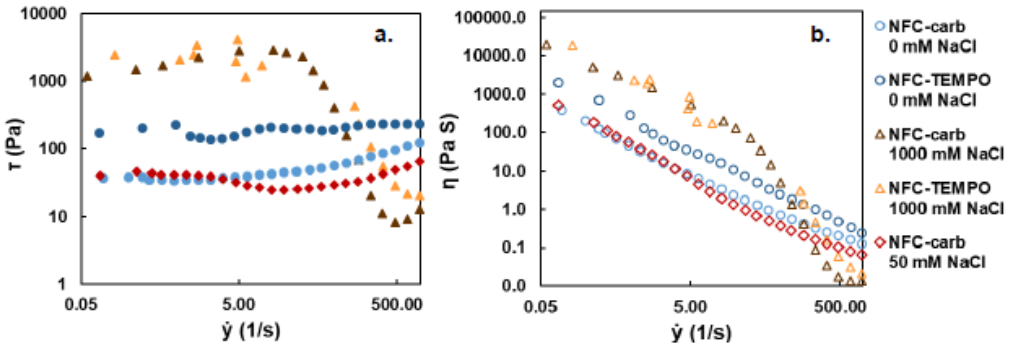

Fig. 10. Controlled rate flow curves of NFC-carb and NFC-TEMPO aqueous suspensions with and without salt addition: effect on the shear stress (a) and on the viscosity (b)

Despite the much lower degree of polymerization of the NFC-TEMPO with respect to NFC-carb (149 *vs* 696), the NFC-TEMPO aqueous suspension without salt addition exhibited a markedly higher shear stress for all studied shear rate ranges than the NFC-carb

(Fig. 10). Because the NFC-TEMPO was much more nanofibrillated than the NFC-carb (Fig. 1), the results emphasized the importance of the particle size, including specific surface area, on the rheological behavior.

Comparing the effect of NaCl addition (Fig. 10) with ethanol or acetone additions (Fig. 3) on both shear stress and apparent viscosity, substantial differences were observed. For NaCl addition (1 M), a sharp decrease in the shear stress occurred for shear rates higher than 20 s^{-1}, suggesting a noticeable structure break, whereas the shear stress remained stable for the corresponding suspension with low ionic strength (0 M NaCl) and ethanol or acetone aqueous medium up to 40%. However, for a 75% ethanol concentration (Fig. 7), the gel structure also broke.

The effect of the ionic strength on the dynamic moduli in oscillatory stress sweep assays performed with roughened surfaces is illustrated in Fig. 11 for the NFC-carb, which showed that a higher NaCl concentration resulted in higher dynamic moduli achieved. Moreover, as shown in Fig. 12, there was a linear increase in the storage modulus with the NaCl concentration, in the range 0.1 M to 1 M. Saarikoski *et al*. (2012) used a mechanically disintegrated pulp (low surface charge) and also reported an increase in the storage modulus (from approximately 120 Pa to approximately 160 Pa, at solid content of 1%) with an increase in NaCl concentration from 0 to 100 mM; further increase in NaCl concentration to 1000 mM only had a marginal effect on storage modulus, and strong microfibril aggregation was reported by the authors. Tanaka *et al*. (2016) also reported a linear increase in storage modulus (50 Pa to 450 Pa) with NaCl increase from 0 to 100 mM, for an NFC with 900 µmol/carboxyl content at a solid content of 0.25 wt%. However, in this study the increase in the storage modulus was observed in the wide range of NaCl (0 to 1000 mM), for both of the studied NFCs with 0.7 mmol/g and 1.9 mmol/g of carboxylate groups. It should also be emphasized that a NaCl concentration above 100 mM had a marginal effect on the viscosity, but in contrast had a huge effect on the storage modulus. This linear increase of storage modulus with the NaCl concentration was also reported for nanocrystalline cellulose (NCC) concentrations above 7%. These authors attributed this increase to the increase of interparticle bonds (Xu *et al*. 2018). The decrease of the effective particle charge (estimated by the streaming current output), observed in Fig. 9, is a pre-requisite for the increase of interparticle bonds; the balance between the attractive and repulsive forces results in favor of the attractive van der Waals forces, including hydrogen bonds, when the repulsive forces diminished (Hubbe *et al*. 2017b).

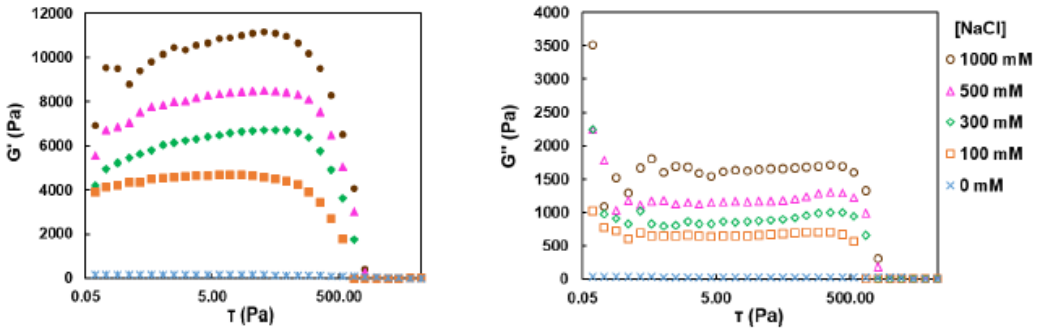

Fig. 11. Storage modulus (a) and loss modulus (b) for NFC-carb suspensions with various NaCl concentrations

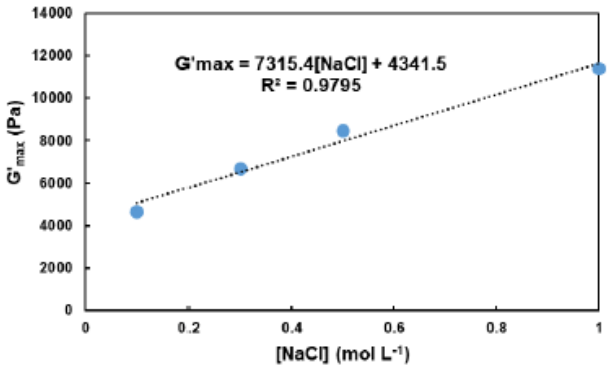

Fig. 12. Effect of NaCl concentration on the maximum storage modulus of NFC-carb suspensions

The comparison of NaCl addition with acetone addition revealed that the NaCl impact on storage modulus was much higher than that of acetone (Fig. 4).

The comparative behavior of NFC-carb and NFC-TEMPO materials regarding the storage and loss moduli is represented in Fig. 13, which revealed the superior performance of the NFC-TEMPO, despite both lower cellulose DP and particle size. The maximum storage modulus increased from close to 80 Pa to 11,000 Pa for the NFC-carb and from approximately 90 Pa to 28,000 Pa for NFC-TEMPO.

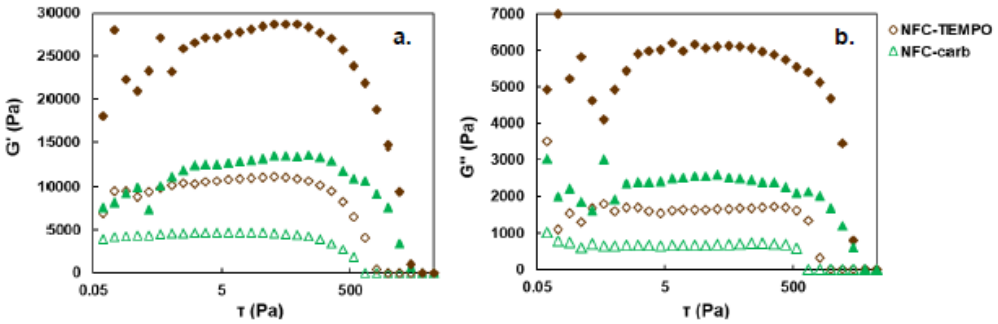

Fig. 13. Storage modulus (a) and loss modulus (b) for NFC-carb and NFC-TEMPO suspensions with 1 M NaCl (filled symbols) and 0.1 M NaCl (open symbols)

The tan δ values for both NFCs are presented in Fig. 14, which indicated that the suspensions exhibited some elastic instability until 5 Pa, followed by a wide plateau until 100 Pa (NFC-carb) and over 500 Pa (NFC-TEMPO), afterwards the viscous behavior began to dominate. Moreover, a comparison of the results between Figs. 14 and 5 clearly indicates that the NaCl addition enabled an extension in the range of elastic behavior to a higher shear stress (from 50 Pa to 500 Pa).

Briefly, both nanofibrillation extents and ionic strengths facilitated the preparation of a cellulosic gel with a storage modulus in the range of 150 Pa to 28000 Pa, at a solids content of 1.3 wt%, which can be useful for several fields of application where the favorable gel properties are preserved.

According to Lowys *et al.* (2001), a small amount of NaCl is expected to cause a moderate electrostatic screening effect, increasing the *G'* to some extent. However, higher NaCl concentrations can result in collapse of the energy barrier and aggregation of the fibrils, which leads to a loss of homogeneous gel structure (Lowys *et al.* 2001; Saarikoski *et al.* 2012). However, in this study this did not occur in the samples until a concentration

of NaCl up to 1000 mM. The gel structure only collapsed under a shear stress higher than 500 Pa applied at a frequency of 1.0 Hz.

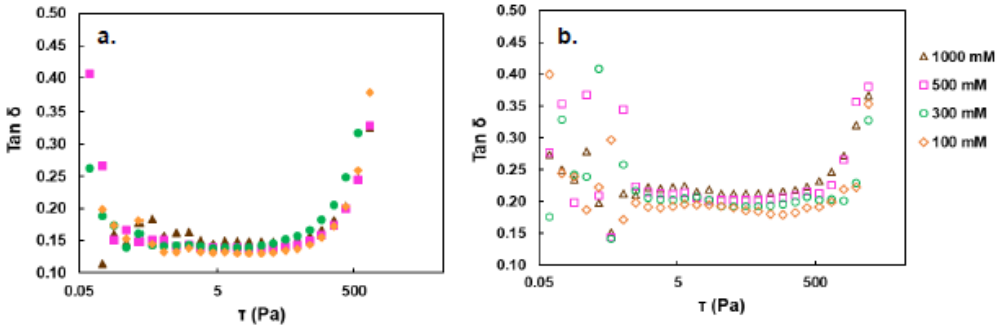

Fig. 14. Loss tangent values for NFC-carb (a) and NFC-TEMPO (b) suspensions with various NaCl concentrations

CONCLUSIONS

1. A small addition of either ethanol or acetone to the NFC aqueous suspension (2.5% (w/w)) decreased the shear stress, the viscosity, and the storage modulus from 150 Pa to 100 or 50 Pa. In contrast, a concentration as high as 40% (w/w) increased both the viscosity and storage modulus to values considerably higher than those of the aqueous suspensions, suggesting higher interfibrillar interaction, which was in accordance with the observed decrease of the absolute value of the zeta potential, from 1175 mV to 565 mV. The corresponding storage modulus increased from 150 to 400 Pa.
2. An increase in the NaCl concentration from 50 mM to 100 mM led to a drastic increase in both the shear stress and viscosity. An addition of over 100 mM of NaCl drastically increased the dynamic moduli, compared to the respective aqueous suspension. The maximum storage modulus linearly increased with the NaCl concentration (in the range of 100 to 1000 mM), and reached 10000 Pa and 28000 Pa for NFC-carb and NFC-TEMPO, respectively, at a solid content of 1.3 wt%. In addition, the elastic behavior of the cellulose gel was substantially extended, enduring much higher shear stress when loaded at a frequency of 1 Hz.
3. The gel formed by NFC-TEMPO, with a higher percentage of nanofibrils and ionic charge than NFC-carb, exhibited a superior performance despite the much lower cellulose DP.

ACKNOWLEDGEMENTS

The research undertaken for this paper was performed under the UBI-Celtejo agreement. The authors would also like to thank Engineer Paulo João and Mapril (Maia, Portugal) for kindly providing the authors with the Mütek PCD-02 Particle Charge Detector.

REFERENCES CITED

Benhamou, K., Dufresne, A., Magnin, A., Mortha, G., and Kaddami, H. (2014). "Control of size and viscoelastic properties of nanofibrillated cellulose from palm tree by varying the TEMPO-mediated oxidation time," *Carbohyd. Polym.* 99, 74-83. DOI: 10.1016/j.carbpol.2013.08.032

Bhushan, B., and Jung, Y. C. (2011). "Natural and biomimetic artificial surfaces for superhydrophobicity, self-cleaning, low adhesion, and drag reduction," *Prog. Mater. Sci.* 56(1), 1-108. DOI: 10.1016/j.pmatsci.2010.04.003

Buscall, R. (2010). "Wall slip in dispersion rheometry," *J. Rheol* 54(6), 1177-1183. DOI: 10.1122/1.3495981

Chen, P., Yu, H., Liu, Y., Chen, W., Wang, X., and Ouyang, M. (2013). "Concentration effects on the isolation and dynamic rheological behavior of cellulose nanofibers *via* ultrasonic processing," *Cellulose* 20(1), 149-157. DOI: 10.1007/s10570-012-9829-7

Fall, A. B., Lindström, S. B., Sundman, O., Odberg, L., and Wågberg, L. (2011). "Colloidal stability of aqueous nanofibrillated cellulose dispersions," *Langmuir* 27(18), 11332-11338. DOI: 10.1021/la201947x

Fukuzumi, H., Tanaka, R., Saito, T., and Isogai, A. (2014). "Dispersion stability and aggregation behavior of TEMPO-oxidized cellulose nanofibrils in water as a function of salt addition," *Cellulose* 21(3), 1553-1559. DOI: 10.1007/s10570-014-0180-z

Haavisto, S., Koponen, A. I., and Salmela, J. (2014). "New insight into rheology and flow properties of complex fluids with Doppler optical coherence tomography," *Front. Chem.* 2, 1-6. DOI: 10.3389/fchem.2014.00027

Håkansson, K. M. O., Fall, A. B., Lundell, F., Yu, S., Krywka, C., Roth, S. V., Santoro, G., Kvick, M., Wittberg, L. P., Wågberg, L., *et al.* (2014). "Hydrodynamic alignment and assembly of nanofibrils resulting in strong cellulose filaments," *Nat. Commun.* 5(4018), 1-10. DOI: 10.1038/ncomms5018

Hauru, L. K. J., Hummel, M., Michud, A., and Sixta, H. (2014). "Dry jet-wet spinning of strong cellulose filaments from ionic liquid solution," *Cellulose* 21(6), 4471−4481. DOI: 10.1007/s10570-014-0414-0

Henriksson, M., Henriksson, G., Berglunda, L. A., and Lindström, T. (2007). "An environmentally friendly method for enzyme-assisted preparation of microfibrillated cellulose (MFC) nanofibers," *Eur. Polym. J.* 43(8), 3434-3441. DOI: 10.1016/j.eurpolymj.2007.05.038

Hubbe, M., Ferrer, A., Tyagi, P., Yin, Y., Salas, C., Pal, L., and Rojas, O. (2017a). "Nanocellulose in thin films, coatings, and plies for packaging applications: A review," *BioResources* 12(1), 2143-2233.

Hubbe, M. A., Tayeb, P., Joyce, M., Tyagi, P., Kehoe, M., Dimic-Misic, K., and Pal, L. (2017b). "Rheology of nanocellulose-rich aqueous suspensions: A Review," *BioResources* 12(4), 9556-9661.

Iwamoto, S., Isogai, A., and Iwata, T. (2011). "Structure and mechanical properties of wet-spun fibers made from natural cellulose nanofibers," *Biomacromolecules* 12(3), 831-836. DOI: 10.1021/bm101510r

Iwamoto, S., Lee, S., and Endo, T. (2013). "Relationship between aspect ratio and suspension viscosity of wood cellulose nanofibers," *Polym. J.* 6(1), 73-76. DOI: 10.1038/pj.2013.64

Iotti, M., Gregersen, Ø. W., Moe, S., and Lenes, M. (2011). "Rheological studies of microfibrillar cellulose water dispersions," *J. Polym. Environ.* 19(1), 137-145. DOI: 10.1007/s10924-010-0248-2

Ishii, D., Saito, T., and Isogai, A. (2011). "Viscoelastic evaluation of average length of cellulose nanofibers prepared by tempo-mediated oxidation," *Biomacromolecules* 12(3), 548-550. DOI: 10.1021/bm1013876

ISO 5351 (2012). "Pulps -- Determination of limiting viscosity number in cupriethylenediamine (CED) solution," International Organization for Standardization, Geneva, Switzerland.

Janardhnan, S., and Sain, M. (2006). "Isolation of cellulose microfibrils - An enzymatic approach," *BioResources* 1(2), 176-188. DOI: 10.15376/biores.1.2.176-188

Jowkarderis, L., and Van de Ven, T. G. M. (2014). "Intrinsic viscosity of aqueous suspensions of cellulose nanofibrils," *Cellulose* 21(4), 2511-2517. DOI: 10.1007/s10570-014-0292-5

Karppinen, A., Saarinen, T., Salmela, J., Laukkanen, A., Nuopponen, M., and Seppälä, J. (2012). "Flocculation of microfibrillated cellulose in shear flow," *Cellulose* 19(6), 1807-1819. DOI: 10.1007/s10570-012-9766-5

Lowys, M. -P., Desbrières, J., and Rinaudo, M. (2001). "Rheological characterization of cellulosic microfibril suspensions. Role of polymeric additives," *Food Hydrocolloid.* 15(1), 25-32. DOI: 10.1016/S0268-005X(00)00046-1

Mendoza, L., Batchelor, W., Tabor, R., and Garnier, G. (2018). "Gelation mechanism of cellulose nanofibre gels: A colloids and interfacial perspective," *J. Colloid Interf. Sci.* 509, 39-46. DOI: 10.1016/j.jcis.2017.08.101

Mohtaschemi, M., Dimic-Misic, K., Puisto, A., Korhonen, M., Maloney, T., Paltakari, J., and Alava, M. J. (2014). "Rheological characterization of fibrillated cellulose suspensions *via* bucket vane viscometer," *Cellulose* 21(3), 1305-1312. DOI: 10.1007/s10570-014-0235-1

Naderi, A., Lindström, T., and Pettersson, T. (2014a). "The state of carboxymethylated nanofibrils after homogenization-aided dilution from concentrated suspensions: A rheological perspective," *Cellulose* 21(4), 2357-2368. DOI: 10.1007/s10570-014-0329-9

Naderi, A., Lindström, T., and Sundström, J. (2014b). "Carboxymethylated nanofibrillated cellulose: Rheological studies," *Cellulose* 21(3), 1561-1571. DOI: 10.1007/s10570-014-0192-8

Naderi, A., and Lindström, T. (2014). "Carboxymethylated nanofibrillated cellulose: Effect of monovalent electrolytes on the rheological properties," *Cellulose* 21(5), 3507-3514. DOI: 10.1007/s10570-014-0394-0

Naderi, A., and Lindström, T. (2015). "Rheological measurements on nanofibrillated cellulose systems: A science in progress," in *Cellulose and Cellulose Derivatives: Synthesis, Modification and Applications*, M. I. H. Mondal (ed.), Nova Science Publishers, Inc., New York, NY, USA.

Naderi, A., Koschellab, A., Heinzeb, T., Shihc, K., Niehc, M., Pfeiferb, A., Change, C., and Erlandssonf, J. (2017). "Sulfoethylated nanofibrillated cellulose: Production and properties," *Carbohyd. Polym.* 179, 515-523. DOI: 10.1016/j.carbpol.2017.04.026

Nechyporchuk, O., Belgacem, M. N., and Pignona, F. (2014). "Rheological properties of micro-/nanofibrillated cellulose suspensions: Wall-slip and shear banding phenomena," *Carbohyd. Polym.* 112, 432-439. DOI: 10.1016/j.carbpol.2014.05.092

Nechyporchuk, O., Belgacem, M. N., and Pignon, F. (2015). "Concentration effect of TEMPO-oxidized nanofibrillated cellulose aqueous suspensions on the flow instabilities and small-angle X-ray scattering structural characterization," *Cellulose* 22(4), 2197-2210. DOI: 10.1007/s10570-015-0640-0

Nechyporchukm, O., Belgacem, M. N., and Bras, J. (2016). "Production of cellulose nanofibrils: A review of recent advances," *Ind. Crop. Prod.* 93, 2-25. DOI: 10.1016/j.indcrop.2016.02.016

Onyianta, A. J., Dorris, M., and Williams, R. L. (2018). "Aqueous morpholine pre-treatment in cellulose nanofibril (CNF) production: Comparison with carboxymethylation and TEMPO oxidization pre-treatment methods," *Cellulose* 25(2), 1047-1064. DOI: 10.1007/s10570-017-1631-0

Ovarlez, G., Rodts, S., Chateau, X., and Coussot, P. (2009). "Phenomenology and physical origin of shear localization and shear banding in complex fluids," *Rheol. Acta* 48(8), 831-844. DOI: 10.1007/s00397-008-0344-6

Pääkkö, M., Ankerfors, M., Kosonen, H., Nykänen, A., Ahola, S., Österberg, M., Ruokolainen, J., Laine, J., Larsson, P. T., Ikkala, O., *et al.* (2007). "Enzymatic hydrolysis combined with mechanical shearing and high-pressure homogenization for nanoscale cellulose fibrils and strong gels," *Biomacromolecules* 8(6), 1934-1941. DOI: 10.1021/bm061215p

Saarikoski, E., Saarinen, T., Salmela, J., and Seppälä, J. (2012). "Flocculated flow of microfibrillated cellulose water suspensions: An imaging approach for characterization of rheological behaviour," *Cellulose* 19(3), 647-659. DOI: 10.1007/s10570-012-9661-0

Saarinen, T., Lille, M., and Seppälä, J. (2009). "Technical aspects on rheological characterization of microfibrillar cellulose water suspensions," *Annu. Trans. Nord. Rheol. Soc.* 17, 121-130.

Saito, T., Kimura, S., Nishiyama, Y., and Isogai, A. (2007). "Cellulose nanofibers prepared by tempo-mediated oxidation of native cellulose," *Biomacromolecules* 8(8), 2485-2491. DOI: 10.1021/bm0703970

SCAN-CM 65:02 (2002). "Total acidic group content," Scandinavian Pulp, Paper and Board Testing Committee, Stockholm, Sweden.

Shinoda, R., Saito, T., Okita, Y., and Isogai, A. (2012). "Relationship between length and degree of polymerization of tempo-oxidized cellulose nanofibrils," *Biomacromolecules* 13(3), 842-849. DOI: 10.1021/bm2017542

Sluiter, A., Hames, B., Ruiz, R., Scarlata, C., Sluiter, J., Templeton, D., and Crocker, D. (2012). *Determination of Structural Carbohydrates and Lignin in Biomass* (NREL/TP-510-42618), National Renewable Energy Laboratory Golden, CO, USA.

Smith, D. K., Bampton, R. F., and Alexander, W. J. (1963). "Use of new solvents for evaluating chemical cellulose for the viscose process," *Ind. Eng. Chem. Proc. DD.* 2(1), 57-62. DOI: 10.1021/i260005a012

Tanaka, R., Saito, T., Hänninen, T., Ono, Y., Hakalahti, M., Tammelin, T., and Isogai, A. (2016). "Viscoelastic properties of core-shell-structured, hemicellulose-rich nanofibrillated cellulose in dispersion and wet-film states," *Biomacromolecules* 17(6), 2104-2111. DOI: 10.1021/acs.biomac.6b00316

Tanaka, R., Saito, T., Hondo, H., and Isogai, A. (2015). "Influence of flexibility and dimensions of nanocelluloses on the flow properties of their aqueous dispersions," *Biomacromolecules* 16(7), 2127-2131. DOI: 10.1021/acs.biomac.5b00539

Tanaka, R., Saito, T., Ishii, D., and Isogai, A. (2014). "Determination of nanocellulose fibril length by shear viscosity measurement," *Cellulose* 21(3), 1581-1589. DOI: 10.1007/s10570-014-0196-4

Wagberg, L., Decher, G., Norgren, M., Lindstrom, T., Ankerfors, M., and Axnas, K. (2008). "The build-up of polyelectrolyte multilayers of microfibrillated cellulose and cationic polyelectrolytes," *Langmuir* 24(3), 784-795. DOI: 10.1021/la702481v

Walther, A., Timonen, J. V., Diez, I., Laukkanen, A., and Ikkala, O. (2011). "Multifunctional high-performance biofibers based on wet-extrusion of renewable native cellulose nanofibrils," *Adv. Mater.* 23(26), 2924-2928. DOI: 10.1002/adma.201100580

Xu, Y., Atrens, A. D., and Stokes, J. R. (2018). " 'Liquid, gel and soft glass' phase transitions and rheology of nanocrystalline cellulose suspensions as a function of concentration and salinity," *Soft Matter* 14, 1953-1963. DOI: 10.1039/C7SM02470C

Article submitted: May 2, 2019; Peer review completed: July 13, 2019; Revised version received and accepted: July 30, 2019; Published: August 5, 2019.
DOI: 10.15376/biores.14.4.7636-7654

3.1.1. Supplementary investigation

Additional controlled rate flow essays were performed on a 1.3 wt.% NFC-carb suspension containing 1000 mM of NaCl in order to determine the effect of smooth *vs* roughened surfaces on the rheology of the suspension. Figure 23 shows the previous and resulting appearance of the suspension during the flow essay with smooth and roughened surfaces.

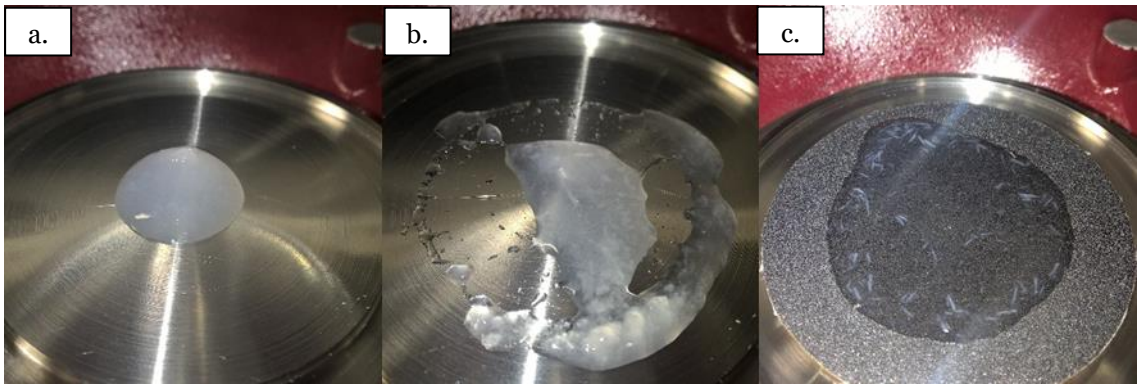

Figure 23. Initial (a.) and final appearances of an NFC-carb suspension with 1 M of NaCl after a controlled rate flow essay performed with smooth (b.) and roughened (c.) surfaces

After a controlled rate flow essay performed with smooth surfaces, phase separation of the suspension could be perceived (figure 23 b). This instability manifested by a gradual phase-separation (de-watering of the sample) and accelerated by an external force has been reported by Naderi and Lindström (2015) on a 2 wt.% enzymatically pre-treated NFC sample, after insertion in a smooth surfaced plate-plate geometry. Furthermore, although NFC suspensions are inherently prone to flocculation, Saarikoski *et al.* (2012) using smooth surfaced concentric cylinders geometries, also reported high-pressure homogenization pretreated 1 wt.% NFCs suspensions increased tendency to flocculate in the presence of NaCl in concentrations of 10^{-3} M and higher, due to the decrease in interfibrillar repulsion.

On the other hand, after essays performed with roughened surfaces, filament-like aggregations could be easily spotted (figure 23 c). These results are in good agreement with those obtained by Gallier *et al.,* (2014) which demonstrated that surface roughness and inter-particle friction can significantly contribute to flocculation within sheared suspensions.

In order to study the structural changes in 1.3 wt.% NFC-carb suspensions with NaCl (100, 300 and 1000 mM) under shear and the formation of the filament-like aggregates, controlled rate time essays were performed at two constant shear rates: 10 and 100 s^{-1}. The essays were stopped at 3, 10, 30, 60 and 180 seconds and pictures of the resulting samples' appearance were gathered. The outcome is portrayed in table 2.

Table 2. Appearance monitorization of NFC-carb samples with different NaCl concentrations during controlled rate flow essays

NaCl (mM)	100		300		1000	
Shear rate (s^{-1}) / Essay time (s)	10	100	10	100	10	100
3						
10						
30						
60						
180						

As we can infer from in table 2, the fibrils collided and entangled to form filament-like aggregates under specific flow conditions. When suspensions of elongated particles like cellulose fibrils in NFC suspensions are exposed to flow, there is a preferential orientation and the fibrils tend to align in the direction of the flow (Hubbe *et al.*, 2017), in this case twisting around and aggregating to form the perceived filaments. According to Saarikoski *et al.*, (2012), under shear, the initial fiber network breaks gradually, and at sufficiently high shear rates, the suspension can flow as individual aggregates.

A lower shear rate favored the formation of these filament-like aggregates, as so did less time under shear, since the flow breaks down the aggregates by eroding their surfaces or by splitting them in smaller pieces (Karppinen *et al.,* 2012; Saarikoski *et al.,* 2012). Thus, a lower shear rate induced larger aggregates. These results are in good agreement with those reported by Karppinen *et al.* (2012) who studied the flow induced flocculation of microfibrillated cellulose suspensions at constant shear rates with a concentric cylinder geometry and image monitoring

throughout the essays. According to these authors after constant shear, the floc size was dependent on the preceding shear interval, and a lower shear rate induced larger flocs.

It is also possible to notice from table 2 that, despite the perceptible formation of aggregates in the first 10 seconds, there was a gradual redispersion of the suspension over time, mainly at higher shear rates and lower NaCl concentration. The same kind of behavior was also reported by Chen *et al.* (2002) who studied the flocculation of pulp and polyethylene terephthalate fiber suspensions with a parallel-plates type rheometer.

Higher concentrations of NaCl also favored the formation of aggregates even at a higher shear rate, which makes sense, since the aggregate strength is determined by the number of contacts and cohesive forces present between the fibers and, as has been previously mentioned, the increase of the NaCl in the suspension decreases the electrostatic repulsion between the fibers, causing their collapse.

In the table 2 it is also noticeable that the essays performed with suspensions with 300 and 1000 mM of NaCl at a shear rate of 100 s-1 and for 60 and 180 seconds, apart from filament-like aggregates, also present some distinct spherical aggregates. Similar results were obtained by Saarikoski *et al.* (2012) which studied the flocculation process by performing imaging monitored flow rheological measurements with a concentric cylinder geometry on microfibrillated cellulose suspensions with added NaCl. These authors have realized that, at low shear rates, the loosened flocs flowed in a chain-like formation and at higher rates, the floc chains buckled and then separated into individual, spherical flocs. The individual spherical floc size was inversely proportional to the shear rate.

3.2. Effect of NFC suspensions solid content and spinning rate on the mechanical properties of wet-spun filaments

Abstract

Commercial bleached sulfite and kraft eucalypt pulps were subjected to beating and to different TEMPO mediated oxidation systems prior to the production of nanofibrillated cellulose aqueous suspensions through high pressure homogenization. The fibrils from both resulting suspensions were morphologically characterized and the suspensions with solid contents from 2.5 to 3.22% were used to produce cellulosic filaments through wet spinning, at spinning rates ranging from 0.45 to 1.7 m min^{-1} into a 1M NaCl coagulation bath, followed by an ethanol fixation bath. Some filaments were subjected to an additional cleaning water bath. All filaments were dried in standard conditions of temperature and relative humidity and were tested for mechanical performance. Results showed that an increase in spinning rate improved the mechanical performance of the filaments, indicating that some level of fibril alignment, while increasing solid content did not, due to higher viscosity and lower capacity for fibril alignment. More fibrillated cellulose exhibited higher mechanical properties denoting the important role of fibril's morphology in the filament's assembly despite the lower cellulose degree of polymerization. An additional cleaning water bath increased the mechanical performance of the filaments due to the removal of the residual NaCl. The wet spinning system enabled the production of cellulosic filaments with a tensile strength up to 223 MPa and an elastic modulus up to 11.7 GPa using a 3 wt.% nanofibrillated cellulose, despite the low spinning rate of 0.85 m min^{-1}.

Keywords

Nanofibrillated cellulose; wet spinning; filaments; mechanical performance.

Introduction

In recent decades, natural fibrous materials like cellulose fibrils have been receiving increasing attention due to their potential to produce high mechanical performance filaments, while respecting industrial, environmental, and social requirements. These fibrils constitute the basic blocks to construct low environmental impact and low production cost biomaterials, with high mechanical performance and susceptible to nanoscale functionalization (Bledzki, 1999; Håkansson *et al.*, 2014).

The obtention of cellulosic filaments from lignocellulosic materials and their transformation into yarns with uniform characteristics, through "green" and energetically sustainable processes is challenging. In order to produce a uniform material, it is necessary to deconstruct the cellulosic fiber structure into cellulose nanofibrils and rebuild them in the form of filament or macrofiber, under such operating conditions that lead to uniformity and consistency of properties (Håkansson *et al.*, 2014). The potential of these filaments when applied as reinforcement in advanced composites, for instance, is ultimately limited by the intrinsic properties and the natural variability of the fibers that gave rise to them (Adusumali *et al.*, 2006).

The highly hydrophilic nature of cellulose and its absence of melting transition prevents the application of melt spinning as a way to manufacture filaments made out of 100% cellulose nanofibrils, although this spinning method can be applied when cellulose nanofibrils are added to either natural or synthetic polymers, giving rise to composite filaments (Clemons, 2016; Lundahl *et al.*, 2016a).

Spinning of continuous filaments from NFC is an interesting option because it has the potential to effectively use the very fine dimensions of the fibrils while maintaining its Cellulose I native structure (Clemons, 2016). In addition, the crystalline structure of regenerated cellulose (referred to as Cellulose II) is different from that of cellulose in its native state (i.e., Cellulose I). While reported values for the mechanical performance of these two types of crystalline structures vary considerably depending on the measurement technique, the values for Cellulose I are reported as considerably higher (Moon *et al.*, 2011).

The production of neat NFC filaments *via* either dry or wet spinning has been accomplished by several authors. Ghasemi *et al.* (2017) studied the influence of different NFC suspensions starting properties and drying temperature on the mechanical properties of filaments produced through dry spinning. Their results showed that, while the drying temperature had no substantial influence on the mechanical properties of the produced NFC filaments, the fibrils morphological properties played an important role in that matter, since the mechanical performance of the filaments improved with increasing grinding time of the starting material, which can be attributed to increased internal hydrogen bonding.

While the morphology of the fibrils is a key aspect related to the overall performance of the spun filaments, several studies indicate that so is the overall fibrils orientation and assembly in the resulting filament: due to the relatively low aspect ratio, NFC cannot be drawn during spinning as easily as dissolved polymers. Hence, alternative approaches are required for creating the extensional flow necessary for effective fibril alignment (Lundahl *et al.*, 2016a).

Iwamoto *et al.*, (2011) reported the production of wet-spun NFC filaments from TEMPO-mediation oxidized wood pulp and tunicate cellulose, varying the spinning rate in order to promote nanofibril alignment. According to the authors, the mechanical properties of the spun filaments were affected by the orientation of the cellulose nanofibers, as increased spinning rate promoted nanofibril alignment along the filaments axis. The wet spun filaments showed higher Young's moduli than natural and regenerated cellulose fibers.

Walther *et al.* (2011) have performed wet spinning of NFC suspensions into neat NFC filaments with decent mechanical performance, but they hypothesized that the mechanical properties could be further increased by post drawing processes, promoting additional alignment to the nanofibrils. Indeed, tensile strength and stiffness are typically improved with high draw ratios as a result of the enhanced alignment (Lundahl *et al.*, 2016a; Kim *et al.* 2019). Torres-Rendon *et al.* (2014) reported a strain-rate controlled wet-stretching of rehydrated NFC and chitin filaments as a way of inducing fibril alignment. This approach consisted of immersing dry filaments in water and taking advantage of the wet filaments' plasticity to stretch them slowly, improving their Young's modulus by more than 300% (from 8.2 to 33.7 GPa) and their tensile strength by close to 150% (from 118 to 289 MPa), regarding unstretched filaments.

Håkansson *et al.* (2014) reported a flow-focusing system where an NFC dispersion ran through a core flow while two additional NaCl solution sheath flows collided with it from the sides. Because these sheath flows have higher velocities than the core flow, they create an extensional flow in the core inducing fibril alignment while promoting gel transition of the NFC dispersion, which locks the aligned fibril structure prior to fixation through solvent exchange in acetone. While air drying, the filaments were not further drawn, nor they were allowed to shrink. Filaments spun through this flow focusing technique attained a Young's modulus up to 18 GPa and a tensile strength up to 490 MPa.

Although both systems enhance fibril alignment, a comparison between wet-stretched and flow focused NFC filaments allows to realize that wet-stretching increases mainly the Young's modulus whereas flow-focusing improves more specifically the tensile strength and ductility, effectively contributing to uniformly pack the NFC. This can be the reason why flow-focused filaments avoid the brittleness associated to wet-stretched filaments (Lundahl *et al.*, 2016b).

Apart from the production of filaments from neat NFC, the addition of cellulose nanofibrils to composites was found to improve the mechanical and thermal properties of produced composite filaments. Several authors have also reported the production of composite filaments

through wet spinning, combining NFC and poly(vinyl alcohol) (PVA): Fahma *et al.* (2019) have accomplished wet spinning of biocompatible composite NFC-PVA filaments from palm oil by-products derived NFC; Endo *et al.* (2013) have also performed wet spinning of composite filaments from a TEMPO-mediation oxidized NFC combined with PVA. These authors have further performed a hot drawing technique (with a drawn ratio of 20), promoting the orientation of amorphous PVA regions in the filaments to which small amounts of NFC had been added. The maximum Young's modulus of the obtained composite drawn filaments reached 57 GPa, which is far higher than that of commercial neat PVA drawn fibers.

Considering the influence of the solid content on the fibril's mobility in the suspension and apparent viscosity, the objective of this study was to investigate the influence of NFC suspensions solid content and wet spinning operation conditions on the mechanical performance of the wet-spun filaments.

Materials and methods

NFC production

Dried commercial bleached sulfite and kraft eucalypt pulps were used as sources of cellulose fibers to produce NFC aqueous suspensions. Both pulps were subjected to beating in a PFI mill according to the ISO 5264-2:2011 standard, for 4500 revolutions at 1.66 N/m. After beating, the sulfite pulp was further subjected to 2,2,6,6-tetramethylpiperidine-1-oxyl radical (TEMPO) mediated oxidation (TEMPO/NaBr/NaClO system) using a method adapted from Saito *et al.* (2007). The treatment took place at room temperature and at a consistency of 1 wt.% in the presence of 0.016 g of TEMPO/g cellulose and 0.1 g of NaBr /g cellulose. 33.3 mL of 13 wt.% NaClO/g cellulose were introduced in the reaction medium in four increasingly larger additions in one-hour intervals, under continuous agitation. The pH was continuously monitored and kept at around 10.5 with small additions of a 1M NaOH solution. After the last NaClO addition the reaction was allowed to continue for an hour and the treated pulp was vacuum filtrated and washed with distilled water. The treated sulfite pulp will henceforth be designated NFC-s.

The kraft pulp was subjected to a different TEMPO mediated oxidation using a TEMPO/NaClO/$NaClO_2$ system based on Tanaka *et al.* (2012a). This method involved the addition of 0.9 g of $NaClO_2$/g cellulose, 0.5 mL of 13 wt.% NaClO/g cellulose and 0.016 g TEMPO/g cellulose to the pulp immersed in a 0.1 M and pH 6.8 phosphate buffer at a consistency of 1 wt.%. The treatment lasted for 24 hours at a temperature of 60ºC. Then, the system was brought to room temperature, the treated pulp was vacuum filtered and washed with distilled water. The treated kraft pulp will from now on be referred to as NFC-k.

After the TEMPO mediated oxidations, both oxidized pulps were resuspended in distilled water at a solid content of 1.5 wt.% and were subjected to high pressure homogenization in 2 successive passes (500 bar and 1000 bar), using a GEA Niro Soavi (Panther NS3006L; GEA, Parma, Italy).

Cellulose degree of polymerization

The limiting viscosity ([η]) of the original and TEMPO oxidized pulps was determined according to the ISO 5351 (2012) standard, with a cupriethylenediamine (CED) solution as a solvent and using a capillary viscometer. The resulting [η] and DP are presented in table 1. The degree of polymerization (DP) was calculated using the following equations [1, 2] (Henriksson *et al.*, 2008).

$[\eta] = 0.42 \times DP; \quad DP < 950$ [1]

$[\eta] = 2.28 \times DP^{0.76}; \quad DP \geq 950$ [2]

Where is [η] is the limiting viscosity (mL/g) and DP is the degree of polymerization.

Table 1. Limiting viscosity and degree of polymerization of the original and TEMPO oxidized pulps

NFC suspension	Before TEMPO mediated oxidation		After TEMPO mediated oxidation	
	[η] (mL/g)	DP	[η] (mL/g)	DP
NFC-s	587	1486	85	202
NFC-k	824	2322	356	848

Fibrils morphological characterization

After homogenization, the NFC-s and NFC-k suspensions were diluted to a solid content of 0.1 wt.% and were dispersed in an ultra-sound bath for 5 minutes. A drop of the diluted suspension was allowed to dry overnight at room temperature on a microscope sample holder. Microscopy observations were performed using scanning electron microscopy (SEM) (Hitachi S-2700) operated at 20 kV. All the samples were previously gold sputtered by cathodic spraying. For transmission electron microscopy (TEM) imaging, aqueous NFC suspensions were diluted to 0.001 wt.% and sonicated. Drops of the suspensions were deposited on carbon coated electron microscope grids and negatively stained with 2 wt. % uranyl acetate. The grids were air dried and observed with a Hitachi HT – 7700 TEM operated at an acceleration voltage of 80 keV.

Wet spinning set-up

NFC-s and NFC-k suspensions were used to produce cellulosic filaments through wet spinning. The original suspensions (with an initial solid content of around 1 wt. %) were let to evaporate at room temperature with occasional mixing until the desired solid content was reached. The NFC-s was adjusted to 3.0 wt. % and the NFC-k was adjusted to 2.5 and 3.22 wt. %.

The wet spinning set-up consisted of a syringe filled with NFC suspension (assembled in a syringe pump) that ejected filaments through a 2.5 cm long blunt needle, with an inner diameter of 1.5 mm, at three different flow rates: 800, 1500 and 3000 μL min^{-1}, (which correspond to spinning rates of 0.45, 0.85 and 1.7 m min^{-1}, respectively) into a 1M NaCl coagulation bath, promoting gelation by decreasing the electrostatic repulsion between the

nanofibrils. Figure 1 provides a schematic representation of the wet spinning setup put together for this study.

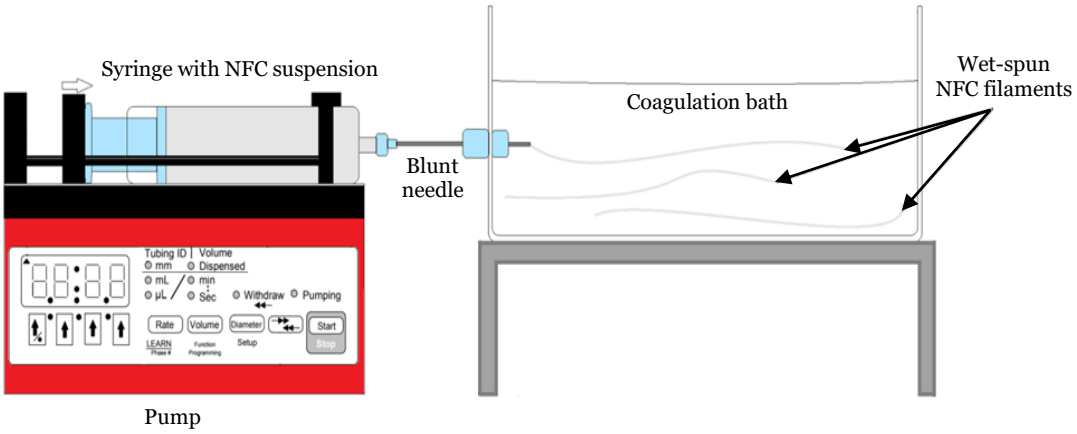

Figure 1. NFC suspensions wet-spinning setup

The wet-spun filaments remained in the coagulation bath for 30 minutes and were then transferred to an ethanol fixation bath for an additional 30 minutes. Then, they were allowed to air dry at room conditions, with fixed length, preventing them from shrinking during drying. As a post-treatment, some of the produced filaments were afterwards submerged in a water bath for 5 minutes, in order to enable the electrolyte diffusion out of the filaments. Finally, the filaments were air dried once again.

Mechanical characterization of the wet-spun filaments

The diameter of the filaments was measured through optic microscopy against a glass slide with a measuring scale, assuming a circular cross section. The produced filaments were conditioned overnight in standard conditions (22ºC and 50% relative humidity), before testing. Tensile tests were carried out using a universal testing machine (Thwing-Albert Co, EJA series) in the same standard environment. The essays were performed at a rate of 0.2 mm/min with a 50 N load cell and at 5 cm span length. A minimum of 6 essays were performed for each type of filament and the arithmetic average is presented for each parameter.

Results and discussion

The fibrils morphology on the suspensions was investigated through SEM and TEM imaging. Figure 2 gives an overview of the morphologic features of NFC-s and NFC-k.

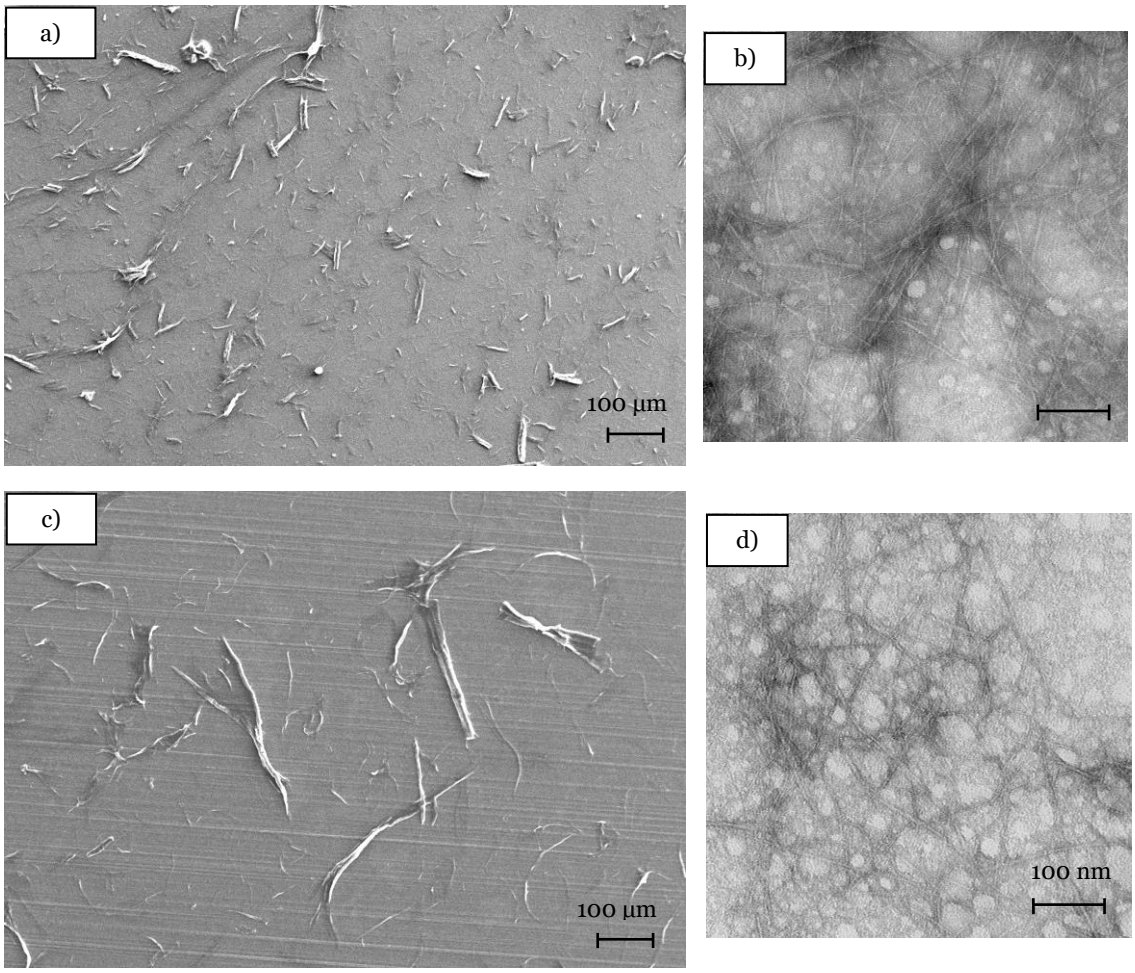

Figure 2. SEM (a, c) and TEM (b, d) images of the NFC-s (a, b) and NFC-k (c,d) suspensions

As it can be seen in figure 2, the fibrillation of the materials appears to be not uniform. Although fine fibrillar structures with diameters in the nanometer range can be spotted, bigger cellulose fibrils with dimensions in the microscale are also clearly visible for both NFC suspensions. Despite that, the NFC-s appears to be more fragmented than the NFC-k, with much more particles on the smaller side (figure 2 a *vs* c), although no major difference between the two materials could be noted at nanoscale (figure 2 b *vs* d).

The treatments underwent by the NFC-s caused a decrease of 86.4% on the polymerization degree (from 1486 to 202), while in the NFC-k case the polymerization degree declined 63.5% (from 2322 to 848), relatively to the initial untreated materials, denoting the grater severity on the NFC-s treatment. This agrees with what is described in the literature for TEMPO/NaBr/NaClO *vs* TEMPO/NaClO/$NaClO_2$ systems, in which the latter is reported to be effective for the preparation of TEMPO-oxidized hardwood celluloses with higher DP values (Tanaka *et al.* 2012b).

Figure 3 shows the resulting NFC-k (2.5 wt. %) wet-spun filaments produced with a spinning rate of 1.7 m min^{-1} and air dried under tension.

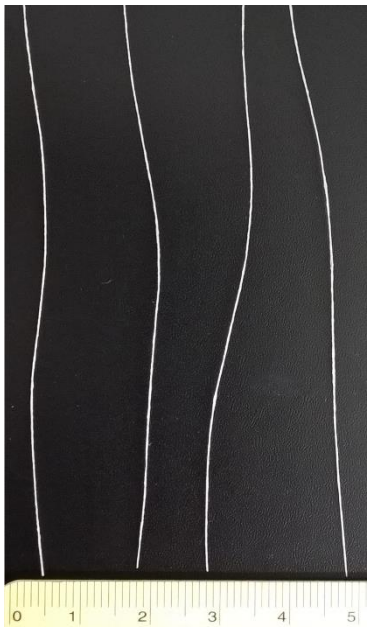

Figure 3. Appearance and dimensions of NFC filaments produced through wet spinning

Figure 4 shows SEM images of wet spun filaments from NFC-k and NFC-s suspensions at a spinning rates of 1.70 and 0.85 m min^{-1}, respectively, after an additional 5-minute water bath.

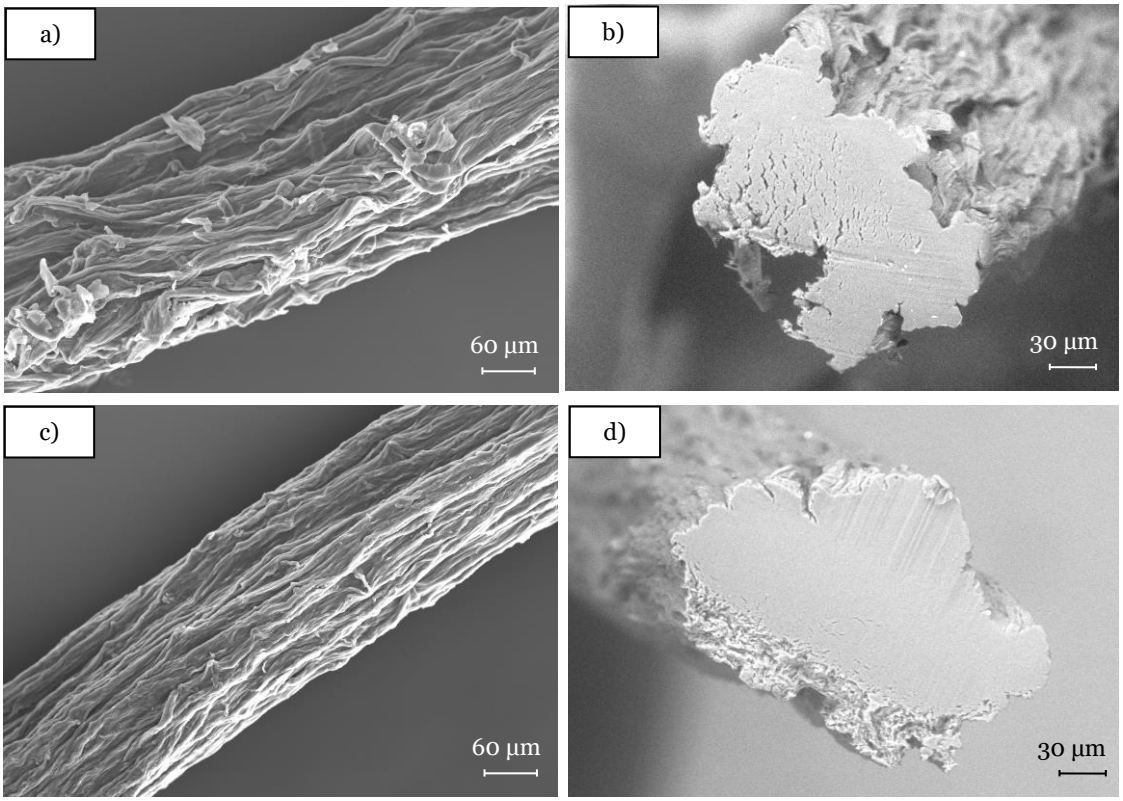

Figure 4. SEM images of filaments wet-spun from a 3.22 wt. % NFC-k suspension at a spinning rate of 1.70 m min^{-1} (a, b) and a 3 wt. % NFC-s suspension at a spinning rate of 0.85 m min^{-1} (c, d) along their length (a, c) and razor cut cross sections (b, d), after a water bath and drying

The produced filaments appear to be void free and their cross section appear to be fairly circular in shape, even after reimersion in a 5-minute water bath and second drying, as can be seen in figure 4 b and d.

The regular cross-sectional shapes of the wet-spun filaments were not significantly affected by the change in spinning rates, unlike what was described by Iwamoto *et al.* (2011), who reported irregular shapes of wet-spun filaments produced from wood nanofibers in an acetone coagulation bath and dried at 105°C, for spinning rates between 0.1 and 1 m min^{-1} and even show a hollow structure at spinning rates above 10 m min^{-1}, probably due to cylindrical coalescence of fibrils sheets during spinning.

Table 2 shows the mechanical performance of all the tested wet-spun filaments. They have been evaluated regarding the maximum force, tensile strength, strain-to-failure, and elastic modulus.

Table 2. Wet-spinning operating conditions and mechanical properties of the produced filaments

NFC susp.	Solid content (wt. %)	Spinning rate (m min^{-1})	Filament diameter (μm)	Filament density (g cm^{-3})	Additional washing	Linear mass (dtex)	Tensile strength (MPa)	Max. force (N)	Tenacity (cN/dtex)	Strain-to-failure (%)	Elastic modulus (GPa)
NFC-k	2.5	0.45	199	1.67	No	5.2	109.3	3.4	65.4	4.5	6.8
		0.85	204	2.02	No	6.6	129.4	4.2	63.6	6.0	7.1
		1.70	221	1.41	No	5.4	139.0	5.3	98.1	7.7	8.2
	3.22	1.70	295	1.17	No	8.0	84.0	5.7	71.3	2.73	7.5
		1.70	246	1.43	Yes	6.8	148.5	7.6	111.8	7.16	6.6
NFC-s	3.0	0.45	210	1.87	No	6.5	123.1	4.3	66.2	6.24	7.7
		0.85	187	2.08	No	5.7	148.2	4.1	71.9	5.98	9.1
		0.85	161	2.06	Yes	4.2	223.0	4.5	107.1	6.29	11.7

Table 2 shows that, in general, an increase in the spinning rate improved the resistance parameters of the wet-spun filaments, which might indicate that some level of fibril alignment is being achieved. This result is in good agreement with what has been reported in the literature (Iwamoto *et al.,* 2011; Håkansson *et al.,* 2014) although in the current investigation the filaments have been spun at much lower rates. The increase in the strain-to-failure is also a good indication on fibril alignment.

Unsurprisingly, an increase in the NFC-k suspension solid content, from 2.5% to 3.22%, caused an increase in the linear mass of filaments produced with the same spinning conditions, from 5.4 to 8.0 dtex (g/10 000m), respectively. However, this did not translate into superior mechanical performance of the filaments. For instance, for a spinning rate of 1.7 m min^{-1} and no additional waching, the tensile strength decreased from 139.0 to 84.0 MPa with the increase of the suspensions solid content, and the tenacity decreases from 98.1 to 71.3 cN/dtex. These

results agree with the ones obtained by Lundahl *et al.* (2016b), who attribute this behavior to the coexistence of higher hydrogel viscosity and hydrogel apparent density as well as lower capacity for fibril alignment upon filament formation in systems with lower water volume fraction. The same authors reported that improved quality of spun filaments can be achieved at low hydrogel concentrations due to flow-induced alignment, with an optimum at 2% solids content, which is not far from the range of solid contents employed in the present study.

Considering the significant decrease of the filament's density from 1.41 (NFC-k, 2.5% solid content) to 1.17 (NFC-k, 3.22% solid content), we can suggest that this parameter can play an important role, as would be expected, probably also indicating lower packing, as a consequence of lower fibril alignment.

To further analyze these results, the filaments' densities were estimated based on the linear mass and the filaments diameters. The results were included in table 2. The values are, in general, higher than those of cellulose (1.5 g cm^{-3}), which suggests that a significant amount of NaCl remains in the filaments.

The effect of an additional filament washing with water was also studied. Filaments produced under the same conditions but submitted to an additional washing (Yes or No, Additional washing column in table 2) exhibited enhanced mechanical properties, mainly in the tensile strength, probably due to the removal of the residual NaCl whose presence might weaken the fibril-fibril interaction. In fact, in figure 5 a. it is possible to perceive NaCl crystals from the coagulation bath completely covering the surface of the filament, while a water bath and successive drying completely cleared the filament's surface (figure 5 b.) A water bath as short as 5 minutes proved to be effective in removing the NaCl from the previously fixed filaments, increasing the tensile strength from 84.0 to 148.5 MPa for NFC-k spun at 1.70 m min^{-1} and from 148.2 to 223.0 MPa for NFC-s spun at 0.85 m min^{-1} (table 2). Additional studies revealed that increasing the water bath residence time did not improve the mechanical performance of the filaments. Actually, longer residence times in the water bath (as long as 15 minutes) damaged the filaments integrity and the structures fell apart. As a consequence of the NaCl removal, both the linear mass and the cross-section of the filaments significantly decreased; the linear mass decreased 15% and 26% and the filaments diameter also decreased 17% and 14% for NFC-K and NFC-s, respectively. Because of these modifications, a drastic increase in tensile strength, tenacity and strain-to-failure was observed.

Regarding the effect of the NFC characteristics, filaments produced from NFC-s at a solid content of 3.0 wt. % had higher tensile strength than those produced from NFC-k at 2.5 wt. % (148.2 and 129.4 MPa respectively) for a spinning rate of 0.85 m min^{-1}, despite the fact that the NFC-s displayed a much lower degree of polymerization when compared to the NFC-k (202 *vs* 848). Therefore, we can hypothesize that fibril morphology and assembling alignment have a much more important role than the degree of polymerization of the cellulose in the material.

This also strongly suggests that the interfibrillar binding is the weak point in the structure, at this level of strength.

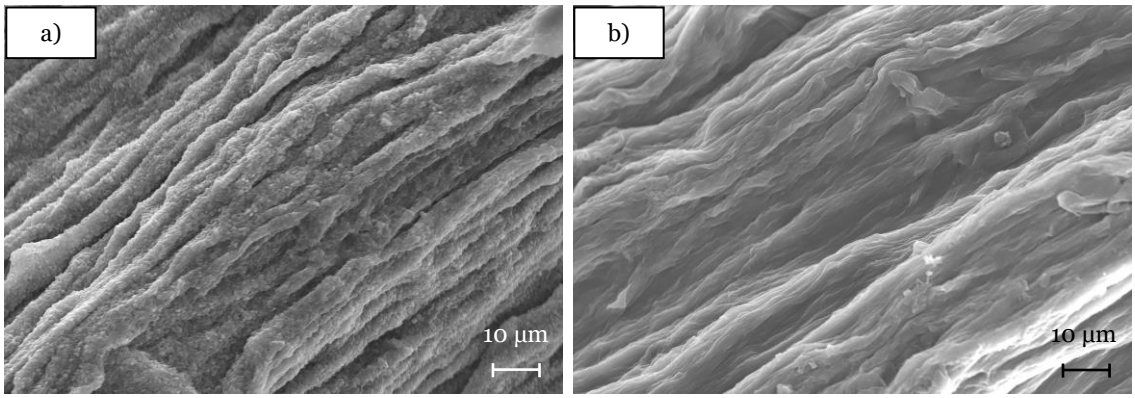

Figure 5. SEM images of a filament wet-spun from a 3 wt. % NFC-s suspension at a spinning rate of 0.85 m min^{-1} before (a) and after (b) a 5-minute water bath

Iwamoto *et al.* (2011) obtained wet spun filaments from a TEMPO-oxidized 2 wt.% NFC suspension using a regular wet spinning system where the filaments were directly spun into a fixation acetone bath and air-dried without drawing. At a spinning rate of 1 m min^{-1}, the authors achieved filaments with a tensile strength and Young's modulus of 192 MPa and 11.6 GPa, respectively, which are in the same order of magnitude of those produced in this study, for similar spinning rates. These authors also increased the spinning rate up to 100 m min^{-1}, leading to an increase of the tensile strength and Young's modulus to 321 MPa and 23.6 GPa, respectively, putting in evidence the role of the increased spinning rate in the fibril orientation in the spun filament, although no major increase of the mechanical performance, especially the tensile strength, was achieved by increasing the spinning rate from 10 to 100 m min^{-1}.

Lundahl *et al.* (2016b) reported the manufacture of 2 wt.% TEMPO-oxidized based wet spun filaments with a tensile strength of 297 MPa and an elastic modulus of 21 GPa, using once again a simple wet spinning assembly with an acetone fixation bath. These results were achieved at a spinning rate of 7.5 m min^{-1}.

In resume, the wet spinning system assembled for the present study enabled the production of cellulosic filaments with a tensile strength up to 223 MPa and an elastic modulus up to 11.7 GPa using a 3 wt.% NFC-s, despite being produced at a spinning rate of just 0.85 m min^{-1}.

Nevertheless, in the context of using NFC based spun filaments to replace industrially produced regenerated cellulose fibers, thus reducing the environmental footprint, the mechanical properties of the spun NFC filaments are still not yet comparable to those of viscose and Lyocell, for instance, which can attain tensile strengths of 340 and 790 MPa, and Young's modulus of 10.8 and 30.5 GPa, respectively (Adusumali *et al.* 2006).

Adjustments need yet to be undertaken on the operating conditions to further improve the fibril orientation during the spinning process, and consequently enhance the mechanical performance of the spun NFC filaments, namely increasing the spinning rate while figuring out suitable conditions for coagulation in other to be able to manufacture resilient continuous filaments, adjusting the solid content and viscosity of the initial NFC suspension and optimizing the drying conditions.

Conclusions

NFC filaments were successfully wet spun from two types of NFC suspensions into a NaCl 1M coagulation bath. After fixation in an ethanol bath and air drying, the filaments had smooth appearance and circular cross-sectional shapes.

The mechanical performance of the obtained filaments has been evaluated regarding the maximum force, tensile strength, strain-to-failure and elastic modulus.

Even for the studied low spinning rate range (0.45 to 1.70 m min^{-1}), an increase in the spinning rate improved the resistance parameters of the filaments, which might indicate that some level of fibril alignment is being achieved. The increase of solid content from 2.5 to 3.22 % did not improve the mechanical performance of the filaments, probably due to a combination of higher hydrogel viscosity and lower capacity for fibril alignment upon filament formation. Fibril's morphology also has an important role in the fibrils assembling in the filament because the more fibrillated NFCs exhibit significantly higher mechanical properties, despite their much lower cellulose degree of polymerization.

An additional filament washing with water and consecutive air-drying led to an increase in the mechanical performance of the filaments, mainly in the tensile strength probably due to the removal of the residual NaCl which might weaken the fibril-fibril interaction.

Despite some improvements on the filaments' mechanical properties have been achieved, nanofibril morphology, hydrodynamic nanofibril alignment, additional treatment and drying conditions have yet to be optimized.

References

Adusumali, R.-B., Reifferscheid, M., Weber, H., Roeder, T., Sixta, H., Gindl, W. (2006). Mechanical properties of regenerated cellulose fibres for composites. Macromolecular Symposia, 244(1), 119–125. Doi: 10.1002/masy.200651211

Bledzki, A. (1999). Composites reinforced with cellulose based fibres. Progress in Polymer Science, 24(2), 221–274. Doi: 10.1016/s0079-6700(98)00018-5

Clemons, C. (2016). Nanocellulose in spun continuous fibers: a review and future outlook. Journal of Renewable Materials, 4(5), 327–339. Doi: 10.7569/jrm.2016.634112

Endo, R., Saito, T., Isogai, A. (2013). TEMPO-oxidized cellulose nanofibril/poly(vinyl alcohol) composite drawn fibers. Polymer, 54(2), 935–941. Doi: 10.1016/j.polymer.2012.12.035

Fahma, F., Lisdayana, N., Abidin, Z., Noviana, D., Sari, Y. W., Mukti, R. R. et al. (2019). Nanocellulose-based fibres derived from palm oil by-products and their in vitro biocompatibility analysis. The Journal of The Textile Institute, 111(9), 1354–1363. Doi: 10.1080/00405000.2019.1694353

Ghasemi, S., Tajvidi, M., Bousfield, D., Gardner, D., Gramlich, W. (2017). Dry-spun neat cellulose nanofibril filaments: influence of drying temperature and nanofibril structure on filament properties. Polymers, 9(12), 392. Doi: 10.3390/polym9090392

Håkansson, K. M. O., Fall, A. B., Lundell, F., Yu, S., Krywka, C., Roth, S. V., et al. (2014). Hydrodynamic alignment and assembly of nanofibrils resulting in strong cellulose filaments. Nature Communications, 5(1). Doi: 10.1038/ncomms5018

Iwamoto, S., Isogai, A., Iwata, T. (2011). Structure and Mechanical Properties of Wet-Spun Fibers Made from Natural Cellulose Nanofibers. Biomacromolecules, 12(3), 831–836. Doi: 10.1021/bm101510r

Kim, H. C., Kim, D., Lee, J. Y., Zhai, L., Kim, J. (2019). Effect of Wet Spinning and Stretching to Enhance Mechanical Properties of Cellulose Nanofiber Filament. International Journal of Precision Engineering and Manufacturing-Green Technology, 6(3), 567–575. Doi: 10.1007/s40684-019-00070-z

Lundahl, M. J., Klar, V., Wang, L., Ago, M., Rojas, O. J. (2016a). Spinning of Cellulose Nanofibrils into Filaments: A Review. Industrial & Engineering Chemistry Research, 56(1), 8–19. Doi: 10.1021/acs.iecr.6b04010

Lundahl, M. J., Cunha, A. G., Rojo, E., Papageorgiou, A. C., Rautkari, L., Arboleda, J. C., Rojas, O. J. (2016b). Strength and Water Interactions of Cellulose I Filaments Wet-Spun from Cellulose Nanofibril Hydrogels. Scientific Reports, 6(1). Doi: 10.1038/srep30695

Moon, R. J., Martini, A., Nairn, J., Simonsen, J., Youngblood, J. (2011). Cellulose nanomaterials review: structure, properties and nanocomposites. Chemical Society Reviews, 40(7), 3941. Doi: 10.1039/c0cs00108b

Saito, T., Isogai, A. (2006). Introduction of aldehyde groups on surfaces of native cellulose fibers by TEMPO-mediated oxidation. Colloids and Surfaces A: Physicochemical and Engineering Aspects, 289(1-3), 219–225. Doi: 10.1016/j.colsurfa.2006.04.038

Torres-Rendon, J. G., Schacher, F. H., Ifuku, S., Walther, A. (2014). Mechanical Performance of Macrofibers of Cellulose and Chitin Nanofibrils Aligned by Wet-Stretching: A Critical Comparison. Biomacromolecules, 15(7), 2709–2717. Doi: 10.1021/bm500566m

Tanaka, A., Seppänen, V., Houni, J., Sneck, A., Pirkonenet, P. (2012a). Biorefinery. Nanocellulose characterization with mechanical fractionation. Nordic Pulp & Paper Research Journal, 27(4), 689–694. Doi: 10.3183/npprj-2012-27-04-p689-694

Tanaka, R., Saito, T., Isogai, A. (2012b). Cellulose nanofibrils prepared from softwood cellulose by TEMPO/NaClO/NaClO2 systems in water at pH 4.8 or 6.8. International Journal of Biological Macromolecules, 51(3), 228–234. Doi: 10.1016/j.ijbiomac.2012.05.016

Walther, A., Timonen, J. V. I., Díez, I., Laukkanen, A., & Ikkala, O. (2011). Multifunctional High-Performance Biofibers Based on Wet-Extrusion of Renewable Native Cellulose Nanofibrils. Advanced Materials, 23(26), 2924–2928. Doi: 10.1002/adma.201100580

3.3. Paper 2 - Effect of hot calendering on physical properties and water vapor transfer resistance of bacterial cellulose films

V. L. D. Costa, A. P. Costa, M. E. Amaral, C. Oliveira, M. Gama, F. Dourado and R. M. Simões
Journal of Materials Science (2016) 51:9562–9572
DOI 10.1007/s10853-016-0112-4

J Mater Sci (2016) 51:9562–9572

Effect of hot calendering on physical properties and water vapor transfer resistance of bacterial cellulose films

V. L. D. Costa[1], A. P. Costa[1,2], M. E. Amaral[1,2], C. Oliveira[3], M. Gama[3], F. Dourado[3], and R. M. Simões[1,2,*]

[1] *Research Unit of Fiber Materials and Environmental Technologies (FibEnTech - UBI), Universidade da Beira Interior, Rua Marquês d'Avila e Bolama, 6201-001 Covilhã, Portugal*
[2] *Department of Chemistry, Universidade da Beira Interior, 6201-001 Covilhã, Portugal*
[3] *CEB—Centre of Biological Engineering, University of Minho, 4710-057 Braga, Portugal*

Received: 23 March 2016
Accepted: 2 June 2016
Published online: 27 July 2016

ABSTRACT

This work investigates the effect of hot calendering on bacterial cellulose (BC) films properties, aiming the achievement of good transparency and barrier property. A comparison was made using vegetal cellulose (VC) films on a similar basis weight of around 40 $g.m^{-2}$. The optical–structural, mechanical, and barrier properties of BC films were studied and compared with those of highly beaten VC films. The Young's moduli and tensile index of the BC films are much higher than those obtained for VC (14.5–16.2 vs 10.8–8.7 GPa and 146.7–64.8 vs 82.8–40.3 $N.m.g^{-1}$), respectively. Calendering increased significantly the transparency of BC films from 53.0 to 73.0 %. The effect of BC ozonation was also studied. Oxidation with ozone somewhat enhanced the brightness and transparency of the BC films, but at the expenses of slightly lower mechanical properties. BC films exhibited a low water vapor transfer rate, when compared to VC films and this property decreased by around 70 % following calendering, for all films tested. These results show that calendering could be used as a process to obtain films suitable for food packaging applications, where transparency, good mechanical performance, and barrier properties are important. The BC films obtained herein are valuable products that could be a good alternative to the highly used plastics in this industry.

Introduction

Cellulose is a bio-based natural polymer, the most abundant polysaccharide in nature. Cellulose is extensively synthesized by plants, but it can also be produced by bacteria and tunicates [1]. Bacterial cellulose (BC) is mainly produced by gram-negative bacteria like *Gluconacetobacter xylinus*, *Gluconacetobacter sucrofermentans*. Using the appropriate growth conditions, these bacteria produce cellulose as a

Address correspondence to E-mail: rmss@ubi.pt

DOI 10.1007/s10853-016-0112-4

primary metabolic product in which the extracellular cellulose nanofibrils (of less than 10 nm width) form a three-dimensional highly hydrated network gel. BC is chemically identical to that produced by plants but has unique physical and chemical properties, i.e., high crystallinity, surface area, degree of polymerization (DP_v), mechanical strength, and purity [2, 3]. In addition, the BC properties depend on the used strain and culture parameters [4]. Unlike the cellulose from wood pulp, BC is free of other contaminating polysaccharides and its isolation and purification are relatively simple, not requiring energy or chemically intensive processes. In addition, the release of cellulose nanofibrils from vegetal fibers can require up to 30,000 $kWh.ton^{-1}$ [5]. Furthermore, the production of vegetal fibers from wood has environmental impacts. These aspects give an added impetus to the study of alternative sources of cellulose [6].

Due to the mentioned properties, BC has a wide field of applications including biomedical, such as artificial skin [7] and tissue regeneration [8], or as a reinforcing agent for the design of nanocomposites [9]. In the field of paper restoration, Santos et al. [4] reported that the use of BC could be more suitable than the currently used Japanese Paper. On the other hand, the combination of BC with recycled paper fibers, for example, has proven to be an efficient technique to improve the mechanical properties of the final product [10–12]. Fragmented BC has also promising prospects in papermaking due to flexural behavior and durability, among other characteristics [10, 13]. In the paper and board industry, there are several products where it might be used in order to improve the physical–mechanical properties of the final product [14]. Furthermore, BC can be modified with cellulose-binding modules to refine these properties and/or introduce bioactive features [15]. In opposition to paper materials, where opacity is a key property in most applications (i.e., printing and writing papers), in films for application in food packaging and other uses, transparency is looked for. Nowadays, the most used films are the affordable polyethylene and polypropylene, which exhibit good transparency and barrier properties for water and oxygen, but are hardly recyclable and produced from oil. On the contrary, cellulose-based materials are renewable, recyclable and therefore have potential to contribute to a sustainable green economy [16]. The potential of nanocellulose to produce films with good levels of transparency is reported by some authors [17, 18]. Several strategies have been explored to improve transparency, namely wet press, while calendering has never been explored so far. Calendering is a thermo-mechanical treatment where the material is passed between several pairs of heated rollers [19]. When applied to paper materials, calendering increases the transparency [20]. To the best of our knowledge, the effect of hot calendering operation on BC films properties has not been yet studied. Here, BC films were produced from BC suspensions using a process similar to papermaking. The behavior of the produced BC films and the effect of calendering on the mechanical, optical–structural, and water vapor transfer rate (WVTR) were studied and compared with VC films processed in a similar way. The effect of BC ozonation (BCO) on brightness and transparency was also studied.

Materials and methods

Production of bacterial cellulose

Gluconacetobacter xylinus (ATCC 53582) was maintained in solid Hestrin–Schramm culture medium (HS) [21] using 2 % (w/v) agar (HiMedia). BC fermentation was done under static culture conditions, using HS at 30 °C for at least four weeks. The composition (in w/v) of the HS medium is as follows: 2 % glucose (Sigma-Aldrich), 0.5 % peptone (Sigma-Aldrich), 0.5 % yeast extract (HiMedia), 0.34 % $Na_2HPO_4{\cdot}2H_2O$ (Sigma-Aldrich), 0.15 % citric acid (Pronolab). The final pH was adjusted to 5.5 using HCl 18 % (v/v) (Sigma-Aldrich). The resulting BC membrane was extensively washed at room temperature with tap water, to remove residual culture medium; afterward it was placed in excess 1.0 N NaOH solution for 24 h, to remove bacteria. The membrane was then washed thoroughly with distilled water until the final pH of the supernatant became that of distilled water, resulting in a whitish pellicle.

Production of bacterial cellulose films

The produced BC membranes were fragmented in a laboratory blender for 3 min, after adding water until a solid content of 0.354 % (w/w), so as to produce a BC suspension.

In order to improve the films brightness and evaluate the effect of oxidation on the carbonyl and carboxyl content and consequently on cellulose nanofibrils dispersion, a fraction of the BC suspension was submitted to ozonation (ozone produced from oxygen at a flow rate of 100 $L.h^{-1}$, with an ozone concentration of 28 $mg.L^{-1}$) during 15 min, under vigorous agitation.

Films with a diameter of 98 mm were manufactured from ozonated (BCO) and non-ozonated suspensions (BC) with a basis weight of around 40 $g.m^{-2}$, by vacuum filtration, using a filter paper as filtration medium (FiltresRS). After the water had been drained, the upper side of BC sheets was adhered to metallic discs with the same diameter. Thereafter, a stacking of disc, BC sheet, filter paper, and blotting paper, was prepared for pressing at 1.45 MPa for 5 min, using a procedure similar to paper production (SCAN-CM 64:00). Then, the filter papers were carefully removed and the BC films were dried overnight, adhered to the metallic discs, between perforated metallic rings under a small pressure applied to the edge of the sheets in order to prevent the films from shrinking, in a standard atmosphere for conditioning (23 °C and 50 % of relative humidity) according to ISO 187:1990. From each material (BC and BCO) sixteen films were produced.

Production of vegetal cellulose films

An eucalypt bleached kraft pulp was beaten to 80° Schopper Riegler (°SR), using a Valley beater. The VC films were produced from this highly beaten pulp, according to standard procedure ISO 5269-1:2005. The film's basis weight was approximately 40 $g.m^{-2}$.

Intrinsic viscosity and degree of polymerization

In order to evaluate the possible cellulose depolymerisation in the ozone treatment, the intrinsic viscosity of the BC/BCO and VC, in the form of films, was measured after dissolution in a cupriethylenediamine (CED) solution (SCAN-CM 15:99). The DP_v was calculated from viscosity [22].

Calendering of the films

The films produced from each type of BC suspension were divided into four sets, each containing four films; one set was not calendered, and the remaining three were submitted to calendering with two metal rolls on a hard calender (HC) (Beloit Wheeler- Model 703) using a linear pressure of 120 $kN.m^{-1}$ at a fixed temperature of 100 °C. The samples were passed 1, 3, or 6 times between the calender roller pair, which will be mentioned as BC_HCX, where X is the number of passes between the roller pair. A similar procedure was followed for the VC films.

Characterization of the films

Non-calendered and calendered BC/BCO and VC films were characterized for their mechanical and optical–structural properties according to the appropriate ISO standards for cellulosic materials, mentioned throughout the procedures and through the determination of the WVTR.

Structural and physical analysis of the films The morphological characterization of BC/BCO and VC films was performed using scanning electron microscopy (SEM) (Hitachi S-2700, operated at 20 kV). All the samples were previously gold-covered by cathodic spraying.

The X-ray diffraction (XRD) technique was employed in order to determine the crystallinity index (CrI) of the samples. The XRD was carried out on a diffractometer DMAX-III/C (Rigaku), using a copper X-ray source. Scans were collected at 1.2° min^{-1} from 5 to 60° 2θ. The CrI was then calculated using the peak height method, according to Eq. (1) [23].

$$\mathrm{CrI}(\%) = \frac{I_{200} - I_{\mathrm{am}}}{I_{200}} \times 100 \quad (1)$$

where I_{200} is the overall intensity 2θ of the crystalline region at about 22.8°; I_{am} is the overall intensity 2θ of the amorphous region at about 18°. The porosity (P) of the different structures was estimated according to the Eq. (2),

$$\mathrm{P}(\%) = 100 \times \left(1 - \frac{\rho_{\mathrm{sample}}}{\rho_{\mathrm{cellulose}}}\right) \quad (2)$$

where ρ_{sample} is the density of the sample, $g.cm^{-3}$; $\rho_{\mathrm{cellulose}}$ is the density of cellulose, which is assumed to be 1.6 $g.cm^{-3}$ [24–26]. BC, BCO, and VC films characterization was performed before and after calendering. In all cases, the samples were tested according to ISO 187:1990. The basis weight was calculated according ISO 536:2012 and samples

thickness was measured with a micrometer (Adamel & Lhomargy, M120 series) and the average of four measurements was calculated (ISO 1974:2012). The apparent film density ($g.cm^{-3}$) was calculated dividing the basis weight ($g.m^{-2}$) by the film thickness (μm).

A spectrophotometer Technidyne Corp., Color Touch 2, Model ISO was used to obtain the optical properties: brightness (ISO 2470-1:2009) and transparency.

Tensile strength, elongation at break, and Young's modulus were determined using a crosshead motion machine (Thwing-Albert Co, EJA series) with a load cell of 100 N and a constant rate of elongation ($20\ mm.min^{-1}$), according to ISO 1924-2:2008. The distance between grips was 50 mm. The dry zero-span tensile tests were performed with a Pulmac tester (Pulmac, TS-100 Troubleshooter), according to ISO 15361:2000. Static bending stiffness was performed by a bending tester (Lorentzen & Wettre) at an angle of 25° and a 50-mm distance, according to an adaptation made from ISO 5628:2012. For all tests, at least four representative specimens of each film set have been tested and the average values were reported.

The WVTR was determined for calendered (6 passes) and non-calendered BC/BCO films and for VC films. The WVTR was determined in home-made recipients, ensuring constant water vapor partial pressures in the both sides of the films throughout the essays. The interior of the recipients contained a given amount of anhydrous calcium chloride (Sigma-Aldrich) that ensured zero water partial vapor pressure inside the recipients. The other side of the film was in contact with standard conditions of temperature and humidity. The amount of water vapor that diffused through the films was accounted by the mass increase of the whole set, including recipient containing the calcium chloride. The whole sets were periodically weighted for 144 h and the mass gain was used to determine the WVTR of each sample, according to TAPPI 448 om-09. For each test, at least two films were used, and the arithmetic mean of the results was calculated.

Results

Aiming to increase the brightness of the films, BC suspension was treated with ozone, an environment friendly bleaching agent used in the bleaching of vegetal pulp fibers. Due to the relatively low selectivity of ozone, carbonyl groups are introduced in the cellulose chain, which can lead to cellulose depolymerization [27]. In fact, Table 1 shows that after ozone treatment, BCO exhibits 10 % lower DP_v (41.7 % lower intrinsic viscosity) than that of the untreated BC. Most of this depolymerization is likely to take place in the intrinsic viscosity determination process itself, since the carbonyl groups introduced in the cellulose chain may lead to its cleavage under the alkaline conditions used in the essay [27]. Calendering at 100 °C had a marginal effect on the DP of BC, BCO, and VC films. The intrinsic viscosity values obtained for the BC are within the value range reported by Tsouko et al. [28] for disintegrated BC. The disintegration process carried out before the film formation also had a significant effect on the BC intrinsic viscosity; actually, the value decreased from $850\ mL.g^{-1}$ (non-disintegrated) to $735\ mL.g^{-1}$ (Table 1). The pulp fibers exhibit a slightly lower intrinsic viscosity than expected for an unbeaten pulp [29]. This value can be due to the intense beating that the vegetal fibers were submitted to produce the VC film.

BC films with a basis weight of around $40\ g.m^{-2}$ were produced by vacuum filtration, from the different cellulose suspensions. The physical properties of the produced films were characterized through several essays. The structural, mechanical, and optical properties of the calendered (1, 3, and 6 passes between calender roller pair) and non-calendered films are shown in Table 2. The calendering process enables the production of vegetal and BC films with very low internal porosity and consequently with apparent densities close to the cellulose itself ($1.6\ g.cm^{-3}$). As expected, the non-calendered films densities for VC and BC are different (0.84 versus $1.13\ g.cm^{-3}$), as a natural consequence of the

Table 1 Intrinsic viscosity and DP_v of calendered (HC1 1 pass) and non-calendered BC/BCO and VC films

Sample	Intrinsic viscosity ($mL.g^{-1}$)	DP_v^a
VC	579	3792
VC_HC1	573	3784
BC	735	3972
BC_HC1	727	3963
BCO	428	3565
BCO_HC1	422	3555

[a] $DP_v = [0.75\ (954\ \log v - 325)]^{1.105}$ [22]

Table 2 Mechanical and optical–structural properties of VC, BC, and BCO films non-calendered (0) and calendered (1, 3, and 6 passes).The coefficients of variation were below 5 %

Properties	VC film				BC film				BCO film			
	0	1	3	6	0	1	3	6	0	1	3	6
Basis weight, $g.m^{-2}$	43.2	42.9	43.5	42.7	45.1	44.4	45.1	45.6	44.5	44.3	44.8	43.2
Apparent density, $g.cm^{-3}$	0.84	1.40	1.45	1.46	1.13	1.45	1.47	1.51	1.20	1.45	1.58	1.58
Porosity, %	47.5	12.5	9.38	8.98	29.6	9.29	7.99	5.44	24.9	9.18	1.47	1.17
Tensile index, $N.m.g^{-1}$	82.8	40.5	40.3	40.7	146.7	64.8	67.8	70.2	152.1	65.8	56.2	52.95
Elongation, %	3.42	1.60	1.50	1.33	5.37	1.00	1.18	1.04	4.88	1.11	1.06	0.93
Dry zero-span tensile index, $N.m.g^{-1}$	130.5	98.4	86.6	93.1	181.4	174.5	166.2	173.4	177.1	169.7	159.0	172.8
Young's modulus, GP_a	10.8	8.7	9.4	9.4	14.5	16.2	16.7	16.7	11.9	12.3	16.2	16.9
Young's modulus[a], GP_a	20.5	10.0	10.4	10.3	20.5	17.8	18.2	17.7	15.9	13.5	16.4	17.1
Bending stiffness, mN	16.3	8.3	8.7	9.5	17.5	16.5	14.5	15.8	17.0	15.7	16.5	15.5
ISO Brightness, %	66.15	57.73	57.85	57.31	71.44	68.38	67.16	67.08	74.43	72.71	70.81	70.64
Transparency, %	49.60	63.67	65.05	64.82	53.03	67.28	72.39	73.03	54.87	69.35	73.49	75.21

[a] Normalized by the cellulose density (1.6 $g.cm^{-3}$); $Young's\ modulus^{a} = \frac{Young's\ modulus \times 1.6}{Apparent\ density}$

dimensions of the constitutive elements. VC fibers have an average width and length of 18 μm and 1 mm, respectively, whereas BC fibrils have an approximate width of 10 nm, while their length varies due to its branching growth nature. The segmental length between branching points was estimated as 580–960 μm [10], although the effect of mechanical treatment on the effective length cannot be neglected. The effect of calendering on apparent density can be observed in Table 2. The most noticeable impact is for the first pass in the hard calender, however, an important enhancement in transparency can be achieved with additional passes for the BC/BCO, which is not the case for VC films. The BC film transparency increased from around 53 to 73 % after 6 passes calendering, which confirms the expected positive effect of this unit operation. However, only a marginal improvement in the BC films transparency was observed between the 3rd and 6th passage. Ozone treatment was here applied to BC, to evaluate if it would improve the brightness levels. Results from Table 2 show that indeed the brightness of the BC films increased with ozone treatment, without losing transparency. Regarding the mechanical properties, BC/BCO presents much higher mechanical resistances than the VC. Since physical properties greatly depend on the basis weight, some properties were normalized taking into account the basis weight or the apparent density. Tensile index at break represents the load normalized with the specimen's width and basis weight. BC/BCO tensile index almost doubled one of the VC films. However, tensile index values were reduced in all cases to about half after the first pass in the calender. Dry zero-span tensile index is similar to normal tensile index, but the distance between grips being zero in this case. Assuming that no slippage occurs between the grips and the testing material, this measure estimates the intrinsic resistance of the constitutive elements of the material, which seems to be much higher for BC/BCO than for VC films. Calendering affects the two materials differently; the intrinsic VC fiber strength decreases with calendering, whereas it remains practically constant for the BC/BCO. Young's modulus and bending stiffness were also measured and are reported in Table 2. As the apparent density of the material changes with calendering, a normalized Young's modulus was also calculated, based on the maximum density that the materials can achieve (1.6 $g.cm^{-3}$), which is the density of the cellulose itself. Interestingly, the two sources of cellulose (BC and VC) exhibit the same value for the normalized Young's modulus (20.5 GPa).

Morphological characterization of the different films was carried out by SEM. Selected micrographs are shown in Fig. 1, highlighting the different morphological dimensions of the constitutive fibers. The

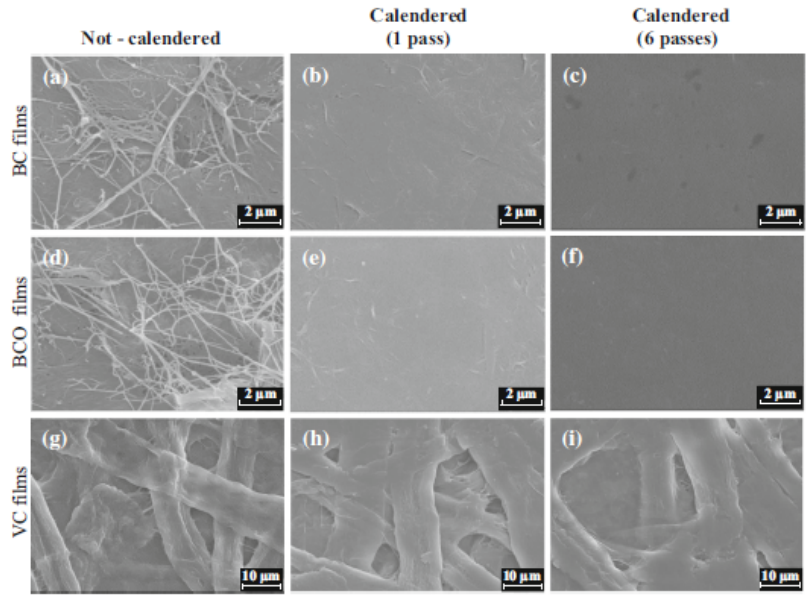

Figure 1 SEM images of the calendering effect on the BC/BCO films (magnification: ×10000), and VC films (magnification: ×1500). **a**, **d**, **g** are non-calendered films, **b**, **e**, **h** are calendered films (1 pass) and **c**, **f**, **i** are calendered films (6 passes).

surface characteristics of the network structures changed with calendering leading to compact structures which agrees well with the lower porosity results presented in Table 2.

The X-ray diffraction technique was employed to determine the crystallinity v (CrI). BC exhibits a higher CrI than the VC fibers (90.0 vs 75.6 %). The vegetal pulp fibers are produced from wood by a chemical process and contain 19 % of hemicelluloses (amorphous material), in addition to cellulose. Therefore, the differences observed for the two sources of cellulose are expected. No significant effect of calendering on the CrI for the three materials was observed. On the contrary, Retegi et al. [30] observed a positive impact of wet pressure (uncompressed vs wet compressed at 10 MPa) on the crystallinity of BC.

For food packaging applications, the water vapor permeability of the films is of critical importance. Figure 2 shows the obtained results for the accumulated water vapor transferred through the films for calendered (6 passes) and non-calendered BC/BCO and VC films. The effect of calendering is notorious for the vegetal films, whereas it is moderate for the BC. These results are consistent with the porosity of the different structures under evaluation (Table 2).

Table 3 resumes the effect of calendering on the WVTR for the different materials, where the much lower WVTR of the BC is evident when compared with the highly beaten VC film. In addition, the results show that the calendering process causes a decrease of around 70 % in the WVTR for all samples. To facilitate the analysis, the global porosity of the materials was included in Table 3. Interestingly, BC structures are less water vapor permeable than VC even when the porosity of BC is higher (BC vs VC_HC6). These results can be due to the high hemicellulose content and lower crystallinity of the vegetal fiber, which both induce higher affinity to water and therefore can enhance diffusion, and also to the different dimensions of the pores in the different materials.

Discussion

The techno-economic viability of nanocellulosic materials, including BC and nanofibrillated VC depends on the performance/costs relationship, where the basic raw-material's costs and the energy intensity of the processing techniques play a crucial

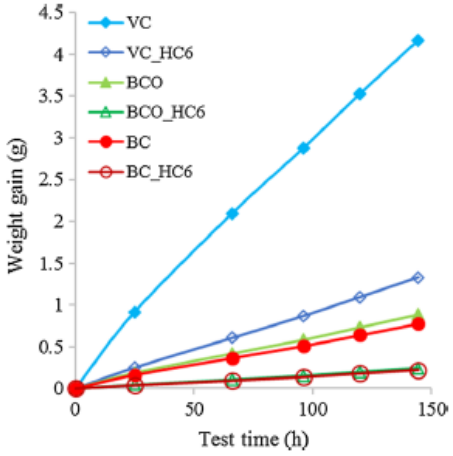

Figure 2 Transferred water vapor as a function of the test time for different cellulosic samples, with (6 passes) and without calendering.

Table 3 WVTRs of BC/BCO and VC films, without and with calendering (6 passes) and global porosity

Sample	WVTR ($g.m^{-2}.day^{-1}$)	Global porosity, %
VC	148.67	47.5
VC_HC6	46.21	9.0
BC	27.12	29.6
BC_HC6	7.53	5.4
BCO	31.14	24.9
BCO_HC6	8.54	1.2

role. To produce nanocellulose films from the corresponding suspensions, the vacuum filtration process seems to be the most promising process, as in papermaking. As expected, filtration time to make sheets from BC depends greatly on the pore size of the used filter medium; filtration time has ranged from 45 min [31] to 3–4 h [32] when fine pore size filter medium is used, but it is reduced to 8 min when woven filter fabric with larger openings and with variable vacuum was used for filtration [33]. In the present work, a qualitative filter paper with an average pore size of 8–11 μm was used and filtration times around 6 min were required, under a vacuum of around 0.9 atm. These filtration times are much higher than for the process of paper formation, but lower than some values reported in the literature [31–33]. In addition, the BC retention in the sheet was close to 90 %, which is comparable with the values reported for paper [34].

The experimental results presented in Table 2 clearly indicate that the films produced from BC/BCO are much denser (1.13 and 1.20 $g.cm^{-3}$) than the ones obtained from the highly beaten pulp VC fibers (0.84 $g.cm^{-3}$), which reveals a much compact and closed structure (as also observed by the lower porosity of the BC films, Table 3), in accordance with the dimension of the constitutive elements. The obtained apparent densities of BC are in good agreement with those reported by Nakagaito et al. [35] for BC films made from disintegrated BC, although they have gone through different pressing and drying processes. The values obtained for VC is also in the same magnitude of those reported by several authors [35, 36].

As it can be seen in Table 2, the non-calendered BC and BCO films porosities are much lower than those of the VC counterparts (29.6 and 24.9 %, against 47.5 %, respectively). After calendering, the porosity of the BC and BCO was extremely low (5.4 and 1.2 %, respectively). To attain similar porosities, Retegi et al. [30] applied a wet pressure of 100 MPa on BC structures, which is certainly a more complex process than calendering. On the other hand, BCO films porosity seems to be more sensitive to successive calendering than BC; as observed in Table 2, the porosity decreases from 9.2 to 1.2 % and 9.3 to 5.4 %, respectively for BCO and BC, when the number of calendering passages increases from 1 to 6 passes. This behavior can tentatively be explained based on the better formation (less agglomerates) or higher nanofibrils mobility of the BCO regarding the BC. The oxidation with ozone introduces carbonyl and some carboxyl groups in cellulose [37], which should increase electrostatic repulsion between fibrils and therefore decrease flocculation [38]. Nakagaito et al. [35] have reported some extent of agglomeration in BC after wet disintegration. A more uniform formation leads to better structure consolidation, as the higher density suggests (1.13 vs 1.20 $g.cm^{-3}$). The higher sensitivity to consolidation, however, suggests higher mobility of the oxidized nanofibrils. It should also be noted that the ozonation was carried out under vigorous agitation, which can diminish the mean BCO fibril length, which also enhances mobility in the calendering process and in the film formation itself.

Regarding the mass transfer properties, the air permeability study revealed that, while the VC films had high air permeability values, the BC films where

completely airtight. These permeability results are also in agreement with those reported by Yousefi et al. [36]. The air barrier properties of the BC films are due to their highly dense and compact nanostructure [39, 40]. Regarding the influence of the film structure on water vapor permeability, an important property for food packaging applications, the following aspects were observed: the calendered VC (VC_HC6), exhibits higher WVTR than the before calendering (BC), in spite of the higher porosity of the latter; the ozonated BC (BCO, before and after calendering) exhibits higher WVTR than the non-ozonated BC (BC, before and after calendering), despite its lower porosity. Based on literature [27, 37], the BC submitted to ozone bleaching should have higher carbonyl and some carboxyl content than the BC, and the vegetal fibers have amorphous material (hemicelluloses). Both features lead to higher water affinity, which probably justifies the observed behavior. In fact, Nair et al. [41] have shown that hydrophobic cellulose films exhibit lower water transfer rate than the corresponding non-modified cellulose films.

Regarding transparency, another important property of films, the inverse correlation between this property and internal porosity is clear (Table 2). Lower porosity led to higher transparency, which is in accordance with Kubelka–Munk theory [20] extensively used in paper physics; a decrease in porosity means a decrease in light scattering surface area (data not shown) and consequently higher transparency. It is noticeable that the VC attains a plateau in porosity, and consequently in transparency, whereas the porosity of BC continues to decrease with calendering, and transparency as well. Moreover, in this respect, the BC films produced from BC submitted to ozonation attained the lowest porosity and consequently the highest transparency. The positive effect of ozone was also revealed on brightness, suggesting the presence of chromophores in the BC.

As expected, the BC structures are much more resistant than its VC counterparts. BC, the tensile index (which normalizes the load at rupture respecting the basis weight) is 146.7 and 82.8 $N.m.g^{-1}$, respectively for BC and VC. The corresponding Young's modulus for BC and VC are 14.5 and 10.8 GPa, respectively. However, it is important to emphasize that both the apparent density (Table 2) and the film thickness of these materials are different. The VC films exhibit lower apparent density, higher light scattering surface area (data not shown) and, by this way, lower inter-fiber bonded area, which, for the same intrinsic strength of the constitutive elements led to lower tensile strength index. Moreover, considering the morphological dimensions of the fibers in each case, the BC has certainly much higher specific surface area for inter-elements bond development, which directly affects the number of hydrogen bonds between them and, consequently, affects the mechanical properties.

The results obtained for the BC Young's modulus (14.5 to 16.7 GPa) are slightly lower than those reported in the literature [10, 42] for films obtained from never disintegrated BC membranes (15.1 to 18.0 GPa). The differences are also notorious for the tensile strength; the same authors have reported values as high as 256 MPa for air-dry non-disintegrated films, whereas in the present study 165.8 MPa (tensile index 146.7 $N.m.g^{-1}$) was obtained for the BC films, produced after disintegration. These differences are certainly due to the disintegration process, which is responsible for the partial disruption of the originally continuous BC three-dimensional structure [36].

In order to better compare the mechanical potential between BC and VC, a normalized Young's modulus was calculated, assuming that all materials have the same density, the one of cellulose itself (1.6 $g.cm^{-3}$), which means considering a void-free material. This calculation reveals no significant differences between VC and BC, regarding their normalized Young's modulus, which is close to 20 GPa. The difference in the tensile index reflects mainly differences in inter-fiber/fibril bonded area and hydrogen bonds. The use of this normalized Youngs modulus allows to better evaluating the effect of calendering on the strength properties of the films. This normalized Young's modulus decreases from 20.5 GPa to around 10 GPa with calendering in the case of VC films. On the contrary, the same treatment on the BC films has only a minor effect on the normalized Young's modulus (20 vs 18 GPa). Interestingly, the zero-span tensile index, that accounts for the intrinsic fiber or nanofibrils tensile strength, presents similar behavior. These results suggest that under the used calendering conditions (dry state films, temperature of rolls of 100 °C, and linear pressure of 120 $kN.m^{-1}$) the supramolecular structure of the fiber was severely deteriorated, whereas the BC nanofibrils were much less affected.

The calendering process submits the constitutive elements of the materials to very high shear stress and eventually crushing. The small dimensions of the BC nanofibrils give them more mobility in the structure and therefore it is expected that the intensity of nanofibrils damage should be lower than those experimented by the microfibrils of the VC.

Regarding ozone effect on mechanical properties, the tensile index increases with ozonation, but this may be a natural consequence of the film densification (from 1.13 to 1.20 $g.cm^{-3}$). Both normalized Youngs modulus and dry zero-span tensile index indicated some degradation of the BC after ozone treatment, which is in agreement with a decrease in the cellulose average DP_v (Table 1).

Another important feature of the data in Table 2 is the drastic decrease of the tensile strength (measured as tensile index), after calendering. The elongation at break also decreases drastically. A similar behavior was observed by Iguchi et al. [10], when the pressure applied to consolidate the BC film was increased from 49 to 1960 kPa; the authors suggested that this can be due to the introduction of defects [10]. With paper structures made with cellulosic fibers (VC), Retulainen et al. [43] have assigned this drastic decrease in tensile index to fiber debonding, due to calendering.

Conclusions

As a consequence of the BC films high density, its mechanical resistance is much higher than those of VC fibers even when they are highly beaten. Ozonation of the BC slightly improved the brightness and enhanced the films transparency, but the WVTR increased, regarding the corresponding non-ozonated BC films, despite the lower porosity of the BCO films. Calendering (6 passes) significantly increased film transparency and decreased the WVTR by around 70 % for all the tested films, but some mechanical properties are impaired. Therefore, a compromise should be established between the benefits of ozonation and calendering, and the decrease in the mechanical performance induced by these processes.

Acknowledgements

The authors thank FCT (Fundação para a Ciência e Tecnologia) and FEDER (Fundo Europeu de Desenvolvimento Regional) for the financial support of the project FCT PTDC/AGR-FOR/3090/2012—FCOMP-01-0124-FEDER-027948 and the awarding of a research grant for Vera Costa.

References

[1] Eichhorn SJ, Dufresne A, Aranguren M, Marcovich NE, Capadona JR, Rowan SJ, Weder C, Thielemans W, Roman M, Renneckar S, Gindl W, Veigel S, Keckes J, Yano H, Abe K, Nogi M, Nakagaito AN, Mangalam A, Simonsen J, Benight AS, Bismarck A, Berglund LA, Peijs T (2010) Review: current international research into cellulose nanofibers and nanocomposites. J Mater Sci 45:1–33. doi:10.12691/jmpc-2-1-1

[2] Castro C, Zuluaga R, Putaux JL, Caro G, Mondragon I, Ganan P (2011) Structural characterization of bacterial cellulose produced by *Gluconacetobacter swingsii* sp. from Colombian agroindustrial wastes. Carbohyd Polym 84:96–102

[3] Basta AH, El-Saied H (2009) Performance of improved bacterial cellulose application in the production of functional paper. J Appl Microbiol 107:2098–2107

[4] Santos SM, Carbajo JM, Gomez N, Quintana E, Ladero M, Sanchez A, Chinga-Carrasco G, Villar JC (2016) Use of bacterial cellulose in degraded paper restoration Part I: application on model papers. J Mater Sci 51(3):1541–1552. doi:10.1007/s10853-015-9476-0

[5] Siró I, Plackett D (2010) Microfibrillated cellulose and new nanocomposite materials: a review. Cellulose 17:459–494

[6] Keshk SM (2014) Bacterial cellulose production and its industrial applications. J Bioprocess Biotech 4:1–10

[7] Jonas R, Farah LF (1998) Production and application of microbial cellulose. Polym Degrad Stabil 59:101–106

[8] Czaja WK, Young DJ, Kawecki M, Brown RM (2007) The future prospects of microbial cellulose in biomedical applications. Biomacromolecules 8:1–12

[9] Yano S, Maeda H, Nakajima M, Hagiwara T, Sawaguchi T (2008) Preparation and mechanical properties of bacterial cellulose nanocomposites loaded with silica nanoparticles. Cellulose 15:111–120

[10] Iguchi M, Yamanaka S, Budhiono A (2000) Review: bacterial cellulose—a masterpiece of nature's arts. J Mater Sci 35:261–270. doi:10.1016/j.carbpol.2012.03.045

[11] Mormino R, Bungay H (2003) Composites of bacterial cellulose and paper made with a rotating disk bioreactor. Appl Microbiol Biotechnol 62:503–506

[12] Delgado-Aguilar M, González I, Pèlach MA, De La Fuente E, Negro C, Mutje P (2015) Improvement of deinked old

newspaper/old magazine pulp suspensions by means of nanofibrillated cellulose addition. Cellulose 22:789–802
[13] Mohite BV, Patil SV (2014) A novel biomaterial: bacterial cellulose and its new era applications. Biotechnol Appl Biochem 61:101–110
[14] Charles LA, Waterhouse JF (1987) The effect of supercalendering on the strength properties of paper. Institute of Paper Chemistry. Technical Paper Series, number 244
[15] Oliveira C, Carvalho V, Domingues L, Gama FM (2015) Recombinant CBM-fusion technology—applications overview. Biotechnol Adv 33(3–4):358–369
[16] Kalia S, Dufresne A, Cherian BM, Kaith BS, Avérous L, Njuguna J (2011) Nassiopoulos (2011) cellulose-based bio- and nanocomposites: a review. Int J Polym Sci 837875:1–35
[17] Lee K-Y, Tammelin T, Schulfter K, Kiiskinen H, Samela J, Bismarck A (2012) High performance cellulose nanocomposites: comparing the reinforcing ability of bacterial cellulose and nanofibrillated cellulose. Appl. Mater. Interfaces 4(8):4078–4086
[18] Dhar P, Bhardwaj U, Kumar A, Katiyar V (2014) Cellulose nanocrystals: a potential nanofiller for food packaging applications. In: Komolprasert V, Turowski P (eds) Food Additives and Packaging, vol 1162. American Chemical Society, Washington, pp 197–239
[19] Vernhes P, Bloch J, Blayo A, Pineaux P (2009) Effect of calendering on paper surface micro-structure: a multi-scale analysis. J Mater Process Technol 209:5204–5210
[20] Leskelä M (1998) Optical properties chapter 4. In: Niskanen K (ed) Paper physics (Book 16). Fapet, Helsinki
[21] Hestrin S, Schramm M (1954) Preparation of freeze-dried cells capable of polymerizing glucose to cellulose. Biochem J 58(2):345–352
[22] Sihtola H, Kyrklund B, Laamanen L, Palenius L (1963) Comparison and conversion of viscosity and DP values by different methods. Paperi Ja Puu 45(4a):225–232
[23] Segal L, Creely JJ, Martin AE Jr, Conrad CM (1962) An empirical method for estimating the degree of crystallinity of native cellulose using the X-ray diffractometer. Tex Res J 29:786–794
[24] Henriksson M, Berglund LA, Isaksson P, Lindström T, Nishino T (2008) Cellulose nanopaper structures of high toughness. Biomacromolecules 9:1579–1585
[25] Saito T, Nishiyama Y, Putaux JL, Vignon M, Isogai A (2006) Homogeneous suspensions of individualized microfibrils from TEMPO-catalyzed oxidation of native cellulose. Biomacromolecules 7(6):1687–1691
[26] González I, Alcalá M, Chinga-Carrasco G, Vilaseca F, Boufi S, Mutjé P (2014) From paper to nanopaper: evolution of mechanical and physical properties. Cellulose 21:2599–2609
[27] Pouyet F, Lachenal D, Das S, Hirat C (2013) Minimizing viscosity loss during totally chlorine-free bleaching of hardwood kraft pulp. BioResources 8(1):238–249
[28] Tsouko E, Kourmentza C, Ladakis D, Kopsahelis N, Mandala I, Papanikolaou S, Paloukis F, Alves V, Koutinas A (2015) Bacterial cellulose production from industrial waste and by-product streams. Int J Mol Sci 16(7):14832–14849
[29] Gil N, Gil C, Amaral ME, Costa AC, Duarte AP (2009) Use of enzymes to improve the refining of a bleached eucalyptus globulus kraft pulp. Biochem Eng J 46:89–95
[30] Retegi A, Gabilondo N, Peña C, Zuluaga R, Castro C, Gañan P, de la Caba K, Mondragon I (2010) Bacterial cellulose films with controlled microstructure–mechanical property relationships. Cellulose 17:661–669
[31] Sehaqui H, Liu A, Zhou Q, Berglund LA (2010) Fast preparation procedure for large, flat cellulose and cellulose/inorganic nanopaper structure. Biomacromolecules 11:2195–2198
[32] Nogi M, Iwamoto S, Nakagaito AN, Yano H (2009) Optically transparent nanofiber paper. Adv Mater 21(16):1595–1598
[33] Zhang L, Batchelor W, Varanasi S, Tsuzuki T, Wan X (2012) Effect of cellulose nanofiber dimensions on sheet forming through filtration. Cellulose 19:561–574
[34] Biermann CJ (1996) Handbook of pulping and papermaking, 2nd edn. Academic Press, San Diego
[35] Nakagaito AN, Iwamoto S, Yano H (2005) Bacterial cellulose: the ultimate nano-scalar cellulose morphology for the production of high-strength composites. Appl Phys A 80:93–97
[36] Yousefi H, Faezipour M, Hedjazi S, Mousavi MM, Azusa M, Heidari AH (2013) Comparative study of paper and nanopaper properties prepared from bacterial cellulose nanofibers and fibers/ground cellulose nanofibers of canola straw. Ind Crop Prod 43:732–737
[37] Chirat C, Lachenal D (1994) Effect of ozone on pulp components application to bleaching of Kraft pulps. Holzforschung 48(Suppl):133–139
[38] Fall AB, Lindström SB, Sundman O, Ödberg L, Wagberg L (2011) Colloidal stability of aqueous nanofibrillated cellulose dispersions. Langmuir 27(18):11332–11338
[39] Fendler A, Villanueva MP, Giminez E, Lagarón JM (2007) Characterization of the barrier properties of composites of HDPE and purified cellulose fibers. Cellulose 14:427–438
[40] Syverud K, Stenius P (2009) Strength and barrier properties of MFC films. Cellulose 16:75–85
[41] Nair SS, Zhu JY, Deng Y, Ragauskas AJ (2014) High performance green barriers based on nanocellulose. Sustain. Chem. Process 2:23

[42] Yamanaka S, Watanabe K, Kitamura N, Iguchi M, Mitsuhashi S, Nishi Y, Uryu M (1989) The structure and mechanical properties of sheets prepared from bacterial cellulose. J Mater Sci 24:3141–3145. doi:10.1007/BF01139032

[43] Retulainen E, Moss P, Nieminen K (1997) Effect of calendering and wetting on paper properties. J Pulp Pap Sci 23(1):J34–J39

3.4. Paper 3 - Hydrophobicity improvement of cellulose nanofibrils films by stearic acid and modified precipitated calcium carbonate coating

V. L. D. Costa and R. M. S. Simões
Journal of Materials Science (2022) 57:11443–11459
DOI 10.1007/s10853-022-07249-x

J Mater Sci (2022) 57:11443–11459

Polymers & biopolymers

Hydrophobicity improvement of cellulose nanofibrils films by stearic acid and modified precipitated calcium carbonate coating

V. L. D. Costa[1,2,*] and R. M. S. Simões[1,2]

[1] Research Unit of Fiber Materials and Environmental Technologies (FibEnTech-UBI), Universidade da Beira Interior, Rua Marquês de Ávila e Bolama, 6200-001 Covilhã, Portugal
[2] Department of Chemistry, University of Beira Interior, 6201-001 Covilhã, Portugal

Received: 23 December 2021
Accepted: 14 April 2022
Published online: 11 May 2022

ABSTRACT

The development of a cellulose nanofibrils film with permanent hydrophobicity using green processes, avoiding hazardous solvents, through easy procedures, is a great challenge. The hydrophobicity of a layer of calcium carbonate modified with stearic acid has already been presented. However, the combination of a cellulose nanofibrils film with a layer of modified calcium carbonate to develop a permanent hydrophobic cellulose-based material rises the additional issue of adhesion between layers. In the present study, a set of cellulose nanofibrils films was coated with a layer of stearic acid and another set was additionally covered with modified precipitated calcium carbonate (0.4–6 μm sized particles with above 50% aragonite crystalline form), previously modified with a stearic acid suspension using ultrasounds. To investigate the issue of adhesion between layers, some films were subjected to heat treatments at 68 and 105 °C. Structural and physical analysis of the films, as well as barrier properties and static/dynamic contact angle measurements were performed. Results show that overall mechanical performance of the films was not substantially affected by the coating and posterior heat treatments. Heat treatments decreased the water vapor transmission rate of stearic acid coated films from 91.9 to 31.6 g m^{-2} day^{-1} and the oxygen permeability of stearic acid and modified calcium carbonate coated films from 26.4 to 2.6 cm^3 μm/(m^2 day kPa). The double layered coated cellulose nanofibrils films attained contact angle hysteresis of 3.1° and 5° and static contact angles of 150° and 140° with no heat treatment and with a heat treatment of 68 °C, respectively. The heat treatment enabled to permanently adhere modified calcium carbonate particles on the film, providing it with persistent hydrophobicity.

Handling Editor: Stephen Eichhorn.

Address correspondence to E-mail: vera.costa@ubi.pt
E-mail Address: rmss@ubi.pt

https://doi.org/10.1007/s10853-022-07249-x

Introduction

In line with the principles of Green Chemistry we should strive to use renewable feedstock and raw materials, design safe chemicals and products and use safe solvents and reactions conditions [1–3]. Out of the renewable materials, cellulose is maybe the most attractive due to its abundance, biodegradability, and non-toxicity [4]. Cellulose nanofibrils (CNFs) have recently been the subject of much interest due to their unique characteristics such as very high aspect ratio, high specific strength, thermal stability, hydrophilicity and broad capacity for chemical modification, among others [2, 5, 6]. These attributes make this material suitable for many industrial applications [7]: for instance, as nanofibrils have the ability to form very dense and entangled networks, freestanding CNF films are a promising platform for the development of food packaging materials [6, 8]. However, the hydrophilicity of cellulose makes it sensitive to moisture, thus often limiting its use where high relative humidity is required. Consequently, extensive research has been devoted to increasing the hydrophobicity of cellulosic materials and enhancing their barrier properties in wet or humid conditions [4, 9–14].

Several methods have reported increasing the hydrophobicity of CNF films, including chemical modification of the cellulose fibrils [13, 15]. Despite the efforts on applying green systems, hydrophobization of cellulose through chemical modification routes usually requires the addition of organic solvents and some environmentally unfriendly reagents [16].

Other methods involve either the incorporation of a hydrophobic component in the structure [17] or coating cellulose-based structures with hydrophobic components [4, 6].

Besides reducing the surface energy, many authors have emphasized a multi-scale roughness profile as an important contributor to the hydrophobic properties of a materials' surface, since it increases the total surface area and allows for the entrapment of air in between the water droplets and the surface. Depending on the wetting regime, the water droplets can either penetrate in between the roughness peaks or remain on top of them [18].

Mertaniemi et al. have successfully super-hydrophobized surfaces with spray-dried chemically modified CNFs leading to hierarchical surface roughness, closely resembling that of lotus leaves [19]. Huang et al. have reported a sprayable superhydrophobic coating produced from a CNF ethanol suspension [20]. Arbatan et al. reported the preparation of a superhydrophobic paper through dip coating a filter paper in an aqueous suspension containing precipitated calcium carbonate (PCC) and CNFs, to increase the papers' surface roughness and a subsequent chemical treatment with a solution of alkyl ketene dimer in n-heptane [21].

While in these last reports, much effort has been paid to attaining nanosized roughness via coating with CNFs, other authors on the other hand, have focused on the hydrophobization through hydrophobic modification of coatings and their adhesion on the surfaces. For instance, Hu et al. have reported a combination of surface coating with a dipping treatment in order to increase the water contact angle to near 150° and water resistance of regular paper, using PCC for roughness control, stearic acid (SA) as a surface hydrophobic modification agent and latex as a polymer binder [22].

Unlike some authors, who have synthesized hydrophobic PCC particles [23–25], in the present work the PCC's surface was modified with stearic acid through a simple and rapid method (the used PCC was mostly under aragonite crystalline form, which is more hydrophilic than calcite). Though such hydrophobic modification of PCC and coating techniques have been applied to paper, as far as we are aware of, they have not been applied on CNF films aiming the increase in hydrophobicity. Besides, while current procedures for manufacture of micro- and nano-scale roughness in hydrophobic surfaces are difficult at an industrial large-scale and the chemicals used to provide hydrophobicity are often expensive and toxic, this method comes as a simple and relatively inexpensive process for increasing the hydrophobicity of CNF films without using hazardous solvents or time-consuming methods, as well disregarding the need of a binding agent between the CNF films and the hydrophobic coating.

In the present work, CNF freestanding films were manufactured though vacuum filtration and were hydrophobized with a layer of stearic acid. Also, a layer-by-layer technique with stearic acid and a modified PCC hydrophobic powder, combined with heat treatment was performed.

Materials and methods

A commercial Totally Chlorine Free (TCF) never dried bleached kraft eucalypt pulp (with an average limiting viscosity of 570 mL/g) was used as a source of native cellulose fibers. Stearic acid (SA), 2,2,6,6-tetramethylpiperidine-1-oxyl radical (TEMPO), sodium hypochlorite, sodium bromide and other reported chemicals were of laboratory grade (Sigma-Aldrich, USA) and were used without further purification. Precipitated calcium carbonate (PCC) (Sturcal® F) with a minimum of 50% aragonite crystalline form content, an apparent density of 0.45–0.56 g/cm^3 and particle size in the range 0.4–6 μm (values as reported by supplier) was provided by J.M. Pereira (Portugal).

CNF suspensions production

A commercial TCF never dried bleached kraft eucalypt pulp (around 80% cellulose and 20% xylan) was used to produce a CNF aqueous suspension. The pulp was subjected to a 2,2,6,6-tetramethylpiperidine-1-oxyl radical (TEMPO)-mediated oxidation pretreatment based on previously reported reaction conditions [26], as follows: 10 g oved dried of pulp fibers were resuspended in a total volume of 3 L of 50 mM sodium carbonate buffer solution with a pH of 10.5, containing 0.025 g of TEMPO and 0.25 g of NaBr. A total of 80 mmol of NaClO were added to the previous mixture divided into 4 equal parts, with 15 min apart between each addition. The mixture was then allowed to react for an additional 60 min, all while in continuous agitation and at room temperature. The reaction was then stopped by vacuum filtrating the resulting fibers in a porous plate funnel and washing them with distilled water until pH 7 was achieved.

The resulting fibers were afterward resuspended in distilled water at a solid content of 1.5 wt% and were subjected to 2 successive homogenization steps (500 bar + 850 bar), using a GEA Niro Soavi (Panther NS3006L; GEA, Parma, Italy).

Microscopy observations

In order to morphologically characterize the cellulose fibrils in the obtained CNF suspension, a drop of 0.01 wt% CNF suspension was allowed to air dry overnight at room temperature on a scanning electron microscope (SEM) sample holder. The CNF films surface imaging was performed by attaching fragments directly on the SEM sample holder with double sided tape. Transversal cuts of the coated and non-coated CNF films were also made into representative samples, and they were attached vertically on the sample holders so as to observe their cross section.

Microscopic observations were performed using either a field emission scanning electron microscope (FE-SEM) (Hitachi SEM SU-70 Hitachi, Tokyo, Japan) operated at 15 kV or SEM (Hitachi S-2700; Hitachi, Tokyo, Japan) operated at 20 kV. All of the samples were previously gold sputtered by cathodic spraying (Quorum Q150R ES; Quorum Technologies, East Sussex, UK).

For the transmission electron microscope (TEM) imaging, drops of 0.001 wt% CNF suspension were deposited on carbon-coated electron microscopic grids and negatively stained with 2 wt% uranyl acetate. The grids were air-dried and analyzed with a Hitachi HT-7700 TEM (Hitachi, Tokyo, Japan) with an acceleration voltage of 80 kV.

Degree of polymerization

The CNFs limiting viscosity [η] was determined according to the ISO 5351 (2012) standard, with a cupriethylenediamine (CED) solution as a solvent and using a capillary viscometer. The degree of polymerization (DP) was calculated using the following Eqs. (1, 2) [27].

$$[\eta] = 0.42 \times DP; DP < 950 \quad (1)$$

$$[\eta] = 2.28 \times DP^{0.76}; DP \geq 950 \quad (2)$$

where is [η] is the limiting viscosity (mL/g) and DP is the degree of polymerization.

Total acidic groups content

The total acidic groups content in the produced CNFs was determined through a conductivity titration method, based on the standard SCAN-CM 65:02. Initially, the CNFs were protonated by resuspension in a HCl solution and then they were washed by sequential cycles of centrifugations, at 3000 g for 15 min, and resuspension in fresh distilled water, until the supernatant attained a conductivity of 5 μS/cm maximum. The CNF suspensions were afterward titrated with a NaOH solution until pH = 11. The

amount of weak acid groups was determined from the break points in the conductivity versus added volume of NaOH from the curves obtained from the conductivity titrations.

Preparation of stearic acid suspension and modified PCC

In a first instance, a stearic acid (SA) aqueous dispersion was prepared using a method adapted from Lozhechnikova et al.: SA was added to distilled water at a concentration of 0.4 wt% and the mixture was heated up on a hot plate until it reached 90 °C. At that point, the hot mixture was sonicated at 20 kHz for 3 min with 2 s interval using an ultrasonic liquid processor equipped with a CV17 probe (Vibra-Cell VC 600-2, Sonics & Materials Danbury, USA) and was afterward transferred to an ice bath and let to cool down. The final dispersion was filtered through a filtering funnel with 40–100 µm nominal maximal pore size [28]. The filtrate was a stable milky looking SA dispersion.

In a second stage, a modified PCC powder was prepared using the following method, described by Arbatan et al.: A 0.7 wt% PCC aqueous suspension was prepared submitting it to homogenization in a mild ultrasound bath (S30H, Elmasonic, Singen, Germany) for 3 min immediately before use [21]. Then, 4 mL of this suspension (28 mg of PCC) was added to 10 mL of the previously prepared SA dispersion (≈ 40 mg of SA), and the mixture was subjected to sonication in the ultrasonic liquid processor for 3 min, followed by overnight water evaporation in an oven at 105 °C. This resulted in a dry white modified PCC powder. The modified PCC powder was manually ground in mortar and pestle to disintegrate lumps and obtain a fine powder which was used afterward as a film coating without further treatment.

Production and coating of CNF films

The previously produced CNF suspension was diluted to a solid content of 0.3 wt% and homogenized (Ultra-Turrax T-25 Digital Homogenizer, Ika Labortechnik, Staufen, Germany) for 2 min at 6000 rpm. The resulting suspension was subjected to a mild ultrasound bath (S30H, Elmasonic, Singen, Germany) for 5 min to release the air bubbles.

Simple CNF films with a diameter of 8.5 cm and a target grammage of 55 g/m^2 were prepared by vacuum filtration in a filtrating funnel, using a 0.65 µm pore size nitrocellulose membrane (Millipore, Bedford, Mass., USA) as filtration medium, attached to a filter paper for added support. Vacuum filtration was carried out at a constant pressure of 0.2 bar, using a vacuum pump, until the water stopped draining, which took around 180 min. Then, the wet CNF filtration cake and filtrating membrane were placed between two pieces of cloth and blotting paper (one cloth piece on each side), and the whole set was pressed for 30 s at 2.19×10^5 N/m^2 in order to remove some of the remaining water and ease the membrane detachment. Then, after carefully removing the membrane, and while still holding the piece of cloth on the opposite side in direct contact with the CNFs, a metallic disk was adhered, and the set was once again pressed for an additional 10 s at the same pressure, just enough for the CNFs to adhere to the metallic disk. Finally, the cloth was gently removed from the top and the CNF film was dried overnight, between perforated metallic rings under pressure applied to the edge of the films in order to prevent them from shrinking, in a standard atmosphere for conditioning (23 °C and 50% of relative humidity). These uncoated CNF films will be designated as CNF from now on.

A second set of SA layered CNF films were produced as follows: the CNF suspension was vacuum filtered under the same previously described conditions. At the end of the water drainage, 3.9 mL of the SA suspension, corresponding to 5 wt% of the film's total dry mass were diluted to a total volume of 10 mL to ensure coverage of the entire filtration cake's surface. The suspension was added on top of the CNF filtration cake, and it was once again let to vacuum filter until the water stopped draining, which took an additional 15 min. The following steps of pressing and drying were as formerly described. This SA layered CNF films will be referred to as CNF-SA.

A third variety of CNF films was prepared from these later ones (CNF-SA) as follows: a small amount of the produced modified PCC powder was gently spread on top of the SA layer of the CNF-SA dried films with a fine bristle brush, just enough to cover the surface, in a layer-by-layer assembling (CNF-LBL). After this, the films were subjected to a heat treatment in an oven at either 68 °C or 105 °C for

15 min to improve adhesion between layers. Similar heat treatment was performed on some CNF-SA films.

Structural and physical analysis of CNF films

All samples were kept in standard atmosphere for conditioning (23 °C and 50% of relative humidity) for at least 24 h before testing (ISO 187:1990).

The basis weight of the films was calculated according to ISO 536:2012 and their thickness was measured with a micrometer (Adamel & Lhomargy, M120 series, New York, USA). The arithmetic average of four measurements was used.

The apparent density of the films was determined from the basis weight and thickness.

The corresponding porosity of the films was estimated according to Eq. (3).

$$\text{Porosity}(\%) = 100 \times 1 - \left(\left(\frac{\rho_{\text{film}}}{\rho_{\text{cellulose}}}\right)\right)^{1} \quad (3)$$

where ρ_{film} is the apparent density of the film, g/cm^3 and $\rho_{\text{cellulose}}$ is the density of crystalline cellulose, which is assumed to be 1.6 g/cm^3.

The surface roughness of the produced uncoated CNF and coated CNF films was also assessed using a Bekk smoothness measuring equipment (Messmer Büchel, model K533, Nederlands), in accordance with the Tappi 479 om-91 standard.

The tensile strength, elongation at break and Young's modulus were determined using a universal tensile testing equipment (Thwing-Albert Instrument Co., EJA series, Philadelphia, USA) with a load cell of 100 N and a constant rate of elongation (20 mm min^{-1}), according to ISO 1924-2:2008. The distance between grips was 50 mm. To avoid slippage at the sample holders, small pieces of paper tape were attached to the edges of the samples.

The dry zero-span tensile tests were performed with a Pulmac tester (Pulmac, TS-100 troubleshooter, Vermont, USA), according to ISO 15361:2000. Static bending stiffness was performed by a bending tester (Lorentzen & Weltre, Sweeden) at an angle of 25 degrees and a 50 mm distance, according to an adaptation made from ISO 5628:2012. For all tests, at least four representative films have been tested and the arithmetic average values are presented.

The optical properties of the films (brightness (ISO 2470-1:2009) and transparency) were determined through spectrophotometry (Technidyne Corp., Color Touch® 2, France).

Barrier properties

The water vapor transmission rate (WVTR) was determined for the produced films according to Tappi 448 om-09. Home customed containers were used, ensuring constant water vapor partial pressures in both sides of the films throughout the essays. The interior of the containers had a given amount of anhydrous granular calcium chloride that ensured zero water vapor partial pressure inside the recipients. The other side of the films was in contact with the standard conditions of temperature and humidity of the laboratory (23 °C and 50% relative humidity). Regarding the coated films (CNF-SA and CNF-LBL) the coated side was facing upward, in contact with the standard conditions. The amount of water vapor that diffused through the films was accounted by the mass increase in the whole set. The whole sets were periodically weighted for as long as 144 h and the mass gain was used to determine the WVTR (g/(m^2 day)) of each sample, according to Eq. (4).

$$\text{WVTR} = \frac{S}{A} \quad (4)$$

where S corresponds to the slope of a liner regression that best fits the plot of weight gain versus testing time (g/days) and A is the area of the films (m^2).

The water vapor permeability (WVP) was calculated according to Eq. (5).

$$\text{WVP} = \frac{\text{WVTR}}{\Delta P/_e} \quad (5)$$

where ΔP is the water vapor pressure difference between the two sides of the films and e is the films thickness. Two replicates were performed for each sample.

The oxygen transmission rate (OTR) of the films was measured according to ASTM F1927:2014, using the Ox-Tran®Model 2/21 system (Mocon, Minnesota, USA). The upper limit of the device measuring range was 9570 cm^3/(m^2 day). The measurements were performed in triplicate at 23 °C and 50% relative humidity. The oxygen permeability (OP) was calculated in a similar manner as the WVP.

[1] Eq. (3) Should be

$$Porosity\ (\%) = 100 \times \left(1 - \frac{\rho\ film}{\rho\ cellulose}\right)$$

Contact angle measurements

Static contact angles (CA) with deionized water were measured with an optical contact angle measuring and contour analysis system (OCAH 200, Dataphysics Instruments, Filderstadt, Germany). The static CA measurements were performed with 4 µL water droplets placed on top of cut out strips of all the produced films, using the sessile drop method. The dynamic (advancing and receding) contact angles (ARCA) were measured by executing consecutive cycles of addition/depletion of 4 µL of water on the 4 µL water droplets already placed on the surface of the samples, using the needle-in-drop method. For every sample, at least 4 measurements were taken, choosing a different spot for each measurement, and the arithmetic average is presented. All measurements were performed at 22 °C and under a relative humidity of 50%.

Statistical analysis

The experimental data were subjected to statistical analysis using SPSS 28 software (SPSS Inc., Chicago, USA) and were examined using analysis of variance (ANOVA). Tukey's test was used to verify the significant differences among the values at $p < 0.05$.

Results and discussion

Morphological characterization of the fibrils

The morphology of the fibrils was investigated through SEM and TEM imaging in order to capture the micro- and nano-scale elements. Figure 1 gives an overview of the morphological characteristics of the produced CNFs.

Although it is possible to observe microscale elements (Fig. 1a), the material has been disintegrated into nanofibrils to a considerable extent (Fig. 1b). In fact, a centrifugation method described elsewhere [29] was carried out in order to roughly quantify the relative proportions of micro- and nano-elements in the CNF suspension, and the experimental results showed that nearly 67% of the material has sedimented, indicating that at least 33% of the material is, in fact, nanofibrils. Moreover, the image analysis of the CNF suspensions enabled to determine that about

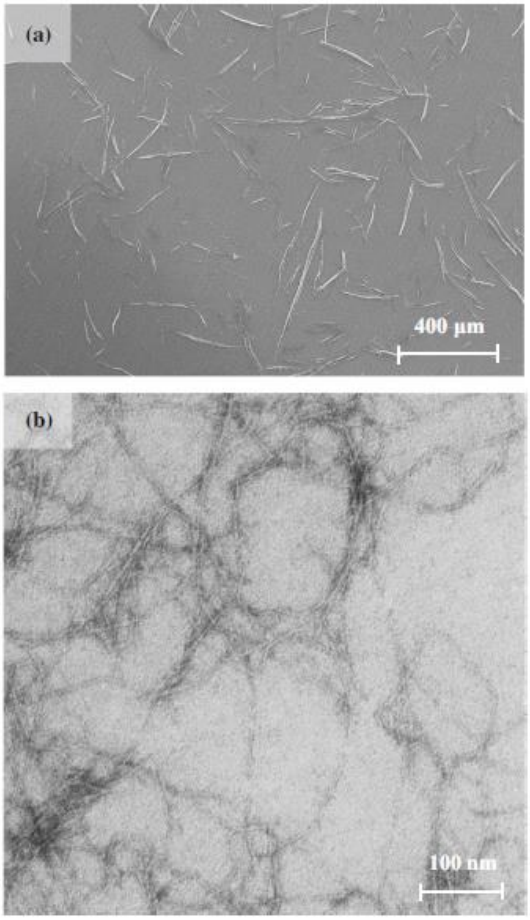

Figure 1 CNFs imaged through SEM with a magnification of ×60 (**a**) and TEM (**b**) with a magnification of ×40 k.

40% of the material has a length higher than 0.2 mm. The whole material was used to produce the films.

Physicochemical characterization of the fibrils

The determined limiting viscosity of the pretreated fibrils was 154 mL/g, which corresponds to a calculated average DP of 367. This indicates that the resulting material from the TEMPO mediated oxidation had far lower DP than that of the original cellulose used as a starting material (DP of 1429). This result is in good agreement with what has been reported by other authors for TEMPO/NaBr/NaClO oxidation systems [30, 31].

The resulting average carboxyl groups content for the produced TEMPO-oxidized CNFs was 997 µmol/g. Both DP and carboxyl groups content were in good agreement with the results reported by other authors for similar pretreatments [32]. The high carboxyl group content of TEMPO-oxidized cellulose fibrils helps in fiber wall disintegration by loosening the adhesion between microfibrils by electrostatic repulsions and improving aqueous dispersions stability [33]. Considering the substantial carboxyl group content and the relatively low content of nanoelements, it would have been possible to increase this value by performing one or two additional steps in the homogenizer, but probably at the expenses of increasing the film forming time.

Mechanical, optical and barrier properties of the CNF films

The average mechanical and optical-structural properties of all the produced CNF films are presented in Table 1.

Regarding the film formation process, it should be emphasized that the whole CNF suspension was used and that no substantial amount of material was lost during the filtration process (with a 0.65 µm pore size nitrocellulose membrane), since the average obtained basis weight for the CNF films (Table 1) was very close to the target basis weight (55 g/m^2). In addition, smooth and translucent CNF films were produced (Fig. 2), in general without the often-reported issue of wrinkling [34]. The produced films were let to air-dry in standard conditions of temperature and humidity, keeping appropriate tension only on the outer edges of the material with metallic rings.

Both apparent density and tensile index of the CNF films measured in this work (Table 1) are in general comparable with the literature results [35–37]. For TEMPO-oxidized kraft pulps, Fukuzumi et al. reported tensile strength between 222 and 233 MPa, which taking in account the density can be converted in tensile index between 153 and 160 N m/g [35]. These values are higher than those of the present work, but the film density is also much higher (around 1.45 g/cm^3) and the authors removed the non-fibrillated and partially fibrillated materials prior to the film formation. Kumar et al., using TEMPO oxidized eucalyptus and the integral material, reported values in the same range of the present work [38]. Wang et al., using bleached Eucalyptus pulp endoglucanase pretreated, reported values on the same order of magnitude of those presented in Table 1 [36]. The Young modulus values reported in Table 1 range from 5.2 to 5.9 GPa, which are similar to those reported by Fukuzumi et al. [35] for TEMPO-oxidized cellulose (6.2 GPa), but drastically lower than the values reported by Henriksson et al. for cellulose nanopapers produced from softwood dissolving pulp after enzymatic pretreatment with DPs ranging from 410 to 1100, although these authors have dried the nanopapers at 55 °C under a 10 kPa pressure, which certainly played an important role in the mechanical performance [27]. Even for a cellulose with a DP of 410 and a nanopaper porosity of 28%, which are close to our own results, these authors reported a Young's modulus of 13.7 GPa and overall superior mechanical performance that can probably be attributed to more favorable interfibrillar adhesion characteristics and more homogeneously distributed defects. Regarding the Young modulus, it should be emphasized the contribution of elongation on the result. The films from the present work have a strain at break around 5%, whereas other exhibit lower values and therefore the higher Young's modulus reported by other authors is not unexpected [38].

The comparison of the values of the tensile index (measured at a span of 50 mm) and the corresponding values for zero-span tensile index enabled to conclude that the major part of the microfibril resistance was retained in the film, suggesting a film relatively free of weak points.

The apparent density slightly decreased with the layer of SA, but consistently increased with the heat treatment (Table 1), which was expected, considering the increased mobility and rearrangement of the SA molecules. This densification process was consistently slightly more pronounced on the samples treated at higher temperature (for the same amount of time). Despite the densification process, the tensile index and overall mechanical performance suffered no major alterations with the heat treatments of any of the films, which makes sense if we acknowledge the CNF layer is the main contributor for the mechanical resistance.

The surface treatment had a significant effect on the films' transparency: it markedly decreases with the LBL assembling as well as with the SA layer. This is in line with the measured light scattering coefficient and with the dimension and particulate nature

Table 1 - Average mechanical and optical-structural properties of the CNF films (neat CNF; CNF-SA: with a SA layer; CNF-LBL: with a SA layer and modified PCC)

Properties	CNF	CNF-SA			CNF-LBL		
Heat treatment	–	–	68 °C	105 °C	–	68 °C	105 °C
Basis weight (g/m^2)	54.8 ± 1.6^a	54.6 ± 1.2^a	55.3 ± 0.9^a	55.1 ± 0.8^a	56.4 ± 1.6^a	55.7 ± 1.3^a	55.8 ± 0.9^a
Thickness (μm)	48.6 ± 1.5^a	49.7 ± 1.3^a	47.0 ± 1.0^a	45.0 ± 0.9^b	49.9 ± 1.1^a	46.6 ± 1.2^a	45.0 ± 1.0^b
Apparent density (g/cm^3)	1.13 ± 0.01^a	1.10 ± 0.01^b	1.18 ± 0.01^c	1.22 ± 0.01^d	1.13 ± 0.01^a	1.20 ± 0.01^d	1.24 ± 0.01^d
Tensile index (Nm/g)	103.7 ± 5.2^a	111.7 ± 4.1^b	103.1 ± 4.7^a	101.6 ± 4.5^a	–	108.5 ± 5.4^a	104.8 ± 3.3^a
Elongation (%)	5.5 ± 0.2^a	5.7 ± 0.3^a	5.1 ± 0.2^b	4.8 ± 0.2^b	–	5.6 ± 0.7^a	4.6 ± 0.3^b
Zero-span tensile index (Nm/g)	139.3 ± 11.2^a	129.2 ± 10.7^a	136.5 ± 12.5^a	124.1 ± 10.2^a	–	127.2 ± 11.5^a	130.5 ± 11.6^a
Young's modulus (GPa)	5.4 ± 0.4^a	5.6 ± 0.5^a	5.9 ± 0.7^a	5.5 ± 0.3^a	–	5.2 ± 0.4^a	5.8 ± 0.8^a
Bending stiffness (mN)	55.0 ± 5.2^a	55.2 ± 5.2^a	55.3 ± 5.2^a	55.3 ± 5.2^a	–	55.0 ± 5.2^a	55.2 ± 5.2^a
ISO Brightness (%)	73.3 ± 0.8^a	76.3 ± 1.4^b	69.9 ± 0.7^c	67.4 ± 0.5^d	78.2 ± 1.4^b	74.5 ± 1.2^a	72.0 ± 1.3^a
Transparency (%)	77.9 ± 2.5^a	59.1 ± 1.2^b	78.0 ± 2.2^a	75.5 ± 2.0^a	52.8 ± 1.3^c	69.0 ± 2.1^d	67.7 ± 1.9^d
Light scattering coefficient (cm^2/g)	5.0 ± 0.2^a	12.5 ± 1.1^b	4.8 ± 0.3^a	5.6 ± 0.6^a	14.4 ± 1.8^b	7.6 ± 1.0^c	8.1 ± 1.0^c
Light absorption coefficient (cm^2/g)	0.18 ± 0.01^a	0.31 ± 0.07^b	0.21 ± 0.01^c	0.27 ± 0.06^b	0.26 ± 0.09^b	0.24 ± 0.02^b	0.31 ± 0.07^b

Means at the same line with different superscript letters are significantly different ($p < 0.05$)

Figure 2 Photograph of a produced translucent free-standing CNF film on top of a conventional copy paper with the UBI logotype.

of the PCC, which is usually incorporated in office paper during production process to provide opacity [39]. Interestingly, the heat treatment of the coated films enabled to fully recover the transparency of the SA coated films. The effect of the heat treatment on the apparent density may suggest that at least a part of the SA migrates into the pores of the neat CNF films, decreasing the non-contacting interfaces of the CNF elements and therefore decreasing the light scattering coefficient of the material. However, the strong increase in the scattering coefficient from 5.0 to 12.5 cm^2/g corroborates the high light scattering power of the SA layer deposited on the CNF films. Actually, as it will be evidenced later on (Fig. 5c), the surface irregularities of the SA layer are under 1 μm, meaning they are in the same order of magnitude of visible light wavelength (400–700 nm), and scattering it. For the CNF-LBL films, an important transparency recovery occurs with heat treatment, but the light scattering power of the PCC in the surface and also possibly inside the film is preserved and the transparency remains lower than that of the neat CNF films (Fig. 3).

Water vapor and oxygen barrier properties

Figure 4 shows the obtained results for the accumulated water vapor transferred over time through the

different produced CNF films, which enabled to estimate the WVTR (Table 2).

The neat CNF films exhibit WVTRs comparable with the values reported for similar films produced from TEMPO-oxidized pulps [40] and higher than those reported for enzymatically treated pulps and bacterial cellulose films (27.1 g/(m^2 day); global porosity = 29.6%) [41]. Migration of molecules between two adjacent volumes separated by a thin film occurs in three basic steps: adsorption of the molecule on the film's surface, diffusion through the film and exit of the diffusing molecule by desorbing from the surface [42]. As any other mass transfer process by diffusion, the WVTR will be proportional to the effective water vapor diffusion and the driving force. In turn, the effective water vapor diffusion depends on the water vapor diffusion in air, but also on porosity and pore tortuosity. In addition, if the pore size is of the same magnitude of the free average path of molecules, Knudsen diffusion takes place. Thus, it is plausible to think that WVTR would escalate with the increase of the fibril's carboxyl group content, due to increased affinity to water on the water vapor exposed film side (the other side is water free; therefore, the driving force increases).

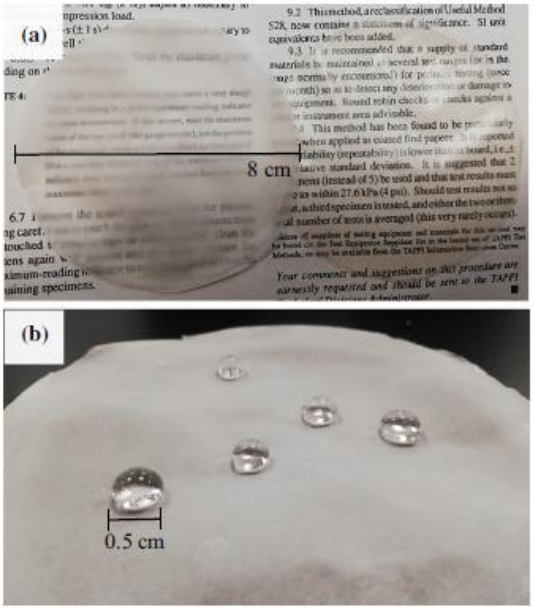

Figure 3 Appearances of an CNF-LBL film (on the left) and an uncoated CNF film (on the right) over conventional copy paper (**a**); water droplets on the surface of an CNF-LBL film (**b**).

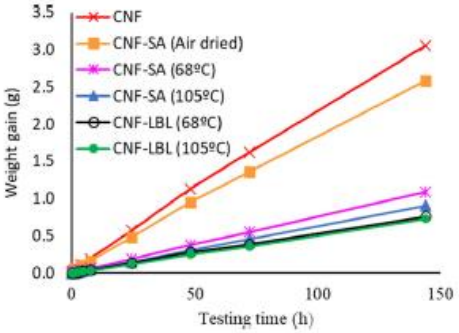

Figure 4 Transferred water vapor as a function of the testing time for different CNF films with and without heat treatment.

Costa et al. have reported extremely low WVTR values (7.53 g m^{-2} day^{-1}) for bacterial cellulose films after hot calendering treatment, with a decrease in global porosity from 29.6 to 5.4% [41].

As it is observable in Fig. 4 and Table 2, the surface treatment with SA has a small positive impact on the WVTR. More importantly, the heat treatment of the CNF-SA films has a tremendous positive impact on the WVTR. The WVTR decreases from 92 to 38 g m^{-2} day^{-1}, when the sample was submitted to a heat treatment during 15 min at 68 °C. This temperature treatment certainly provides some fluidity to the SA layer (the melting point of SA is 69.3 °C). Furthermore, the increase in heat temperature from 68 to 105 °C slightly decreased the WVTR of the films, which validates the supposition that the SA layer melts during heat treatment and the SA molecules fill the interstitial pore space in the fiber network as they gain more mobility with increasing temperature.

This migration of the SA with temperature to the internal pores of the CNF films is also consistent with the decrease in the light scattering coefficient of the heat-treated CNF-SA films (Table 1).

CNF-LBL films showed even lower WVTR relatively to the CNF-SA films, although in this case the effect of increasing heat treatment is not so evident.

Spence et al. reported that coating microfibrillated cellulose (MFC) composite films with beeswax or paraffin decreases the WVTR and hypothesized that this could be due to surface pore closure and filling of the pore network [43]. On another study, paraffin wax (8.6 wt%) was incorporated on pretreated bleached softwood and resulted in a decrease of the WVTR of the produced films, in agreement with a

Table 2 WVTR and OTR of the produced CNF films

Sample	WVTR (g/(m^2 day)	WVP ($\times 10^3$ g/(m day kPa))	OTR (cm^3/(m^2 day)	OP (cm^3 µm/(m^2 day kPa))	Global porosity (%)
CNF	109.0	4.0	55 ± 20	26.4	29.5
CNF-SA	91.9	3.5	–	–	31.3
CNF-SA 68 °C	38.2	1.4	–	–	26.5
CNF-SA 105 °C	31.6	1.1	–	–	23.5
CNF-LBL 68 °C	27.1	1.0	5.3 ± 0.5	2.6	25.3
CNF-LBL 105 °C	25.6	0.9	–	–	22.5

pore filling mechanism [44]. However, the decrease in global porosity alone (from around 30 to 25%) is not enough to justify the drastic decrease in the WVTR and the decrease in surface porosity may be the key factor.

Oxygen transmission rate

The oxygen transmission rate values measured in the neat CNF films are, in general, consistently higher than those reported in the literature [45, 46]. Syverud and Stenius, working with mechanically fibrillated cellulose, have reported values of OP in the range 3.52–5.03 cm^3 µm/(m^2 day kPa) [47]. For CNF produced after TEMPO oxidation, the reported values are even much lower [6, 35, 45]. Österberg et al. have reported values of 0.6 cm^3 µm/(m^2 day kPa). In the present work, the oxygen permeability is around 26.4 cm^3 µm/(m^2 day kPa) and present a very high standard deviation [6]. The morphological evaluation of the CNF suspension by image analysis enabled to detect a significant fraction of fibrous material in the class length of > 0.2 mm (see also Fig. 1). The presence of this significant amount of fiber fragments and the reported low crystallinity index of the CNFs pretreated with TEMPO are the main possible reasons behind the observed higher than expected OP values. Padberg et al. have shown that TEMPO oxidized pulp exhibits lower crystallinity index, which induces higher oxygen permeability [48]. In addition, the high standard deviation suggests the existence of some nonuniformities in the film at nanoscale levels. The effect of the LBL coating on the OTR and OP is notorious. The OP decreased from 26.4 to 2.6 cm^3 µm/(m^2 day kPa) after surface modification with SA and modified PCC. The closure of superficial pores by the stearic acid and the PCC mineral is probably the reasons behind these results. Unfortunately, the OTR was not measured in the stearic acid coated samples and therefore the relative contribution of the SA and mineral coating cannot be disclosed. In addition, it should be emphasized that OTR of these coated CNF films compare favorably with the synthetic ones (p.e. Ethylene vinyl alcohol: 3–5 cm^3/(m^2 day) [49].

Figure 5 depicts the microscopic appearance of an uncoated CNF film and SA coated CNF films, before and after heat treatment at both tested temperatures.

As it is possible to see in Fig. 5, unlike an uncoated CNF film (Fig. 5a) the SA layers without any heat treatment present the engraved marks from the cloths with which they were in contact during the pressing stage (Fig. 5b). The perceptible surface smoothness of the SA layer after heat treatment at 68 °C (Fig. 5d, e) and 105 °C (Fig. 5f, g) is an indicator of a melting process. It is not visually perceptible any major difference between the SA surfaces treated at the two different temperatures (Fig. 5d, f), but the nanoscale irregularities are clear on the surface of the air-dried CNF-SA (c), which may also contribute to the observed light scattering (Table 1).

To modify the surface roughness at a micro- and nano-scale as a way to enhance hydrophobicity, a modified PCC powder was applied on the CNF-SA films.

The modified PCC powder could be easily spread on the top of previously SA coated CNF films, producing CNF-LBL films. Although water droplets placed on these films could smoothly slide across their surface, clearly exhibiting lotus effect (Fig. 3b), the PCC powder layer was just loosely attached to the SA layer and could easily be removed with touch or friction. In order to overcome this critical issue and strengthen the bonding between the SA layer and the modified PCC heat treatment was performed on the films. After a preliminary study, we concluded that

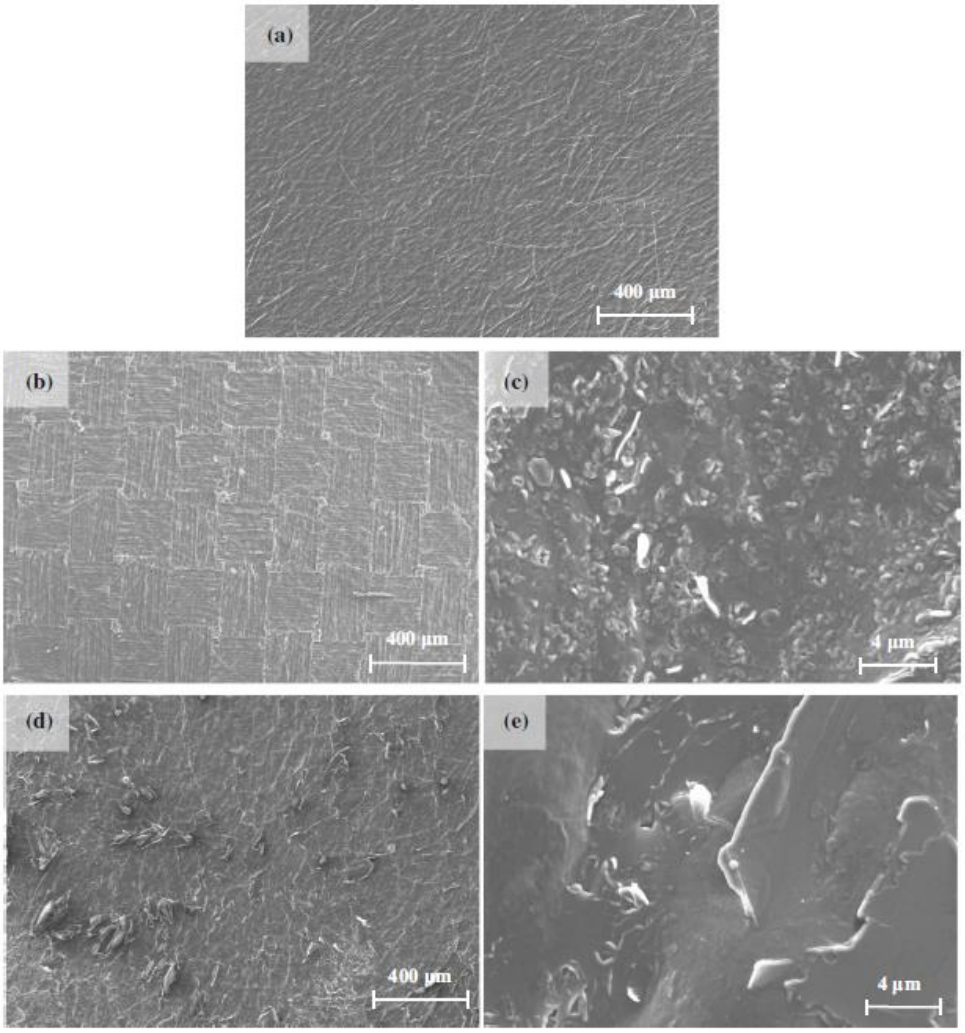

Figure 5 FE-SEM images of the surface of an uncoated CNF film (**a**), SA coated CNF films with no heat treatment (**b**, **c**) and submitted to 68 °C (**d**, **e**) (magnification: **a**, **b** and **d** are ×60; **c** and **e** are ×5 k).

68 °C was the minimum temperature at which the modified PCC powder was able to strongly adhere to the SA surface, in which case the partially melted SA layer acted as a glue between the modified PCC powder layer and the CNF film. On the one hand, a small part of the SA layer migrated into the pores of the neat CNF film, providing mechanical strength between the SA layer and the CNFs; on the other hand, a small portion of the SA molecules on the surface of the modified PCC merged on the underlying SA layer, providing adhesion to the PCC particles. The PCC layer on the top of the produced heat-treated CNF-LBL films (68 and 105 °C) was resistance to touch and friction, maintaining their hydrophobic properties after handling or rubbing with a finger across their surface.

Contact angle measurements

The hydrophilic nature of untreated CNF films is a well-known feature that arises from their high hydroxyl and carboxyl content which may in turn

lead to low resistance to water [35]. The most common method for determining the hydrophilic/hydrophobic nature of a solid is the measurement of its contact angle (CA) with water. The static CA is specific to any given system and can be defined as the angle at which a droplet of probing fluid (water, in this case) meets a given solid, being determined by the interactions across the three-phase line. Generally, the CA is lower than 90° for hydrophilic materials, while hydrophobic ones display a CA higher than 90° [11]. A particular case of hydrophobicity is superhydrophobicity which is characterized by a static contact angle above 150° and also a very small sliding angle, typically lower than 5° [50].

Figure 6 shows the variation of CA over time of a water droplet placed on a neat CNF film and an CNF-SA film with no heat treatment.

Predictably, the neat CNF films were hydrophilic with an initial CA of around 45°. The contact angle decreased with time as a result of partial penetration of water into the film, coming down to 35° after 3 s (Fig. 6). The CA of CNF films can differ according to many different factors, not only chemical composition, but the fibrillation degree of the obtained fibrils as well: a more fibrillated material leads to a more compact and less porous surface, which consequently increases the observed CA [51].

The CA of the neat CNF films is in good agreement with Fukuzumi et al., who reported an initial CA of 47° on an CNF film prepared from TEMPO-oxidized softwood cellulose with a carboxyl group content of 1300–1600 µmol/g, and likewise described the same phenomenon of CA decreasing over time due to partial water penetration [35].

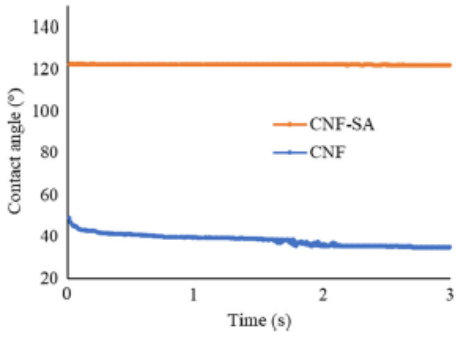

Figure 6 Variation of the CA over time of a water droplet on the surface of CNF and CNF-SA films with no heat treatment.

The CNF-SA film turned out to be hydrophobic, since their measured CA was around 122°. This result resembles that reported by Österberg et al. where CNF films were surface coated using a commercial paraffin wax and the CA increased from 40 to 110° for uncoated and wax coated films, respectively [6].

While the CA of the neat CNF films decreased over time due to swelling, the CA for CNF-SA remained constant for the whole measuring time (3 s), since there was no water penetration into the film due to decreased wettability.

The CA of all the produced films was determined and the results are presented in Table 3. The reported values of CA correspond to the measurement at 3 s to avoid initial instability due to the water droplet wobbling. For visual comparison, the snapshots of the correspondent water droplets at 3 s measurements are also shown.

As presented in Table 3, the application of a SA layer on the surface of the films with no heat treatment was sufficient for providing them with hydrophobicity, attaining a CA of 122°. While the layer of SA successfully hydrophobized the simply air-dried films, heat treatment at 68 °C and 105 °C decreased their CA to 96° and 92°, respectively (Table 3), possibly due to melting of the SA, causing the surface to be smoother (Fig. 5). Forsman et al. applied a carnauba wax dispersion on CNF films using a layer-by-layer coating method and have also performed heat treatment at 103 °C in order to investigate melting of the wax particles and its effect on the coating. They came to the conclusion that the melting of the wax smooths the surface of the films, causing a slight decrease in CA when compared to the untreated films, which is in good agreement with our result [4].

The addition of modified PCC particles, combined with a heat treatment at 68 °C for adhesion, had a notorious positive effect, increasing the CA from 96 to 140°, probably due to the increase in roughness. In order to assess the surface roughness (as an opposite of smoothness) of the uncoated and coated films, Bekk smoothness tests were performed in triplicate on the surface of all produced films and the mean values are reported in Table 4. While the SA coating and especially the LBL coating with no heat treatment drastically increased the surface roughness (Bekk smoothness decreased from 268 to 34 s), heat treatment was able to restore some smoothness to

Table 3 Average CA measured at 3 s for CNF, CNF-SA and CNF-LBL films, with and without heat treatment

Film	Heat treatment (°C)	CA (°)	Water droplet image
CNF	–	35	
CNF-SA	–	122	
CNF-SA	68	96	
CNF-SA	105	92	
CNF-LBL	–	150	
CNF-LBL	68	140	
CNF-LBL	105	135	

those surfaces, particularly for the films treated at 105 °C.

Figure 7 shows the microscopic surface appearance and a cross section of an CNF-LBL film, after heat treatment at 68 °C.

In Fig. 7 it is possible to identify micro- and nano-sized particles of modified PCC powder spread across the surface of the heat-treated CNF-LBL film (Fig. 7a, b). Despite the melting process of the SA layer acting as a binder between the CNF film and the modified PCC, the powder did not completely sink into the SA layer, generating roughness on its surface (Fig. 7c). The PCC particles uniformly covered all the surface of the film (Fig. 7b), providing hydrophobicity since it had a measured CA of 140° (Table 3), although the literature reports that only partial

Table 4 Bekk smoothness test results for the different CNF films

Sample	Bekk smoothness (s)
CNF	268 ± 28
CNF-SA	55 ± 8
CNF-SA 68 °C	86 ± 9
CNF-SA 105 °C	99 ± 9
CNF-LBL	34 ± 6
CNF-LBL 68 °C	50 ± 6
CNF-LBL 105 °C	102 ± 2

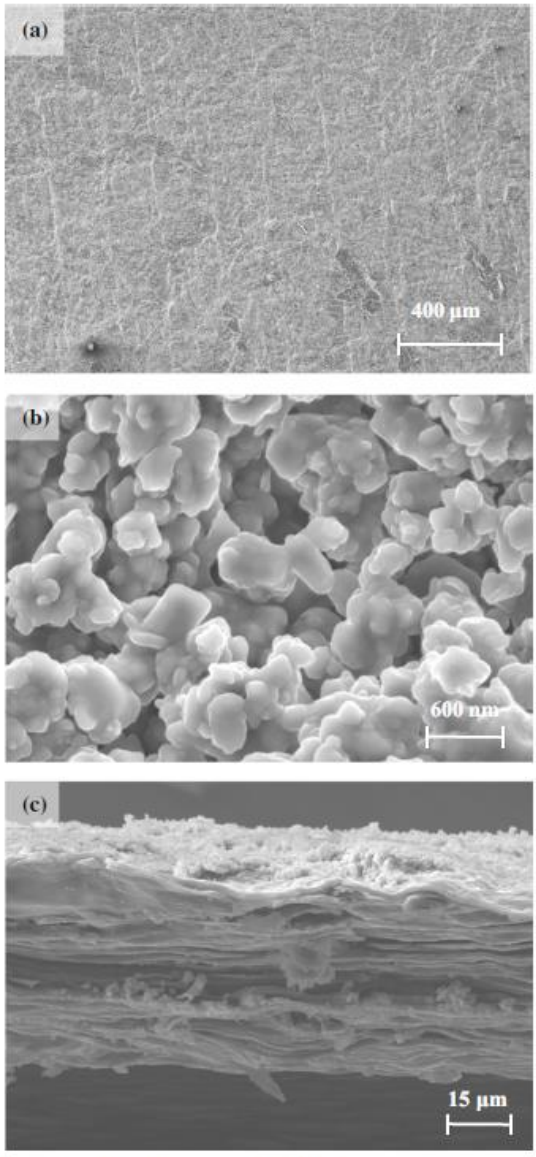

Figure 7 FE-SEM images of CNF-LBL film surface (**a** and **b**) and cross section (**c**) treated at 68 °C (magnifications: **a** is ×60; **b** is ×30 k; **c** is ×1 k).

nanoparticle coverage can be enough to significantly change the wetting properties of a surface [4, 52]. Furthermore, while surfaces with high macroscale roughness may cause inconsistent contact angle measurements, the positive effect of micro- and nanoscale roughness on hydrophobicity has been reported by many authors [53–55].

The cross section of an CNF-LBL film, shown in Fig. 7c with the modified PCC powder facing upward, enabled to perceive that the layered film is actually quite compact and uniform, with no distinguishable layered fractions, which certainly contributes to the physical integrity of the whole set.

According to Table 3, the increase in temperature in the heat treatment from 68 to 105 °C slightly decreased the CA of the CNF-LBL films from 140 to 135°, probably because the SA layer became melted enough for some modified PCC particles to completely sink in, slightly decreasing the overall surface's roughness (Table 4). Even though the SA layer only constitutes 5% of the total weight of the layered film, this result shows that adjustments in the amount of SA used to coat the CNF films, eventually reducing the thickness of the SA layer, might come as advantageous.

Another important parameter when researching hydrophobic surfaces is their CA hysteresis, i.e., the difference between the advancing CA and the receding CA [11, 56]. ARCA measurements were performed as follows: the advancing CA was measured by gradually increasing the volume of a probe droplet until the three-phase (solid–liquid–gas) contact line begins to expand, at which point a maximum CA was reached. Reciprocally, the receding CA was measured by gradually decreasing the volume of a sessile droplet until the contact line began to shrink, at which point the receding CA can be obtained [57].

For a super-hydrophobic surface for instance, apart from having a static CA above 150 °C, the water droplet shall not stick to the surface of the sample, having thus low CA hysteresis [11, 19].

ARCA measurements were performed on CNF-SA and CNF-LBL films with and without heat treatment.

The obtained CA hystereses for the CNF films are plotted in Fig. 8, as ARCA cycles (succeeding increase and decrease of the probe droplet's volume as a function of time).

It is worth mentioning that the initial CAs registered in Fig. 8 are somewhat lower than those previously reported as static CAs for the respective films in Table 3. The reason for this is related to the different CA measuring techniques: while a typical static CA measurement is carried out using a sessile drop method, where the probe droplet is placed on top of the sample and the needle is removed before the measurement, an ARCA cycle involves CA measurements performed using a needle-in-drop method, which is a requirement for increasing and decreasing its volume. The decrease in the CA arises as a consequence of the additional adhesion between the water and the needle, which slightly changes the water droplet geometry, leading to lower measured contact angles. From the results, it is evident that the CNF-LBL samples exhibit higher contact angles and lower hysteresis values than the CNF-SA samples, highlighting the role of the micro/nanoscale roughness on the hydrophobic and super hydrophobic behavior.

Hu and Deng used a comparable approach to achieve a superhydrophobic layer through chemically modifying PCC particles in water with oleic acid. They studied the CA hysteresis of the modified material and reported a CA hysteresis of 2.5° for an oleic acid content of 1.09 wt% and a CA hysteresis of nearly zero for an optimum oleic acid content of 2.51 wt%, with a corresponding advancing water CA of 164° [58]. These results are not far from those achieved in the present work, where an CNF-LBL film with no heat treatment attained a CA hysteresis of 3.1° (149.5–146.4°) and a static CA of 150°. Even

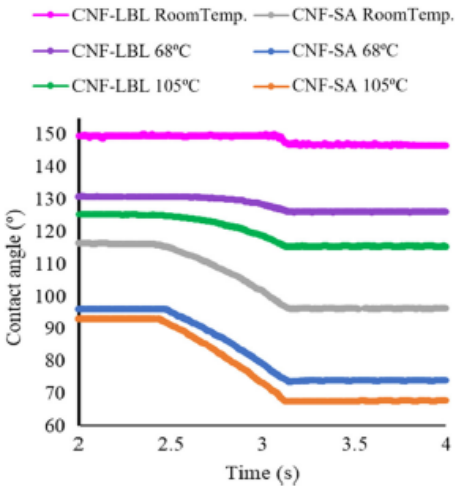

Figure 8 Plot of the CA hysteresis for the different produced films.

after the heat treatment at 68 °C, a CA hysteresis of 5° (131–126°) was reached, with a static CA of 140°. Furthermore, while Hu and Deng performed CA measurements on the modified PCC particles using double-sided adhesive tape as the substrate, in the present work, through a simple heat treatment, we were able to permanently adhere modified PCC particles on CNF films surface, using an intermediate layer of stearic acid as a binder [58].

Conclusions

Smooth and translucent CNF films were produced through vacuum filtration using 0.65 µm pore size nitrocellulose membranes as filtration media, with no substantial loss of material during the filtration process.

Both apparent density and tensile index of the produced CNF films, varying from 1.10 and 1.24 g/cm^3, and from 101.6 and 111.7 Nm/g, respectively, are in general comparable with the literature results. The overall mechanical performance of the films suffered no major alterations after surface treatment with SA and modified PCC and with posterior heat treatments.

Concerning barrier properties, heat treatments decreased the WVTR of SA layered CNF films from 91.9 down to 31.6 g m^{-2} day^{-1}, probably due to SA melting, filling the interstitial pore space in the fiber network. The closure of superficial pores by SA and modified PCC also caused a drastic decrease in the oxygen permeability from 26.4 to 2.6 cm^3 µm/(m^2 day kPa).

Surface coating CNF films with a SA layer rendered them hydrophobic, increasing the water CA from 45 to 122°. Heat treatments at 68 °C and 105 °C decreased the CA to 96° and 92°, respectively, due to melting of the SA layer, causing the surface to be smoother. On the other hand, the addition of modified PCC increased the CA from 96 to 140° with a heat treatment of 68 °C, and to 150 °C, with no heat treatment, most likely due to nanoscale roughness provided by the modified PCC particles.

The heat treatment was a key stage in the process, enabling the adherence of the modified PCC particles onto the stearic acid layer and the later to the CNF network, providing a *quasi*-superhydrophobic film with good resistance to handling and rubbing, using an easy and green process.

Acknowledgements

The research undertaken for this paper was performed under the UBI-Celtejo cooperation protocol. The authors are very grateful for the support given by research unit Fiber Materials and Environmental Technologies (FibEnTech-UBI), on the extent of the project reference UIDB/00195/2020, funded by the Fundação para a Ciência e a Tecnologia, IP/MCTES through national funds (PIDDAC).

Declarations

Conflict of interest The authors declare that they have no conflict of interest.

References

[1] Jenck JF, Agterberg F, Droescher MJ (2004) Products and processes for a sustainable chemical industry: a review of achievements and prospects. Green Chem 6(11):544

[2] Abdul Khalil HPS, Bhat AH, Ireana Yusra AF (2012) Green composites from sustainable cellulose nanofibrils: a review. Carbohyd Polym 87(2):963–979

[3] Ivanković A, Dronjić A, Bevanda AM, Talić S (2017) Review of 12 principles of green chemistry in practice. Int J Sustain Green Energy 6(3):39–48

[4] Forsman N, Lozhechnikova A, Khakalo A, Johansson L-S, Vartiainen J, Österberg M (2017) Layer-by-layer assembled hydrophobic coatings for cellulose nanofibril films and textiles, made of polylysine and natural wax particles. Carbohyd Polym 173:392–402

[5] Zimmermann T, Bordeanu N, Strub E (2010) Properties of nanofibrillated cellulose from different raw materials and its reinforcement potential. Carbohyd Polym 79(4):1086–1093
[6] Österberg M, Vartiainen J, Lucenius J, Hippi U, Seppälä J, Serimaa R, Laine J (2013) A fast method to produce strong NFC films as a platform for barrier and functional materials. ACS Appl Mater Interfaces 5(11):4640–4647
[7] Kalia S, Boufi S, Celli A, Kango S (2014) Nanofibrillated cellulose: surface modification and potential applications. Colloid Polym Sci 292(1):5–31
[8] Stark NM (2016) Opportunities for cellulose nanomaterials in packaging films: a review and future trends. J Renew Mater 4(5):313–326
[9] Gonçalves G, Marques PAAP, Trindade T, Neto CP, Gandini A (2008) Superhydrophobic cellulose nanocomposites. J Colloid Interface Sci 324(1–2):42–46
[10] Jonoobi M, Harun J, Mathew AP, Hussein MZB, Oksman K (2010) Preparation of cellulose nanofibers with hydrophobic surface characteristics. Cellulose 17(2):299–307
[11] Song J, Rojas OJ (2013) Paper chemistry: approaching super-hydrophobicity from cellulosic materials: a review. Nord Pulp Pap Res J 28(2):216–238
[12] Rastogi V, Stanssens D, Samyn P (2014) Mechanism for tuning the hydrophobicity of microfibrillated cellulose films by controlled thermal release of encapsulated wax. Materials 7(11):7196–7216
[13] Sehaqui H, Zimmermann T, Tingaut P (2014) Hydrophobic cellulose nanopaper through a mild esterification procedure. Cellulose 21(1):367–382
[14] Yuan Z, Wen Y (2018) Enhancement of hydrophobicity of nanofibrillated cellulose through grafting of alkyl ketene dimer. Cellulose 25(12):6863–6871
[15] Rol F, Belgacem MN, Gandini A, Bras J (2019) Recent advances in surface-modified cellulose nanofibrils. Prog Polym Sci 88:241–264
[16] Kalia S, Thakur K, Celli A, Kiechel MA, Schauer CL (2013) Surface modification of plant fibers using environment friendly methods for their application in polymer composites, textile industry and antimicrobial activities: a review. J Environ Chem Eng 1(3):97–112
[17] Liimatainen H, Ezekiel N, Sliz R, Ohenoja K, Sirviö JA, Berglund L et al (2013) High-strength nanocellulose-talc hybrid barrier films. ACS Appl Mater Interfaces 5(24):13412–13418
[18] Samyn P (2013) Wetting and hydrophobic modification of cellulose surfaces for paper applications. J Mater Sci 48(19):6455–6498. https://doi.org/10.1007/s10853-013-7519-y
[19] Mertaniemi H, Laukkanen A, Teirfolk J-E, Ikkala O, Ras RHA (2012) Functionalized porous microparticles of nanofibrillated cellulose for biomimetic hierarchically structured superhydrophobic surfaces. RSC Adv 2(7):2882
[20] Huang J, Lyu S, Fu F, Chang H, Wang S (2016) Preparation of superhydrophobic coating with excellent abrasion resistance and durability using nanofibrillated cellulose. RSC Adv 6(108):106194–106200
[21] Arbatan T, Fang X, Shen W (2011) Superhydrophobic and oleophilic calcium carbonate powder as a selective oil sorbent with potential use in oil spill clean-ups. Chem Eng J 166(2):787–791
[22] Hu Z, Zen X, Gong J, Deng Y (2009) Water resistance improvement of paper by superhydrophobic modification with microsized $CaCO_3$ and fatty acid coating. Colloids Surf, A 351(1–3):65–70
[23] El-Sheikh SM, Barhoum A, El-Sherbiny S, Morsy F, El-Midany AA-H, Rahier H (2019) Preparation of superhydrophobic nanocalcite crystals using Box-Behnken design. Arab J Chem 12(7):1479–1486
[24] Wang C, Sheng Y, Zhao X, Pan Y, Hari-Bala WZ (2006) Synthesis of hydrophobic CaCO3 nanoparticles. Mater Lett 60(6):854–857
[25] Wang C, Piao C, Zhai X, Hickman FN, Li J (2010) Synthesis and characterization of hydrophobic calcium carbonate particles via a dodecanoic acid inducing process. Powder Technol 198(1):131–134
[26] Xu M, Dai H, Sun X, Wang S, Wu W (2012) Influence of buffer solution on tempo-mediated oxidation. BioResources 7(2):1633–1642. https://doi.org/10.15376/biores.7.2.1633-1642
[27] Henriksson M, Berglund LA, Isaksson P, Lindström T, Nishino T (2008) Cellulose nanopaper structures of high toughness. Biomacromolecules 9(6):1579–1585
[28] Lozhechnikova A, Bellanger H, Michen B, Burgert I, Österberg M (2017) Surfactant-free carnauba wax dispersion and its use for layer-by-layer assembled protective surface coatings on wood. Appl Surf Sci 396:1273–1281
[29] Costa VLD, Costa AP, Simões RMS (2019) Nanofibrillated cellulose rheology: effects of morphology, ethanol/acetone addition and high NaCl concentration. BioResources 14(4):7636–7654
[30] Besbes I, Alila S, Boufi S (2011) Nanofibrillated cellulose from TEMPO-oxidized eucalyptus fibres: effect of the carboxyl content. Carbohyd Polym 84(3):975–983
[31] Isogai A, Saito T, Fukuzumi H (2011) TEMPO-oxidized cellulose nanofibers. Nanoscale 3(1):71–85
[32] Shinoda R, Saito T, Okita Y, Isogai A (2012) Relationship between length and degree of polymerization of TEMPO-oxidized cellulose nanofibrils. Biomacromolecules 13(3):842–849

[33] Saito T, Nishiyama Y, Putaux J-L, Vignon M, Isogai A (2006) Homogeneous suspensions of individualized microfibrils from TEMPO-catalyzed oxidation of native cellulose. Biomacromolecules 7(6):1687–1691
[34] Sehaqui H, Liu A, Zhou Q, Berglund LA (2010) Fast preparation procedure for large, flat cellulose and cellulose/inorganic nanopaper structures. Biomacromolecules 11(9):2195–2198
[35] Fukuzumi H, Saito T, Iwata T, Kumamoto Y, Isogai A (2009) Transparent and high gas barrier films of cellulose nanofibers prepared by TEMPO-mediated oxidation. Biomacromolecules 10(1):162–165
[36] Wang W, Sabo RC, Mozuch MD, Kersten P, Zhu JY, Jin Y (2015) Physical and mechanical properties of cellulose nanofibril films from bleached eucalyptus pulp by endoglucanase treatment and microfluidization. J Polym Environ 23(4):551–558
[37] Lindström T (2017) Aspects on nanofibrillated cellulose (NFC) processing, rheology and NFC-film properties. Curr Opin Colloid Interface Sci 29:68–75
[38] Kumar V, Bollström R, Yang A, Chen Q, Chen G, Salminen P, Bousfield D, Toivakka M (2014) Comparison of nano- and microfibrillated cellulose films. Cellulose 21:3443–3456
[39] Shen J, Song Z, Qian X, Liu W (2009) Modification of papermaking grade fillers: a brief review. BioResources 4(3):1190–1209
[40] Bedane AH, Eić M, Farmahini-Farahani M, Xiao H (2015) Water vapor transport properties of regenerated cellulose and nanofibrillated cellulose films. J Membr Sci 493:46–57
[41] Costa VLD, Costa AP, Amaral ME, Oliveira C, Gama M, Dourado F, Simões RM (2016) Effect of hot calendering on physical properties and water vapor transfer resistance of bacterial cellulose films. J Mater Sci 51(21):9562–9572 https://doi.org/10.1007/s10853-016-0112-4
[42] Nair SS, Zhu J, Deng Y, Ragausks AJ (2014) High performance green barriers based on nanocellulose. Sustain Chem Process 2(23):1–7. https://doi.org/10.1186/s40508-014-0023-0
[43] Spence K, Venditti R, Rojas O, Pawlak J, Hubbe M (2011) Water vapor barrier properties of coated and filled microfibrillated cellulose composite films. BioResources 6(4):4370–4388
[44] Spence KL, Venditti RA, Rojas OJ, Habibi Y, Pawlak JJ (2010) The effect of chemical composition on microfibrillar cellulose films from wood pulps: water interactions and physical properties for packaging applications. Cellulose 17(4):835–848
[45] Aulin C, Gällstedt M, Lindström T (2010) Oxygen and oil barrier properties of microfibrillated cellulose films and coatings. Cellulose 17:559–574
[46] Lavoine N, Desloges I, Dufresne A, Bras J (2012) Microfibrillated cellulose – its barrier properties and applications in cellulosic materials: a review. Carbohyd Polym 90(2):735–764
[47] Syverud K, Stenius P (2009) Strength and barrier properties of MFC films. Cellulose 16(1):75–85
[48] Padberg J, Bauer W, Gliese T (2016) The influence of fibrillation on the oxygen barrier properties of films from microfibrillated cellulose. Nord Pulp Pap Res J 31(4):548–560
[49] Kim D, Kwon H, Seo J (2013) EVOH nanocomposite films with enhanced barrier properties under high humidity conditions. Polym Compos 53(4):644–654
[50] Lv C, Yang C, Hao P, He F, Zheng Q (2010) Sliding of water droplets on microstructured hydrophobic surfaces. Langmuir 26(11):8704–8708
[51] Sharma S, Nair SS, Zhang Z, Ragauskas AJ, Deng Y (2015) Characterization of micro fibrillation process of cellulose and mercerized cellulose pulp. RSC Adv 5(77):63111–63122
[52] Dong L, Nypelö T, Österberg M, Laine J, Alava M (2010) Modifying the wettability of surfaces by nanoparticles: experiments and modeling using the Wenzel law. Langmuir 26(18):14563–14566
[53] Cao L, Hu H-H, Gao D (2007) Design and fabrication of micro-textures for inducing a superhydrophobic behavior on hydrophilic materials. Langmuir 23(8):4310–4314
[54] Bhushan B, Koch K, Jung YC (2008) Biomimetic hierarchical structure for self-cleaning. Appl Phys Lett 93(9):093101
[55] Rodionova G, Eriksen Ø, Gregersen Ø (2012) TEMPO-oxidized cellulose nanofiber films: effect of surface morphology on water resistance. Cellulose 19(4):1115–1123
[56] Kusumaatmaja H, Yeomans JM (2007) Modeling contact angle hysteresis on chemically patterned and superhydrophobic surfaces. Langmuir 23(11):6019–6032
[57] Ras RHA, Tian X, Bayer IS (2017) Superhydrophobic and superoleophobic nanostructured cellulose and cellulose composites. In: Kargarzadeh H, Ahmad I, Thomas S, Dufresne A (eds) Handbook of nanocellulose and cellulose nanocomposites. Wiley, Weinheim, pp 731–760
[58] Hu Z, Deng Y (2010) Superhydrophobic surface fabricated from fatty acid-modified precipitated calcium carbonate. Ind Eng Chem Res 49(12):5625–5630

3.5. Paper 4 - Effect of Ethanol Addition on the Drainage Time of Aqueous/Ethanol NFC Suspensions and on Barrier and Mechanical Properties of the Produced Films

V. L. D. Costa and R. M. S. Simões
Journal of Material Sciences and Applications (2021) 6:102
DOI 10.17303/jmsa.2022.6.102

Journal of
Materials Sciences and Applications

JScholar
Fostering Scholarly Communication

Research Article Open Access

Effect of Ethanol Addition on the Drainage Time of Aqueous/Ethanol NFC Suspensions and on Barrier and Mechanical Properties of the Produced Films

VLD Costa[1,2*] and RMS Simões[1,2]

[1]Research unit of Fiber Materials and Environmental Technologies (FibEnTech-UBI), Universidade da Beira Interior, Covilhã, Portugal

[2]Department of Chemistry, University of Beira Interior, Covilha, Portugal

***Corresponding author:** Vera Lúcia Dias da Costa, Research Unit of Fiber Materials and Environmental Technologies (FibEnTech-UBI) Universidade da Beira Interior, Rua Marquês d'Avila e Bolama, 6200-001 Covilhã, Portugal, Tel: +351275319739, E-mail: vera. costa@ubi.pt

Received Date: December 24, 2021 **Accepted Date:** January 22, 2022 **Published Date:** January 25, 2022

Citation: VLD Costa (2022) Effect of Ethanol Addition on the Drainage Time of Aqueous/Ethanol NFC Suspensions and on Barrier and Mechanical Properties of the Produced Films. J Mater sci Appl 6: 1-13

Abstract

NFC aqueous/ethanol suspensions with a solid content 0.3 wt.% were produced from a TEMPO-oxidized bleached kraft eucalypt pulp, with ethanol content varying from o to 75 wt.%. Films were manufactured from these suspensions through vacuum filtration at a constant absolute pressure, and the draining progression was monitored by measuring the collected filtrate. The NFC filtration cakes were adhered to metallic discs and kept under pressure applied to the edges while they dried either in standard conditions of temperature and humidity or in an oven at 70ºC for 4 hours. The resulting films were tested for mechanical and optical performance and water vapor barrier properties. Results show that filtrating time decreases drastically with the increase of ethanol content, from about 2 hours to 2 minutes for 0 and 75 wt.% ethanol suspensions, respectively. The films' porosity generally increased with the increase of ethanol content. The mechanical performance of standard dried films was not affected by increasing ethanol content, despite the global porosity increase from 18.8% to 31.3%. On the other hand, the tensile index drastically increased for oven-dried films up to 124 and 90.2 N m g^{-1} for 0 and 75 wt.% ethanol suspensions, respectively, despite significant increase in elongation and scattering coefficient. Water vapor transmission rate increased up to 207.48 g m^{-2} day^{-1} for films produced from 75 wt.% ethanol suspensions.

Keywords: Nano Fibrillated Cellulose; Ethanol; Films Production; Drainage Time; Mechanical Performance; Water Vapor Barrier.

Introduction

Nanotechnology is a field that researches nanomaterials, which are materials with structural units on a nanometer scale in at least one direction. These materials have enhanced and desirable chemical and physical properties, that can be tailored and harvested according to several diverse applications, such as light-harvesting and bioelectricity [1]; scaffolds for bone tissue engineering [2, 3] and composite thermally insulating materials [4].

Nanocellulosic materials have strong self-association tendency and an inherent predisposition to form films upon drying through strong interactions within the numerous surface hydroxyl groups. These films have unique physical properties such as high strength and translucency or even fully transparency, depending on the overall dimensions of the individual fibrils [5].

The inherent strength of crystalline cellulose combined with the strong interfibrillar interaction can be harvested in order to manufacture mechanically robust NFC-based films with excellent oxygen barrier properties in dry conditions and susceptible to functionalization [6,7].

NFC films usually have a good mechanical resistance, with tensile strength and Young's modulus typically varying within 100–200 MPa and 5–10 GPa, respectively, although large variation in mechanical behavior can be expected due to numerous reasons such as the chemical composition of the NFC raw material and chemical/ mechanical pretreatments, which directly influence the fibril size and size distribution as well as the amount of interfibrillar contacts within the formed films [5].

The resistance to solvents, even to water, is another useful property of dried films made from NFC aqueous suspensions: while soaking normal dried pulp sheets in water causes weakening and structure disintegration into individual fibers due to their strong interaction with water through hydrogen bonding, NFC films, on the other hand, remain resilient after extended contact with solvents such as ethanol, acetone, and toluene or even water. Hornification due to additional hydrogen bonding in the amorphous regions of cellulose and consequent irreversible fibril agglomeration has been suggested as the reason behind this observed solvent resistance [8-10].

Several authors have reported the manufacture of NFC based films through filtration of NFC suspensions, followed by hot-pressing the NFC filtering cake under high loads in order to avoid wrinkling and considerably reduce the drying time, besides improving the mechanical properties due to the densification of the structure [10 - 12] but, depending on the material used in the filtration and pressing processes, the films can end up not being entirely smooth, or with some level of irregularities on their surface [10].

Furthermore, the most acknowledged drawback of the majority of the reported approaches concerning pure NFC films formation is the extremely slow dewatering of NFC aqueous suspensions, making the process extremely time-consuming, usually requiring several hours to a few days and with complicated manipulations [10].

Many authors have reported filtrating times that go anywhere from 45 minutes [11] to 3-4 hours [13] using fine pore size filter media (0.65 µm and 0.1 µm), depending on the filtrated volume, operating conditions, intended grammage and on the morphology of the fibrils, which can also play an important role in the draining progression [14].

In an effort to fasten the filtrating process, some authors have tried increasing the pore size of the filtrating medium [10,14], but it came with a drawback. Österberg *et al.* have reported a fast method for producing NFC films through pressurized filtration using an open mesh fabric with a 10 µm pore size at 2.5 bar pressure [10]. The filtration process took less than an hour, but at the expenses of losing 40% of the material through the pores during the process, for every produced film. Lower drainage time (up to 3 minutes) and with 94% fibril retention was reported by Varanasi and Batchelor, applying vacuum of 25 MPa through a 125 µm woven copper wire mesh filter medium [12].

Another reported technique for filtration aid is the addition of high molecular weight cationic polyacrylamide [15]. The authors have analyzed the flocculation and water drainability of an MFC gel as a function of the polyelectrolyte dosage, charge density and molecular weight, and reported a drainage time as low as to 9.5 minutes, giving rise to highly porous films, suggesting a retention of a more open colloidal structure of the material upon drying. Despite the fast film formation process, the resulting material was a cellulose-based composite rather

than a purely nanocellulosic film, since both cellulosic fibrils and added polyelectrolyte were combined in on single structure.

While solvent exchange to a non-aqueous media of previously drained or casted NFC aqueous suspensions is extensively performed either to prevent structural changes during subsequent surface modification, tailor the porosity of the film or to fasten the drying process [6, 16 -19], to the best of our knowledge, no studies have been undertaken concerning the formation of neat NFC films from ethanol/aqueous suspensions.

The present work aims to study the effect of NFC aqueous/ethanol suspensions composition on the drainage time and specific resistance of the NFC cake during NFC films formation through vacuum filtration and on barrier/mechanical properties of the resulting films.

Materials and Methods

A commercial Totally Chlorine Free (TCF) never dried bleached kraft eucalypt pulp (average limiting viscosity was 570 mL/g) was utilized as a source of native cellulose fibers. Ethanol 99% (Sigma-Aldrich, USA) was used without further purification.

NFC suspensions production

The NFC suspension was produced in an analogous way to a previously reported work [20]. In resume, a commercial never dried bleached kraft eucalypt pulp was submitted to 2 successive homogenization steps at 500 and 850 bar, using a GEA Niro Soavi high pressure homogenizer (Panther NS3006L; GEA, Parma, Italy), and was afterwards submitted to 2,2,6,6-tetramethylpiperidine-1-oxyl radical (TEMPO) mediated oxidation.

Morphological characterization of the fibrils

In order to morphologically characterize the cellulose fibrils in the obtained NFC suspension, a drop of 0.01 wt.% NFC suspension was allowed to air dry overnight at room temperature on a scanning electron microscope (SEM) sample holder.

The samples were previously gold sputtered by cathodic spraying (Quorum Q150R ES; Quorum Technologies, East Sussex, UK) and microscopic observations were performed using SEM (Hitachi S-2700; Hitachi, Tokyo, Japan) operated at 20 kV.

For the transmission electron microscope (TEM) imaging, drops of 0.001 wt% NFC suspension were deposited on carbon-coated electron microscopic grids and negatively stained with 2 wt% uranyl acetate. The grids were air-dried and analyzed with a Hitachi HT-7700 TEM (Hitachi, Tokyo, Japan) with an acceleration voltage of 80 kV.

Cellulose degree of polymerization

The NFC limiting viscosity (η) was determined according to the ISO 5351 (2012) standard, with a cupriethylenediamine (CED) solution as a solvent and using a capillary viscometer. The degree of polymerization (DP) was calculated using the literature' equations [6].

Total acidic groups content

The total acidic groups content in the produced NFC was determined through a conductivity titration method, based on the standard SCAN-CM 65:02, as described in a previous paper [20].

Production of films from NFC aqueous/ethanol suspensions

The previously produced NFC suspension was diluted to a solid content of 0.3 wt.%, using the required amounts of water and ethanol, and homogenized (Ultra-Turrax T-25 Digital Homogenizer, Ika Labortechnik, Staufen, Germany) for 2 minutes at 6000 rpm. The resulting suspension was subjected to a mild ultrasound bath (S30H, Elmasonic, Singen, Germany) for 5 minutes to release the air bubbles.

Simple NFC films with a diameter of 8.5 cm and a target grammage of 50 g m^{-2} were prepared by vacuum filtration in a filtrating funnel, using a 0.65 µm pore size nitrocellulose membrane (Millipore, Bedford, Mass., USA) as filtration medium, attached to a filter paper for added support. Vacuum filtration was carried out at a constant absolute pressure of 0.2 bar, using a vacuum pump. The draining progression was monitored by collecting the filtrate and weighing it along the filtration time. The filtrations were considered to be over whenever the drainage stopped.

The NFC wet filtration cake and filtrating membrane were placed between blotting papers, followed by pressing for 5 minutes at 2.19 x 10^5 N m^{-2}. Then, a metallic disc was thorough-

ly placed on top of the film, and the whole set was once again pressed for an additional 10 seconds at the same pressure, just enough for the NFC film to adhere to the metallic disc. The filtrating membrane was removed at this stage. Finally, the NFC films were dried, between perforated metallic rings under pressure applied to the edge of the films in order to prevent them from shrinking. The films were dried either overnight in a standard atmosphere for conditioning (23 °C and 50 % of relative humidity), or in an oven at 70°C for 4 hours. The oven dried films were conditioned in standard conditions overnight before testing.

Characterization of films produced from NFC aqueous/ethanol suspensions

The basis weight of the films was calculated according to ISO 536:2012 and their thickness was measured with a micrometer (Adamel & Lhomargy, M120 series, New York, USA). The arithmetic average of four measurements was used.

The apparent density of the films was determined from the basis weight and thickness.

The corresponding porosity of the films was estimated according to the equation (1).

$$Porosity\ (\%) = 100 \times 1 - \left(\frac{\rho_{film}}{\rho_{cellulose}}\right)^{2} \quad (1)$$

Where ρ_{film} is the apparent density of the film, g/cm^3 and $\rho_{cellulose}$ is the density of crystalline cellulose, which is assumed to be 1.6 g/cm^3.

The tensile properties of the produced films were tested according to ISO 187:1990. The tensile strength, elongation at break and Young's modulus were determined using an universal tensile testing equipment (Thwing-Albert Instrument Co., EJA series, Philadelphia, USA) with a load cell of 100 N and a constant rate of elongation (20 mm.min^{-1}), according to ISO 1924-2:2008. The distance between grips was 50 mm. To avoid slippage at the sample holders, small pieces of paper tape were attached to the edges of the samples.

Static bending stiffness was performed by a bending tester (Lorentzen & Weltre, Sweeden) at an angle of 25 degrees and a 50 mm distance, according to an adaptation made from ISO 5628:2012. For all tests, at least four representative films have been tested and the arithmetic average values are presented. The optical properties of the films (brightness (ISO 2470-1:2009) and transparency) were determined through spectrophotometry (Technidyne Corp., Color Touch® 2, France).

Water vapor barrier properties

The water vapor transmission rate (WVTR) was determined for the produced films according to Tappi 448 om-09. Home customed containers were used, ensuring constant water vapor partial pressures in both sides of the films throughout the essays. The interior of the containers had a given amount of anhydrous granular calcium chloride that ensured zero water vapor partial pressure inside the recipients. The other side of the films was in contact with the standard conditions of temperature and humidity of the laboratory. The amount of water vapor that diffused through the films was accounted by the mass increase of the whole set. The whole sets were periodically weighted for as long as 144 hours and the mass gain was used to determine the WVTR (g (m^2 day)$^{-1}$) of each sample, according to the equation (2).

$$WVTR = \frac{S}{A} \quad (2)$$

Where S corresponds to the slope of a liner regression that best fits the plot of weight gain *vs* testing time (g days^{-1}) and A is the area of the films (m^2).

Statistical analysis

The experimental data were subjected to statistical analysis using SPSS 28 software (SPSS Inc., Chicago, USA) and were examined using analysis of variance (ANOVA). Tukey's test was used to verify the significant differences among the values at $p<0.05$.

Results and Discussion

Morphological characterization of the fibrils

The morphology of the fibrils was investigated through observations with SEM and TEM in order to give an overview on the present micro- and nanoscale elements. Figure 1 depicts the morphological characteristics of the produced NFC.

[2] Equation (1) Should be

$$Porosity\ (\%) = \ 100 \times \left(1 - \frac{\rho\ film}{\rho\ cellulose}\right)$$

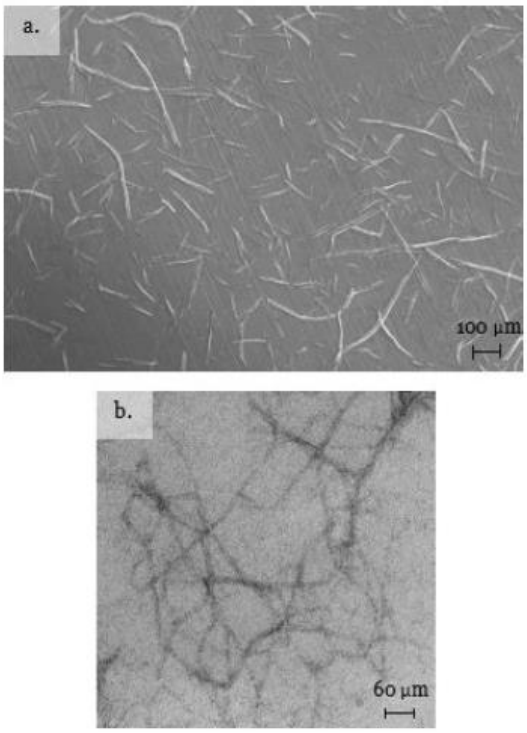

Figure 1: NFC fibrils imaged through SEM (a) and TEM (b)

As Figure 1 shows, the pulp has been disintegrated into nanofibrils (Figure 1, b), although many microscale elements are also observable (Figure 1, a).

Physico-chemical characterization of the fibrils

The TEMPO-oxidized fibrils had a determined limiting viscosity of 154 mL/g, corresponding to a calculated average DP of 367, which are by far lower than those of the starting material (limiting viscosity of 570 ml/g, corresponding to a DP of 1429). The resulting average carboxyl groups content was 997 µmol/g. These results are in good agreement with what has been reported in the literature for similar pretreatments using TEMPO/NaBr/NaClO oxidation systems [21 - 23].

Draining evaluation

The drainage progression throughout filtration of the aqueous/ethanol NFC suspensions is depicted in Figure 2.

At the end of the filtration process, the total recovered filtrate was not the same in every essay due to some evaporation, but Figure 2 makes clear that the filtrating rate increases drastically with the increase of ethanol content in the suspension. While an aqueous NFC suspension (0 wt.% ethanol) took around 180 minutes, increasing the ethanol content to 50, 60 and 75 wt.% fastened the filtration process to around 120, 18 and 2 minutes, respectively, using a 0.65 µm pore size nitrocellulose membrane as a filtration medium.

To further characterize the NFC suspension filtration process, the data was analyzed based on the Hagen-Poiseuille's equation (equation 3), taking in account that the transmembrane pressure (ΔP) is constant (0.8×10^5 N m^{-2}).

$$\frac{At}{V} = \frac{\mu \alpha \rho_0}{2 \Delta P} \times \frac{V}{A} + \frac{\mu R_M}{\Delta P} \qquad (3)$$

Where A is the filtrating membrane area (m^2); t is the filtrating time (s); V is the filtrate volume (m^3); µ is the filtrate viscosity (Pa s); α is the cake specific resistance; R_M is the membrane specific resistance; ρ_0 is the weight of cake per unit volume of filtrate (kg m^{-3}); ΔP is the transmembrane pressure (N m^{-2}).

Under these circumstances, the representation of At/V as function of V/A should give a linear plot, where intercept of the linear regression is related to the R_M and the slope is related to the α, if the cake is incompressible.

Figure 3 represents this profile for the NFC aqueous suspension (0 wt.% ethanol).

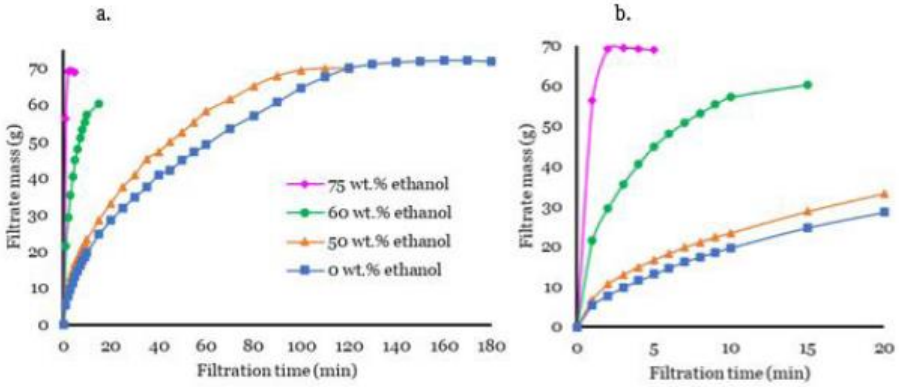

Figure 2: Monitorization of drainage during the manufacture of films from NFC suspensions with different ethanol contents: a.) total filtration time; b.) zoom in of the first 20 minutes of filtration

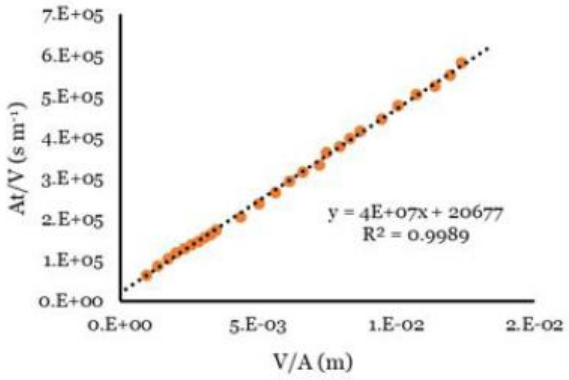

Figure 3: Linear regression of At/V as function of V/A in an NFC aqueous suspension filtration process

As we can see in Figure 3, the experimental values have an excellent linear fitting, with an R^2 over 0.99, confirming that this cake is incompressible and thus it is possible to estimate both α and R_M. The same data treatment was performed on the subsequent essays with increasing ethanol content; the fittings were also good, but the specific membrane resistance appears negative, which indicates some deviation from the model. The calculated α and R_M are presented in Table 1, taking into account the change of the viscosity of the medium, which increases somewhat with ethanol addition.

As expected from the drainage profiles in Figure 2, the NFC cake specific resistance decreases drastically with the addition of ethanol to the aqueous NFC suspension. Theoretically, the cake specific filtration resistance depends on the cake porosity and specific surface area of the particles. As we will see later in the paper, the porosity of the dry film increases significantly from 18.8% for 0 and 50 wt.% ethanol to 25.5% and 31.3%, respectively for 60 and 75wt.% ethanol (Table 2). The wet thickness of the cake could not be measured due to the fragile nature of the film, but the dry thickness suggests that the porosity of the wet

cake increases with the ethanol content of the aqueous suspension. Considering that ethanol induces some fibrils aggregation, we can speculate that the specific surface area of the particles was also reduced.

Table 1: Calculated cake specific resistance (α) membrane specific resistance (R_M) and for filtration of NFC suspensions with different ethanol contents

Ethanol content (wt.%)	α	R_M
0	2.13×10^{15}	1.65×10^{12}
50	6.95×10^{14}	-3.07×10^{10}
60	1.04×10^{14}	-2.29×10^{11}
75	3.82×10^{13}	-4.79×10^{11}

Mechanical and optical characterization of the films

In order to study the effect of the suspensions' composition and drying conditions on the mechanical and optical properties, the produced films were either air dried in standard temperature and relative humidity conditions (22ºC and 50% RH) or in an oven at 70ºC for 4 hours. Oven dried films were conditioned in standard conditions for 24 hours before testing. Table 2 shows the results.

As it was aforementioned, the porosity of the films dried in standard conditions generally increases with the increase of ethanol content. While the high surface tension of water (about 70 dyne/cm) promotes pore collapse between fibrils and hydrogen bond area development upon drying, the ethanol with its much lower surface tension (about 20 dyne/cm) and lower boiling point is less effective in the interfibrillar pores collapse, leading to structures with higher global porosities. In addition, when exposed to less polar media, the cellulosic fibrils' network undergoes partly irreversible reorganization, like aggregation, tending to the energetically most favorable state and thus more porous structures arise from this process [9, 24]. On the other hand, while NFC films made from 0 wt.% ethanol suspensions exhibited the same porosity either when dried in standard conditions or in the oven, oven dried films made from 50, 60 and 75 wt.% ethanol NFC suspensions increased the porosity by over 60% concerning their dry standard conditions counterparts. The oven drying process decreases even more the surface tension of ethanol and provides energy for fast ethanol evaporation, further increasing the global film porosity.

Regarding the mechanical properties of the films dried in standard conditions, the results put in evidence that the tensile index and Young's modulus of the NFC films (Table 2) are not substantially affected by the increase of ethanol content in the suspension from which they were produced, which is a very positive result taking in account that the film formation time decreases from close to 2 hours to around 2 minutes. What is even more interesting is the drastic increase of the tensile index when the films were dried in an oven during 4 hours at 70ºC; for the 0 wt.% ethanol/aqueous suspension, the increase in tensile index reaches 73% (71.6 to 124 N m g^{-1}), despite the significant increase in elongation (from 1.7% to 6.1%). For the ethanol/water suspensions, the relative tensile index increase is in the range of 30-40%, despite both increase in elongation and porosity. For the films made from 75 wt.% ethanol/aqueous suspensions, the higher performance of the oven dried films, regarding the standard dry films, persisted; the tensile index increased about 31%, despite the much higher elongation and scattering coefficient (2.1 *vs* 6.3% and 6.49 *vs* 15.05 cm^2/g, respectively). In resume, the oven dried films produced from 75 wt.% ethanol/water NFC suspension exhibited higher mechanical performance (92.2 N.m/g *vs* 71.6 N.m/g) than the dry standard films produced from 100 wt.% water NFC suspension. This performance is obtained, despite the much higher global porosity of the film (50% *vs* 18.8%) and higher elongation 6.3% *vs* 1.7%), which highlights the potential of both ethanol addition to the NFC suspension and the oven drying process.

Usually, the increase in mechanical resistance takes place at the expenses of a loss in elongation and an increase in contact between structural elements (evidenced in a decrease in the scattering coefficient). In the present study this was not the

case; both the elongation and the scattering coefficient increase considerably, whereas the tensile index also increases drastically, which puts in evidence the role of curing temperature on the film's properties.

Österberg *et al.* performed hot-pressing of films produced through filtration of NFC aqueous suspensions, at about 100 °C and 1800 Pa, varying the pressing time between 0.5 and 2 hours. The authors reported an increase from 121 MPa to 180 MPa (corresponding to an increase in tensile index from 149.6 N.m/g to 219.3 N.m/g), which puts in evidence the positive role of the temperature on the mechanical properties of the NFC films. Elongation, however, decreased substantially when the pressing time increased from o.5 to 2h, from 7.9 to 5.1% [10]

Regarding the optical properties, Table 2 shows that films produced from purely aqueous NFC suspensions (0 wt.% ethanol) reached a transparency of over 83 % for standard dried films and over 71 % for oven dried films, which is in the same transparency range of the results reported by Huang *et al.* [25]. These authors produced nanopapers through filtration of a TEMPO oxidized NFC aqueous suspension using a 0.65 µm pore size nitrocellulose ester filter membrane, followed by hot pressing at 105°C, and obtained NFC films with transparencies of around 90% [25]. Furthermore, Fukuzumi *et al.* reported transmittances at 600 nm of about 90% and 78% for NFC films prepared through vacuum filtration from softwood cellulose and from hardwood cellulose, respectively [26].

In the present research, the transparency of the films dried under standard conditions remains constant until 60% of ethanol content and decreases substantially for the 75 wt.% ethanol NFC suspension. The transparency decreases considerably for the oven dry process relative to the standard dry one. These results generally agree with the scattering coefficient since films with higher scattering coefficients are likely to appear less transparent. Increasing scattering coefficient and brightness generally coincided with a decrease in apparent density and an increase in the porosity of the films, which is in good agreement with Zhu *et al.* who reported that light transmittance and scattering in transparent nanopapaers do not only depend on the fibrils size but also on the packing density of the structure [27].

Table 2: Mechanical and optical characterization of NFC films produced from NFC suspensions with different ethanol compositions

Suspensions' ethanol content (wt.%)	Drying conditions*	Grammage ($g\ m^{-2}$)	Apparent density ($g\ cm^{-3}$)	Porosity (%)	Tensile index ($N\ m\ g^{-1}$)	Elongation (%)	Young's modulus (GPa)	Bending stiffness (mN)	ISO Brightness (%)	ISO Opacity (%)	Transparency (%)	Scattering coefficient ($cm^2\ g^{-1}$)
0	Standard	47.5± 2.6^a	1.3± 0.05^a	18.8± 3.0^a	71.6± 8.3^a	1.7± 0.3^a	6.4 ± 0.4^a	72.5± 0.2^a	36.42± 1.09	26.91± 2.51	83.81± 1.61	0.04±0.07
	Oven	46.9± 1.3^a	1.3± 0.06^a	18.8± 3.6^a	124.0± 15.4^b	6.1± 2.4^b	5.9± 1.4^d	76.3± 0.1^e	36.01± 1.03	47.03± 1.93	71.96± 1.31	2.00±0.02
50	Standard	51.8± 0.5^b	1.3± 0.05^a	18.8± 3.3^a	75.4± 11.8^a	1.6± 0.5^a	6.9± 0.6^a	85.0± 1.3^b	38.19± 0.48	26.49± 1.14	83.43± 0.78	0.14±0.01
	Oven	50.3± 0.6^b	1.1± 0.01^b	31.3± 0.9^c	99.7± 13.2^c	6.5± 1.4^b	4.5± 0.8^e	88.8± 0.1^f	41.67± 0.57	39.70± 1.19	75.22± 0.65	3.41±0.03
60	Standard	50.3± 1.0^b	1.2± 0.01^b	25.0± 0.8^b	62.2± 7.1^b	1.5± 0.4^a	6.2± 0.5^b	91.3± 0.2^c	40.15± 0.60	27.30± 1.32	82.86± 0.92	2.91±0.21
	Oven	50.3± 0.8^b	0.9± 0.01^b	43.8± 0.5^d	87.3± 6.2^d	6.8± 0.6^b	3.3± 0.1^f	97.5± 0.2^g	69.31± 0.65	71.20± 2.03	47.52± 0.10	15.74±0.14
75	Standard	51.5± 1.7^b	1.1± 0.05^b	31.3± 3.0^c	70.4± 11.3^a	2.1± 0.6^a	5.4± 0.2^c	82.5± 0.3^d	43.16± 3.36	36.29± 4.13	72.92± 3.19	6.49±0.99
	Oven	51.0± 0.1^b	0.8± 0.01^b	50.0± 0.7^e	92.2± 7.1^e	6.3± 1.1^b	3.2± 0.1^f	110.0± 0.3^h	58.01± 2.21	69.52± 3.74	48.83± 2.45	15.05±0.85

* Drying conditions: Standard is air dried overnight at 22°C and 50% RH; Oven is oven dried at 70°C for 4 hours

Means at the same column with different superscript letters are significantly different ($p < 0.05$)

Figure 4 shows a side-by-side comparison of films produced from 75wt.% ethanol and 0 wt.% ethanol NFC suspensions, dried under standard conditions. The higher opacity of the former film is in accordance with its higher light scattering coefficient (6.49 cm^2/g *vs* 0.04 cm^2/g) and higher global porosity. The combination of drying in the oven and film production from ethanol/water suspension provided the opportunity to manipulate film transparency, preserving the mechanical performance.

The bending stiffness of the films, in general, increases as the global porosity increase, due to the increase in film thickness

Water vapor transmission through the films

Regarding the water vapor transmission though the films, the WVTR of films made from solely aqueous NFC suspensions are on the same range as those reported by other authors [28, 29].

As it is evidenced in Figure 5 and Table 3, the WVTR is not substantially affected when the ethanol content of the NFC suspension increases up to 60 wt.%, even though the film's porosity increases from 18.8 to 25% for 0 or 50 and 60 wt.% ethanol, respectively. However, a notorious increase from 134.83 to 207.48 g m^{-2} day^{-1} takes place by increasing the ethanol content to 75%, accordingly accompanied by an increase in the porosity from 25.0 to 31.3%.

The oven drying process caused a further increase of over 40% in the WVTR of the films made from a 75 wt.% ethanol suspension (207.48 to 291.19 g m^{-2} day^{-1}), against an increase of around 60% on the porosity (31.3 to 50%). Interestingly, the oven dried NFC films made from 0 wt.% ethanol suspensions increased the WVTR by 19% (137.82 to 163.83 g m^{-2} day^{-1}) despite the porosity remained unaltered.

In resume, filtrating a 75 wt.% ethanol/aqueous NFC suspension and oven drying at 70°C for 4 hours, decreased the film formation time from around 2 hours to 2 minutes, providing a film with tensile properties higher than those exhibited by an air-dried film produced from an aqueous NFC suspension. Furthermore, the films produced from this method exhibited higher WVTR and porosity.

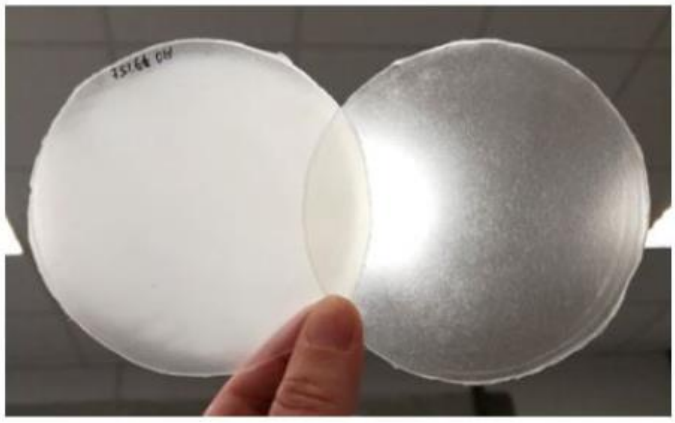

Figure 4: Films produced from a 75wt.% ethanol NFC suspension (left) and from a purely aqueous NFC suspension (right) dried under standard conditions

Table 3: Calculated water vapor transfer rate for films produced from different ethanol content NFC suspensions and different drying conditions

Ethanol content (wt.%)	Drying conditions	WVTR (g m^{-2} day^{-1})	Porosity (%)
0	Standard	137.82	18.8
50		137.52	18.8
60		134.83	25.0
75		207.48	31.3
0	Oven	163.83	18.8
75		291.19	50.0

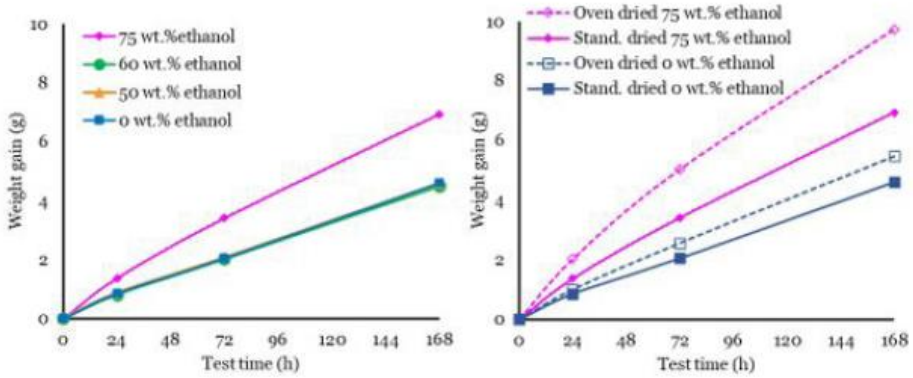

Figure 5: Transferred water vapor as a function of test time for NFC films produced from different ethanol content NFC suspensions

Conclusions

The main specific conclusions of the work are the following:

• The addition of ethanol to the NFC aqueous suspension to attain a 75 wt.% ethanol content enabled to decrease the filtration time from about 2 hours to about 2 minutes. Using a constant transmembrane pressure of 0.8x 10^5 N/m^2, it was possible to estimate the NFC cake specific resistance. This value decreased from 2.1 x 10^{15} m/kg to 3.8 x 10^{13} m/kg with the ethanol addition (75 wt%. ethanol/aqueous NFC suspension).

• The tensile index and Young's modulus of the standard dried NFC films were not, in general, substantially affected by the increase of ethanol content in the NFC suspensions.

• Oven drying the films (70ºC, 4 hours) enabled to drastically increase the film's tensile index, regarding the standard dried ones. These results were obtained with films with higher global porosity and surprisingly with much higher elongation.

• The porosity of the produced films generally increased with the increase of ethanol content. Oven drying the films made from 50 to 75 wt.% ethanol NFC suspensions resulted in an increase in porosity of over 60%.

• WVTR was not substantially affected when the ethanol content of the NFC suspension increased up to 60 wt.%, but there was a notorious increase from 134.83 to 207.48 g m^{-2} day^{-1} for the films made from 75 wt.% ethanol NFC suspensions. The oven drying process of these films caused a further increase of over 40% in the WVTR.

• The combination of both film drying in oven and film production from ethanol/water suspension provided the opportunity to manipulate film transparency and water vapor transmission rate, preserving the mechanical performance of the films.

In resume, with this study we propose a relatively fast and simple method to produce neat NFC films with potentially desirable mechanical and barrier properties for membrane applications where mechanical strength, toughness, low density, controlled permeability and porosity and high surface area are important, such as fuel cells, liquid purification and filtering, tissue engineering, protein immobilization and separation, and protective clothing.

Acknowledgements

The research undertaken for this paper was performed under the UBI-Celtejo cooperation protocol. The authors would also like to acknowledge the support from the FibEnTech - Research Unit of Fiber Materials and Environmental Technologies of Universidade da Beira Interior.

References

1. Mouhib M, Antonucci A, Reggente M, Amirjani A, Gillen AJ, et al. (2019) Enhancing bioelectricity generation in microbial fuel cells and biophotovoltaics using nanomaterials. Nano Res 12: 2184-99.

2. Sadeghpour S, Amirjani A, Hafezi M, Zamanian A (2014) Fabrication of a novel nanostructured calcium zirconium silicate scaffolds prepared by a freeze-casting method for bone tissue engineering. Ceramics Int 40: 16107-14.

3. Amirjani A, Hafezi M, Zamanian A, Yasaee M, Abu Osman N (2016) Synthesis of nano-structured sphene and mechanical properties optimization of its scaffold via response surface methodology. J Advanced Materials and Processing 4: 56-62.

4. Guo W, Wang X, Zhang P, Liu J, Song L, et al. (2018) Nano-fibrillated cellulose-hydroxyapatite based composite foams with excellent fire resistance. Carbohydrate Polymers 195: 71-8.

5. Tammelin T, Vartiainen J (2014) Nanocellulose Films and Barriers. In: Handbook of Green Material. World Scientific Publishing Co. Pte. Ltd: 213-29.

6. Henriksson M, Berglund LA, Isaksson P, Lindström T, Nishino T (2008) Cellulose Nanopaper Structures of High Toughness. Biomacromolecules 9: 1579-85.

7. Lavoine N, Desloges I, Dufresne A, Bras J (2012) Microfibrillated cellulose - Its barrier properties and applications in cellulosic materials: A review. Carbohydrate Polymers 90: 735-64.

8. Hult EL, Larsson PT, Iversen T (2001) Cellulose fibril aggregation — an inherent property of kraft pulps. Polymer 42: 3309-14.

9. Johansson LS, Tammelin T, Campbell JM, Setälä H, Österberg M (2011) Experimental evidence on medium driven cellulose surface adaptation demonstrated using nanofibrillated cellulose. Soft Matter, 7: 10917.

10. Österberg M, Vartiainen J, Lucenius J, Hippi U, Seppälä J, et al. (2013) A Fast Method to Produce Strong NFC Films as a Platform for Barrier and Functional Materials. ACS Applied Materials & Interfaces 5: 4640-7.

11. Sehaqui H, Liu A, Zhou Q, Berglund LA (2010) Fast Preparation Procedure for Large, Flat Cellulose and Cellulose/Inorganic Nanopaper Structures. Biomacromolecules 11: 2195-8.

12. Varanasi S, Batchelor WJ (2013) Rapid preparation of cellulose nanofibre sheet. Cellulose 20: 211-5.

13. Nogi M, Iwamoto S, Nakagaito AN, Yano H (2009) Optically transparent nanofiber paper. Advanced Materials 21: 1595-8.

14. Zhang L, Batchelor W, Varanasi S, Tsuzuki T, Wan X (2012) Effect of cellulose nanofiber dimensions on sheet forming through filtration. Cellulose 19: 561-74.

15. Raj P, Varanasi S, Batchelor W, Garnier G (2015) Effect of cationic polyacrylamide on the processing and properties of nanocellulose films. J Colloid and Interface Sci 447: 113-9.

16. Sehaqui H, Zhou Q, Ikkala O, Berglund LA (2011) Strong and Tough Cellulose Nanopaper with High Specific Surface Area and Porosity. Biomacromolecules 12: 3638-44.

17. Sim K, Ryu J, Youn HJ (2015) Structural characteristics of nanofibrillated cellulose mats: Effect of preparation conditions. Fibers and Polymers 16: 294-301.

18. Toivonen MS, Kurki-Suonio S, Schacher FH, Hietala S, Rojas OJ, et al. (2015) Water-Resistant, Transparent Hybrid Nanopaper by Physical Cross-Linking with Chitosan. Biomacromolecules, 16: 1062-71.

19. Solala I, Bordes R, Larsson A (2017) Water vapor mass transport across nanofibrillated cellulose films: effect of surface hydrophobization. Cellulose 25: 347-56.

20. Costa VL, Costa AP, Simões RM (2019) Nanofibrillated Cellulose Rheology: Effects of Morphology, Ethanol/Acetone Addition, and High NaCl Concentration. BioResources 14: 7636-54.

21. Besbes I, Alila S, Boufi S (2011) Nanofibrillated cellulose from TEMPO-oxidized eucalyptus fibres: Effect of the carboxyl content. Carbohydrate Polymers 84: 975-83.

22. Isogai A, Saito T, Fukuzumi H (2011) TEMPO-oxidized

cellulose nanofibers. Nanoscale 3: 71–85.

23. Shinoda R, Saito T, Okita Y, Isogai A (2012) Relationship between Length and Degree of Polymerization of TEMPO-Oxidized Cellulose Nanofibrils. Biomacromolecules 13: 842-9.

24. Moon RJ, Martini A, Nairn J, Simonsen J, Youngblood J (2011) Cellulose nanomaterials review: structure, properties and nanocomposites. Chemical Society Reviews 40: 3941.

25. Huang J, Zhu H, Chen Y, Preston C, Rohrbach K, et al. (2013) Highly Transparent and Flexible Nanopaper Transistors. ACS Nano 7: 2106-13.

26. Fukuzumi H, Saito T, Iwata T, Kumamoto Y, Isogai A (2008) Transparent and High Gas Barrier Films of Cellulose Nanofibers Prepared by TEMPO-Mediated Oxidation. Biomacromolecules 10: 162-5.

27. Zhu H, Parvinian S, Preston C, Vaaland O, Ruan Z, et al. (2013) Transparent nanopaper with tailored optical properties. Nanoscale 5: 3787.

28. Bedane AH, Eić M, Farmahini-Farahani M, Xiao H (2015) Water vapor transport properties of regenerated cellulose and nanofibrillated cellulose films. J Membrane Sci 493: 46-57.

29. Souza G, Belgacem MN, Gandini A, Carvalho AJF (2021) Low permeable hydrophobic nanofibrilated cellulose films modified by dipping and heating processing technique. Cellulose 28: 1617-32.

Chapter 4 - General conclusions and future perspectives

Cellulose is the most abundant, renewable, and sustainable biopolymer on earth, having many desirable characteristics that make it a suitable material for several applications. Cellulose nanofibrils harvested from renewable resources have recently gained attention owing to their sustainable and biodegradable nature, combined with other mechanical, optical, thermal, and fluidic properties. Cellulose nanofibrils are thus appealing in the fabrication of several materials ranging from composites to porous membranes and gels, filaments, and films. The investigation undertaken throughout this work was divided in five sections that focus on exploring either the rheologic behavior of cellulose nanofibrils in different liquid media or the mechanical, optical and barrier properties of structures produced from this material.

In the first section, the effects of morphology, ethanol/acetone addition and NaCl concentration on nanofibrillated cellulose suspensions' rheology were studied. Either ethanol or acetone in concentrations of 2.5 up to 40 wt.% were added to a carboxymethylated and a 2,2,6,6-tetramethylpiperidine-1-oxyl oxidized nanofibrillated cellulose suspensions and the ionic strength was increased by adding 50 to 1000 mM of NaCl. Rheological measurements were performed on the suspensions at a solid content of 1.3%, using a stress-controlled rheometer equipped with cone and plate geometry. Results showed that a 2.5 wt.% addition of either ethanol or acetone decreased the viscosity and the dynamic moduli, while a 40 wt.% addition increased the viscosity to values higher than those of the aqueous suspensions, doubled the energy storage modulus, and extended the gel-like behavior. An increment on NaCl concentration from 50 to 100 mM drastically increased viscosity while energy storage modulus in the elastic region linearly increased with increasing NaCl concentration from 100 to 1000 mM, suggesting increased interparticle bonds with NaCl addition.

In the second section, two 2,2,6,6-tetramethylpiperidine-1-oxyl oxidized nanofibrillated cellulose suspensions obtained from two different eucalypt pulps, with solid contents from 2.5 to 3.22% were used to produce cellulosic filaments through wet spinning, at spinning rates ranging from 0.45 to 1.7 m min-1 into a 1M NaCl coagulation bath, followed by an ethanol fixation bath. The filaments were dried in standard conditions of temperature and relative humidity and their mechanical performance was tested. Results showed that an increase in spinning rate improved the mechanical performance of the filaments, indicating some level of fibril alignment. On the other hand, increasing solid content did not improve the filament's resistance, due to higher viscosity and lower capacity for fibril alignment. Higher mechanical performance was exhibited by more fibrillated cellulose meaning that fibril's morphology plays an important role in the filament's assembly, despite the lower cellulose degree of polymerization of the more fibrillated cellulose.

In the third section, the effect of hot calendering on optical–structural, mechanical, and barrier properties of bacterial cellulose films was studied and compared with those of highly beaten vegetal cellulose films. The Young's modulus and tensile index of the bacterial cellulose films were much higher than those obtained for vegetal cellulose. Calendering substantially increased the transparency of bacterial cellulose films. Ozonation enhanced the brightness and transparency of bacterial cellulose films, but slightly decreased their mechanical performance. The water vapor transfer rate was lower for bacterial cellulose films than for vegetal ones and decreased by 70 % with calendering. Calendering could be used to obtain films suitable for food packaging applications, as a good alternative to plastics.

In the fourth section, nanofibrillated cellulose films were produced and coated with either a layer of stearic acid or stearic acid and precipitated calcium carbonate, in a layer-by-layer assembly. Some films were treated at 68ºC and 105ºC. Structural and physical analysis of the films, barrier properties and static/dynamic contact angle measurements were performed. Results showed that the coatings and heat treatments did not affect the films' mechanical performance. Heat treatments decreased the water vapor transmission rate and oxygen permeability of both stearic acid and layer-by-layer coated films. Stearic acid coating rendered the films hydrophobic, with static contact angle up to 122º. Layer-by-layer coated films attained a contact angle up to 150º and a contact angle hysteresis of 3.1º with no heat treatment. Rubbing and handling resistant *quasi* superhydrophobicity was obtained for layer-by-layer films treated at 68ºC, with a contact angle up to 140º and a contact angle hysteresis of 5º.

Finally, in the fifth section, nanofibrillated aqueous/ethanol cellulose suspensions with an ethanol content up to 75 wt.% were used to manufacture films through vacuum filtration, monitoring the draining progression by measuring the collected filtrate. The films were either dried in standard conditions of temperature and humidity or in an oven at 70ºC for 4 hours. The resulting films were tested for mechanical and optical performance and water vapor barrier properties. Results showed that filtrating time decreases drastically with the increase of the suspension ethanol content, from about 2 hours to 2 minutes for 0 (aqueous suspension) and 75 wt.% ethanol/aqueous suspensions, respectively. Increasing the ethanol content in the fibril suspension did not affect the mechanical performance of standard dried films, despite the global porosity increase. On the other hand, oven drying provided the films with tensile properties higher than those exhibited by air-dried films produced from purely aqueous suspensions, despite the increase in elongation and light scattering coefficient. Water vapor transmission rate increased for films produced from 75 wt.% ethanol suspensions and was further increased for oven dried films.

In resume, the different approaches put in evidence the huge potential of nanofibrillated cellulose for several applications, namely for film production. Regarding the NFC film production, the important issue is the prohibitive time for film formation from highly fibrillated cellulose. This work makes a positive contribution in this respect, showing that the film

formation time can be strongly reduced by modifying the suspension medium with ethanol, which is an easily recovered solvent. In addition, the mechanical properties of the corresponding films are well preserved.

Another issue that impairs other NFC applications is the hydrophilic nature of the fibrillated cellulose and its corresponding films. In this work, a green and scalable procedure based on stearic acid and precipitated calcium carbonate was proposed to produce strongly hydrophobic NFC films. Appropriate heat treatment of the coated films provided rubbing and handling resistance.

As future perspectives, following the studies already carried out, the work to be developed may include the following aspects:

- In the context of producing NFC based filaments to replace industrial regenerated cellulose fibers, although some level of fibril orientation and enhanced mechanical resistance were achieved, the mechanical properties of the spun NFC filaments are not yet comparable to those of viscose and Lyocell. Thus, adjustments on the operating conditions need to be undertaken to further improve the fibril alignment during the spinning process, such as increasing the spinning rate while figuring out suitable conditions for coagulation, adjusting the initial NFC suspension morphology, solid content and viscosity, and optimizing the drying conditions in other to spin resilient continuous filaments, suitable for several applications.

- Although a layer-by-layer assembly using stearic acid and modified PCC particles, combined with a heat treatment turned out to be a simple, environmentally friendly and effective way of providing persistent hydrophobicity to NFC films, some measures may be carried out to optimize the production conditions and further enhance the hydrophobicity of the films, namely optimize the proportions of stearic acid and PCC in the PCC modification process as well as ajust the operating conditions so as to control the modified PCC particle size, and consequently architecting the micro and nanosized roughness of the coated films in order to enhance the hydrophobicity.

- The addition of ethanol to aqueous NFC suspensions proved to be an efficient way of considerably reducing the filtrating time during the production of NFC films, without compromising the mechanical resistance. Therefore, applying on these films the aforementioned hydrophobization techniques through stearic acid/ modified PCC deposition and oven drying may be an interesting way of achieving permanently hydrophobic and resilient NFC films in a very fast and simple manner.

Chapter 5 - References

Aarne, N., Kontturi, E., Laine, J. (2012). Carboxymethyl cellulose on a fiber substrate: the interactions with cationic polyelectrolytes. Cellulose, 19(6), 2217–2231. Doi: 10.1007/s10570-012-9793-2

Agarwal, D., Hewson, L., Foster, T. J. (2018). A comparison of the sensory and rheological properties of different cellulosic fibres for food. Food & Function, 9(2), 1144–1151. Doi: 10.1039/c7fo01495c

Alcalá, M., González, I., Boufi, S., Vilaseca, F., Mutjé, P. (2013). All-cellulose composites from unbleached hardwood kraft pulp reinforced with nanofibrillated cellulose. Cellulose, 20(6), 2909–2921. Doi: 10.1007/s10570-013-0085-2

Alemdar, A., Sain, M. (2008). Isolation and characterization of nanofibers from agricultural residues – Wheat straw and soy hulls. Bioresource Technology, 99(6), 1664–1671. Doi: 10.1016/j.biortech.2007.04.029

Alila, S., Besbes, I., Vilar, M. R., Mutjé, P., Boufi, S. (2013). Non-woody plants as raw materials for production of microfibrillated cellulose (MFC): A comparative study. Industrial Crops and Products, 41, 250–259. Doi: 10.1016/j.indcrop.2012.04.028

Andresen, M., Johansson, L. -S., Tanem, B. S., Stenius, P. (2006). Properties and characterization of hydrophobized microfibrillated cellulose. Cellulose, 13(6), 665–677. Doi: 10.1007/s10570-006-9072-1

Ankerfors, M., Lindström, T., Henriksson, G. (2013). Method for the manufacture of microfibrillated cellulose. US patent no8,546,558

Ashori, A., Babaee, M., Jonoobi, M., Hamzeh, Y. (2014). Solvent-free acetylation of cellulose nanofibers for improving compatibility and dispersion. Carbohydrate Polymers, 102, 369–375. Doi: 10.1016/j.carbpol.2013.11.067

Aulin, C., Ahola, S., Josefsson, P., Nishino, T., Hirose, Y., Österberg, M., Wågberg, L. (2009). Nanoscale cellulose films with different crystallinities and mesostructures - their surface properties and interaction with water. Langmuir, 25(13), 7675–7685. Doi: 10.1021/la900323n

Azzam, F., Heux, L., Putaux, J. -L., Jean, B. (2010). Preparation by grafting onto, characterization, and properties of thermally responsive polymer-decorated cellulose nanocrystals. Biomacromolecules, 11(12), 3652–3659. Doi: 10.1021/bm101106c

Azzam, F., Siqueira, E., Fort, S., Hassaini, R., Pignon, F., Travelet, C., *et al.* (2016). Tunable aggregation and gelation of thermoresponsive suspensions of polymer-grafted cellulose nanocrystals. Biomacromolecules, 17(6), 2112–2119. Doi: 10.1021/acs.biomac.6b00344

Bacakova, L.; Pajorova, J.; Bacakova, M.; Skogberg, A.; Kallio, P.; Kolarova, K.; Svorcik, V. (2019). Versatile application of nanocellulose: from industry to skin tissue engineering and wound healing. Nanomaterials, 9(164), 1–39. Doi: 10.3390/nano9020164

Bechtold, T., Manian, A. P., Öztürk, H. B., Paul, U., Široká, B., Široký, J. *et al.* (2013). Ion-interactions as driving force in polysaccharide assembly. Carbohydrate Polymers, 93(1), 316–323. Doi: 10.1016/j.carbpol.2012.01.064

Benhamou, K., Dufresne, A., Magnin, A., Mortha, G., Kaddami, H. (2014). Control of size and viscoelastic properties of nanofibrillated cellulose from palm tree by varying the TEMPO-mediated oxidation time. Carbohydrate Polymers, 99, 74–83. Doi: 10.1016/j.carbpol.2013.08.032

Besbes, I., Alila, S., Boufi, S. (2011). Nanofibrillated cellulose from TEMPO-oxidized eucalyptus fibres: Effect of the carboxyl content. Carbohydrate Polymers, 84(3), 975–983. Doi: 10.1016/j.carbpol.2010.12.052

Bhushan, B., Nosonovsky, M. (2010). The rose petal effect and the modes of superhydrophobicity. Philosophical Transactions of the Royal Society A: Mathematical, Physical and Engineering Sciences, 368(1929), 4713–4728. Doi: 10.1098/rsta.2010.0203

Bledzki, A. (1999). Composites reinforced with cellulose based fibres. Progress in Polymer Science, 24(2), 221–274. Doi: 10.1016/s0079-6700(98)00018-5

Bledzki, A. K., Mamun, A. A., Lucka-Gabor, M., Gutowski, V. S. (2008). The effects of acetylation on properties of flax fibre and its polypropylene composites. Express Polymer Letters, 2(6), 413–422. Doi: 10.3144/expresspolymlett.2008.50

Bredereck, K., Hermanutz, F. (2008). Man-made cellulosics. Review of Progress in Coloration and Related Topics, 35(1), 59–75. Doi: 10.1111/j.1478-4408.2005.tb00160.x

Brinchi, L., Cotana, F., Fortunati, E., Kenny, J. M. (2013). Production of nanocrystalline cellulose from lignocellulosic biomass: Technology and applications. Carbohydrate Polymers, 94(1), 154–169. Doi: 10.1016/j.carbpol.2013.01.033

Brodin, F. W., Gregersen, Ø. W., Syverud, K. (2014). Cellulose nanofibrils: Challenges and possibilities as a paper additive or coating material – A review. Nordic Pulp & Paper Research Journal, 29(1), 156–166. Doi: 10.3183/npprj-2014-29-01-p156-166

Bulota, M., Kreitsmann, K., Hughes, M., Paltakari, J. (2012). Acetylated microfibrillated cellulose as a toughening agent in poly(lactic acid). Journal of Applied Polymer Science, 126(S1), E449–E458. Doi: 10.1002/app.36787

Cao, Y., Wu, J., Zhang, J., Li, H., Zhang, Y., He, J. (2009). Room temperature ionic liquids (RTILs): A new and versatile platform for cellulose processing and derivatization. Chemical Engineering Journal, 147(1), 13–21. Doi: 10.1016/j.cej.2008.11.011

Cassie, A. B. D., Baxter, S. (1944). Wettability of porous surfaces. Transactions of the Faraday Society, 40, 546. Doi: 10.1039/tf9444000546

Cha, T. -G., Yi, J. W., Moon, M. -W., Lee, K. -R., Kim, H. -Y. (2010). Nanoscale patterning of microtextured surfaces to control superhydrophobic robustness. Langmuir, 26(11), 8319–8326. Doi: 10.1021/la9047402

Chaker, A., Mutjé, P., Vilar, M. R., Boufi, S. (2014). Agriculture crop residues as a source for the production of nanofibrillated cellulose with low energy demand. Cellulose, 21(6), 4247–4259. Doi: 10.1007/s10570-014-0454-5

Chakraborty, A., Sain, M., Kortschot, M. (2005). Cellulose microfibrils: A novel method of preparation using high shear refining and cryocrushing. Holzforschung, 59(1), 102–107. Doi: 10.1515/hf.2005.016

Chaudemanche, C., Navard, P. (2011). Swelling and dissolution mechanisms of regenerated Lyocell cellulose fibers. Cellulose, 18(1), 1–15. Doi: 10.1007/s10570-010-9460-4

Chauhan V. S., Chakrabarti S. K. (2012). Use of nanotechnology for high performance cellulosic and papermaking products. Cellulose Chemistry and Technology 46(5-6):389-400

Chavan, R. B., Patra, A. K. (2004) Review article: development and processing of lyocell. Indian Journal of Fibre & Textile Research 29:483–492

Chen, B., Tatsumi, D., Matsumoto, T. (2002). Floc structure and flow properties of pulp fiber suspensions. Nihon Reoroji Gakkaishi, 30(1), 19–25. Doi: 10.1678/rheology.30.19

Chen, S., Schueneman, G., Pipes, R. B., Youngblood, J., Moon, R. J. (2014). Effects of crystal orientation on cellulose nanocrystals–cellulose acetate nanocomposite fibers prepared by dry spinning. Biomacromolecules, 15(10), 3827–3835. Doi: 10.1021/bm501161v

Chi, K., Catchmark, J. M. (2018). Improved eco-friendly barrier materials based on crystalline nanocellulose/chitosan/carboxymethyl cellulose polyelectrolyte complexes. Food Hydrocolloids, 80, 195–205. Doi: 10.1016/j.foodhyd.2018.02.003

Chinga-Carrasco, G. (2011). Cellulose fibres, nanofibrils and microfibrils: The morphological sequence of MFC components from a plant physiology and fibre technology point of view. Nanoscale Research Letters, 6(1). Doi: 10.1186/1556-276x-6-417

Chinga-Carrasco, G., Kuznetsova, N., Garaeva, M., Leirset, I., Galiullina, G., Kostochko, A., Syverud, K. (2012). Bleached and unbleached MFC nanobarriers: properties and hydrophobisation with hexamethyldisilazane. Journal of Nanoparticle Research, 14(12). Doi: 10.1007/s11051-012-1280-z

Chu, Y., Sun, Y., Wu, W., Xiao, H. (2020). Dispersion properties of nanocellulose: a review. Carbohydrate Polymers, 250, 116892. Doi: 10.1016/j.carbpol.2020.116892

Clemons, C. (2016). Nanocellulose in spun continuous fibers: a review and future outlook. Journal of Renewable Materials, 4(5), 327–339. Doi: 10.7569/jrm.2016.634112

Cranston, E. D., Gray, D. G. (2006). Morphological and optical characterization of polyelectrolyte multilayers incorporating nanocrystalline cellulose. Biomacromolecules, 7(9), 2522–2530. Doi: 10.1021/bm0602886

Cunha, A. G., Zhou, Q., Larsson, P. T., Berglund, L. A. (2014). Topochemical acetylation of cellulose nanopaper structures for biocomposites: mechanisms for reduced water vapour sorption. Cellulose, 21(4), 2773–2787. Doi: 10.1007/s10570-014-0334-z

de Coninck, J., de Ruijter, M. J., Voué, M. (2001). Dynamics of wetting. Current Opinion in Colloid & Interface Science, 6(1), 49–53. Doi: 10.1016/s1359-0294(00)00087-x

de France, K. J., Hoare, T., Cranston, E. D. (2017). Review of hydrogels and aerogels containing nanocellulose. Chemistry of Materials, 29(11), 4609–4631. Doi: 10.1021/acs.chemmater.7b00531

de Menezes, A. J., Pasquini, D., Curvelo, A. A. d. S. *et al.* (2009). Self-reinforced composites obtained by the partial oxypropylation of cellulose fibers. 2. Effect of catalyst on the mechanical and dynamic mechanical properties. Cellulose 16, 239–246. Doi: 10.1007/s10570-008-9271-z

Dersch, R., Liu, T., Schaper, A. K., Greiner, A., Wendorff, J. H. (2003). Electrospun nanofibers: Internal structure and intrinsic orientation. Journal of Polymer Science Part A: Polymer Chemistry, 41(4), 545–553. Doi: 10.1002/pola.10609

Di Giorgio, L., Martín, L., Salgado, P. R., Mauri, A. N. (2020). Synthesis and conservation of cellulose nanocrystals. Carbohydrate Polymers, 238, 116187. Doi: 10.1016/j.carbpol.2020.116187

Diniz, J. M. B. F., Gil, M. H., Castro, J. A. A. M. (2004). Hornification - its origin and interpretation in wood pulps. Wood Science and Technology, 37(6), 489–494. Doi: 10.1007/s00226-003-0216-2

Dong, H., Strawhecker, K. E., Snyder, J. F., Orlicki, J. A., Reiner, R. S., Rudie, A. W. (2012). Cellulose nanocrystals as a reinforcing material for electrospun poly(methyl methacrylate) fibers: Formation, properties and nanomechanical characterization. Carbohydrate Polymers, 87(4), 2488–2495. Doi: 10.1016/j.carbpol.2011.11.015

Duchesne I., Hult E., Molin U., Daniel G., Iversen T., Lennholm H. (2001). The influence of hemicellulose on fibril aggregation of kraft pulp fibres as revealed by FE-SEM and CP/MAS 13C-NMR. Cellulose, 8:103-111. Doi: 10.1023/A:1016645809958

Dufresne, A.; Cavaill, J. -Y.; Vignon, M. R. (1997). Mechanical behavior of sheets prepared from sugar beet cellulose microfibrils. Journal of Applied Polymer Science, 64(6), 1185–1194. Doi: 10.1002/(SICI)1097-4628(19970509)64:6<1185::AID-APP19>3.0.CO;2-V

Dufresne, A., Dupeyre, D., Vignon, M. R. (2000). Cellulose microfibrils from potato tuber cells: Processing and characterization of starch-cellulose microfibril composites. Journal of Applied Polymer Science, 76(14), 2080–2092. Doi: 10.1002/(SICI)1097-4628(20000628)76:14<2080::AID-APP12>3.0.CO;2-U

Dunlop, M. J., Acharya, B., Bissessur, R. (2018). Isolation of nanocrystalline cellulose from tunicates. Journal of Environmental Chemical Engineering, 6(4), 4408–4412. Doi: 10.1016/j.jece.2018.06.056

Eichhorn, S. J., Dufresne, A., Aranguren, M., Marcovich, N. E., Capadona, J. R., Rowan, S. J., *et al.* (2010). Review: current international research into cellulose nanofibres and nanocomposites. Journal of Materials Science, 45(1), 1–33. Doi: 10.1007/s10853-009-3874-0

Endo, R., Saito, T., Isogai, A. (2013). TEMPO-oxidized cellulose nanofibril/poly(vinyl alcohol) composite drawn fibers. Polymer, 54(2), 935–941. Doi: 10.1016/j.polymer.2012.12.035

Ertas, Y., Uyar, T. (2017). Fabrication of cellulose acetate/polybenzoxazine cross-linked electrospun nanofibrous membrane for water treatment. Carbohydrate Polymers, 177, 378–387. Doi: 10.1016/j.carbpol.2017.08.127

Fang, Z., Zhu, H., Bao, W., Preston, C., Liu, Z., Dai, J., *et al.* (2014). Highly transparent paper with tunable haze for green electronics. Energy Environ. Sci., 7(10), 3313–3319. Doi: 10.1039/c4ee02236j

Fengel, D., Wegener G. (1984). Wood: Chemistry, Ultrastructure, Reactions. De Gruyter, Berlin.

Foster, E. J., Moon, R. J., Agarwal, U. P., Bortner, M. J., Bras, J., Camarero-Espinosa, S., *et al.* (2018). Current characterization methods for cellulose nanomaterials. Chemical Society Reviews, 47(8), 2609–2679. Doi: 10.1039/c6cs00895j

Freire, C. S. R., Silvestre, A. J. D., Neto, C. P., Belgacem, M. N., Gandini, A. (2006). Controlled heterogeneous modification of cellulose fibers with fatty acids: Effect of reaction conditions on the extent of esterification and fiber properties. Journal of Applied Polymer Science, 100(2), 1093–1102. Doi: 10.1002/app.23454

Frey, M. W. (2008). Electrospinning cellulose and cellulose derivatives. Polymer Reviews 48(2), 378-391. Doi: 10.1080/15583720802022281

Fukuzumi, H., Saito, T., Iwata, T., Kumamoto, Y., Isogai, A. (2009). Transparent and high gas barrier films of cellulose nanofibers prepared by TEMPO-mediated oxidation. Biomacromolecules, 10(1), 162–165. Doi: 10.1021/bm801065u

Gallier, S., Lemaire, E., Peters, F., Lobry, L. (2014). Rheology of sheared suspensions of rough frictional particles. Journal of Fluid Mechanics, 757, 514–549. Doi: 10.1017/jfm.2014.507

Galván, M. V., Peresin, M. S., Mocchiutti, P., Granqvist, N., Zanuttini, M. A., Tammelin, T. (2015). Effects of charge ratios of xylan-poly(allylamine hydrochloride) complexes on their adsorption onto different surfaces. Cellulose, 22(5) 2955–2970. Doi: 10.1007/s10570-015-0706-z

Gandini, A., da Silva Curvelo, A. A., Pasquini, D., de Menezes, A. J. (2005). Direct transformation of cellulose fibres into self-reinforced composites by partial oxypropylation. Polymer, 46(24), 10611–10613. Doi: 10.1016/j.polymer.2005.09.004

Gandini, A., Belgacem, M. N. (2015). The surface and in-depth modification of cellulose fibers. Cellulose Chemistry and Properties: Fibers, Nanocelluloses and Advanced Materials, 169–206. Doi: 10.1007/12_2015_305

Ganster, J., Fink, H. -P. (2013). Cellulose and cellulose acetate. Bio-Based Plastics, 35–62. Doi: 10.1002/9781118676646.ch3

González, I., Boufi, S., Pèlach, M. A., Alcalà, M., Vilaseca, F., Mutjé, P. (2012). Nanofibrillated cellulose as paper additive in eucalyptus pulps. BioResources, 7(4). Doi: 10.15376/biores.7.4.5167-5180

González, I., Vilaseca, F., Alcalá, M., Pèlach, M. A., Boufi, S., Mutjé, P. (2013). Effect of the combination of biobeating and NFC on the physico-mechanical properties of paper. Cellulose, 20(3), 1425–1435. Doi: 10.1007/s10570-013-9927-1

González, I., Alcalà, M., Chinga-Carrasco, G., Vilaseca, F., Boufi, S., Mutjé, P. (2014). From paper to nanopaper: evolution of mechanical and physical properties. Cellulose, 21(4), 2599–2609. Doi: 10.1007/s10570-014-0341-0

Gorgieva, S. Trček, J. (2019). Bacterial cellulose: production, modification and perspectives in biomedical applications. Nanomaterials, 9(10), 1352. Doi: 10.3390/nano9101352

Goussé, C., Chanzy, H., Cerrada, M. L., Fleury, E. (2004). Surface silylation of cellulose microfibrils: preparation and rheological properties. Polymer, 45(5), 1569–1575. Doi: 10.1016/j.polymer.2003.12.028

Habibi, Y., Goffin, A. -L., Schiltz, N., Duquesne, E., Dubois, P., Dufresne, A. (2008). Bionanocomposites based on poly(ε-caprolactone)-grafted cellulose nanocrystals by ring-opening polymerization. Journal of Materials Chemistry, 18(41), 5002. Doi: 10.1039/b809212e

Habibi, Y., Lucia, L. A., Rojas, O. J. (2010). Cellulose nanocrystals: chemistry, self-assembly, and applications. Chemical Reviews, 110(6), 3479–3500. Doi: 10.1021/cr900339w

Han, S. O., Youk, J. H., Min, K. D., Kang, Y. O., Park, W. H. (2008). Electrospinning of cellulose acetate nanofibers using a mixed solvent of acetic acid/water: Effects of solvent composition on the fiber diameter. Materials Letters, 62(4-5), 759–762. Doi: 10.1016/j.matlet.2007.06.059

Hansson, S., Trouillet, V., Tischer, T., Goldmann, A. S., Carlmark, A., Barner-Kowollik, C., Malmström, E. (2012). Grafting efficiency of synthetic polymers onto biomaterials: a comparative study of grafting-from *versus* grafting-to. Biomacromolecules, 14(1), 64–74. Doi: 10.1021/bm3013132

Harrisson, S., Drisko, G. L., Malmström, E., Hult, A., Wooley, K. L. (2011). Hybrid rigid/soft and biologic/synthetic materials: polymers grafted onto cellulose microcrystals. Biomacromolecules, 12(4), 1214–1223. Doi: 10.1021/bm101506j

Hatton, F. L., Malmström, E., Carlmark, A. (2015). Tailor-made copolymers for the adsorption to cellulosic surfaces. European Polymer Journal, 65, 325–339. Doi: 10.1016/j.eurpolymj.2015.01.026

Hauru, L. K. J., Hummel, M., Michud, A., Sixta, H. (2014). Dry jet-wet spinning of strong cellulose filaments from ionic liquid solution. Cellulose, 21(6), 4471–4481. Doi: 10.1007/s10570-014-0414-0

Henriksson, M., Henriksson, G., Berglund, L. A., Lindström, T. (2007). An environmentally friendly method for enzyme-assisted preparation of microfibrillated cellulose (MFC) nanofibers. European Polymer Journal, 43(8), 3434–3441. Doi: 10.1016/j.eurpolymj.2007.05.038

Henriksson, M., Berglund, L. A., Isaksson, P., Lindström, T., Nishino, T. (2008). Cellulose Nanopaper Structures of High Toughness. Biomacromolecules, 9(6), 1579–1585. Doi: 10.1021/bm800038n

Hirose, E. (2009). Ascidian tunic cells: morphology and functional diversity of free cells outside the epidermis. Invertebrate Biology, 128(1), 83–96. Doi: 10.1111/j.1744-7410.2008.00153.x

Hospodarova, V., Singovszka, E., Stevulova, N. (2018). Characterization of cellulosic fibers by ftir spectroscopy for their further implementation to building materials. American Journal of Analytical Chemistry, 09(06), 303–310. Doi: 10.4236/ajac.2018.96023

Huang, Z. -M., Zhang, Y. -Z., Kotaki, M., Ramakrishna, S. (2003). A review on polymer nanofibers by electrospinning and their applications in nanocomposites. Composites Science and Technology, 63(15), 2223–2253. Doi: 10.1016/s0266-3538(03)00178-7

Huang, J., Zhu, H., Chen, Y., Preston, C., Rohrbach, K., Cumings, J., Hu, L. (2013). Highly Transparent and Flexible Nanopaper Transistors. ACS Nano, 7(3), 2106–2113. Doi: 10.1021/nn304407r

Hubbe M. A., Rojas O. J., Lucia L. A., Sain M. (2008). Cellulosic nanocomposites: A review. BioResources, 3:929-980. Doi: 10.15376/biores.3.3.929-980

Hubbe, M. A., Gardner, D. J., Shen, W. (2015). Contact Angles and Wettability of Cellulosic Surfaces: A Review of Proposed Mechanisms and Test Strategies. BioResources, 10(4). Doi: 10.15376/biores.10.4.hubbe_gardner_shen

Hubbe, M. A.; Tayeb, P.; Joyce, M.; Tyagi, P.; Kehoe, M.; Dimic-Misic, K.; Pal, L. (2017). Rheology of nanocellulose-rich aqueous suspensions: A review. BioResources, 12, 9556–9661. Doi: 10.15376/biores.12.4.Hubbe

Huhtamäki, T., Tian, X., Korhonen, J. T., Ras, R. H. A. (2018). Surface-wetting characterization using contact-angle measurements. Nature Protocols, 13(7), 1521–1538. Doi: 10.1038/s41596-018-0003-z

Ifuku, S., Yano, H. (2015). Effect of a silane coupling agent on the mechanical properties of a microfibrillated cellulose composite. International Journal of Biological Macromolecules, 74, 428–432. Doi: 10.1016/j.ijbiomac.2014.12.029

Iguchi, M., Yamanaka, S. Budhiono, A. (2000). Bacterial cellulose - a masterpiece of nature's arts. Journal of materials science, 35, 261– 270. Doi: 10.1023/A:1004775229149

Imura, Y., Hogan, R. M. C., Jaffe, M. (2014). Dry spinning of synthetic polymer fibers. Advances in Filament Yarn Spinning of Textiles and Polymers, 187–202. Doi: 10.1533/9780857099174.2.187

Islam, M. N., Rahman, F. (2019). Production and modification of nanofibrillated cellulose composites and potential applications. In: Green Composites for Automotive Applications. Elsevier, 115–141. Doi: 10.1016/b978-0-08-102177-4.00006-9

Isogai, A., Saito, T., Fukuzumi, H. (2011). TEMPO-oxidized cellulose nanofibers. Nanoscale, 3(1), 71–85. Doi: 10.1039/c0nr00583e

Iwamoto, S., Nakagaito, A. N., Yano, H., Nogi, M. (2005). Optically transparent composites reinforced with plant fiber-based nanofibers. Applied Physics A, 81(6), 1109–1112. Doi: 10.1007/s00339-005-3316-z

Iwamoto, S., Nakagaito, A. N., Yano, H. (2007). Nano-fibrillation of pulp fibers for the processing of transparent nanocomposites. Applied Physics A, 89(2), 461–466. Doi: 10.1007/s00339-007-4175-6

Iwamoto, S., Kai, W., Isogai, A., Iwata, T. (2009). Elastic Modulus of Single Cellulose Microfibrils from Tunicate Measured by Atomic Force Microscopy. Biomacromolecules, 10(9), 2571–2576. Doi:10.1021/bm900520n

Janardhnan, S., Sain, M. (2011). Isolation of Cellulose Nanofibers: Effect of Biotreatment on Hydrogen Bonding Network in Wood Fibers. International Journal of Polymer Science, 2011, 1–6. Doi: 10.1155/2011/279610

Jiang, X., Bai, Y., Chen, X., Liu, W. (2020). A review on raw materials, commercial production and properties of lyocell fiber. Journal of BioResources and Bioproducts, 5(1), 16–25. Doi: 10.1016/j.jobab.2020.03.002

Jonoobi, M., Harun, J., Mathew, A. P., Hussein, M. Z. B., Oksman, K. (2010). Preparation of cellulose nanofibers with hydrophobic surface characteristics. Cellulose, 17(2), 299–307. Doi: 10.1007/s10570-009-9387-9

Kaboorani, A., Riedl, B. (2015). Surface modification of cellulose nanocrystals (CNC) by a cationic surfactant. Industrial Crops and Products, 65, 45–55. Doi: 10.1016/j.indcrop.2014.11.027

Kalia, S., Boufi, S., Celli, A., Kango, S. (2013). Nanofibrillated cellulose: surface modification and potential applications. Colloid and Polymer Science, 292(1), 5–31. Doi: 10.1007/s00396-013-3112-9

Kamide, K., Nishiyama, K. (2001). Cuprammonium processes. In: Regenerated Cellulose Fibres. Woodhead Publishing, 88–155. Doi: 10.1533/9781855737587.88

Karppinen, A., Saarinen, T., Salmela, J., Laukkanen, A., Nuopponen, M., Seppälä, J. (2012). Flocculation of microfibrillated cellulose in shear flow. Cellulose, 19(6), 1807–1819. Doi: 10.1007/s10570-012-9766-5

Keshk, S. M. (2014). Bacterial Cellulose Production and its Industrial Applications. Journal of Bioprocessing & Biotechniques, 04(02). Doi: 10.4172/2155-9821.1000150

Khalil, H. P. S. A., Davoudpour, Y., Islam, M. N., Mustapha, A., Sudesh, K., Dungani, R., Jawaid, M. (2014a). Production and modification of nanofibrillated cellulose using various mechanical processes: A review. Carbohydrate Polymers, 99, 649–665. Doi: 10.1016/j.carbpol.2013.08.069

Khalil, H. P. S. A., Davoudpour, Y., Aprilia, N. A. S., Mustapha, A., Hossain, S., Islam, N., Dungani, R. (2014b). Nanocellulose-Based Polymer Nanocomposite: Isolation, Characterization and Applications. In: Nanocellulose Polymer Nanocomposites. John Wiley & Sons, Inc. 273–309. Doi: 10.1002/9781118872246.ch11

Kim, D. Y., Nishiyama, Y., Kuga, S. (2002). Surface acetylation of bacterial cellulose. Cellulose, 9:361-7. Doi: 10.1023/A:1021140726936

Kim, D. B., Pak, J. J., Jo, S. M., Lee, W. S. (2005a). Dry Jet-Wet Spinning of Cellulose/N-Methylmorpholine N-oxide Hydrate Solutions and Physical Properties of Lyocell Fibers. Textile Research Journal, 75(4), 331–341. Doi: 10.1177/0040517505054852

Kim, C. -W., Frey, M. W., Marquez, M., Joo, Y. L. (2005b). Preparation of submicron-scale, electrospun cellulose fibers via direct dissolution. Journal of Polymer Science Part B: Polymer Physics, 43(13), 1673–1683. Doi: 10.1002/polb.20475

Kim, C. -W., Kim, D. -S., Kang, S. -Y., Marquez, M., Joo, Y. L. (2006). Structural studies of electrospun cellulose nanofibers. Polymer, 47(14), 5097–5107. Doi: 10.1016/j.polymer.2006.05.033

Kimura, S., Itoh, T. (2007). Biogenesis and Function of Cellulose in the Tunicates. In: Cellulose: Molecular and Structural Biology. Springer, 217–236. Doi: 10.1007/978-1-4020-5380-1_13

Klemm, D., Kramer, F., Moritz, S., Lindström, T., Ankerfors, M., Gray, D., Dorris, A. (2011). Nanocelluloses: A New Family of Nature-Based Materials. Angewandte Chemie International Edition, 50(24), 5438–5466. Doi: 10.1002/anie.201001273

Koch, K., Bhushan, B., Barthlott, W. (2008). Diversity of structure, morphology and wetting of plant surfaces. Soft Matter, 4(10), 1943. Doi:10.1039/b804854a

Konwarh, R., Karak, N., Misra, M. (2013). Electrospun cellulose acetate nanofibers: The present status and gamut of biotechnological applications. Biotechnology Advances, 31(4), 421–437. Doi: 10.1016/j.biotechadv.2013.01.002

Kosan, B., Michels, C., Meister, F. (2008). Dissolution and forming of cellulose with ionic liquids. Cellulose, 15(1), 59–66. Doi: 10.1007/s10570-007-9160-x

Larsson, E., Sanchez, C. C., Porsch, C., Karabulut, E., Wågberg, L., Carlmark, A. (2013). Thermo-responsive nanofibrillated cellulose by polyelectrolyte adsorption. European Polymer Journal, 49(9), 2689–2696. Doi: 10.1016/j.eurpolymj.2013.05.023

Lavoine, N., Desloges, I., Dufresne, A., Bras, J. (2012). Microfibrillated cellulose – Its barrier properties and applications in cellulosic materials: A review. Carbohydrate Polymers, 90(2), 735–764. Doi: 10.1016/j.carbpol.2012.05.026

Law, K. -Y. (2014). Definitions for Hydrophilicity, Hydrophobicity, and Superhydrophobicity: Getting the Basics Right. The Journal of Physical Chemistry Letters, 5(4), 686–688. Doi: 10.1021/jz402762h

Lee, K. -Y., Tammelin, T., Schulfter, K., Kiiskinen, H., Samela, J., Bismarck, A. (2012). High Performance Cellulose Nanocomposites: Comparing the Reinforcing Ability of Bacterial Cellulose and Nanofibrillated Cellulose. ACS Applied Materials & Interfaces, 4(8), 4078–4086. Doi: 10.1021/am300852a

Lee, H., Sundaram, J., Mani, S. (2017). Production of Cellulose Nanofibrils and Their Application to Food: A Review. In: Nanotechnology, 1–33. Doi: 10.1007/978-981-10-4678-0_1

Li, S., Xiao, M., Zheng, A., Xiao, H. (2011). Cellulose Microfibrils Grafted with PBA via Surface-Initiated Atom Transfer Radical Polymerization for Biocomposite Reinforcement. Biomacromolecules, 12(9), 3305–3312. Doi: 10.1021/bm200797a

Li, J., Wei, X., Wang, Q., Chen, J., Chang, G., Kong, L., *et al.* (2012). Homogeneous isolation of nanocellulose from sugarcane bagasse by high pressure homogenization. Carbohydrate Polymers, 90(4), 1609–1613. Doi: 10.1016/j.carbpol.2012.07.038

Li, J., Nawaz, H., Wu, J., Zhang, J., Wan, J., Mi, Q., *et al.* (2018). All-cellulose composites based on the self-reinforced effect. Composites Communications, 9, 42–53. Doi: 10.1016/j.coco.2018.04.008

Lin, F., Cousin, F., Putaux, J. -L., Jean, B. (2019). Temperature-Controlled Star-Shaped Cellulose Nanocrystal Assemblies Resulting from Asymmetric Polymer Grafting. ACS Macro Letters, 8(4), 345–351. Doi: 10.1021/acsmacrolett.8b01005

Lindström, T., Aulin, C., Naderi, A., Ankerfors, M. (2014). Microfibrillated cellulose. In Encyclopedia of polymerscience and technology. John Wiley & Sons, Inc. 1-34. Doi: 10.1002/0471440264.pst614

Lingström, R., Notley, S. M., Wågberg, L. (2007). Wettability changes in the formation of polymeric multilayers on cellulose fibres and their influence on wet adhesion. Journal of Colloid and Interface Science, 314(1), 1–9. Doi: 10.1016/j.jcis.2007.04.046

Liu, H. Hsieh, Y -L. (2002). Ultrafine fibrous cellulose membranes from electrospinning of cellulose acetate. Polymer Physics, 40(18), 2119-2129. Doi: 10.1002/polb.10261

Liu, Y., Chen, X., Xin, J. H. (2009). Can superhydrophobic surfaces repel hot water? Journal of Materials Chemistry, 19(31), 5602. Doi: 10.1039/b822168e

Lourenço, A. F., Gamelas, J. A. F., Nunes, T., Amaral, J., Mutjé, P., & Ferreira, P. J. (2017). Influence of TEMPO-oxidised cellulose nanofibrils on the properties of filler-containing papers. Cellulose, 24(1), 349–362. Doi: 10.1007/s10570-016-1121-9

Luu W. T., Bousfiels D. W., Kettle J. (2011). Application of nano-fibrillated cellulose as a paper surface treatment for inkjet printing. Paper presented in PaperCon Conference, Covington, USA, 1152-1163.

Ly, M., Mekonnen, T. H. (2020). Cationic surfactant modified cellulose nanocrystals for corrosion protective nanocomposite surface coatings. Journal of Industrial and Engineering Chemistry, 83 409–420. Doi: 10.1016/j.jiec.2019.12.014

Mahmud, M. M., Perveen, A., Jahan, R. A., Matin, M. A., Wong, S. Y., Li, X., Arafat, M. T. (2019). Preparation of different polymorphs of cellulose from different acid hydrolysis medium. International Journal of Biological Macromolecules, 130, 969–976. Doi: 10.1016/j.ijbiomac.2019.03.027

Marmur, A. (2006). Soft contact: measurement and interpretation of contact angles. Soft Matter, 2(1), 12–17. Doi: 10.1039/b514811c

Marmur, A. (2008). From Hygrophilic to Superhygrophobic: Theoretical Conditions for Making High-Contact-Angle Surfaces from Low-Contact-Angle Materials. Langmuir, 24(14), 7573–7579. Doi: 10.1021/la800304r

Mashkour, M., Afra, E., Resalati, H., Mashkour, M. (2015). Moderate surface acetylation of nanofibrillated cellulose for the improvement of paper strength and barrier properties. RSC Advances, 5(74), 60179–60187. Doi: 10.1039/c5ra08161k

Matsumura, H., Sugiyama, J., Glasser, W. G. (2000). Cellulosic nanocomposites. I. Thermally deformable cellulose hexanoates from heterogeneous reaction. Journal of Applied Polymer Science, 78(13), 2242–2253. Doi: 10.1002/1097-4628(20001220)78:13<2242::aid-app20>3.0.co;2-5

Mazeau, K., Heux, L. (2003). Molecular Dynamics Simulations of Bulk Native Crystalline and Amorphous Structures of Cellulose. The Journal of Physical Chemistry B, 107(10), 2394–2403. Doi: 10.1021/jp0219395

McHale, G., Shirtcliffe, N. J., Newton, M. I. (2004). Contact-Angle Hysteresis on Super-Hydrophobic Surfaces. Langmuir, 20(23) 10146–10149. Doi: 10.1021/la0486584

Medronho, B., Lindman, B. (2014). Competing forces during cellulose dissolution: From solvents to mechanisms. Current Opinion in Colloid & Interface Science, 19(1), 32–40. Doi: 10.1016/j.cocis.2013.12.001

Mekonnen, T. H., Haile, T., Ly, M. (2021). Hydrophobic functionalization of cellulose nanocrystals for enhanced corrosion resistance of polyurethane nanocomposite coatings. Applied Surface Science, 540, 148299. Doi: 10.1016/j.apsusc.2020.148299

Missoum, K., Belgacem, M., Bras, J. (2013). Nanofibrillated Cellulose Surface Modification: A Review. Materials, 6(5), 1745–1766. Doi: 10.3390/ma6051745

Modaressi, H.; Garnier, G. (2002). Mechanism of Wetting and Absorption of Water Droplets on Sized Paper: Effects of Chemical and Physical Heterogeneity. Langmuir, 18(3), 642–649. Doi: 10.1021/la0104931

Mohamed, M. A., Jaafar, J., Ismail, A. F., Othman, M. H. D., Rahman, M. A. (2017). Fourier Transform Infrared (FTIR) Spectroscopy. In: Membrane Characterization, 3–29. Doi: 10.1016/b978-0-444-63776-5.00001-2

Moon, R. J., Martini, A., Nairn, J., Simonsen, J., Youngblood, J. (2011). Cellulose nanomaterials review: structure, properties and nanocomposites. Chemical Society Reviews, 40(7), 3941. Doi: 10.1039/c0cs00108b

Mount, E. M. (2017). Extrusion Processes. In: Applied Plastics Engineering Handbook. Elsevier, 217–264. Doi: 10.1016/b978-0-323-39040-8.00012-2

Naderi, A., Lindström, T., Sundström, J. (2015). Repeated homogenization, a route for decreasing the energy consumption in the manufacturing process of carboxymethylated nanofibrillated cellulose? Cellulose, 22(2), 1147–1157. Doi: 10.1007/s10570-015-0576-4

Naderi, A., Lindström, T. (2015). Rheological measurements on nanofibrillated cellulose systems: a science in progress. In: Cellulose and Cellulose Derivatives. Nova Science Publishers Inc., 187-202. ISBN 978-1-63483-127-7

Naderi, A. (2017). Nanofibrillated cellulose: properties reinvestigated. Cellulose, 24(5), 1933–1945. Doi: 10.1007/s10570-017-1258-1

Nakagaito, A. N., Yano, H. (2004). The effect of morphological changes from pulp fiber towards nano-scale fibrillated cellulose on the mechanical properties of high-strength plant fiber based composites. Applied Physics A: Materials Science & Processing, 78(4), 547–552. Doi: 10.1007/s00339-003-2453-5

Nakamura, K., Hatakeyama, T., Hatakeyama, H. (1983). Relationship between hydrogen bonding and bound water in polyhydroxystyrene derivatives. Polymer, 24(7), 871–876. Doi: 10.1016/0032-3861(83)90206-9

Nechyporchuk, O., Belgacem, M. N., Bras, J. (2016). Production of cellulose nanofibrils: A review of recent advances. Industrial Crops and Products, 93, 2–25. Doi: 10.1016/j.indcrop.2016.02.016

Nishino, T., Matsuda, I., Hirao, K. (2004). All-Cellulose Composite. Macromolecules, 37(20), 7683–7687. Doi: 10.1021/ma049300h

Nogi, M., Abe, K., Handa, K., Nakatsubo, F., Ifuku, S., Yano, H. (2006). Property enhancement of optically transparent bionanofiber composites by acetylation. Applied Physics Letters, 89(23), 233123. Doi: 10.1063/1.2403901

Nogi, M., Komoda, N., Otsuka, K., Suganuma, K. (2013). Foldable nanopaper antennas for origami electronics. Nanoscale, 5(10), 4395. Doi: 10.1039/c3nr00231d

Olsson, C., Westman, G. (2012). Wet spinning of cellulose from ionic liquid solutions-viscometry and mechanical performance. Journal of Applied Polymer Science, 127(6), 4542–4548. Doi: 10.1002/app.38064

Osong, S. H., Norgren, S., Engstrand, P. (2016). Processing of wood-based microfibrillated cellulose and nanofibrillated cellulose, and applications relating to papermaking: a review. Cellulose, 23(1), 93–123. Doi: 10.1007/s10570-015-0798-5

Österberg, M., Vartiainen, J., Lucenius, J., Hippi, U., Seppälä, J., Serimaa, R., Laine, J. (2013). A Fast Method to Produce Strong NFC Films as a Platform for Barrier and Functional Materials. ACS Applied Materials & Interfaces, 5(11), 4640–4647. Doi: 10.1021/am401046x

O'sullivan, A. (1997). Cellulose: the structure slowly unravels. Cellulose 4, 173-207. Doi: 10.1023/A:1018431705579

Pääkkö, M., Ankerfors, M., Kosonen, H., Nykänen, A., Ahola, S., Österberg, M., *et al.* (2007). Enzymatic Hydrolysis Combined with Mechanical Shearing and High-Pressure Homogenization for Nanoscale Cellulose Fibrils and Strong Gels. Biomacromolecules, 8(6), 1934–1941. Doi: 10.1021/bm061215p

Paunonen, S. (2013). Strength and Barrier Enhancements of Cellophane and Cellulose Derivative Films: A Review. BioResources, 8(2). Doi: 10.15376/biores.8.2.3098-3121

Perepelkin, K. E. (2007). Lyocell fibres based on direct dissolution of cellulose in N-methylmorpholine N-oxide: Development and prospects. Fibre Chemistry, 39(2), 163–172. Doi: 10.1007/s10692-007-0032-9

Perez, D. S., Montanari, S., Vignon, M. R. (2003). TEMPO-Mediated Oxidation of Cellulose III. Biomacromolecules, 4(5), 1417–1425. Doi: 10.1021/bm034144s

Perissi, I., Bardi, U., Caporali, S., Lavacchi, A. (2006). High temperature corrosion properties of ionic liquids. Corrosion Science, 48(9), 2349–2362. Doi: 10.1016/j.corsci.2006.06.010

Plummer, C. J. G., Galland, S., Ansari, F., Leterrier, Y., Bourban, P. -E., Berglund, L. A., Månson, J.-A. E. (2015). Influence of processing routes on morphology and low strain stiffness of polymer/nanofibrillated cellulose composites. Plastics, Rubber and Composites, 44(3), 81–86. Doi: 10.1179/1743289814y.0000000111

Podsiadlo, P., Choi, S. -Y., Shim, B., Lee, J., Cuddihy, M., Kotov, N. A. (2005). Molecularly Engineered Nanocomposites: Layer-by-Layer Assembly of Cellulose Nanocrystals. Biomacromolecules, 6(6), 2914–2918. Doi: 10.1021/bm050333u

Poletto, M., Pistor, V. J. A. (2013). Structural Characteristics and Thermal Properties of Native Cellulose. Cellulose - Fundamental Aspects. Doi: 10.5772/50452

Postek, M. T., Vladár, A., Dagata, J., Farkas, N., Ming, B., Wagner, R., *et al.* (2010). Development of the metrology and imaging of cellulose nanocrystals. Measurement Science and Technology, 22(2), 024005. Doi: 10.1088/0957-0233/22/2/024005

Prabhu, D. M. Li. W. (2015). The most abundant natural resource: cellulose and its derivatives and their applications. In: Cellulose and Cellulose Derivatives. Nova Science Publishers Inc., 3-15. ISBN 978-1-63483-127-7

Puls, J., Wilson, S. A., Hölter, D. (2011). Degradation of Cellulose Acetate-Based Materials: A Review. Journal of Polymers and the Environment, 19(1), 152–165. Doi: 10.1007/s10924-010-0258-0

Qi, W., Xu, H. -N., Zhang, L. (2015). The aggregation behavior of cellulose micro/nanoparticles in aqueous media. RSC Advances, 5(12), 8770–8777. Doi: 10.1039/c4ra08844a

Raj, P., Varanasi, S., Batchelor, W., Garnier, G. (2015). Effect of cationic polyacrylamide on the processing and properties of nanocellulose films. Journal of Colloid and Interface Science, 447, 113–119. Doi: 10.1016/j.jcis.2015.01.019

Raj, P., Batchelor, W., Blanco, A., de la Fuente, E., Negro, C., Garnier, G. (2016). Effect of polyelectrolyte morphology and adsorption on the mechanism of nanocellulose flocculation. Journal of Colloid and Interface Science, 481, 158–167. Doi: 10.1016/j.jcis.2016.07.048

Ramé, E. (1997). The Interpretation of Dynamic Contact Angles Measured by the Wilhelmy Plate Method. Journal of Colloid and Interface Science, 189(2), 382–383. Doi: 10.1006/jcis.1997.4914

Rana, S., Pichandi, S., Parveen, S., Fangueiro, R. (2014). Regenerated Cellulosic Fibers and Their Implications on Sustainability. Roadmap to Sustainable Textiles and Clothing, 239–276. Doi: 10.1007/978-981-287-065-0_8

Raven, P. H., Johnson, G. B., Mason, K. A., Losos, J. B., Singer, S. R. (2011). Vertebrates. In: Biology. McGraw-Hill Education, 948-949. ISBN 978-0-07353-222-6

Rodríguez-Valverde, M. A., Cabrerizo-Vílchez, M. A., Rosales-López, P., Páez-Dueñas, A., Hidalgo-Álvarez, R. (2002). Contact angle measurements on two (wood and stone) non-ideal surfaces. Colloids and Surfaces A: Physicochemical and Engineering Aspects, 206(1-3), 485–495. Doi: 10.1016/s0927-7757(02)00054-7

Rojas, J., Bedoya, M., Ciro, Y. (2015). Current Trends in the Production of Cellulose Nanoparticles and Nanocomposites for Biomedical Applications. Cellulose - Fundamental Aspects and Current Trends. Doi: 10.5772/61334

Rol, F., Belgacem, M. N., Gandini, A., Bras, J. (2019). Recent advances in surface-modified cellulose nanofibrils. Progress in Polymer Science, 88, 241–264. Doi: 10.1016/j.progpolymsci.2018.09.002

Rose, M., Palkovits, R. (2011). Cellulose-Based Sustainable Polymers: State of the Art and Future Trends. Macromolecular Rapid Communications, 32(17), 1299–1311. Doi: 10.1002/marc.201100230

Saarikoski, E., Saarinen, T., Salmela, J., Seppälä, J. (2012). Flocculated flow of microfibrillated cellulose water suspensions: an imaging approach for characterisation of rheological behaviour. Cellulose, 19(3), 647–659. Doi: 10.1007/s10570-012-9661-0

Saito, T., Isogai, A. (2004). TEMPO-Mediated Oxidation of Native Cellulose. The Effect of Oxidation Conditions on Chemical and Crystal Structures of the Water-Insoluble Fractions. Biomacromolecules, 5(5), 1983–1989. Doi: 10.1021/bm0497769

Saito, T., Kimura, S., Nishiyama, Y., Isogai, A. (2007). Cellulose Nanofibers Prepared by TEMPO-Mediated Oxidation of Native Cellulose. Biomacromolecules, 8(8), 2485–2491. Doi: 10.1021/bm0703970

Saito, T., Hirota, M., Tamura, N., Kimura, S., Fukuzumi, H., Heux, L., Isogai, A. (2009). Individualization of Nano-Sized Plant Cellulose Fibrils by Direct Surface Carboxylation Using TEMPO Catalyst under Neutral Conditions. Biomacromolecules, 10(7), 1992–1996. Doi: 10.1021/bm900414t

Salas, C., Hubbe, M., Rojas, O. J. (2019). Nanocellulose Applications in Papermaking. Biofuels and Biorefineries. Springer, 61–96. Doi: 10.1007/978-981-13-3768-0_3

Samir, M. A. S., Alloin, F., Dufresne, A. (2005). Review of Recent Research into Cellulosic Whiskers, Their Properties and Their Application in Nanocomposite Field. Biomacromolecules, 6(2), 612–626. Doi: 10.1021/bm0493685

Samyn, P. (2013). Wetting and hydrophobic modification of cellulose surfaces for paper applications. Journal of Materials Science, 48(19), 6455–6498. Doi: 10.1007/s10853-013-7519-y

Samarasekara, A. M. P. B., Kahavita, K. D. H. N., Amarasinghe, D. A. S., Karunanayake, L. (2018). Fabrication and Characterization of Nanofibrillated Cellulose (NFC) Reinforced Polymer Composite. Proceedings Article published in 2018 Moratuwa Engineering Research Conference (MERCon). Doi: 10.1109/mercon.2018.8421934

Sayyed, A.J., Deshmukh, N.A., Pinjari, D.V. (2019). A critical review of manufacturing processes used in regenerated cellulosic fibres: viscose, cellulose acetate, cuprammonium, LiCl/DMAc, ionic liquids, and NMMO based lyocell. Cellulose, 26, 2913–2940. Doi: 10.1007/s10570-019-02318-y

Sehaqui, H., Allais, M., Zhou, Q., Berglund, L. A. (2011). Wood cellulose biocomposites with fibrous structures at micro- and nanoscale. Composites Science and Technology, 71(3), 382–387. Doi: 10.1016/j.compscitech.2010.12.007

Sehaqui, H., Berglund, L. A., Zhou, Q. (2013). Biorefinery: Nanofibrillated cellulose for enhancement of strength in high-density paper structures. Nordic Pulp & Paper Research Journal, 28(2), 182–189. Doi: 10.3183/npprj-2013-28-02-p182-189

Sharma, A., Thakur, M., Bhattacharya, M., Mandal, T., Goswami, S. (2019). Commercial application of cellulose nano-composites – A review. Biotechnology Reports, 21, e00316. Doi: 10.1016/j.btre.2019.e00316 0.1016/j.progpolymsci.2018.09.002

Shibata, I., Isogai, A. (2003). Depolymerization of cellouronic acid during TEMPO-mediated oxidation. Cellulose 10, 151–158. Doi: 10.1023/A:1024051514026

Singh, Z., Bhalla, S. (2017). Toxicity of Synthetic Fibres & Health. Advance Research in Textile Engineering, 2(1). Doi: 10.26420/advrestexteng.2017.1012

Siqueira, G., Bras, J., Dufresne, A. (2009). Cellulose Whiskers versus Microfibrils: Influence of the Nature of the Nanoparticle and its Surface Functionalization on the Thermal and Mechanical Properties of Nanocomposites. Biomacromolecules, 10(2), 425–432. Doi: 10.1021/bm801193d

Siqueira, G., Bras, J., Dufresne, A. (2010). Cellulosic Bionanocomposites: A Review of Preparation, Properties and Applications. Polymers, 2(4), 728–765. Doi: 10.3390/polym2040728

Siró, I., Plackett, D. (2010). Microfibrillated cellulose and new nanocomposite materials: a review. Cellulose, 17(3), 459–494. Doi: 10.1007/s10570-010-9405-y

Sixta, H. (2016). Cellulose Chemistry Lyocell Fibers. https://mycourses.aalto.fi/pluginfile.php/243898/mod_resource/content/1/Lyocell%20fibers_%20June%202016.pdf Accessed September 2020.

Soleimani-Gorgani, A. (2016). Inkjet Printing. In: Printing on Polymers, 231–246. Doi: 10.1016/b978-0-323-37468-2.00014-2

Spence, K. L., Venditti, R. A., Rojas, O. J., Habibi, Y., Pawlak, J. J. (2011). A comparative study of energy consumption and physical properties of microfibrillated cellulose produced by different processing methods. Cellulose, 18(4), 1097–1111. Doi: 10.1007/s10570-011-9533-z

Stenstad, P., Andresen, M., Tanem, B. S., Stenius, P. (2008). Chemical surface modifications of microfibrillated cellulose. Cellulose, 15(1), 35–45. Doi: 10.1007/s10570-007-9143-y

Storaenso (2020). Microfibrillated cellulose (MFC) – A natural performance enhancer for bio-based packaging materials.

https://www.storaenso.com/en/products/bio-based-materials/mfc-for-packaging Accessed August 2020.

Svagan, A. J., Samir, M. A. S. A., Berglund, L. A. (2008). Biomimetic Foams of High Mechanical Performance Based on Nanostructured Cell Walls Reinforced by Native Cellulose Nanofibrils. Advanced Materials, 20(7), 1263–1269. Doi: 10.1002/adma.200701215

Svensson, A., Nicklasson, E., Harrah, T., Panilaitis, B., Kaplan, D. L., Brittberg, M., Gatenholm, P. (2005). Bacterial cellulose as a potential scaffold for tissue engineering of cartilage. Biomaterials, 26(4), 419–431. Doi: 10.1016/j.biomaterials.2004.02.049

Swatloski, R. P., Spear, S. K., Holbrey, J. D., Rogers, R. D. (2002). Dissolution of Cellose with Ionic Liquids. Journal of the American Chemical Society, 124(18), 4974–4975. Doi: 10.1021/ja025790m

Taipale, T., Österberg, M., Nykänen, A., Ruokolainen, J., Laine, J. (2010). Effect of microfibrillated cellulose and fines on the drainage of kraft pulp suspension and paper strength. Cellulose, 17(5), 1005–1020. Doi: 10.1007/s10570-010-9431-9

Talik, P., Hubicka, U. (2018). The DSC approach to study non-freezing water contents of hydrated hydroxypropylcellulose (HPC). Journal of Thermal Analysis and Calorimetry, 132(1), 445–451. Doi: 10.1007/s10973-017-6889-9

Tang, J., Sisler, J., Grishkewich, N., Tam, K. C. (2017). Functionalization of cellulose nanocrystals for advanced applications. Journal of Colloid and Interface Science, 494, 397–409. Doi: 10.1016/j.jcis.2017.01.077

Tappa, K., Jammalamadaka, U. (2018). Novel Biomaterials Used in Medical 3D Printing Techniques. Journal of Functional Biomaterials, 9(1), 17. Doi: 10.3390/jfb9010017

Tayeb, A., Amini, E., Ghasemi, S., & Tajvidi, M. (2018). Cellulose Nanomaterials — Binding Properties and Applications: A Review. Molecules, 23(10), 2684. Doi: 10.3390/molecules23102684

Thomas, B., Raj, M. C., B, A. K., H, R. M., Joy, J., Moores, A., *et al.* (2018). Nanocellulose, a Versatile Green Platform: From Biosources to Materials and Their Applications. Chemical Reviews, 118(24), 11575–11625. Doi: 10.1021/acs.chemrev.7b00627

Tingaut, P., Zimmermann, T., Lopez-Suevos, F. (2010). Synthesis and Characterization of Bionanocomposites with Tunable Properties from Poly(lactic acid) and Acetylated Microfibrillated Cellulose. Biomacromolecules, 11(2), 454–464. Doi: 10.1021/bm901186u

Torvinen, K., Sievänen, J., Hjelt, T., Hellén, E. (2012). Smooth and flexible filler-nanocellulose composite structure for printed electronics applications. Cellulose, 19(3), 821–829. Doi: 10.1007/s10570-012-9677-5

Tungprapa, S., Puangparn, T., Weerasombut, M., Jangchud, I., Fakum, P., Semongkhol, S., *et al.* (2007). Electrospun cellulose acetate fibers: effect of solvent system on morphology and fiber diameter. Cellulose, 14(6), 563–575. Doi: 10.1007/s10570-007-9113-4

Utsel, S., Malmström, E. E., Carlmark, A., Wågberg, L. (2010). Thermoresponsive nanocomposites from multilayers of nanofibrillated cellulose and specially designed N-isopropylacrylamide based polymers. Soft Matter 6(2), 342–352

Vecchiato, S., Skopek, L., Jankova, S., Pellis, A., Ipsmiller, W., Aldrian, A., *et al.* (2017). Enzymatic Recycling of High-Value Phosphor Flame-Retardant Pigment and Glucose from Rayon Fibers. ACS Sustainable Chemistry & Engineering, 6(2), 2386–2394. Doi: 10.1021/acssuschemeng.7b03840

Virginia Tech (2008). Invention controls weavers of nanoscale biomaterials. https://vtnews.vt.edu/articles/2008/11/2008-693.html Accessed June 2020.

Wågberg, L. (2000). Polyelectrolyte adsorption onto cellulose fibres – A review. Nordic Pulp & Paper Research Journal, 15(5), 586–597. Doi: 10.3183/npprj-2000-15-05-p586-597

Wågberg, L., Decher, G., Norgren, M., Lindström, T., Ankerfors, M., Axnäs, K. (2008). The Build-Up of Polyelectrolyte Multilayers of Microfibrillated Cellulose and Cationic Polyelectrolytes. Langmuir, 24(3), 784–795. Doi: 10.1021/la702481v

Wang, B., Sain, M. (2007). Isolation of nanofibers from soybean source and their reinforcing capability on synthetic polymers. Composites Science and Technology, 67(11-12), 2521–2527. Doi: 10.1016/j.colavoinempscitech.2006.12.015

Wang, X., Cheng, F., Liu, J., Smått, J. -H., Gepperth, D., Lastusaari, M., *et al.* (2016a). Biocomposites of copper-containing mesoporous bioactive glass and nanofibrillated cellulose: Biocompatibility and angiogenic promotion in chronic wound healing application. Acta Biomaterialia, 46, 286–298. Doi: 10.1016/j.actbio.2016.09.021

Wang, S., Lu, A., Zhang, L. (2016b). Recent advances in regenerated cellulose materials. Progress in Polymer Science, 53, 169–206. Doi: 10.1016/j.progpolymsci.2015.07.003

Wang, X., Yao, C., Wang, F., Li, Z. (2017). Cellulose-Based Nanomaterials for Energy Applications. Small, 14(10), 1704152. Doi: 10.1002/smll.201704152

Wasim, M. (2020). An Overview of Synthesized Bacterial Cellulose Nanocomposites for Biomedical Applications. Biomedical Journal of Scientific & Technical Research, 27(2). Doi: 10.26717/bjstr.2020.27.004483

Watabe, Y., Suzuki, Y., Koike, S., Shimamoto, S., Kobayashi, Y. (2018). Cellulose acetate, a new candidate feed supplement for ruminant animals: In vitro evaluations. Journal of Dairy Science, 101(12), 10929–10938. Doi: 10.3168/jds.2018-14969

Wenzel, R. N. (1936). Resistance of solid surfaces to wetting by water. Industrial & Engineering Chemistry, 28(8), 988–994. Doi: 10.1021/ie50320a024

Wilkes, A. G. (2001). The viscose process. Regenerated Cellulose Fibres, 37–61. Doi: 10.1533/9781855737587.37

Wise, M. (2014). Advances in Microfibrillated Cellulose Films - Promises for Composite Materials. https://www.fpl.fs.fed.us/labnotes/?p=3974 Accessed August 2020.

Wolansky, G., Marmur, A. (1999). Apparent contact angles on rough surfaces: the Wenzel equation revisited. Colloids and Surfaces A: Physicochemical and Engineering Aspects, 156(1-3) 381–388. Doi: 10.1016/s0927-7757(99)00098-9

Xhanari, K., Syverud, K., Chinga-Carrasco, G., Paso, K., Stenius, P. (2010). Reduction of water wettability of nanofibrillated cellulose by adsorption of cationic surfactants. Cellulose, 18(2), 257–270. Doi: 10.1007/s10570-010-9482-y

Xu, M., Dai, H., Sun, X., Wang, S., Wu, W. (2012). Influence of buffer solution on tempo-mediated oxidation. BioResources, 7(2). Doi: 10.15376/biores.7.2.1633-1642

Yang, C., Tartaglino, U., Persson, B. N. J. (2006). Influence of Surface Roughness on Superhydrophobicity. Physical Review Letters, 97(11). Doi: 10.1103/physrevlett.97.116103

Yang, S., Xie, Q., Liu, X., Wu, M., Wang, S., Song, X. (2018). Acetylation improves thermal stability and transmittance in FOLED substrates based on nanocellulose films. RSC Advances, 8(7), 3619–3625. Doi: 10.1039/c7ra11134g

Yang, Z., Dou, F., Yu, T., Song, M., Shi, H., Yao, X., *et al.* (2019). On the cross-section of shaped fibers in the dry spinning process: Physical explanation by the geometric potential theory. Results in Physics, 14, 102347. Doi: 10.1016/j.rinp.2019.102347

Yeo, J. -S., Hwang, S. -H. (2014). Preparation and characteristics of polypropylene-graft-maleic anhydride anchored micro-fibriled cellulose: its composites with polypropylene. Journal of Adhesion Science and Technology, 29(3), 185–194. Doi: 10.1080/01694243.2014.980632

Yetiş, F., Liu, X., Sampson, W. W., Gong, R. H. (2020). Acetylation of lignin containing microfibrillated cellulose and its reinforcing effect for polylactic acid. European Polymer Journal, 134, 109803. Doi: 10.1016/j.eurpolymj.2020.109803

Zhang, W., Hallström, B. (1990). Membrane characterization using the contact angle technique I. methodology of the captive bubble technique. Desalination, 79(1), 1–12. Doi: 10.1016/0011-9164(90)80067-l

Zhang, Z., Sèbe, G., Rentsch, D., Zimmermann, T., Tingaut, P. (2014). Ultralightweight and Flexible Silylated Nanocellulose Sponges for the Selective Removal of Oil from Water. Chemistry of Materials, 26(8), 2659–2668. Doi: 10.1021/cm5004164

Zhang, M., Feng, S., Wang, L., Zheng, Y. (2016). Lotus effect in wetting and self-cleaning. Biotribology, 5, 31–43. Doi: 10.1016/j.biotri.2015.08.002

Zhang, S., Chen, C., Duan, C., Hu, H., Li, H., Li, J., Liu, Y., Ma, X., Stavik, J., Ni, Y. (2018). Regenerated cellulose by the lyocell process, a brief review of the process and properties. BioResources 13(2), 4577-4592. Doi: 10.15376/biores.13.2.Zhang

Zhang, H., Liu, Y., Cui, S., Zhou, Y., Hu, J., Ma, J., Liu, Y. (2020). Cellulose nanofibers electrospun from aqueous conditions. Cellulose. Doi: 10.1007/s10570-020-03366-5

Zhao, Y., Li, J. (2014). Excellent chemical and material cellulose from tunicates: diversity in cellulose production yield and chemical and morphological structures from different tunicate species. Cellulose, 21(5), 3427–3441. Doi: 10.1007/s10570-014-0348-6

Zhao, S., Zhang, Z., Sèbe, G., Wu, R., Rivera Virtudazo, R. V., Tingaut, P., Koebel, M. M. (2015). Multiscale Assembly of Superinsulating Silica Aerogels Within Silylated Nanocellulosic Scaffolds: Improved Mechanical Properties Promoted by Nanoscale Chemical Compatibilization. Advanced Functional Materials, 25(15), 2326–2334. Doi: 10.1002/adfm.201404368

Zhou, Y. M., Fu, S. Y., Zheng, L. M., Zhan, H. Y. (2012). Effect of nanocellulose isolation techniques on the formation of reinforced poly(vinyl alcohol) nanocomposite films. Express Polymer Letters, 6(10), 794–804. Doi: 10.3144/expresspolymlett.2012.85

Ziabari, M., Mottaghitalab, V., Haghi, A. K. (2009). Application of direct tracking method for measuring electrospun nanofiber diameter. Brazilian Journal of Chemical Engineering, 26(1), 53–62. Doi: 10.1590/s0104-66322009000100006

Zimmermann, T., Bordeanu, N., Strub, E. (2010). Properties of nanofibrillated cellulose from different raw materials and its reinforcement potential. Carbohydrate Polymers, 79(4), 1086–1093. Doi: 10.1016/j.carbpol.2009.10.045

Zhu, S., Chen, R., Wu, Y., Chen, Q., Zhang, X., Yub, Z. (2009). A mini review on greenness of ionic liquids. Chemical and Biochemical Engineering Quarterly, 23 (2), 207-211.

Zugenmaier, P. (2021). Order in cellulosics: Historical review of crystal structure research on cellulose. Carbohydrate Polymers, 254, 117417. Doi: 10.1016/j.carbpol.2020.117417